Development of a simplified model for phase change in presence of natural convection and radiation : application to a novel heat storage translucent superinsulated wall

Farah Souayfane

UNIVERSITÉ CÔTE D'AZUR

ÉCOLE DOCTORALE
SCIENCES FONDAMENTALES ET APPLIQUÉES

Université Libanaise

Modèle simplifié de changement de phase en présence de convection et rayonnement : Application à un mur translucide associant superisolation et stockage d'énergie thermiques

Development of a simplified model for phase change in presence of natural convection and radiation: Application to a novel heat storage translucent superinsulated wall

Farah SOUAYFANE

Laboratoire Jean Alexandre Dieudonné LJAD

Présentée en vue de l'obtention
du grade de docteur en Science pour l'ingénieur
de l'Université côte d'Azur
et de l'Université Libanaise
Dirigée par : Pascal Henry Biwole / Farouk Fardoun
Soutenue le : 26 Novembre 2018

Devant le jury, composé de :
Farouk Fardoun, Professeur, Université Libanaise
Hassane Naji, Professeur, Université d'Artois
Luisa Cabeza, Professeur, Université de Lleida
Pascal Henry Biwole, Professeur, Université Clermont Auvergne
Patrick Achard, Directeur de recherche, Mines-ParisTech
Richard Pasquetti, Directeur de recherche, CNRS

Modèle simplifié de changement de phase en présence de convection et rayonnement : Application à un mur translucide associant superisolation et stockage d'énergie thermiques

Development of a simplified model for phase change in presence of natural convection and radiation: Application to a novel heat storage translucent superinsulated wall

Jury :

Rapporteurs

Hassane Naji, Professeur, Université d'Artois

Luisa Cabeza, Professeur, Université de Lleida

Examinateurs

Patrick Achard, Directeur de recherche, Mines-ParisTech

Richard Pasquetti, Directeur de recherche, CNRS

Directeurs de thèse

Farouk Fardoun, Professeur, Université Libanaise

Pascal Henry Biwole, Professeur, Université Clermont Auvergne

Modèle simplifié de changement de phase en présence de convection et rayonnement : Application à un mur translucide associant superisolation et stockage d'énergie thermiques

Résumé

Au Liban comme en France, la consommation énergétique des bâtiments représente plus de 40% de l'énergie finale totale. Une proportion significative de la consommation d'énergie dans les bâtiments est utilisée pour le refroidissement et le chauffage. Une alternative pour atteindre l'objectif de réduction de la consommation d'énergie dans le bâtiment est d'améliorer la performance énergétique de son enveloppe en intégrant des matériaux à changement de phase (MCP). De plus, une partie importante de la conception du bâtiment consiste à utiliser au mieux les ressources externes et en particulier l'exploitation du rayonnement solaire. La fusion des MCP s'accompagne de différents phénomènes, à savoir, la convection naturelle et l'absorption ou transmission du rayonnement. Dans les bâtiments, où une évaluation thermique annuelle est nécessaire, la plupart des études sur les façades translucides intégrant du MCP ont négligé l'effet de la convection naturelle pendant la fusion et ont supposé des transferts unidimensionnels par conduction et rayonnement. Parce que cette hypothèse n'est pas toujours adéquate, le développement d'un modèle numérique simplifié prenant en compte la convection naturelle et le rayonnement lors du changement de phase, adapté à une évaluation thermique annuelle, est nécessaire. Ainsi, dans cette thèse, un modèle numérique simplifié bidimensionnel a été développé, en premier temps, dans le but de modéliser la convection naturelle pendant le processus de fusion d'un matériau à changement de phase. Une validation du modèle est faite à l'aide d'un modèle CFD précédemment développé, et des résultats numériques et expérimentaux trouvés dans la littérature pour le cas : fusion d'Octadécane dans une cavité carrée. Ensuite, un modèle numérique simplifié en 2D pour la fusion du MCP en présence de la convection naturelle et du rayonnement courte longueur d'onde (CLO) a été développé. Le modèle a été validé à l'aide d'une méthode de Boltzmann sur réseau couplé avec la méthode des ordonnées discrètes (LBM-DOM) trouvée dans la littérature pour le cas : fusion d'acide gras dans une cavité rectangulaire. En outre, dans le contexte d'efficacité énergétique et d'exploitation optimale des ressources environnementales, le projet INERTRANS a proposé le développement d'une façade solaire translucide innovante. Cette façade fournit un éclairage naturel et est composé d'une couche d'aérogel de silice assurant une isolation thermique et acoustique importante, et d'un matériau à changement de phase (MCP). Ce dernier est contenu dans des briques de verre et assure l'absorption, le stockage et la restitution de la chaleur. Ce mur a été caractérisé expérimentalement en ambiance contrôlée et in-situ sur un bâtiment à dimensions réelles et localisé au sein du centre PERSEE à Sophia Antipolis.

Son impact sur le bâtiment en termes de contribution aux apports énergétiques et lumineux a été mis en évidence. Il a été remarqué que la performance thermique du mur est très élevée en hiver, tandis qu'un problème de surchauffe a été rencontré en été lorsque le MCP reste à l'état liquide et n'arrive plus à dissiper la chaleur stockée. Pour optimiser la performance du mur MCP-aérogels en été, un modèle numérique simplifié décrivant les mécanismes de transfert de chaleur à travers le mur a été développé sous MATLAB basé sur les deux modèles validés précédents. Ce modèle est trouvé simple à mettre en œuvre et assez rapide pour être couplé à TRNSYS afin d'évaluer la performance thermique de l'ensemble du bâtiment. Le modèle couplé MATLAB-TRNSYS a été validé expérimentalement en été et en hiver à l'aide de la cellule expérimentale du centre PERSEE. Le comportement thermique du mur est testé sous différentes conditions climatiques, et des solutions passives sont proposées pour assurer le confort thermique en été. Les résultats ont montré que même si le MCP ne cycle pas en été, le confort thermique peut être assuré à l'aide des dispositifs d'ombrage. Enfin, le modèle validé a permis d'étudier le comportement thermique annuel d'un bâtiment intégrant un mur MCP- aérogel dans son enveloppe, et ceci dans six climats différents. De plus, une étude économique a été réalisée. Ces études ont confirmé l'intérêt du mur vis-à-vis de l'amélioration des performances énergétiques du bâtiment. La faisabilité économique de l'application du mur MCP-aérogel dépend principalement des conditions climatiques, des coûts de l'énergie, ainsi que de la situation économique du pays et du coût d'investissement.

Mots clés : mur MCP-aérogel, matériau à changement de phase, modélisation, validation expérimentale, convection naturelle, rayonnement, étude économique.

Development of a simplified model for phase change in presence of natural convection and radiation: Application to a novel heat storage translucent superinsulated wall

Abstract

In Lebanon as in France, the building sector is the largest consumer of energy and accounts for about 40% of the total energy consumption. A significant proportion of the energy consumption in buildings is used for cooling and heating applications. One way to reduce energy consumption and improve thermal comfort in the building is by integrating phase change materials (PCM) in its envelope. In addition, an important part of the building design is to make the best use of external resources and particularly the optimal exploitation of solar radiation. During phase change process, different phenomena occur, namely, natural convection in the liquid phase and radiation absorption or transmission. In building applications, where yearly thermal evaluation is needed, most studies on translucent facades with integrated PCM have neglected the natural convection effect during melting and have assumed one-dimensional transfers by conduction and radiation. Because this assumption is not always adequate, the development of a validated simplified numerical model coupling natural convection and radiation during phase change, suitable for annual thermal assessment, is needed. Thus, in this thesis, a two-dimensional simplified numerical model for PCM melting in presence of natural convection is first developed and coded on MATLAB. The model is validated using a CFD model, in addition to experimental and numerical benchmark solutions for a test case: melting of Octadecane in a square cavity. Then, a 2D simplified numerical model for PCM melting in presence of both natural convection and radiation is developed. The model is validated against LBM-DOM method found in the literature for a test case: melting of Fatty acids in rectangular cavity. Moreover, in the context of energy efficiency and exploiting environmental resources, the INERTRANS project has proposed the development of an innovative translucent solar façade. This wall is composed of glazing, silica aerogel used as a transparent insulation material (TIM) and glass bricks filled with a fatty acids mixture. The wall provides, concurrently, storage and restitution of heat, super thermal-acoustic insulation and daylighting to the interior environment. The thermal performance of the TIM-PCM wall was tested in a full-sized test cell located in Sophia Antipolis, Southern France, within the center for Processes, Renewable Energies and Energy Systems (PERSEE) of Mines ParisTech graduate school. In winter season, particularly in sunny cold days, the PCM absorbs solar radiation, melts, and then releases the stored heat to the building at night by solidifying. However, during the summer, an overheating problem is encountered mainly due to solar gains, the PCM remaining in its liquid state and is unable to release the stored heat at night. To enhance the energy performance of

the wall in summertime, a numerical model describing the heat transfer mechanisms occurring in the PCM layer in combination with the other transparent wall layers is developed on MATLAB based on the two previous validated models. The developed model was found simple to implement and fast enough to be linked to TRNSYS software to assess the thermal performance of the whole building. The MATLAB-TRNSYS model is validated experimentally using PERSEE test cell and a good agreement is shown when comparing the simulated values with the measured data for seven consecutive days in summer and winter. The thermal behavior of the wall is tested under different climatic conditions, and passive solutions are proposed to ensure thermal comfort in summer. The results showed that even if the PCM does not cycle in summertime, thermal comfort can be ensured using shading devices. Also, the use of a glazing with special optical characteristics (Prisma solar glass) instead of the ordinary glass in the TIM-PCM wall composition is shown to be an effective technology solving the encountered overheating problem in summer, while preserving the TIM-PCM advantages during winter. Finally, the validated model is used to study the annual thermal behavior of a building integrating TIM-PCM wall in its envelope under six different climates. In addition, an economic study is conducted. These studies confirmed the interest of the wall vis-à-vis the improvement of energy performance of the building. The economic feasibility of applying the TIM-PCM wall depends mainly on climatic conditions, energy costs, as well as the economic situation of the country and the cost of investment.

Keywords: TIM-PCM wall, phase change materials, numerical model, experimental validation, natural convection, radiation, economic analysis.

Acknowledgment

First and foremost, I want to express my sincere gratitude to my supervisors Pr. Farouk FARDOUN and Pr. Pascal Henry BIWOLE for their help and support during the past three years. It has been an honor to be their Ph.D. student. Without their assistance and encouragement, this work would not have been achieved.

I would also like to show my gratitude for the honorable jury members who accepted to examine my project: Mrs. Luisa Cabeza, Mr. Hassane Naji, Mr. Patrick Achard and Mr. Richard Pasquetti.

I also want to acknowledge the support and help of all the staff members of Jean Alexandre Dieudonné laboratory, EDST at Lebanese university, and the PERSEE research center at Mines ParisTech in Sohpia Antipolis.

My deepest thanks go to the Lebanese university, the Côte d'Azur University and Embassy of France in Lebanon. Their financial support is greatly appreciated.

My biggest love and gratitude goes to my family who gave me everything possible to enable me reach higher education levels. I only hope that they know how their love, support and patience encouraged me to fulfill my and their dream...

Nomenclature

ACH	Air change per hour	
averfl	Average fraction of liquid in the PCM layer	
B(T)	Numerical step function, Eq.2-22	
C	Numerical constant	kg/ (m^3.s)
c_1, c_2, c_3	dimensionless coefficient (Eq. 3-37)	
CFD	Computational fluid dynamics	
COP	Coefficient of performance	
Cp	Specific heat capacity	(J/kg·K)
CSTB	Scientific and technical center for building research	
d	optical thickness	
D(T)	Numerical Gaussian function, Eq.2-28	
DOM	Discrete Ordinate Method	
EC	Energy cost	($)
e_i	Experimental value	
EN	European norm	
ESC	Energy savings cost	($)
f_l	Liquid fraction	
Fo	Fourier number $\frac{\alpha t}{H^2}$	
G	Gravitational acceleration	(m/s^2)
Gr	Grashof number	
H	Height of enclosure	(m)
H	Height of the vertical surface (Eq. 3-21)	(m)
h_{in}	Indoor convective coefficient	(W/ m^2K)
h_{out}	Outdoor convective coefficient	(W/ m^2K)
HVAC	Heating, ventilation and air conditioning	
IC	Initial cost	($)
k	Thermal conductivity	(W/m·K)
L	Length of enclosure	(m)
LBM	Lattice Boltzmann Method	
LCC	Life cycle cost	($)

L_H	Latent heat of fusion	(J/kg)
N	Total number of nodes	
N	Total number of nodes in each layer (chapter 2)	
N	Lifetime (chapter 4)	(years)
N-S	Navier Stokes equations	
Nu_H	Nusselt number function of H, Table 2-1	
Nu_L	Nusselt number function of L, Table 2-1	
Nu_z	Nusselt number function of z, Table 2-5	
Nx	Nodes number in horizontal direction	
Ny	Nodes number in vertical direction	
OP	Overhang projection	(m)
P	Pressure	(Pa)
PCM	Phase change materials	
PERSEE	center for processes, renewable energies and energy systems	
PP	Payback period	(years)
Pr	Prandtl number	
PRMSE	Percentage root mean square error	
PWF	Present worth factor	
q	Numerical constant (chapter 2)	
Q_{sol}	Total incident solar radiation	(W/m^2)
$Q_{sol-ref}$	Reflected solar radiation	(W/m^2)
$Q_{sol-total}$	Total incident solar radiation	(W/m^2)
$Q_{sol-trans}$	Transmitted solar radiation	(W/m^2)
R	Thermal resistance	(m^2K/W)
r	Discount rate	
R^2	R-squared	
Ra_H	Rayleigh number function of H, Eq.2-15	
Ra_L	Rayleigh number function of L, Table 2-1	
Ra_z	Rayleigh number function of z, Eq.2-17	
RIM	Radiosity irradiosity method	

RMSE	Root mean square error	
RTE	Radiative transfer equation	
s	Position of the melting front, Eq.2-14	(m)
S	Physical thickness, Eq.2-33	(m)
s_i	Simulated value	
Ste	Stefan number	
STIME	Simulation time	
t	Time	(s)
T	Temperature	(K)
T_0	Initial temperature	(K)
T_{air}	Outdoor air temperature	(ºC)
T_c	Cold temperature	(K)
T_h	Hot temperature	(K)
TIM	Transparent insulation material	
T_m	Melting temperature	(K), (ºC)
u	Velocity vector	(m/s)
v	Wind velocity	(m/s)
x,y	Coordinates	(m)
z	Height of convective zone	(m)

Greek letters

$\emptyset_{LW,in}$	Radiative heat exchange with the indoor environment	(W/m^2)
$\emptyset_{LW,out}$	Radiative heat exchange with the outdoor environment	(W/m^2)
$\emptyset_{cond}$	Conductive heat flux	(W/m^2)
$\emptyset_{sol}$	Radiative source term	(W/m^2)
μ	Dynamic viscosity	(Pa.s)
α	Thermal diffusivity (Table 3-1)	(m^2/s)
α	Solar absorptivity coefficient	
α_{PCM}	Solar absorption coefficient, Eq.2-34	
β	Thermal expansion coefficient	(1/K)
δ	Average position of melting front in Table 2-2	

δ	Overall fractional change in transmittance, Eq.2-30	
Δt	Time increment	(s)
ΔT	Temperature difference between walls T_h- T_c	(K)
ε	Surface emissivity	
η	Adjustment constant of order 1 (chapter 2)	
η	Kinematic viscosity	(m^2/s)
η	Boiler efficiency	(%)
θ	Dimensionless time	
ρ	Solar reflectivity coefficient	
ρ	Density (Table 3-1)	(kg/m^3)
ρ	Solar reflectivity coefficient	
σ	Extinction coefficient	(m^{-1})
τ	Solar transmissivity coefficient	
τ_{PCM}	Solar transmittance coefficient, Eq.2-32	

Subscripts and superscripts

0	Previous time step
av	Average
c	Cooling
conv	Conventional
e	Electricity
enh	Enhanced
enh,p	Enhanced at node p
h	Heating
in	Indoor
l	Liquid
ng	Natural gas
Pc	Phase change
s	Solid
sol	Solar
surf	Surface

W, E, P, S, N	West, east, center, south and north node
w, e, s, n	West, east, south and north interface

Contents

List of Figures

List of Tables

GENERAL INTRODUCTION

General Introduction

There is global concern related to energy consumption in the built environment as one of the major contributors to greenhouse gas emissions responsible for causing climate change and its associated impacts. A significant proportion of the energy consumption in buildings is used for cooling and heating application. In Lebanon, as in France, the energy consumption of buildings represents more than 40% of total final energy and almost 25% of greenhouse gas emissions [1].

An alternative to achieve the goal of reducing energy consumption in the building is to improve the energy performance of its envelope. This envelope acts as a filter, it reduces heat exchange between the outside and the indoor environment, and protects the occupants from wind, rain, and other conditions, contributing to thermal and visual comfort. To achieve these purposes, combining insulation with latent heat storage materials is shown as an effective way. In addition, an important part of the building design is to make the best use of external resources and particularly the exploitation of solar radiation that is considered as an important resource in some areas.

Numerous studies have shown that the integration of phase change materials (PCM) in the building envelope can significantly improve the energy performance of the building and save up to 80% of heating energy in winter, as the material captures the heat of the sun, melts, then restitutes the heat to the building by re-solidifying. However, one of the encountered problems is the high risk of summer overheating when the material can no longer destock the stored heat and remains in its the liquid state. However, the possibility, feasibility, thermal performance and economic analysis of using PCM call a series of theoretical and experiential investigations. The experimental approaches offer a better indication of the actual PCM behavior and performance in comparison to theoretical analysis. However, the experiments are unachievable in some cases, such as the large scale or unsteady around environment, are time and cost consuming. In addition, there are still some unavoidable testing errors. However, the theoretical methods can avoid these weaknesses and predicate the PCM performance suitably. The major advantage of the theoretical/numerical approaches is that various conditions can be carried out by changing the variables in a numerical model, the main drawback being the accuracy of the model used. Therefore, more and more investigators prefer to study the phase change problems by mathematical solutions and numerical simulations.

Usually, when modeling phase change, numerical studies have some assumptions in their mathematical modeling [2] e.g. neglecting convective heat transfer within PCM [3] or neglecting radiative heat transfer [4], whereas the impact of those assumptions on simulation results are poorly discussed in the literature. However, recent researches have demonstrated that natural convection

plays an important role in latent heat thermal energy systems, especially during the melting process and conduction-only models may incur an unacceptable loss of accuracy.

Basically, the modeling of natural convection in liquid PCM could be classified in two major categories. The first category includes the simplified methods including the enhanced conductivity approach using dimensionless numbers. These approaches normally oversimplify the process. On the other hand, detailed computational fluid dynamics (CFD) methods, which require long computational time, are greatly complicated and complex, and might be limited to the investigated case. In addition, CFD simulations are rarely appropriate for the initial design stages especially for long period thermal assessment. However, between these two extremes, a model offering a good compromise between simplicity and accuracy is needed, which will be the first purpose of the current thesis.

On the other hand, most studies on translucent facades with integrated PCM have assumed one-dimensional transfers by conduction and radiation neglecting convection [5]–[7] and numerical models were specifically developed to take the interaction of PCM with solar radiation into account [8]–[11]. However, very few studies were found in the literature for the melting of PCM in presence of both natural convection and radiation. This will be our second research question.

The ANR INERTRANS project [12] proposed the development of an innovative wall that addresses the issue of energy efficiency and optimal use of environmental resources. This wall provides, concurrently, storage and restitution of heat, super thermal-acoustic insulation and daylighting to the interior environment. It allows exploiting the solar radiation during cold periods to heat the interior of the building. To do this, it combines new generation materials, such as silica aerogel for thermal insulation and phase change materials (PCM) for absorption and storage of heat. The quasi-constant restitution of the heat by convection and long wave radiation contributes to the increase of the sensation of thermal comfort of the inhabitant. An acronym for this wall is proposed: TIM-PCM wall which stands for “Translucent Insulating Material – Phase Change Material wall”.

The establishment of such facade in the building is conditioned by the knowledge of its behavior, its performance and its energy impact. However, this knowledge on many case studies is accessible only through numerical modeling. It is, therefore, necessary to ensure the availability and reliability of a numerical model representing the physics of such wall. Particularly, during the melting and solidification of the PCM, the latter can be subjected to different modes of heat transfer depending on the presence or not of sunshine and thus significantly change the kinetics of the phase change. The development of this numerical model will be our third aim.

The wall has been characterized experimentally in a full-scale test cell located in Sophia Antipolis, Southern France, within the center for Processes, Renewable Energies and Energy Systems (PERSEE) of Mines ParisTech graduate school [13]. In their experimental study, Berthou et al [13]

found that, in the winter season, particularly in sunny cold days, the thermal performance of the wall is very effective. While during the summer, an overheating problem is encountered mainly due to solar gains, the PCM remains in its liquid state and it is unable to release the stored heat at night. Thus, the optimization of the wall thermal performance in summer is needed and solutions for overheating and PCM cycling must be proposed.

Consequently, two research issues were identified in this thesis. The first one is scientific: simplified models using a modified heat diffusion equation to consider energy storage (enthalpy method [14], [15], equivalent heat capacity method [16] , [17], source term method [18]) do not consider the natural convection during the melting which can nevertheless become predominant when the PCM container is of sufficiently large dimensions. On the other hand, sophisticated models using numerical solution of Navier-Stokes equations (enthalpy-porosity method [19]–[26], temperature transformation model [27]–[30], modified heat capacity method [31], lattice Boltzmann method (LBM) [32]–[35]are computationally time-consuming and are not at all adapted to perform yearly energy performance evaluation of the building. The second one is technological: in the summer season, the PCM integrated in the TIM-PCM wall can no longer solidify at night and remains in its liquid state, causing summer overheating.

Broadly speaking, the present thesis proposes at first to perform the modeling of the phenomena involved in the translucent TIM-PCM wall to understand the influence and the interaction of the different modes of heat transfer. This includes the development of a simplified model for phase change, in presence of both natural convection and radiation, that offers a good compromise between simplicity and accuracy. And then to develop a mathematical model representing the physics of the wall to be coupled with energy simulation tool for yearly performance evaluation. The aim is to produce an easy and simplified calculation tool that may help in bridging the gap between the research products and concepts (as the TIM-PCM wall) and their development and implementation into the built environment.

The manuscript is composed of four chapters:

- The first chapter presents a state of the art of the heat transfer mechanisms that occurs during the phase change process, and the different numerical models of phase change considering natural convection in liquid PCM. In addition, a literature review of PCM applications within translucent facades and Trombe walls is presented. The TIM-PCM wall system is described and a history related to studies conducted in the framework of the INERTRANS project is presented. Based on the limitations of the previous works, the problematic and the objectives of the present thesis are determined.

- The second chapter presents the development of a simplified numerical model for melting of PCM in presence of natural convection and radiation. The mathematical model is coded on MATLAB using two-dimensional implicit finite volume method. The results are then validated using a complete CFD model created on COMSOL Multiphysics, as well as experimental and numerical benchmark solutions for a test case found in the literature.
- In the third chapter, a numerical model describing the heat transfer mechanisms through the wall is developed on MATLAB and then coupled with TRNSYS to evaluate the thermal performance of the whole building. The numerical model is experimentally validated in summer and winter seasons using the experimental cell located in the PERSEE center. The developed numerical model aims to provide an easy tool to use and fast enough to be adopted as a design tool, to investigate the potentials and disadvantages of the novel TIM-PCM wall under different operative conditions and different climates and to propose solutions to optimize its performance in summer, without the need of performing extensive and expensive experimental analysis.
- The fourth chapter presents an annual assessment of the energy performance of the solar wall integrated into a typical office building envelope under different climatic conditions. The optimal surface of the TIM-PCM wall is economically evaluated for each climate through a life-cycle cost analysis (LCC) as well as the evaluation of the payback period (PP).
- Finally, since the cooling demand is significantly increasing worldwide, we have extended our bibliographical study to PCM applications for cooling purposes, as detailed in Annex A. This aims to get a comprehensive vision of PCM applications for cooling in buildings and problems encountered in these applications. Difficulties in selecting these materials and the factors affecting the success and the effective use of the PCM are also discussed.

Noting that this thesis is presented as a series of journal papers. Consequently, chapters 2,3, 4 and Annex A can be read independently; and some overlap may be found between We have the copyright permission from the editor to reproduce the published articles.

The articles are first-authored by the PhD candidate and co-authored by the thesis supervisors Pascal henry Biwole and Farouk Fardoun, and are published or submitted as separate articles in international peer-reviewed scientific journals as:

- Chapter 2: **Farah Souayfane**, Pascal Henry Biwole, Farouk Fardoun. “Melting of a phase change material in presence of natural convection and radiation: A simplified model”. ***Published in Applied Thermal Engineering, Elsevier, 2018, 130, pp.660 – 671.***
- Chapter 3: **Farah Souayfane**, Pascal Henry Biwole, Farouk Fardoun. “Thermal behavior of a translucent superinsulated latent heat energy storage wall in summertime”. ***Published in Applied Energy, 2018, 217, pp. 390-408.***

- Chapter 4: **Farah Souayfane**, Farouk Fardoun, Pascal Henry Biwole. "Energy Performance and Economic Analysis of a TIM-PCM Wall Under Different Climates". ***Submitted to Energy, revision requested, 2018*.**
- Annex A: **Farah Souayfane**, Farouk Fardoun, Pascal Henry Biwole. "Phase Change Materials (PCM) for cooling applications in buildings: A review". ***Published in Energy and Buildings, Elsevier, 2016, 129, pp.396-431*.**

These articles comprise my own original work except where otherwise stated and all the work is done by the PhD candidate under the supervision of thesis directors.
All published journal papers and international conference papers during this thesis are listed in Annex C.

Introduction Générale

Il y a une préoccupation mondiale relative à la consommation d'énergie dans l'environnement bâti. Celui-ci est en effet l'un des principaux contributeurs aux émissions de gaz à effet de serre responsables du changement climatique et de ses impacts associés. Une proportion significative de la consommation d'énergie dans les bâtiments est utilisée pour le refroidissement et le chauffage. Au Liban comme en France, la consommation énergétique des bâtiments représente plus de 40% de l'énergie finale totale et près de 25% des émissions de gaz à effet de serre [1].

Une alternative pour atteindre l'objectif de réduction de la consommation d'énergie dans le bâtiment est d'améliorer la performance énergétique de son enveloppe. Cette enveloppe agit comme un filtre qui réduit les échanges thermiques entre l'extérieur et l'intérieur et protège les occupants contre le vent, la pluie et d'autres conditions, contribuant ainsi au confort thermique, acoustique et visuel. Pour mieux satisfaire ces fonctions, la combinaison de l'isolation avec des matériaux de stockage de chaleur latente est montrée comme un moyen efficace. En outre, une partie importante de la conception du bâtiment consiste à utiliser au mieux les ressources externes et en particulier l'exploitation du rayonnement solaire.

De nombreuses études ont montré que l'utilisation des matériaux à changement de phase (MCP) en paroi de bâtiment permet d'améliorer remarquablement la performance énergétique du bâtiment et d'économiser jusqu'à 80% d'énergie de chauffage l'hiver, dans la mesure où le matériau capte la chaleur du soleil, fond, puis redonne cette chaleur au bâtiment en se re-solidifiant. Mais l'un des problèmes rencontrés lors de l'utilisation de MCP dans les parois de bâtiment est le fort risque de la surchauffe estival lorsque le matériau n'arrive plus à déstocker la chaleur emmagasinée et reste à l'état liquide. Un cyclage du matériau y compris l'été lui permettrait de jouer pleinement son rôle de barrière thermique ou de puits de chaleur en diminuant le besoin de froid.

Cependant, la possibilité, la faisabilité, la performance thermique et l'analyse économique de l'utilisation des MCP appellent une série d'études théoriques et expérimentales. Les approches expérimentales offrent une meilleure indication du comportement et de la performance réels des MCP par rapport à l'analyse théorique. Cependant, les expériences sont irréalisables dans certains cas, tels que la grande échelle ou l'instabilité autour de l'environnement, sont coûteuses en temps et en argent, en plus, il existe des erreurs de test inévitables. Cependant, les méthodes théoriques peuvent éviter ces faiblesses et prédire d'une manière appropriée la performance des MCP.

Le principal avantage des approches théoriques / numériques est que différentes conditions peuvent être réalisées en modifiant les variables dans le modèle numérique. Par conséquent, de plus en plus

de chercheurs préfèrent étudier les problèmes de changement de phase par des solutions mathématiques et des simulations numériques.

Habituellement, lors de la modélisation du changement de phase, les études numériques ont des hypothèses dans leur modélisation mathématique [2]. Par exemple, en négligeant le transfert de chaleur par convection dans le MCP liquide [3] ou en négligeant le transfert de chaleur radiatif [4], alors que l'impact de ces hypothèses sur les résultats de la simulation est peu discuté dans la littérature. Cependant, des recherches récentes ont démontré que la convection naturelle joue un rôle important pendant le processus de fusion et que les modèles à conduction seule peuvent entraîner une perte de précision inacceptable.

Fondamentalement, la modélisation de la convection naturelle dans les MCP liquides peuvent être classée en deux grandes catégories. La première catégorie comprend les méthodes simplifiées, y compris l'approche de conductivité thermique efficace utilisant les nombres adimensionnels. Ces approches normalement simplifier le processus. En revanche, les méthodes détaillées de la dynamique des fluides (CFD), qui exigent un temps de calcul long, sont grandement compliqué et complexe et peuvent être limités au cas étudié. En outre, les simulations CFD sont rarement appropriées pour les étapes de la conception initiale en particulier pour une évaluation thermique longue durée. Toutefois, entre ces deux extrêmes, un modèle qui offre un bon compromis entre simplicité et précision est nécessaire, qui sera le premier objectif de la thèse actuelle.

D'autre part, la plupart des études sur les façades translucides intégrant des MCP ont supposé des transferts unidimensionnels par conduction et par radiation sans convection [5]–[7], et les modèles numériques ont été spécifiquement développés pour prendre en compte l'interaction des MCP avec le rayonnement solaire [8]–[11]. Cependant, très peu d'études ont été trouvées dans la littérature sur la fusion des MCP en présence de la convection naturelle et de rayonnement. Ce sera notre deuxième question de recherche.

Le projet INTERTRANS [12] a proposé le développement d’un mur solaire passif translucide innovant intégré dans l’enveloppe du bâtiment s’inscrivant directement dans la problématique d’efficacité énergétique et d’exploitation optimale des ressources environnementale. Ce mur solaire assure, simultanément, stockage et restitution de la chaleur, super isolation thermo-acoustique et éclairage naturel contribuant au confort visuel. Il permet d’exploiter le rayonnement solaire lors des périodes froides pour chauffer l’intérieur du bâtiment. Pour ce faire, le mur associe des matériaux de nouvelle génération, tel que l’aérogel de silice pour l’isolation thermique et les matériaux à changement de phase (MCP) pour l’absorption et le stockage de la chaleur issue du rayonnement solaire. La restitution quasi constante de la chaleur par convection et rayonnement grande longueur contribue à l’augmentation de la sensation de confort thermique de l’habitant.

La mise en place d'une telle façade dans le bâtiment est conditionnée par la connaissance de son comportement, de sa performance et de son impact énergétique. Or, cette connaissance sur un nombre important de cas d'études n'est accessible que par la modélisation numérique. Il est donc nécessaire de s'assurer de la disponibilité et de la fiabilité d'un modèle numérique susceptible de représenter la physique d'une telle paroi. En particulier lors de la fusion et de la solidification du MCP, ce dernier peut être soumis à différents modes de transferts de chaleur en fonction de la présence ou non d'ensoleillement et ainsi modifier considérablement la cinétique du changement d'état. Le développement de ce modèle numérique sera notre troisième objectif.

Ce mur a été caractérisé expérimentalement en ambiance contrôlée et in situ sur un bâtiment grandeur nature situé au sein du laboratoire PERSEE de l'Ecole des Mines de Paris à Sophia Antipolis, dans le sud de la France [13]. Dans leur étude expérimentale, Berthou et al [13] ont constaté que la performance thermique du mur est très élevée en hiver, tandis qu'en été les gains de chaleur à travers le mur provoquent un problème de surchauffe et le MCP n'arrive pas à se solidifier. Ainsi, l'optimisation de la performance thermique de cette paroi en été est nécessaire et des solutions pour la surchauffe et le cyclage du MCP doivent être proposées.

Deux verrous ont été alors identifiés dans cette étude. Le premier est scientifique : les modèles simplifiés utilisant une modification de l'équation de diffusion de la chaleur pour tenir compte du stockage de chaleur (méthode enthalpique [14], [15], méthode de la capacité thermique équivalente [16] , [17], méthode du terme source [18]) ne prennent pas en compte la convection naturelle lors de la fusion qui peut pourtant devenir prédominante lorsque le contenant du MCP est de dimensions suffisamment grandes. D'autre part, les modèles sophistiqués utilisant une résolution numérique des équations de Navier Stokes (méthode d'enthalpie-porosité [19]–[26], modèle de transformation de la température [27]–[30], méthode de la capacité calorifique modifiée [31], méthode de Boltzmann sur réseau (LBM) [32]–[35]) sont eux gourmands en temps de calcul et ne sont pas du tout adaptés aux échelles de temps et d'espace caractéristiques de la simulation thermique annuelle du bâtiment. Le deuxième verrou est technologique : en été le MCP n'arrive plus à se resolidifier la nuit, provoquant ainsi une surchauffe estivale.

En gros, cette thèse propose dans un premier temps de réaliser la modélisation des phénomènes mis en jeu au sein du mur translucide MCP-aérogels afin de comprendre l'influence et l'interaction des différents modes de transfert de chaleur. Cela inclut le développement d'un modèle simplifié pour le changement de phase, en présence de convection naturelle et de rayonnement, qui offre un bon compromis entre simplicité et précision. Et ensuite, développer un modèle mathématique représentant la physique du mur afin de le coupler avec un outil de simulation énergétique pour effectuer une évaluation thermique annuelle. L'objectif est de produire un outil de calcul simple et simplifié pouvant

aider à combler le fossé entre les produits et les concepts de recherche (comme le mur MCP-aérogels) et leur développement et leur mise en œuvre dans l'environnement bâti.

Le présent manuscrit est articulé en quatre chapitres :

-Le premier chapitre présente l'état de l'art des mécanismes de transfert de chaleur qui se produisent pendant le processus de changement de phase, ainsi que les différents modèles numériques de changement de phase prenant en compte la convection naturelle dans le MCP liquide. En plus, une revue sur les applications des façades translucides et du mur Trombe intégrant des matériaux à changement de phase est présenté. Le système du mur MCP-aérogel est décrit et un historique lié aux études menées dans le cadre du projet INERTRANS est présenté. Sur la base des limitations des travaux précédents, la problématique et les objectifs de la présente thèse sont déterminés.

- Le deuxième chapitre présente le développement d'un modèle numérique simplifié pour modéliser la convection naturelle et le rayonnement courte longueur d'onde pendant le processus de fusion d'un matériau à changement de phase. Le modèle mathématique est codé sous MATLAB en utilisant la méthode des volumes finis en deux dimensions. Les résultats sont ensuite comparés à ceux d'un modèle CFD complet créé dans COMSOL Multiphysics, et aux résultats numériques et expérimentaux des benchmarks trouvés dans la littérature.

- Dans le troisième chapitre, le modèle numérique décrivant les mécanismes de transfert de chaleur à travers le mur est développé sur MATLAB et ensuite couplé à TRNSYS pour évaluer la performance thermique de l'ensemble du bâtiment. Le modèle numérique est validé expérimentalement en été et en hiver par l'utilisation de la cellule expérimentale présente au sein du laboratoire PERSEE. Ce modèle validé vise à fournir un outil facile à utiliser et assez rapide pour étudier le potentiel ainsi que les inconvénients du mur solaire dans différentes conditions opératoires et dans différents climats, et pour proposer des solutions pour optimiser sa performance en été.

- Le quatrième chapitre, présente une évaluation annuelle de la performance énergétique du mur solaire intégré dans l'enveloppe d'un immeuble de bureaux typique sous différentes conditions climatiques. La surface optimale du mur MCP-aérogel est enfin évaluée économiquement pour chaque climat grâce à une analyse en coût global basé sur le coût durant le cycle de vie des matériaux (CCV) et par l'évaluation du temps de retour sur investissement (TRI).

- Finalement, comme la demande de refroidissement augmente de manière significative dans le monde entier, nous avons étendu notre recherche bibliographique aux applications de MCP pour le refroidissement (voir Annexe A). Ceci a pour objectif d'avoir une vision globale de l'emploi des MCP dans les bâtiments dans un contexte de refroidissement, ainsi que problèmes pouvant être

rencontrés dans ces applications. Les difficultés liées à la sélection de ces matériaux et les facteurs affectant l'utilisation réussie et efficace des MCP sont également discutés.

Notant que cette thèse est présentée comme une série d'articles de revues. Par conséquent, les chapitres 2, 3 et 4 et l'annexe A peuvent être lus indépendamment, et un certain chevauchement peut être trouvé entre eux. L'autorisation préalable des éditeurs a été obtenue pour la diffusion des articles publiés dans le cadre de ce manuscrit.

La doctorante est la première auteure de ces articles, les co-auteurs sont les directeurs de thèse Pascal Henry Biwole et Farouk Fardoun. Pendant la thèse, quatre articles sont publiés et un article est soumis dans des journaux internationaux de rang A à comité de lecture :

- Chapitre 2: **Farah Souayfane**, Pascal Henry Biwole, Farouk Fardoun. "Melting of a phase change material in presence of natural convection and radiation: A simplified model". ***Published in Applied Thermal Engineering, Elsevier, 2018, 130, pp.660 – 671.***
- Chapitre 3: **Farah Souayfane**, Pascal Henry Biwole, Farouk Fardoun. "Thermal behavior of a translucent superinsulated latent heat energy storage wall in summertime". ***Published in Applied Energy, 2018, 217, pp. 390-408.***
- Chapitre 4: **Farah Souayfane**, Farouk Fardoun, Pascal Henry Biwole. "Energy Performance and Economic Analysis of a TIM-PCM Wall Under Different Climates". ***Submitted to Energy, revision requested, 2018***.
- Annexe A: **Farah Souayfane**, Farouk Fardoun, Pascal Henry Biwole. "Phase Change Materials (PCM) for cooling applications in buildings: A review". ***Published in Energy and Buildings, Elsevier, 2016, 129, pp.396-431***.

Ces articles comprennent mon propre travail, sauf indication contraire, et tout le travail est effectué par la doctorante sous la supervision des directeurs de thèse.

Tous les articles de revues publiés et les publications dans des conférences internationales au cours de cette thèse sont énumérés dans l'annexe C.

References

[1] "Agence de l'Environnement et de la Maîtrise de l'Énergie Changement climatique - transition écologique, énergétique." [Online]. Available: http://www.ademe.fr/?sort=-1&cid=96&m=3&catid=12846. [Accessed: 20-Feb-2018].

[2] "Atkin P, Farid MM. Improving the efficiency of photovoltaic cells using PCM infused graphite and aluminium fins. Sol Energy 2015;114:217–28."

[3] Z. Luo *et al.*, "Numerical and experimental study on temperature control of solar panels with form-stable paraffin/expanded graphite composite PCM," *Energy Convers. Manag.*, vol. 149, pp. 416–423, Oct. 2017.

[4] "Hendricks J, Sark W. Annual performance enhancement of building integrated photovoltaic modules by applying phase change materials. Prog Photovolt Res Appl 2013;21:620–30."

[5] F. Goia, "Thermo-physical behaviour and energy performance assessment of PCM glazing system configurations: A numerical analysis," *Front. Archit. Res.*, vol. 1, no. 4, pp. 341–347, Dec. 2012.

[6] K. Zhong, S. Li, G. Sun, S. Li, and X. Zhang, "Simulation study on dynamic heat transfer performance of PCM-filled glass window with different thermophysical parameters of phase change material," *Energy Build.*, vol. 106, pp. 87–95, 2015.

[7] K. A. R. Ismail, C. T. Salinas, and J. R. Henriquez, "Comparison between PCM filled glass windows and absorbing gas filled windows," *Energy Build.*, vol. 40, no. 5, pp. 710–719, Jan. 2008.

[8] F. Goia, M. Perino, and M. Haase, "A numerical model to evaluate the thermal behaviour of PCM glazing system configurations," *Energy Build.*, vol. 54, pp. 141–153, 2012.

[9] K. A. R. Ismail and J. R. Henrıquez, "Parametric study on composite and PCM glass systems," *Energy Convers. Manag.*, vol. 43, no. 7, pp. 973–993, 2002.

[10] C. Liu, Y. Zhou, D. Li, F. Meng, Y. Zheng, and X. Liu, "Numerical analysis on thermal performance of a PCM-filled double glazing roof," *Energy Build.*, vol. 125, pp. 267–275, 2016.

[11] C. Liu, Y. Zheng, D. Li, H. Qi, and X. Liu, "A Model to Determine Thermal Performance of a Non-ventilated Double Glazing Unit with PCM and Experimental Validation," *Procedia Eng.*, vol. 157, pp. 293–300, 2016.

[12] K. Johannes, F. Kuznik, F. Jay, P. Roquette, P. Achard, and Y. Berthou, "CRISTOPIA ENERGY SYSTEMS, SAVERBAT SAS,Elément d'enveloppe d'un bâtiment et ensemble comprenant un tel élément," Brevet Francais FR 1158194, 15-Mar-2013.

[13] Y. Berthou, P. H. Biwole, P. Achard, H. Sallée, M. Tantot-Neirac, and F. Jay, "Full scale experimentation on a new translucent passive solar wall combining silica aerogels and phase change materials," *Sol. Energy*, vol. 115, pp. 733–742, May 2015.

[14] A. . Brent and V. R. Voller, "Enthalpy-porosity technique for modeling convection-diffusion phase change: application to the melting of a pure metal," *Numerical Heat Transfer*, vol. Vol. 13, pp. 297–318, 1988.

[15] B. Binet and M. Lacroix, "Melting from heat sources flush mounted on a conducting vertical wall," *Int. J. Num. Meth. Heat & Fluid Flow*, vol. Vol. 10, pp. 286-306., 2000.

[16] K. Morgan, "A numerical analysis of freezing and melting with convection," *Comp. Meth. App. Eng.*, vol. Vol. 28, pp. 275–84, 1981.

[17] J. Hsiao, "An efficient algorithm for finite difference analysis of heat transfer with melting and solidification," *ASME Paper No. WA/HT-42*, 1984.

[18] Y. Cao and A. Faghri, "A numerical analysis of phase change problem including natural convection," *J HEAT TRANSFER*, vol. 112, pp. 812–15, 1990.

[19] V. Voller and M. Cross, "An enthalpy method for convection/ diffusion phase change," *Int J Numer Methods Eng*, vol. 24:271–84., 1987.

[20] V. Shatikian, G. Ziskind, and R. Letan, "Numerical investigation of a PCM-based heat sink with internal fins," *Int. J. Heat Mass Transf.*, vol. 48, no. 17, pp. 3689–3706, Aug. 2005.

[21] M. Faraji and H. El Qarnia, "Numerical study of melting in an enclosure with discrete protruding heat sources," *Appl. Math. Model.*, vol. 34, no. 5, pp. 1258–1275, May 2010.

[22] A. R. Archibold, M. M. Rahman, D. Y. Goswami, and E. K. Stefanakos, "Analysis of heat transfer and fluid flow during melting inside a spherical container for thermal energy storage," *Appl. Therm. Eng.*, vol. 64, no. 1–2, pp. 396–407, Mar. 2014.

[23] P. Wang, H. Yao, Z. Lan, Z. Peng, Y. Huang, and Y. Ding, "Numerical investigation of PCM melting process in sleeve tube with internal fins," *Energy Convers. Manag.*, vol. 110, pp. 428–435, Feb. 2016.
[24] Z. Liu, Y. Yao, and H. Wu, "Numerical modeling for solid–liquid phase change phenomena in porous media: Shell-and-tube type latent heat thermal energy storage," *Appl. Energy*, vol. 112, pp. 1222–1232, Dec. 2013.
[25] W.-B. Ye, D.-S. Zhu, and N. Wang, "Fluid flow and heat transfer in a latent thermal energy unit with different phase change material (PCM) cavity volume fractions," *Appl. Therm. Eng.*, vol. 42, pp. 49–57, Sep. 2012.
[26] P. Goyal, A. Dutta, V. Verma, and I. T. R. Singh, "Enthalpy Porosity Method for CFD Simulation of Natural Convection Phenomenon for Phase Change Problems in the Molten Pool and its Importance during Melting of Solids."
[27] S. Wang, A. Faghri, and T. L. Bergman, "A comprehensive numerical model for melting with natural convection," *Int. J. Heat Mass Transf.*, vol. 53, no. 9–10, pp. 1986–2000, Apr. 2010.
[28] A. Faghri and Y. Cao, "Performance characteristics of a thermal energy storage module: a transient PCM/forced convection conjugate analysis," *Int. J. HeatMass Transfer*, pp. 93–101, 1991.
[29] P. Damronglerd and Zhang, "Modified temperature-transforming model for convection-controlled melting," *AIAA J. Thermophy. Heat Transfer 21*, pp. 203–208., 2007.
[30] x zeng and A. Faghri, "A temperature transforming model for binary solid–liquid phase change problems: Part I – mathematical modeling and numerical methodology," pp. 467–480, 1994.
[31] D. Groulx and P. H. Biwole, "Solar PV Passive Temperature Control Using Phase Change Materials," 2014.
[32] J. M. Fuentes, F. Kuznik, K. Johannes, and J. Virgone, "Development and validation of a new LBM-MRT hybrid model with enthalpy formulation for melting with natural convection," *Phys. Lett. A*, vol. 378, no. 4, pp. 374–381, 2014.
[33] D. Chatterjee and S. Chakraborty, "An enthalpy-based lattice Boltzmann model for diffusion dominated solid–liquid phase transformation," *Phys. Lett. A*, vol. 341, no. 1–4, pp. 320–330, Jun. 2005.
[34] E. A. Semma, M. El Ganaoui, and R. Bennacer, "Lattice Boltzmann method for melting/solidification problems," *Comptes Rendus Mécanique*, vol. 335, no. 5–6, pp. 295–303, May 2007.
[35] C. Huber, A. Parmigiani, B. Chopard, M. Manga, and O. Bachmann, "Lattice Boltzmann model for melting with natural convection," *Int. J. Heat Fluid Flow*, vol. 29, no. 5, pp. 1469–1480, Oct. 2008.

CHAPTER 1

STATE OF THE ART AND THESIS PROBLEMATIC

Chapter 1. State of the art and thesis problematic

Résumé du chapitre en français :

Etat de l'art et problématique

D'abord, ce chapitre présente les mécanismes de transfert de chaleur qui se produisent pendant le processus de changement de phase. Les différents modèles numériques de changement de phase prenant en compte la convection naturelle dans le MCP liquide sont présentés et le phénomène physique mise en jeu est expliqué. Ces modèles numériques comprennent les modèles CFD et les approches simplifiées. Ensuite, l'état de l'art des différentes études considérant la convection naturelle pendant la fusion des MCP dans des enceintes est présenté. Sur la base de ce qui précède, Il a été constaté que : - la convection naturelle doit être prise en compte dans la phase liquide du MCP pendant la fusion ; - les modèles 'CFD' sophistiqués utilisés pour modéliser la convection naturelle pendant la fusion, nécessitent la résolution numérique des équations de Navier Stokes (méthode d'enthalpie-porosité, modèle de transformation de la température, méthode de la capacité calorifique modifiée, méthode de Boltzmann sur réseau (LBM)) sont eux gourmands en temps de calcul et ne sont pas du tout adaptés aux échelles de temps et d'espace caractéristiques de la simulation thermique annuelle du bâtiment. L'approche de conductivité thermique efficace, largement utilisée, est rapide et simple, mais elle présente plusieurs lacunes, en particulier elle est incapable de montrer les caractéristiques du changement de phase et ne peut pas fournir d'informations sur la position du front de fusion ; - le processus de fusion comprend principalement trois régimes : régime dominé par la conduction, régime mixte de conduction et de convection et régime dominé par la convection. Ces régimes sont reflétés par la courbe du nombre de Nusselt en fonction du temps. Cependant, aucun consensus n'a été trouvé dans la littérature sur lequel est le mécanisme de transfert de chaleur dominant, lequel peut être ignoré et comment combiner ces deux mécanismes pendant la modélisation du changement de phase ; - le nombre de Nusselt est un paramètre clé dans les problèmes dominés par la convection. ; - à ce jour, de nombreuses corrélations de nombre de Nusselt développées dans la littérature ne conviennent que pour une géométrie et / ou un PCM spécifiques.

De plus, dans le cadre de l'amélioration de l'enveloppe des bâtiments et de l'exploitation optimale des ressources environnementales pour diminuer la consommation de l'énergie, une étude bibliographique concernant l'application des façades translucides et du mur Trombe intégrant des matériaux à changement de phase est présentée. En se basant sur cette étude bibliographique, il a été constaté que : - l'intégration des MCP dans les façades translucides augmente le confort thermique

intérieur du bâtiment et par conséquent la satisfaction des occupants ; - la plupart des travaux antérieurs sur les façades transparentes intégrant des MCP ont été principalement développés pour la saison de chauffage et leurs avantages en termes d'efficacité énergétique sont peu quantifiés en été. - la plupart des études sur les façades translucides ont supposé des transferts unidimensionnels par conduction et par rayonnement sans prise en compte de la convection ; l'interaction de la convection et du rayonnement a rarement été étudiée dans la littérature.

Dans le même contexte, le mur solaire innovant issu du projet ANR INERTRANS (2008-2011) est présenté. Le mur est composé d'un lit d'aérogel de silice pour l'isolation thermique-acoustique permettant la transmission du rayonnement solaire, et de briques de verre remplies d'un matériau à changement de phase eutectique à base d'acides gras pour le stockage et la restitution de la chaleur. Le mur entier est translucide et a été mise en place à Sophia Antipolis, au sein du centre PERSEE (Procédés, Énergies Renouvelables et Systèmes Énergétiques) de Mines ParisTech dans le but d'étudier son comportement thermique sous climat réel, et dans la cellule climatique MINIBAT du Centre d'Energétique et de Thermique de Lyon dans le but de déterminer le comportement du mur MCP-aérogel pour des scénarios climatiques imposés et répétables.

Plusieurs études ont été menées dans le cadre du projet INTERTRANS et sont citées ci-après.

Le mur a été caractérisé expérimentalement par Berthou et al. [121], en ambiance contrôlée et in-situ sur un bâtiment grandeur nature situé au sein du laboratoire PERSEE. Les résultats expérimentaux ont montré que la performance thermique du mur est très élevée en hiver, alors que durant l'été, les gains de chaleur à travers le mur provoquent un problème de surchauffe et le MCP n'arrive pas à se solidifier. Ainsi, la performance du mur doit être optimisée, et des solutions pour surmonter la surchauffe estivale et le cyclage du MCP doivent être proposées. Le modèle numérique du mur issu de ce travail présente de fortes différences avec les mesures expérimentales. Ceci est vraisemblablement dû au fait que la convection naturelle n'a pas été correctement prise en compte dans le modèle. Ainsi, la question d'un modèle numérique validé expérimentalement et qui permette l'optimisation d'une telle paroi sous différentes conditions est toujours ouverte.

Fuentes et al. [85] ont développé un modèle de Lattice Boltzmann sur gaz réseau couplé à la méthode des ordonnées discrètes (LBM-DOM) dans le but d'étudier la fusion d'un acide gras contenu dans les briques de verre du mur innovant en présence de convection naturelle et de rayonnement. Ils ont souligné l'importance de considérer la convection naturelle dans le MCP liquide. Cependant, le modèle développé nécessite un temps de calcul très élevé. Ainsi, il ne peut pas être utilisé pour effectuer une évaluation annuelle de la performance énergétique de bâtiments intégrant un tel mur. Un modèle plus simplifié de rayonnement et de convection naturelle pendant la fusion est toujours une question ouverte.

Gong et al. [122] ont concentré leurs travaux expérimentaux et numériques, sur la question importante du processus de fusion d'un MCP à l'intérieur d'une brique de verre. Le rayonnement dans la brique n'a pas été pris en compte, et le modèle développé n'était pas adapté pour être couplé avec TRNSYS ou Energy Plus, afin d'évaluer la performance thermique annuelle de l'ensemble du bâtiment.
Il résulte des points évoqués ci-dessus que des travaux supplémentaires restent à faire dans le cadre du projet INERTRANS, et principalement la mise en place d'un modèle numérique simplifié pouvant convenablement représenter la physique du mur MCP-aérogel, tout en tenant compte de la convection naturelle et du rayonnement lors de la fusion du MCP. Le modèle doit être suffisamment rapide pour être couplé avec un outil de simulation énergétique globale (tel que TRNSYS), afin d'évaluer la performance thermique annuelle de l'ensemble du bâtiment intégrant un tel mur. Une fois le modèle validé expérimentalement, il doit servir à l'optimisation de la performance de la paroi MCP-aérogel sous différentes conditions climatiques et configurations.

Dans ce chapitre, le mur MCP-aérogel est décrit ainsi que la problématique de la thèse. Dans le chapitre suivant, un modèle simplifié prenant en compte la convection naturelle et le rayonnement lors du changement de phase sera développé. Les équations régissant ces phénomènes ainsi que leurs hypothèses simplificatrices et les méthodes numériques adaptées à leur résolution seront présentées.

1. Introduction

By 2035 it is expected that the energy consumption in the building sector increases 29%, which represents an average annual rate of 1% [1]. The European Union EU has introduced some policies and goals to improve the energy efficiency of the building sector, such as [2]–[4]:

1. The Energy Service Directive and Renewables Directive propose respectively a 9% of energy savings by 2016 and 20% of all energies should be prevenient from renewable energy sources by 2020;

2. All new buildings by 2020 must be nearly-zero energy buildings (NZEBs) and after 2018 new public buildings should be NZEBs;

3. The Energy strategy of the European Union added targets to 2020, known as "20-20-20" that have the objective of 20% reduction of the greenhouse gas emissions, comparatively to the 1990 levels, increase of 20% of energy production from renewable energy sources;

4. Besides of the Energy Strategy, the EU added individual rules and directives for each state members for the use of renewable sources and to improve the energy efficiency until 2020.

5. In France, the Climate Plan adopted in 2005 aims at dividing by 4 the amount of greenhouse gases emissions by 2050, compared to the 1990 baseline. About 24% of the country's greenhouse gases emissions are due to building heating [refer to the document I have sent]. Reducing energy demand and increasing the share of renewable energy in the built environment are key steps to reach this objective.

The incorporation of phase change materials (PCM) into building elements is a growing trend for improving the thermal energy storage capacity in the latent form. PCM represent a good option to enhance the building's ability to smooth the peak loads and to reduce the thermal energy needs. The working principle of the PCM is to exploit the considerable capacity of these materials of accumulating heat when they subdue a phase transition. Therefore, compared with the most common strategy, less material is necessary to store the same amount of thermal energy. Currently, the external envelope, mainly in offices and commercial spaces, is systematically composed by large glazed areas that lead to the increase of energy consumption of the building [5]–[7]. These areas are crucial because these are the areas where high energy transfer occurs between the indoor and outdoor spaces, that can lead to thermal and visual discomfort conditions [7]–[11]. Therefore, solutions resourcing to the use of phase change materials to improve the energy efficiency of the glazing areas and transparent/translucent areas have been carried out in the last 20– 25 years with promising results [12]. Some examples of research activities in this field can be found in the literature [13]–[16]. The first concepts of PCM glazing systems were developed mainly for cold climates, but more recent

analysis [17] showed that the adoption of PCM glazing systems may have a positive effect in warmer climates too. The general aim of this technology is to reduce the energy fluctuations along the time, by acting as thermal energy storage device that is charged, mainly, by solar energy. Today, transparent insulation materials with excellent optical and thermal properties are commercially available. Thus, the combination of these improved materials with PCM in transparent building facades may result a better thermal performance.

However, to fully investigate PCM potentials and drawbacks, the availability of robust and reliable numerical tools is fundamental. Thanks to these tools it would be possible to test different configurations of PCM integrated in glazing or transparent systems (e.g. with various PCM, layered-structures) under different operative conditions without the need of performing extensive and expensive experimental analysis. It would also be possible to assess the effectiveness of this technology in different climates and for different building types.

The major challenge of the mathematical modeling of phase change process is to properly represent the moving boundary of the solid–liquid interface and the associated thermophysical property change. The solid–liquid phase change is characterized by a moving melting/freezing front, accompanied with latent heat absorption/release and sharp variations of thermophysical properties, including thermal conductivity, specific heat, viscosity and density. In addition, most of the real applications of solid–liquid phase change occurs in multidimensional configurations, and natural convection in the liquid phase often plays an important role in controlling heat transfer, which substantially complicates the problem and makes analytical solutions impossible.

In fact, during the phase transformation especially melting process, the temperature and concentration gradients in the liquid phase of PCM keep varying, which results in the movement of the liquid PCM, named convection occurring under the action of buoyancy forces due to the density gradients. In the previous numerical investigations, the convection heat flow in the liquid phase received less attention than conduction owing to the limited computational capabilities of computer and the mathematical complexities to formulate the convection heat transfer during the phase transformation. However, recent researches have demonstrated that natural convection plays an important role in latent heat thermal energy systems, especially during the melting process and should not be ignored. In addition, the radiative heat transfer in the case of PCM integrated in translucent facades should be considered in combination with both conduction and convection heat transfers during phase change.

Therefore, this chapter discusses, in section 2, the heat transfer mechanisms that occur during the charging and discharging periods of the phase change materials (PCM) and defines the Stephan and Neumann problems. Section 3 deals with the phase change process considering natural convection in liquid PCM. The physical phenomenon is explained in section 3.1 and the numerical methods

including CFD models and simplified approaches to model natural convection during melting process are presented in section 3.2. In section 3.3 we present the state of the art of different studies on phase change with natural convection in enclosures. A literature review of PCM applications within translucent facades considering radiation heat transfer during phase change is presented in Section 4. Section 5 presents a literature review of PCM applications within Trombe walls and definition of transparent insulation materials. In section 6 we present an innovative wall, proposed by the INERTRANS project, composed of transparent insulation material layer, silica aerogels, and a PCM layer. This wall provides heat storage and insulation while allowing daylighting at the same time. The description of the system and the physical phenomena involved are presented in 6.1 and 6.2. A history related to studies conducted in the framework of the INERTRANS project are presented in section 6.3. In section 7, the previous works and their limitations are discussed, and consequently the problematic and the objectives of the thesis are identified.

2. Heat transfer mechanisms during the phase change

2.1.Conduction and convection heat transfer

The possible heat transfer mechanisms during melting and solidification of phase change materials are conduction, convection or a combination of both. Therefore, the simulation methods in the literature are based on the considered heat transfer mechanism: the pure conduction model and the combined conduction and natural convection model. The pure conduction model is a hypothetical model, which assumes that conduction is the sole heat transfer mechanism during melting.

In 1831, Lamé and Clapeyron [18] conducted the first study on phase change problem by considering only the conduction heat transfer and the effect of natural convection has received less attention.

However, in the last two decades, convection dominated phase change problems have become the subject of numerous studies, and some researchers persist that natural convection is a more significant mechanism in the liquid PCM region whenever convection motion has enough room to develop. In fact, due to the variations of density gradients, the convection in the liquid PCM occurs under the action of buoyancy forces during the melting process.

Modeling phase change taking into account the natural convection in the liquid PCM was firstly considered by Sparrow et al. [19] in 1977, they concluded that the effect of natural convection should not be ignored. In 1978 they conducted another study [20] showing that the natural convection must be accounted for and that it is first order important in phase change problems. In 1980, Yao and Chen [21] investigated the influence of natural convection using an approximate solution; they found that it highly depends on Rayleigh number. Some researchers [22] [23] [24], between 1978 and 1985, have stated that the convection influences the melting rate and the resulting distribution of the liquid

phase of the PCM in a multi-component system. Later, in 1988 Buddhi et al. [25] explained the phenomena that causes the convection in the liquid PCM by the density differences that induce the buoyancy forces. In 1990, Farid et al [26] accounted for the natural convection during melting process using an effective thermal conductivity method ($k_{eff}/k_l = cRa^n$). In 1994, Hasan [27] concluded that the melting process cannot be described correctly if the heat transfer by conduction only is considered. Later, in 1998, Lacroix et al [28] also found that during the melting process, natural convection is the key heat transfer mechanism. In 1999, Zhang and Yi [29] believed that the convection is the dominant heat transfer mechanism due to the continuous increase of the PCM volume during melting. In the same year, Velraj and Seeniraj [30] concluded that during melting, convection occurs in the liquid PCM leading to an increase in the heat transfer rate, compared with the solidification process. In 2001, Sari et al. [31] found that the natural convection had a large effect on the heat transferred from a heat exchanger to a stearic acid PCM. After that, in 2004, Lamberg et al. [32] studied the impact of the natural convection on the melting and solidification procedures. They showed that, compared with the experimental results, unsatisfactory numerical results were obtained when the effect of natural convection is absent during the melting process, whilst good estimation during the solidification process were showed. Figure 1-1 shows the difference between the predicted temperature, with and without convection, during the melting of a fatty acid eutectic of melting temperature 21ºC. It turns out that the differences are negligible for thicknesses less than 1 cm, while beyond that, the difference between the predicted temperature with and without convection can reach up to 18 °C [33].

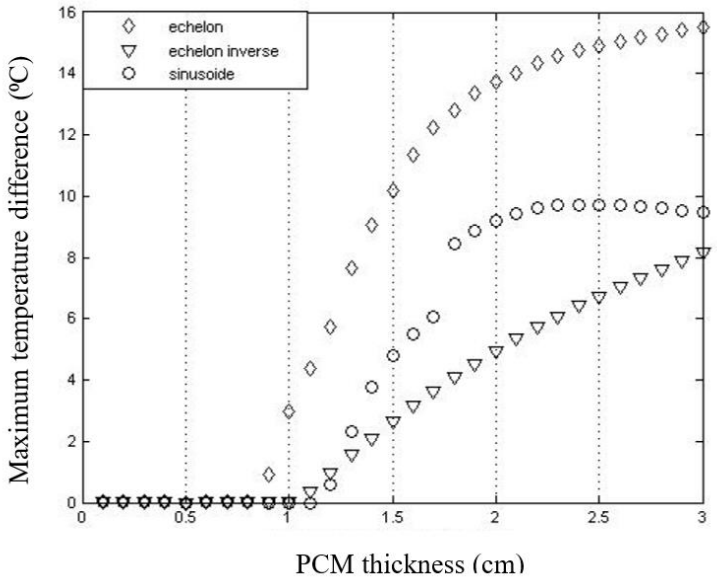

Figure 1-1: Influence of natural convection on the temperature function of PCM thickness [33]

For the melting process, the PCM changes its phase from solid to a mushy state, and then liquid, which is reversible during the solidification process. Therefore, it is possible during the phase

transformation process that more than one kind of heat transfer mechanisms acting at work, but how to weight the percentages of conduction and convection heat transfer in each stage has been the main challenge for the researchers currently. Section 3 will review the most common methods used to model the convection heat transfer during phase change.

2.2.Stefan problem and Neuman problem

The simplest of the Stefan problems, or moving boundary problems, is the one-phase Stefan problem since only one-phase involved. The term of 'one-phase' designates only the liquid phases active in the transformation and the solid phase stay at its melting temperature. Stefan's solution with constant thermophysical properties shows that the rate of melting or solidification in a semi-infinite region is governed by a dimensionless number, known as the Stefan number (Ste),

$$Ste = \frac{C_l(T_l - T_m)}{L} \qquad \text{Eq. 1-1}$$

where, C_l is the heat capacity of the liquid PCM, L is the latent heat of fusion, and T_l and T_m are the surrounding and melting temperatures, respectively.

With the heat transfer continuing, the interface boundary is constantly moving as the liquid and solid phases shrinking and growing, which disable the prediction of the boundary location [34]. Because of that the solid– liquid interface is not fixed, but moving with time, the heat transfer mechanisms during a PCM phase transformation process are complex. Therefore, the phase change transition is difficult to analyze owing to the three reasons: the solid–liquid interface is moving; the interface location is nonlinear; it consists of thermal conduction and natural convection heat transfer mechanisms. Due to these three factors, the non-linearity of the governing equations is introduced to the moving boundary, and the precise analytical solutions are only possible for a limited number of scenarios

The Stefan problem was extended to the two-phase problem, the so-called Neumann problem which is more realistic [35]. In Neumann problem, the initial state of the PCM is assumed to be solid, during the melting process, its initial temperature does not equal to the phase change temperature, and the melting temperature does not maintain at a constant value. Consider that the melting happens in a semi-infinite slab ($0 < x < \infty$), the solid PCM is initially at a uniform temperature $T_s < T_m$ and a constant temperature T_0 is imposed on the slab surface x=0, with the assumptions of constant thermo-physical properties of the PCM, the heat conduction in solid and liquid region and the heat fluxes transferring from the liquid phase to the solid–liquid interface are given as shown in Figure 1-2. Where ρ is the density, C is the specific heat, k is the thermal conductivity, t and x are the time and space coordinates respectively and L is latent heat of fusion.

Neumann analytical solution can be written as:

Position of the solid–liquid interface (melting front)

$$\delta(t) = 2\lambda\sqrt{\mu_l t} \quad \text{Eq. 1-2}$$

Temperature of the liquid phase:

$$T(x,t) = T_l - (T_l - T_m)\frac{\mathrm{erf}(x/2\sqrt{\mu_l t})}{\mathrm{erf}(\lambda)} \quad \text{Eq. 1-3}$$

Temperature of the solid phase:

$$T(x,t) = T_s + (T_m - T_s)\frac{\mathrm{erfc}(x/2\sqrt{\mu_s t})}{\mathrm{erfc}(\lambda\sqrt{\mu_l/\mu_s})} \quad \text{Eq. 1-4}$$

where, T_s ,T_l and T_m the initial temperature of solid and liquid PCM (K) and melting temperature respectively. λ is the solution to the transcendental equation [18] and μ is the thermal diffusivity of PCM (m^2/s).

However, the Neumann's solution is applicable only for moving boundary problems in the rectangular coordinate system and needs an existing initial liquid layer.

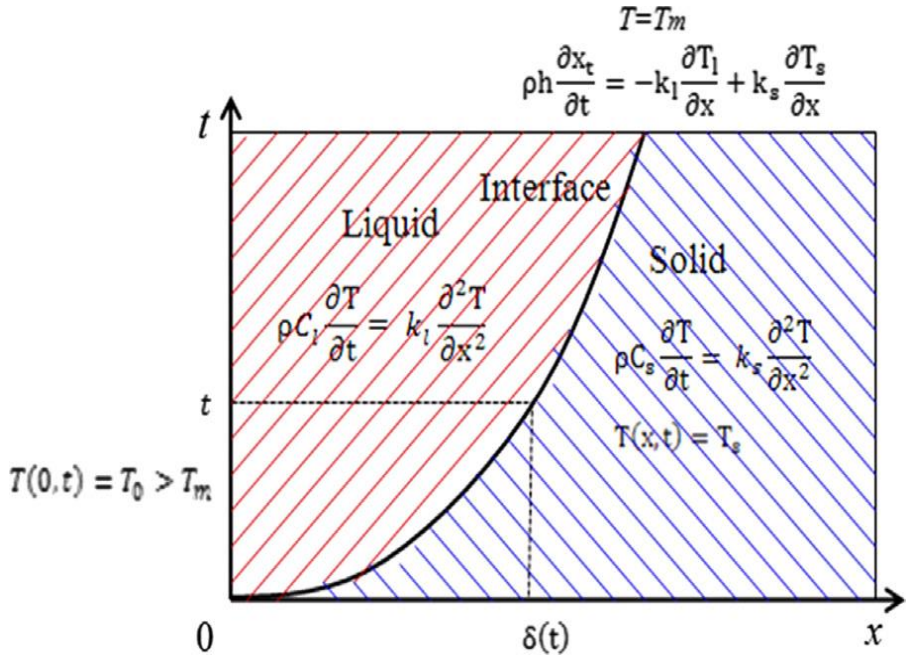

Figure 1-2 : Schematic illustration of the two-phase Stefan problem

Furthermore, there are several other issues with the use of a theoretical approach in the study of PCM. There were many mechanisms involved during a PCM phase transition, such like a change in volume, density, thermal conductivity, specific heat capacity, super-cooling, etc [36]. Another major issue with PCM is that they act as self-insulating materials. When PCM solidification occurs from the top of the heat surface, solid insulating layer will be developed which moves inward during the whole solidification process. With the increase in the size and thickness of the solid layer, the heat transfer rate from the liquid PCM to the heat exchanger surface decreases until it becomes so small that will not be possible to maintain at an acceptable heat transfer rate.

Logical heat transfer mechanisms during the charging and discharging periods of the PCM are the essential elements to develop any accurate mathematical model. However, there are quite a few issues to properly describe the heat transfer mechanisms: conduction and natural convention during the phase change process. In the next section, physical phenomenon and mathematical solutions of phase change with natural convection will be presented.

3. Melting with natural convection

Melting in the presence of significant natural convection is an important phenomenon in the field of thermal energy storage in phase-change materials. Considerable empirical and theoretical work has been devoted already to this phenomenon, and one conclusion was that this phenomenon is quite complicated [37]. The complications stem from the strong coupling that exists between the flow of the liquid phase and the melting rate of the solid. It is this coupling that determines the instantaneous shape of the two-phase interface, which constitutes one of the unknowns in each problem. It should be noted that according to many authors [38] [39], convection heat transfer is less important than conduction during solidification process.

3.1.Physical phenomenon

The evolution of the process is as follows. At first, when a small layer of liquid forms, heat transfer is dominated by conduction and the melting front moves parallel to the left heated wall (see Figure 1-3 (a)). Then, because of the variation in density, the hot fluid rises and brings the heat to the solid via the interface between the two. This causes a non-uniform distribution of heat, and therefore a slight deformation of the melting front. At this time, the heat transfer is mixed combining transfer by convection in the superior part of the enclosure and conduction in the lower part (see Figure 1-3 (b)). As the temperatures rise, the fluid motion is more important, the liquid gives more heat to the interface and it cools coming down, therefore, the heat transfer is larger at the top than the bottom of the interface, leading to an irregular shape of the latter. The deformation of the melt front is more important and dominated by the convective heat transfer (see Figure 1-3 (c)). The process continues until the arrival of the melt front to the cold wall.

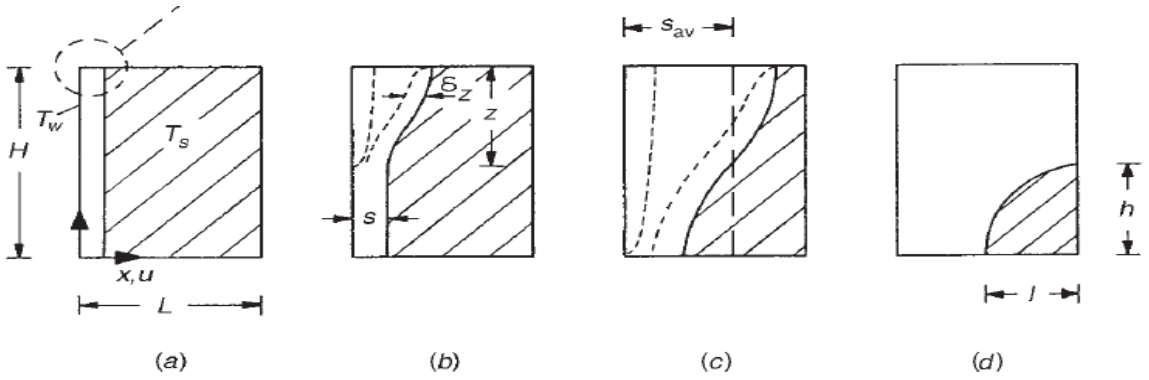

Figure 1-3: Regimes for melting in the presence of significant natural convection when the phase-change material is being heated from the side [40]

3.2.Mathematical solutions

The main challenge of the mathematical modeling of phase change process is to properly represent the moving melting front. The numerical modeling of solid–liquid phase change problems can be divided into two main groups: fixed grid methods and deforming grid methods.

In fixed grid schemes, the melting front is not tracked explicitly, but instead is determined by the temperature/enthalpy distribution, and the mathematical calculations become much simpler with reasonable accuracy. The most widely used fixed grid methods to formulate the energy conservation of the phase change process are the equivalent heat capacity method proposed by Morgan, 1981 [41] and Hsiao, 1984 [42] and the enthalpy method first introduced by Eyres et al., 1946, then reformulated for fixed grids by Voller et al., 1987 [43] and Binet and Lacroix, 2000 [44]. Cao and Faghri (1990) [45] proposed an enhanced temperature-based equivalent heat capacity method named the temperature transforming model (TTM), an enhanced temperature-based equivalent heat capacity method, in which the enthalpy-based energy equation is converted into a nonlinear equation with a single dependent variable. But this method suffered from inconsistency [46][47]. On the other hand, the enthalpy method treats both isothermal and mushy phase-change problems, but it suffered from temperature oscillation.

On the other hand, in deforming grid methods or front-tracking methods the mesh moves to track the phase interface which complicate the mathematical operations and transformed coordinate systems must be used. At each time step, the location of the moving boundary is calculated on a grid, which can lead to high computational costs.

When natural convection in the liquid phase is taken into account, the problem becomes more complicated and analytical solutions cannot be used [46]. In addition to the moving boundary issue, these problems are strongly non-linear, and the Navier-Stokes equations i.e, the coupled energy equations in the solid and liquid phases, together with the continuity and momentum equations in the liquid, must be solved.

Numerically, various methods are currently explored and used to model phase change accounting for natural convection, mainly the enthalpy-porosity approach [48][49][50][51][52][53][54][55], the temperature transforming model (TTM) [46][56][57][58], the equivalent thermal capacity method [41], the modified heat capacity method [59], in addition to the integral method, the boundary fixing method, the unstructured finite-element method, and the coordinate transformation method [18]. If no simplification is made, one must consider at least: the conservation of mass, equations of momentum and energy equation. In addition, Lattice Boltzmann Method (LBM) [60][61][62] can be used to model the fluid flow during phase change.

The solution of these equations can be done using finite volume methods (FVM) like the commercial software FLUENT or finite element method (FEM) using COMSOL Multiphysics software.

3.2.1. Temperature transforming model (TTM)

The temperature transforming model TTM was suggested by Cao and Faghri (1990) [45] to model phase-change problems with the effect of natural convection. In this method, continuity and momentum equations are used same as fluid flow problems, while the energy equation is different from the enthalpy-based energy equations.

Continuity equation

$$\frac{\partial(\rho u)}{\partial x}+\frac{\partial(\rho v)}{\partial y}=0 \qquad \textbf{Eq. 1-5}$$

Momentum equations:

$$\frac{\partial(\rho u)}{\partial t}+\frac{\partial(\rho uu)}{\partial x}+\frac{\partial(\rho vu)}{\partial y}=-\frac{\partial p}{\partial x}+\frac{\partial}{\partial x}\left(\mu\frac{\partial u}{\partial x}\right)+\frac{\partial}{\partial y}\left(\mu\frac{\partial u}{\partial y}\right) \qquad \textbf{Eq. 1-6}$$

$$\frac{\partial(\rho v)}{\partial t}+\frac{\partial(\rho uv)}{\partial x}+\frac{\partial(\rho vv)}{\partial y}=-\frac{\partial p}{\partial y}+\frac{\partial}{\partial x}\left(\mu\frac{\partial v}{\partial x}\right)+\frac{\partial}{\partial y}\left(\mu\frac{\partial v}{\partial y}\right)+\rho g[\beta(T-Tm)-1] \qquad \textbf{Eq. 1-7}$$

Energy equation:

$$\frac{\partial(\rho h)}{\partial t}+\frac{\partial(\rho uh)}{\partial x}+\frac{\partial(\rho vh)}{\partial y}=\frac{\partial}{\partial x}\left(k\frac{\partial T}{\partial x}\right)+\frac{\partial}{\partial y}\left(k\frac{\partial T}{\partial y}\right) \qquad \textbf{Eq. 1-8}$$

h is the total enthalpy including sensible and latent terms, u and v are the velocities in *x* and *y* directions (m/s), p is the pressure (Pa), k is the thermal conductivity (W/m. K).

Scaled temperature $T^* = T\text{-}Tm$ is defined, and the enthalpy is expressed by the temperature transforming model:

$$h = c\,(T^* + s) \qquad \textbf{Eq. 1-9}$$

$$\begin{cases} c = cs & if\ T^* < -\delta T \\ c = \dfrac{(cs+sl)}{2}+\dfrac{hsl}{2\delta T} & if -\delta T \le T^* \le \delta T \\ c = cl & if\ T^* > \delta T \end{cases} \qquad \textbf{Eq. 1-10}$$

$$\begin{cases} s = \delta T & if\ \mathrm{T}^* < -\delta T \\ s = \delta T & if -\delta T \le \mathrm{T}^* \le \delta T \\ s = \left(\frac{cs}{cl}\right)\delta T + \frac{hsl}{cl} & if\ \mathrm{T}^* > \delta T \end{cases} \quad \text{Eq. 1-11}$$

$$\begin{cases} k = ks & if\ \mathrm{T}^* < -\delta T \\ k = ks + \frac{(kl - ks)(\mathrm{T}^* + \delta T)}{2\delta T} & if -\delta T \le \mathrm{T}^* \le \delta T \\ k = kl & if\ \mathrm{T}^* > \delta T \end{cases} \quad \text{Eq. 1-12}$$

where *hsl* is the latent heat (J/kg), δT is half width of mushy zone temperature range, cp is the specific heat (kJ/kg˚C). $T^* < -\delta T$ corresponds to the solid phase, $-\delta T \le T^* \le \delta T$ to the mushy region, and $T^* > \delta T$ to the liquid phase.

The energy equation becomes:

$$\partial\frac{\rho c\mathrm{T}^*}{\partial t} + \partial\frac{\rho uc\mathrm{T}^*}{\partial x} + \partial\frac{\rho vc\mathrm{T}^*}{\partial y} = \frac{\partial}{\partial x}\left(\frac{k\partial\mathrm{T}^*}{\partial x}\right) + \frac{\partial}{\partial y}\left(\frac{k\partial\mathrm{T}^*}{\partial y}\right) - \partial\frac{\rho cs}{\partial t} - \partial\frac{\rho ucs}{\partial x} - \partial\frac{\rho vcs}{\partial y} \quad \text{Eq. 1-13}$$

The TTM method was used by several authors[56][57][58] , Wang et al. [46] developed a 2D numerical model for melting including natural convection applied in a square cavity. They have used the TTM employing a new method for solid velocity correction, and the velocity–pressure coupling is solved by the CUT algorithm. Z. Ma and Y. Zhang [47] proposed numerous solid correction schemes to ensure zero velocity in the solid phase namely switch-off, ramped switch-off , Darcy source term, ramped source term and variable viscosity.

3.2.2. Enthalpy-Porosity method

The enthalpy-porosity approach is the most widely used method to model phase change including the natural convection [14]. Using enthalpy-porosity method, the liquid fraction is calculated at each iteration. The region where the liquid fraction is between 0 and 1 is called the mushy zone. This zone is considered as a quasi-porous medium, as the material melts the porosity increases from 0 to 1 and decreases to zero for the solid region and therefore the velocities also vanish [55].

The energy equation can be expressed in the form:

$$\partial\frac{\rho h}{\partial t} + \partial\frac{\rho uh}{\partial x} + \partial\frac{\rho vh}{\partial y} = \frac{\partial}{\partial x}\left(\alpha\frac{\partial h}{\partial x}\right) + \frac{\partial}{\partial y}\left(\alpha\frac{\partial h}{\partial y}\right) - Sh \quad \text{Eq. 1-14}$$

where h is the sensible enthalpy, α=k/cp and Sh is the source term.

Total enthalpy:

$$H = h + \Delta H \quad \text{Eq. 1-15}$$

The latent heat in the enthalpy-porosity approach is accounted for by a source term in the energy equation expressed by:

$$Sh = \partial\,(\rho \Delta H)/\partial t\; + \partial\,(\rho \Delta H)/\partial x\; + \partial\,(\rho \Delta H)/\partial y \quad \textbf{Eq. 1-16}$$

$$\Delta H = fl.L \quad \textbf{Eq. 1-17}$$

where *fl* is the liquid fraction (equal to 1 for liquid state and 0 for solid state) and *L* is the latent heat (J/kg).

$$\rho = \rho l\, fl + (1 - fl)\, \rho s \quad \textbf{Eq. 1-18}$$

$$\lambda = \lambda l\, fl + (1 - fl)\, \lambda s$$

$$cp = cpl\, fl + (1 - fl)\, cps$$

where ρ is the density (kg/m^3), λ is the thermal conductivity (W/m˚C) and *Cp* is the specific heat (kJ/kg˚C).

Momentum equations:

$$\partial \frac{\rho u}{\partial t} + \partial \frac{\rho u u}{\partial x} + \partial \frac{\rho v u}{\partial y} = -\frac{\partial p}{\partial x} + \frac{\partial}{\partial x}\left(\mu \frac{\partial u}{\partial x}\right) + \frac{\partial}{\partial y}\left(\mu \frac{\partial u}{\partial y}\right) + Au \quad \textbf{Eq. 1-19}$$

$$\partial \frac{\rho v}{\partial t} + \partial \frac{\rho u v}{\partial x} + \partial \frac{\rho v v}{\partial y} = -\frac{\partial p}{\partial y} + \frac{\partial}{\partial x}\left(\mu \frac{\partial v}{\partial x}\right) + \frac{\partial}{\partial y}\left(\mu \frac{\partial v}{\partial y}\right) + Av + Sb \quad \textbf{Eq. 1-20}$$

$$Sb = \rho ref g \beta\, (h - href)/Cp \quad \textbf{Eq. 1-21}$$

where *href* and *ρref* are reference values of enthalpy and density respectively, β is a thermal expansion coefficient (1/K) and *Au* and *Av* are the Darcy terms ensuring zero velocity in the solid control volumes.

The porosity function *(A)* defined in momentum equations reduces velocities gradually in the solid phase until it vanishes. A is given as:

$$A = -\eta\,(1 - fl)^{\,2} / (fl^3 + b) \quad \textbf{Eq. 1-22}$$

where *b* is a small number (0.001) to avoid division by zero and η is a very large number (10^9).

3.2.3. Enthalpy based -Lattice Boltzmann Method

Natural convection during melting of PCM can also be studied through Lattice Boltzmann Method (LBM)[60][61][62]. The LBM offers an important alternative method for simulation of phase change including fluid flow. the main advantages of LBM are the numerical stability, ability to set up, in complex geometries, no-slip boundary conditions, accuracy, and the high parallel implementation of the algorithm [63]. The enthalpy approach is used to model phase change, while lattice Boltzmann method is used to solve fluid flow equations.

3.2.4. Enhanced conductivity approach - simplified method

Usually in thermal engineering applications, the phase change problem is simplified, and building models with integrated PCM ignore the convection effect in the liquid region, due to the complexity of CFD models and the high computational time. Therefore, the convective term in the transport equations is neglected and hence only the unsteady heat conduction term in the energy equation is considered [64]. However, because the assumption of conduction alone is not always adequate, and the inclusion of the convective phenomena is costly in terms of computation time when modeled numerically using CFD methods, the buoyancy effect during the melting process was accounted using the common effective thermal conductivity ($k_{enh} = \overline{Nu}.\, k_l$; $k_{enh} = cRa^n$) [26][65][66][67][68][69]. Nevertheless, this approach has many disadvantages, mainly it cannot provide information about the melting front location since it is essentially a conduction model, the determination of an appropriate value of the modified conductivity function of dimensionless number is not a trivial task, a constant value cannot be designated to the effective thermal conductivity of a fluid with varying temperature [70] and the four regimes during melting process cannot be expressed. The average Nusselt number is considered as a main parameter in this approach, since it defines the convection heat transfer coefficient, and strongly affects the dynamics of the process [71]. Thus, several authors, have presented correlations of the average Nusselt number during the melting process based on the aspect ratio, Ra and Pr number restrictions. These correlations are based on experimental or numerical observations. Therefore, their validity will always be restricted to the specific range, geometry configurations, thermal boundary conditions and variables the studies were performed for [71]. It is worthy also to mention that the choice of the characteristic length in the Ra and Nu formulas is very critical. Either the height of the enclosure (H) or the average thickness of the liquid zone (sav) could be used as the characteristic length scale [40]. Moreover, Webb and Viskanta [72] concluded that caution is advised when using correlations in the literature for design purposes or as quantitative comparisons with independent investigators, and that the proper characteristic length in melting/solidification problems needs more research attention.

3.3.Literature review on melting with natural convection in enclosures

Conduction and convection-dominated melting along a heated isothermal wall in a rectangular or square enclosure has received great attention due to its wide-ranging technological and engineering applications in such fields as casting, metallurgy and thermal energy storage. This phenomenon was investigated using both experimental and numerical/theoretical approaches. Even though the experimental studies show more accurately the real behavior of PCM, researchers prefer to study the phase change problems by mathematical solutions and numerical simulations due to the fact that that numerous conditions can be carried out by changing the variables in a numerical model [18].

Beckermann and Viskanta [73] investigated experimentally and numerically the melting of a pure metal (gallium) inside a vertical rectangular enclosure, with natural convection heat transfer in the liquid region and conduction in the solid one. The numerical results were validated through comparisons with a number of experiments. It was found that the melting process consisted of four regimes: a conduction-dominated regime, a mixed conduction-convection regime characterized by convection in the upper part of the enclosure and conduction in the lower part, a convection-dominated regime, and a regime where melting process is extremely influenced by heat extraction by cold wall (the melting process approached to the steady-state condition). It was also concluded that additional research is needed to arrive at general correlations for the dependence of the average Nusselt numbers on the governing dimensionless parameters (Ra and Pr). Brent et al. [74] also conducted a numerical investigation of the melting of pure gallium in a rectangular cavity, the temperature at the left wall was maintained at 38ºC while the right wall boundary was at an initial temperature of 28.3ºC, and the other walls at the top and the bottom were adiabatic. They modeled combined convection-diffusion phase change using the enthalpy-porosity approach. The results showed an excellent agreement between the numerical predictions and experimental findings available in literature. They also indicated different features of the enthalpy-porosity method such as, convergence speed, applicability and the ability to predict accurately the position of the melting front at different times.

Wang et al. [75] investigated experimentally the thermal characteristics of the melting process in a rectangular enclosure heated from a vertical wall using a flat plate heat pipe to provide a uniform temperature. Based on the experimental results, they developed correlations for the melted volume fraction and the time-averaged Nusselt number as a function of different parametric dimensionless variables (Ra, Ste, Pr and Fo). The results showed that during the melting procedure the temporal variation of the Nusselt number reflects the existence of three different regimes: conduction regime, transition regime (mixed conduction-convection), and convection-dominated regime. Gong et al. [76] studied numerically the melting of a phase change material in a rectangular cavity with an isothermally-heated vertical wall. The enthalpy-porosity approach was used to model the evolution of the flow at the solid/liquid interface. They found that inverting the container at an appropriate stage during the melting process is an effective way to enhance the effect of natural convection.

Younsi et al. [77] investigated numerically the thermal characteristics of the melting process of hydrated salt in a rectangular enclosure heated from a vertical wall, using an enthalpy-based mathematical model. The finite volume method (FVM) was used to solve the governing equations. The convection dominated melting in a rectangular cavity was also investigated numerically using the commercial code FLUENT 6. It was shown an excellent agreement between the numerical

methods (2D FVM and FLUENT code) and the experimental results. Wang et al. [46] developed a comprehensive model based on the finite volume method and temperature transforming model for solving the problem of 2D melting with natural convection in a square cavity for four different cases. The consistent update technique (CUT) algorithm was used to solve the velocity–pressure coupling. The results showed that the used algorithm is much more efficient, in terms of CPU time, than the SIMPLE algorithm for solving melting problems. Besides, a new solid velocity correction scheme that does not introduce large numbers to vanish velocity in the solid was used. This scheme eliminated effectively the inconsistencies found in earlier studies and was able to accelerate the convergence significantly. The results showed a reasonable agreement between the numerical model compared to previous theoretical and experimental results.

Murray and Groulx [78] modeled natural convection during melting of Octadecane in a square enclosure using the COMSOL Multiphysics package (versions 4.0a and 4.1). The left vertical wall was heated to a temperature of 313 K, while the right wall was maintained at initial temperature Tm of 303 K. The influence of the temperature range ΔT was established in the simulation. In addition, the authors discussed the impact of the numerical definition of viscosity on the onset and strength of natural convection, and the resulting melting front position. The results showed that the variation in PCM properties such as thermal conductivity and viscosity affects the shape of the melting interface and the amount of melted PCM. Finally, it was pointed to the importance of accounting for natural convection during melting in a PCM.

Yanxia et al. [79] investigated experimentally the melting process of ethanolamine–water binary mixture used as PCM in a rectangular enclosure heated from its vertical side. They studied the effect of natural convection in terms of liquid fraction and the position of the melting front. Moreover, empirical correlations of time-averaged Nusselt number and liquid fraction were developed in convection-dominated melting regime. The results showed that pure conduction regime only occurs at the early stage of the melting process and that natural convection improves the rate of melting compared with the pure conduction model. Finally, a conduction– convection model is essential for predicting melting process accurately.

Ho and Viskanta [80] investigated experimentally the melting of n-octadecane from an isothermal vertical wall of a rectangular cavity. Initially, the PCM was solid with a uniform temperature that was either preselected amount below or very close to the melting temperature. Heat transfer coefficients at the heat source surface and the solid-liquid interface were recorded photographically. The experimental results showed that the rates of heat transfer and melting were significantly influenced by the buoyancy driven convection in the liquid region, except in the earlier stage of the melting process.

Yao and Cherney [81] studied the effect of the natural convection on the melting of a solid PCM around a hot horizontal cylinder by using the integral method. The results demonstrated that the integral solution had surprising accuracy when it was compared with the quasi-steady solution when Stefan number was small. Rieger et al.[82] investigated numerically the melting process of a PCM inside a heated horizontal circular cylinder. Both heat conduction and convection have been taken into account to treat this moving boundary problem, and the complex structure of the timewise changing physical domain (melt region) have been successfully overcome by applying body fitted coordinate technique. Ismail and Silva [83] developed a 2D mathematical model to study the melting of a PCM around a horizontal circular cylinder considering the presence of the natural convection in the melt region. A coordinate transformation technique was used to fix the
moving front. The numerical predictions were compared with available results to establish the validity of the model, and a satisfactory agreement was found. They concluded that the numerical model was adequate to represent the physical situation of the proposed system. Furzerland [84] investigated the enthalpy method and the coordinate transformation method through the comparison of the solutions of specific problems of one dimensional heat transfer by considering pure convection. One of his conclusions was that the enthalpy method is very attractive owing to these: it is easy to program and there are no computational overheads associated with tracking the moving interface within a specific range of fusion temperatures.

Concerning the computational time, it can be quite large, depending on the used method, the simulated problem and the spatial and temporal discretization [85]. The melting of Tin, filled in a square enclosure of height 0.1m, in presence of natural convection has been studied by different authors [85] [86] [87]. The computational time for the melting of Tin was found 450 hours for a total simulation time of 700 seconds with a mesh size of 400 × 400 in [86]; the simulations were conducted using a Compaq Alpha ES40 machine. While the computational time using the LBM in [85], for a simulation time of 1000 seconds is found 76 hours with a mesh size of 400 × 400, the simulations were conducted using an Intel Xeon X5472. Moreover, Hannoun et al. [87] reported 2400 hours of CPU to simulate 2500 seconds of the melting of Tin with a mesh size of 200 × 200, using Compaq Alpha ev67 machine. In addition, the simulation of 5000 seconds of the melting of Octadecane, filled in square enclosure of height 0.1m, with natural convection took 34 hours with a mesh size of 225 × 225 [85].

4. Literature review of phase change with radiation

Transparent envelope components are key elements in buildings, especially in offices and commercial buildings, that affect the energy performance and daylighting [88]–[90].

To accomplish its energy storage function, and at the same time to allow the transmission of light into the indoor environment, some researchers [13] [91] [16] have been interested in transparent PCM. The integration of PCM in a transparent element of the building envelope enhances the ability for energy storage, since the PCM will be directly exposed to the solar radiation. This technology aims to smooth the indoor temperature and decrease the energy fluctuations, providing daylighting at the same time.

Numerous experimental and numerical work of heat storage solutions for transparent envelope containing PCM have been developed, especially for double glazed unit, which has been attracted much more attention as a valid method for reducing building energy consumption. Phase change materials were integrated within double [92] [93] or triple glazing units [94], within more complex glazing components [95] and within translucent solar walls [13]. The performance of glazing with integrated PCM was investigated both experimentally [92]–[94], [96], [97] and numerically [98]–[100]. A literature review of the use of PCM in transparent and translucent building envelope components can be found in [101].

Buddhi and Sharma [91], measured the transmittance of stearic acid, transparent PCM, as a function of temperature and thickness. At 60 ºC (melting temperature Tm = 64.6ºC) they found an average transmittance of 99% for a thickness of 1 cm, and 81% for a thickness of 5 cm.

Manz et al. [13] studied a translucent wall for solar heating and daylighting composed of glass pan, air gap, a translucent PCM and a transparent insulation material (TIM). They investigated experimentally the optical PCM properties and a prototype of the TIM-PCM wall was constructed in 1994 in Swiss. Also, a one-dimensional numerical model (side effects were neglected) was developed considering only heat transfer by conduction and the optical properties were simulated using a Monte Carlo technique. The results show that the thermal and optical performance of the wall is very promising and that the chosen PCM in solid state reduces the heat and light gains. Thus, they proposed considering another PCM with a melting temperature of 21ºC instead of 26.5ºC. Weinläder et al. [16] investigated experimentally the thermal behavior of three glazing systems incorporated with a plastic container filled with different PCM. However, in both studies, the behavior of the system was not investigated in detail in the hot season and inferences on thermal comfort were not evaluated according to standards.

To improve the poor thermal inertia of conventional glazing systems, Goa et al. [12] studied the implementation of a PCM layer in combination with glass panes. They developed a one-dimensional numerical model for heat and shortwave wave transmission. The numerical model is divided in two sub-models: to solve the heat transfer process and to calculate the solar irradiance transmitted and

absorbed. The energy balance of the radiative heat fluxes for each layer (node) is solved iteratively using the following equation:

$$q_{sol,n} = (I_{n-1\to n} + I_{n+1\to n}) - (I_{n\to n+1} + I_{n\to n-1}) \quad \text{Eq. 1-23}$$

where $q_{sol,n}$ is the absorbed solar radiation in the nth layer [W/m^2] and the $I_{x\to y}$ variables are the short-wave radiative fluxes [W/m^2] that enter/leave the nth layer. the first step of the calculation procedure is aimed at assessing the component that is reflected by the layer. The second step calculates the amount of shortwave radiation that is absorbed by the layer. The amount of shortwave energy that is eventually transmitted by the layer is then obtained by difference between the total impinging radiation and the reflected and absorbed parts. The enthalpy method in one dimension was used to model phase change. The model was validated experimentally using a PCM glazing prototype (1.4 m x 1.15 m) composed by two layers of glass (6 mm and 8 mm) and one PCM layer (paraffin, 15 mm thick with melting temperature of 35 °C). They found that the numerical tool represents a good base for simulations on different configurations of PCM glazing systems.

Liu et al [97] investigated numerically the thermal performance of a PCM-filled double glazing roof with different thickness of PCM in the cold area of Northeast China. They also studied the effect of the semi-transparent property of the glazing roof and zenith angle on the thermal performance. The heat transfer through the glazing unit is simplified to one dimensional unsteady heat transfer process and the convection within the PCM layer (when in liquid state) is neglected. The phase change is modeled using enthalpy formulation and the radiation is accounted for by adding a radiative source term to the energy equation. The one-dimensional unsteady energy equation for PCM regions is given as:

$$\rho \frac{\partial h}{\partial \tau} = k \frac{\partial^2 T}{\partial x^2} + \emptyset \quad \text{Eq. 1-24}$$

where, h is the specific enthalpy of PCM (J/kg). ρ and k are the density (kg/m^3) and the thermal conductivity (W/mK) of PCM, respectively. The radiative source term $\emptyset$ is calculated for each layer, for example when the calculation node is in the phase 2 of PCM layer as shown in Figure 1-4:

$$\emptyset = \frac{T_{g1} T_{p1} A_{p2} I_{sol} cos\theta}{L_{p2}} \quad \text{Eq. 1-25}$$

where, I_{sol} is the solar radiation (W/m^2), T_{g1}, T_{p1} are the solar transmittance of glass 1 layer and phase 1 layer respectively. A_{p2} is the solar absorptance of phase 2 layer. L_{p2} is the thickness (m) of phase 2 layer and glass 2 layer. The results showed that when the PCM thickness increases, the temperature time lag increases. When the extinction coefficients of PCM increase, PCM thickness effect on thermal performance parameters turns bigger except for the temperature time lag.

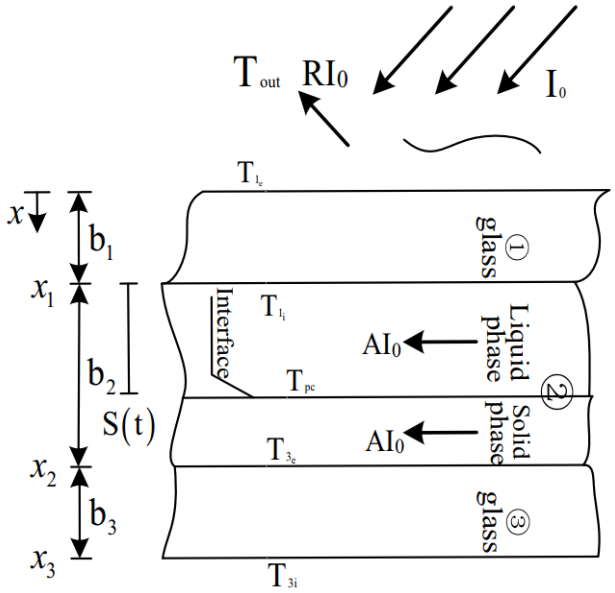

Figure 1-4: layout of double glazed roof filled with PCM

Ismail et al. [15] investigated the thermal and optical properties of double-glazed units filled with PCM, through numerical and experimental analysis. For the numerical model, a one-dimensional formulation was developed, and a moving grid procedure was used within the PCM layer. They found that the PCM filled glass window system was practical and thermally effective.

Ismail et al. [14] developed a numerical model of two concepts of glass windows, that is, double glass window filled with infrared absorbing gases and the other one is filled with phase change materials. For the PCM glass system, the concept is as follow: the external glass receives the solar radiation, where part of it is absorbed, another part is reflected, and the rest is transmitted to the PCM, which absorbs part of the energy received. At the interface between the external glass sheet and PCM, the radiation absorbed by the PCM and the heat conducted by the glass surface raise the PCM temperature until reaching its fusion temperature and converts a layer of the PCM to a liquid. To model the double glass window filled with a PCM a relative simple and effective radiation conduction one dimensional formulation is used and convection in the liquid phase of the PCM is neglected. The double glass window filled with an absorbing gas mixture and using reflective glass is more efficient and has a coefficient of heat gain F factor, in the range of 0.55–0.65. The double glass window filled with PCM has F factor in the range of 0.65–0.80.

Diaz and Viskanta [102] studied the melting process using one-dimensional radiation and conduction model. They solved the energy equation with the temperature formulation, and Stefan's condition at the interface. For this case of conduction and radiation, this formulation has the advantage of allowing the explicit introduction of the radiative flux at the interface.

Zhong et al. [99] established a numerical model and an experimental setup in order to determine the effects of PCM thermophysical parameters on the dynamic heat transfer progress of PCM-filled glass

window (PCMW). The heat transfer process of the PCMW is shown in Figure 1-5. The heat transfer through the window is simplified to one-dimensional unsteady heat transfer process in double-glazed window and the convective process is neglected in the PCM. Results showed that when PCM (paraffin MG29) is used, the thermal insulation of PCMW and peak cooling load shifting effects were remarkable in the hot summer and cold winter area of China, and the heat entered the building through the PCMW is reduced by 18.3% in the typical sunny summer day.

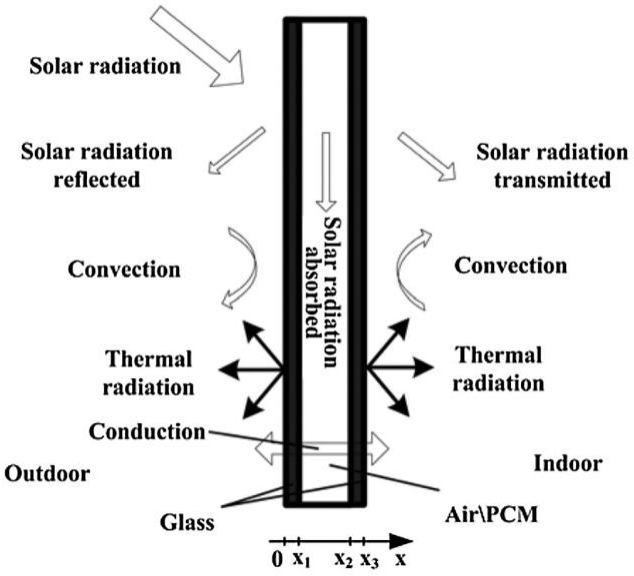

Figure 1-5: Heat transfer process of the PCM-filled glass window (PCMW)

Although the inclusion of PCM in glazing systems can have a positive effect on thermal comfort and contributes to improvements in the energy performance of buildings [96], the introduction of PCM, instead of gas or vacuum, in a double-glazing unit, results in a reduced thermal resistance, negatively affecting the thermal performance of the system. In addition, due to the complete melting of the PCM within the double-glazing unit during summer, the internal surface temperature of the glazing may increase to a level that may negatively affect thermal comfort [96].

Additionally, we present in Table 1-1 five common radiation models to solve the RTE found in the literature. In fact, within the medium, radiative heat transfer is described by the general radiative heat transfer equation (RTE) [103] that accounts for the variation of the intensity radiation field, and it is usually divided into three additive terms: absorption, emission and scattering.

Table 1-1 Common radiation models to solve the radiative heat transfer equation (RTE)

Radiation model	Advantages	Limitations
Discrete ordinates model (DOM)	– Solution method similar to that for the other conservation equations. – Conservative method leads to heat balance for coarse discretization.	Solving a problem with a large number of ordinates is CPU-intensive

	– Accuracy can be increased by using a finer discretization. – Accounts for scattering, semi-transparent media, specular surfaces. – Banded-gray option for wavelength-dependent transmission.	
Discrete transfer radiation model (DTRM)	– Relatively simple model. – Can increase accuracy by increasing number of rays. – Applies to wide range of optical thicknesses.	– Assumes all surfaces are diffuse (isotropic reflection). – Effect of scattering not included. – Solving a problem with a large number of rays is CPU-intensive.
P-1 model	– Radiative transfer equation easy to solve with little CPU demand. – Works reasonably well for combustion applications where optical thickness is large. – Easily applied to complicated geometries with curvilinear coordinates. – Effects of particles, droplets, and soot can be included.	– Assumes all surfaces are diffuse. – May result in loss of accuracy, depending on complexity of geometry, if optical thickness is small. – Tends to overpredict radiative fluxes from localized heat sources or sinks.
Rosseland model	Does not require any boundary conditions since surfaces are treated as black (Emissivity = 1.0)	–Only valid for optically thick and linearly anisotropic material (thickness/depth greater than 10) –Not valid near walls
The Monte Carlo Model	– Very general-purpose method - allows you to do gray/non-gray, scattering, emission and absorption – It is the recommended choice for a transparent media radiation calculation	– Computationally intensive: Samples and ray traces the domain every solution step. – always contains statistical error $\approx 1/\sqrt{N}$

5. Trombe wall with integrated PCM

Trombe wall integrating phase change materials (PCM) is a particular passive solar technique that has shown great potentialities and can reduce effectively the building energy consumption. Basically, traditional Trombe walls [104]–[108] consist of an external glazing, an air channel, and a high heat capacitance wall in contact with the indoor environment (Figure 1-6) . The solar radiation heats the air channel between the glazing and the wall and the heat is absorbed by the outer surface of the wall. Then, the heat is transmitted inwards, by conduction within the wall, by convection and by radiation towards the room. This type of walls can reduce the energy bill by 20 to 30% virtually in all climates especially when the air gap is vented [107].

Among disadvantages often cited for Trombe wall, are the cost, the delicate design and operation for the air gap and vents, the absence of light transmission through the wall, the problem of overheating in summer and the large thermal losses in winter when there is little sunshine. To improve the Trombe wall heat storage performance, phase change materials were implemented in the wall composition and this technique has been investigated by numerous researchers [109]–[114]. During the day, this

wall is heated due to the incident solar radiation, melting the PCM. At night, when the outdoor temperature falls below the phase change temperature, the heat stored by the PCM is released, warming the building.

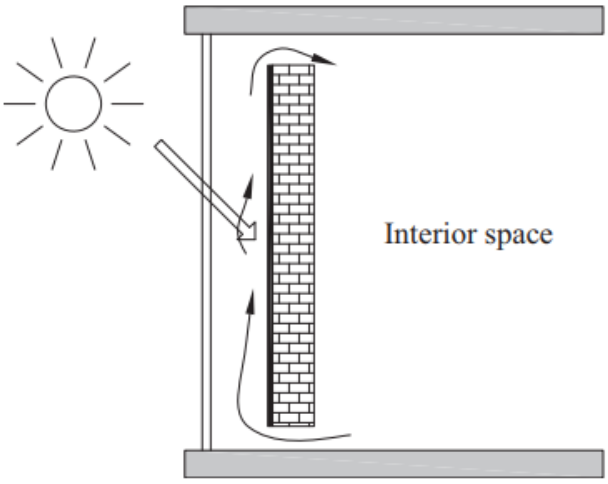

Figure 1-6: schematic of TROMBE wall [115]

Fiorito (2012) [110] conducted a parametric study on the use of PCM in Trombe walls by varying the PCM position and the melting point temperature for five different climates. They found enhanced performances for the modified Trombe wall.

Zalewski et al. [111] studied experimentally a Trombe wall with PCM components filled in the air channel and an insulating board replacing the high capacitance wall. They found that the heat storage capacity of the wall was increased.

Also, an experimental Trombe wall (ventilated façade) with PCM was studied by De Gracia et al. [112] during winter season. They found that the use of the ventilated facade with PCM improves significantly the thermal behavior of the whole building.

Kara and Kurnuç [116] investigated a PCM Trombe wall with a novel triple glass (NTG) to improve the performance of the conventional Trombe wall system and overcome its main disadvantage: the overheating during the summer. However, in all these applications, the light transmission was still absent.

Transparent insulation

Insulation materials are used to reduce the transmission of heat through conduction, convection and radiation in walls [117]. Usually, These materials are opaque, however, many studies were interested in transparent insulation materials (TIM) [117] [118] which, in addition to insulation, allow light to pass through. This is especially important in winter when, in addition to insulation, it is needed to increase solar gains. Such gains can reach 50 W/m^2 during a sunny week in January [118]. On the

other hand, these gains may become a problem during the summer, causing overheating. TIM are classified into four different types in accordance with the geometrical layout of the materials. Each type has a unique pattern of solar transmission and physical behavior as illustrated in Figure 1-7, where the bold line represents the absorbing surface (a wall with PCM for example): Absorber-parallel structures (Figure 1-7,a) are constructed from several layers parallel to the absorber surface. The degree of insulation can be increased, by adding more layers, resulting in an increase in optical reflection and solar gain reduction. Such systems do not meet the criteria of high transmission and low heat loss. Absorber-perpendicular structures (Figure 1-7,b) have low optical reflection losses and reflect and transmit the incoming beam radiation effectively towards the absorber. The cavity structures (Figure 1-7,c) are combination of both absorber-parallel and absorber-perpendicular structures. Finally, quasi-homogeneous structures (Figure 1-7,d) that include TIM made of glass fiber or aerogel, are similar to porous materials. Here, the incident rays pass through the TIM, always undergoing multiple reflections at the surfaces of the pores and the effect is then the diffusion of the radiation.

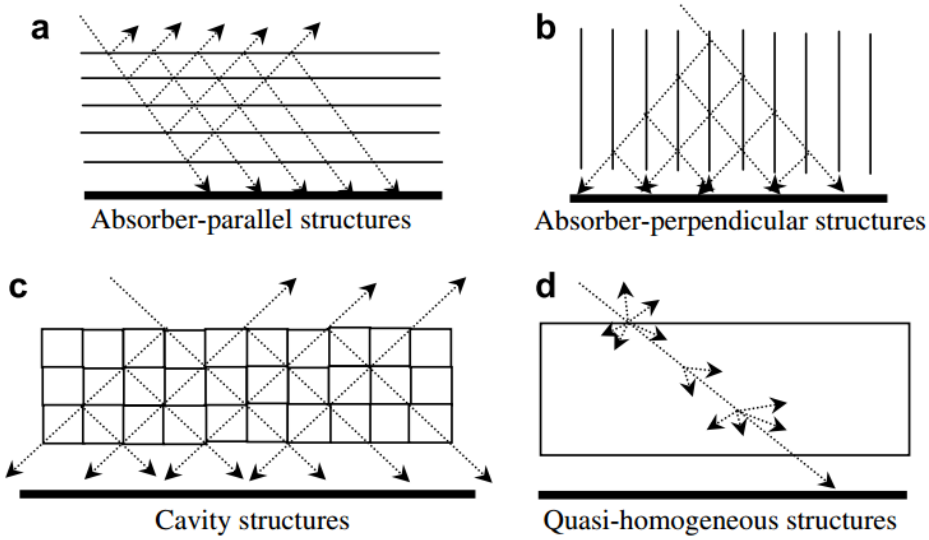

Figure 1-7: Classification of transparent insulation materials [118]

For decades, a number of investigations have been carried out to improve the properties of transparent insulations. A great deal of research work has been done to improve the honeycomb structures used as transparent insulation material (TIM). The application of these improved TIM on external walls as a passive solar heating element similar to the Trombe wall was proposed and experimentally investigated by Goetzberger et al.[119]. In addition, over the past 30 years, different types of materials, such as plastics, glass, and aerogels, have been used to produce TIM [118].

6. INERTRANS wall

6.1.System description

The ANR INERTRANS project (2018-2011) [120] proposed the development of an innovative wall that addresses the issue of energy efficiency and optimal use of environmental resources. The wall is composed of a silica aerogels bed for high insulation and solar radiation transmission and of glass bricks filled with a eutectic phase change material (fatty acids) for heat storage and restitution. The whole wall is translucent. The best conditioning of these elements has been studied, retaining as a solution, the assembly of a single glazing exterior side, followed by a space filled with insulation, and then glass bricks filled with PCM on the inside (Figure 1-8). An acronym for this wall is proposed: TIM-PCM wall which stands for “Translucent Insulating Material – Phase Change Material wall". Many features, that are not found in a conventional Trombe wall, are combined by such wall: it provides heat gains from solar radiation, high thermal insulation, heat storage and release, natural daylighting and visual communication to the outside world.

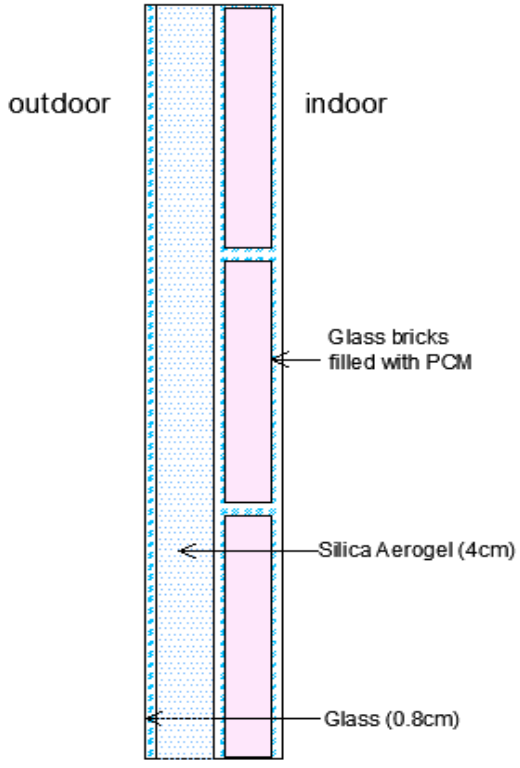

Figure 1-8: Schematic of the TIM-PCM wall

The wall has been set up in Sophia Antipolis, Southern France, within the center for Processes, Renewable Energies and Energy Systems (PERSEE) of Mines Paristech graduate school in the aim of studying its thermal behavior (Figure 1-9). Also, a TIM-PCM wall was constructed in the MINIBAT climatic chamber of the CETHIL (*Centre d’Energétique et de Thermique de Lyon*) in

Lyon, with the aim of determining the behavior of the wall for imposed and repeatable climate scenarios (Figure 1-10).

Figure 1-9: (a) TIM-PCM wall from the outside, (b) PCM in solid phase (left) and liquid phase (right), from the inside (PERSEE center in Sophia Antipolis)

Figure 1-10: Interior and exterior photo of the TIM-PCM wall of CETHIL

6.2.Physical phenomena

The thermal study of the wall requires the knowledge of the different heat transfer mechanisms that take place, especially the melting of fatty acids filled in glass bricks with combined natural convection and radiation. The natural convection is developed in the liquid PCM and could dramatically impact the heat transfer. The evolution of the melting process in presence of natural convection is explained in section 3.1.

In addition, during the day, the solid PCM absorbs the solar radiation, thus increasing its temperature until the melting, and at that moment, a small layer of liquid begins to form and the liquid PCM transmits solar radiation. Thus, the radiation through the PCM must be coupled to the natural convection phenomena during melting process. Noting that the TIM-PCM wall is supposed to be opaque for the longwave radiation due to the presence of the silica aerogel layer.

6.3.Previous works related to the INERTRANS project

Some studies have already been conducted within the framework of the INERTRANS project.

The TIM-PCM wall was studied experimentally by Berthou et al [121] in-situ, under real life conditions, in the full-sized test cell located in Sophia Antipolis in PERSEE center (Figure 1-11). Besides, experimentations were carried out at the French Scientific and Technical Center for Building research (CSTB) to characterize thermal and optical properties of the materials used. The outer (TIM) layer is composed of a 0.8 cm large glass pane while the inner layer is composed of glass bricks of dimension 19 cm x19 cm x 5 cm filled with PCM. There is a 4-cm gap between the outer and inner layer, which is filled with silica aerogel granulates. The test room is equipped with 4.41 m^2 of TIM–PCM wall facing south.

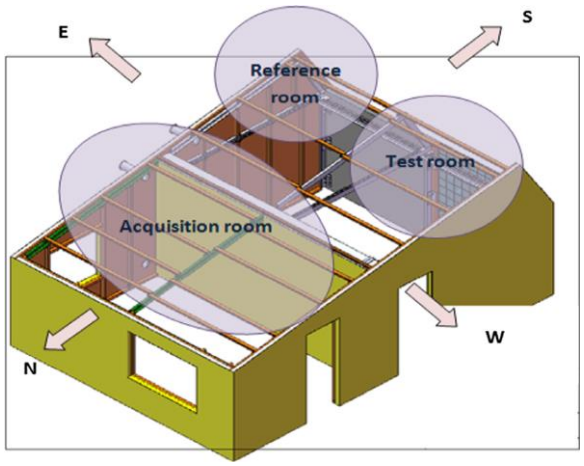

Figure 1-11: Schematic presentation of the full-scale test cell

Experimental results obtained by Berthou et al. [69] have shown that the heat losses through the wall are very low while the heat and light gains are high. In addition, it was shown that the tested wall is very effective in winter and shoulder season, particularly for cold sunny climates (the recorded indoor air temperature varied from 17 to 20 ºC), but when the solar radiation is very low, the wall does not bring any additional heat. In summer, the PCM does not cycle and stays in liquid state, causing overheating, the indoor air temperature in the test cell reaching up to 40ºC (Figure 1-12).

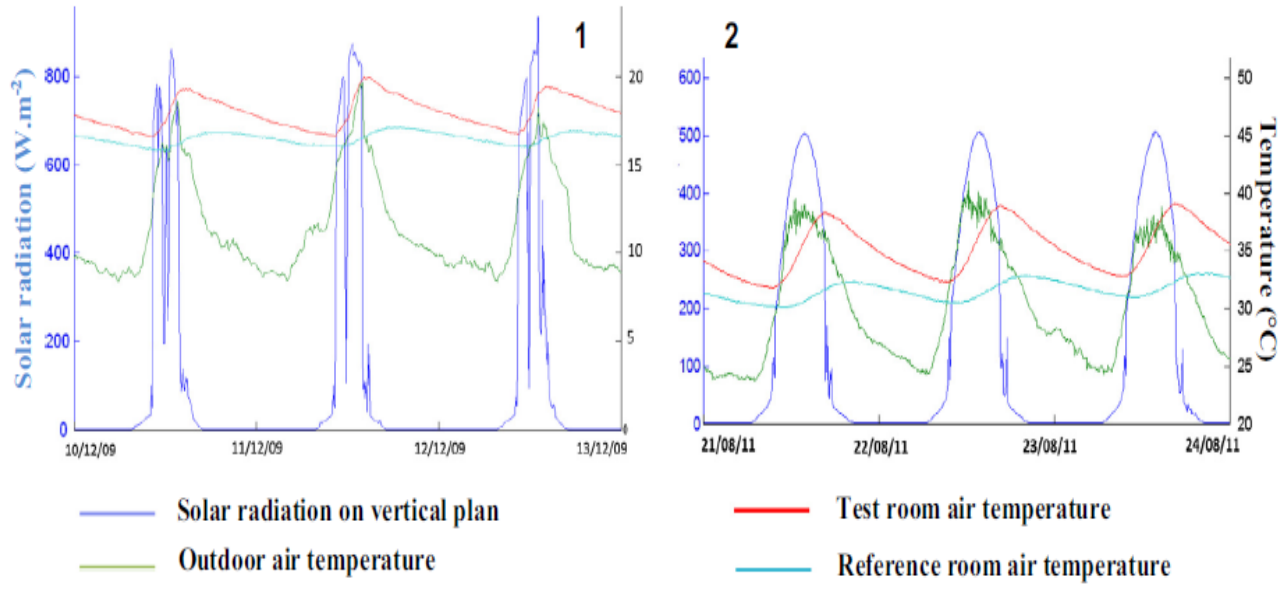

Figure 1-12: Solar radiation and air temperatures for three days in December2009 and August 2011

Numerically, Berthou developed a 1D numerical model considering natural convection and short-wave radiation during melting of PCM. He assumed that the wall is opaque for longwave radiation. The radiation was modeled using the equation of Beer-Lambert, this relation defines in a simple way the evolution of the radiative short-wave flow in the semitransparent medium and it is given as:

$$\emptyset(x) = k\emptyset_0 e^{-kx} \quad \text{Eq. 1-26}$$

where $\emptyset(x)$ is shortwave wave radiation entering the vertical PCM layer of abscissa *x* and *k* is the linear attenuation coefficient of the medium.

The natural convection was accounted for using dimensionless numbers and thermal transfers in the liquid PCM were calculated by Newton's law:

$$\emptyset conv = h(T)S(T_f - T_s) \quad \text{Eq. 1-27}$$

where T_f is the melting temperature, T_s is the surface temperature and the convective coefficient *h(T)* is given by:

$$h(T) = \frac{\lambda Nu}{L_c} \quad \text{Eq. 1-28}$$

where *Lc* is the characteristic length of the phase change, λ is the PCM conductivity and *Nu* is the Nusselt number given by the following correlation:

$$Nu = 0.35Ra^{0.25} \quad \text{Eq. 1-29}$$

where Ra is the Rayleigh number.

In this work, the model has not been reasonably experimentally validated. In Figure 1-13, the yellow and the red curves represent respectively the internal surface temperature of the wall for the model with and without natural convection respectively. The results of the model without natural convection are found closer to the experimental results as in the square 1. Moreover, during the melting, there is

a difference up to 5°C between the numerical model with convection and the experiment (square 1). The reason may be that the natural convection was not correctly introduced in the numerical model. As future work, they insisted that the performance of the wall needed to be optimized in summer and solutions for overheating and PCM cycling must be proposed.

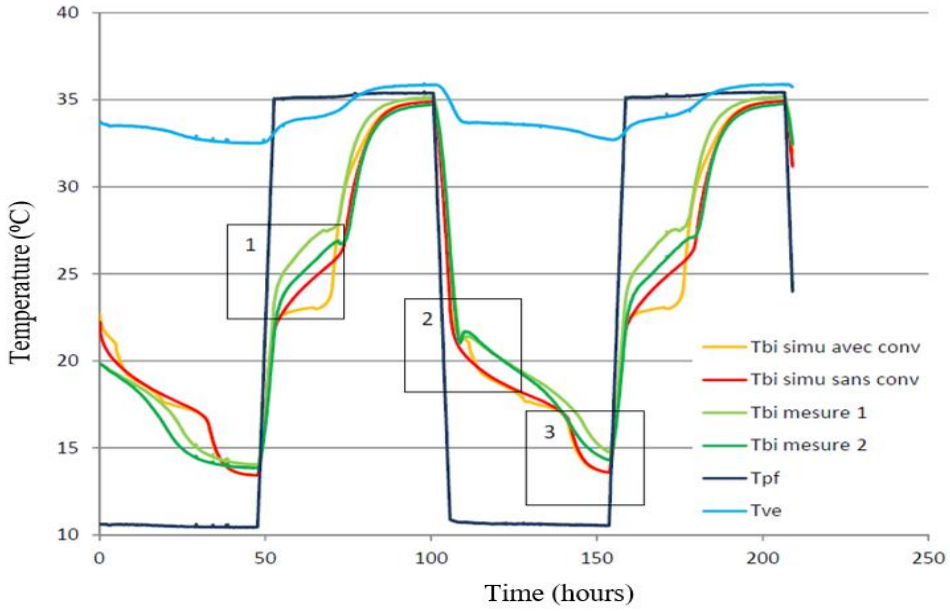

Figure 1-13: Comparison simulation / experimentation of the internal surface temperature of the wall for the model with and without natural convection

Regarding the part of the INERTRANS project executed in Lyon, Fuentes et al. [85] studied the melting of fatty acids filled in glass bricks of the INERTRANS wall in presence of natural convection and radiation. First, they developed a lattice Boltzmann Model (LBM) to study the melting of Octadecane and Tin in presence of natural convection in a square cavity (Figure 1-14,a). For the phase change problem, the enthalpy formulation used is given as:

$$h = c_p T + f_l L_h \qquad \textbf{Eq. 1-30}$$

where h is the enthalpy, C_p is the specific heat capacity, L_h is the latent heat of fusion and f_l is the liquid fraction:

$$f_l = \begin{cases} 0 & if\ h \le h_s \\ \dfrac{h - h_s}{h_l - h_s} & if\ h_s < h < h_l \\ 1 & if\ h \ge h_l \end{cases} \qquad \textbf{Eq. 1-31}$$

The energy equation, including convection and radiation, is expressed as:

$$\rho c_p \left(\frac{\partial T}{\partial t} + u.\nabla T \right) = \nabla.(k \nabla T) - L_h \frac{\partial f_l}{\partial t} - \nabla.\overrightarrow{q_r} \qquad \textbf{Eq. 1-32}$$

where $\overrightarrow{q_r}$ is the radiation heat flux (W/m^2)

The energy equation is solved by finite differences, whereas fluid flow equations are solved by the lattice Boltzmann method. The LBM equation is expressed by:

$$f_i(\vec{x} + \overrightarrow{c_i}, t+1) - f_i(\vec{x}, t) = \Omega_i \quad \text{Eq. 1-33}$$

where f_i is the particle distribution function, which is the probability of finding a particle in position *x*, time *t* and velocity c_i *(i =0, ... , q - 1)*, and Ω_i is the collision operator, giving the relaxation towards an equilibrium state.

The developed LBM was validated using numerical Benchmark solutions found in the literature.

Later, they modeled the radiation using the Discrete Ordinates Method (DOM), and radiation flux is added into the energy equation. The Discrete Ordinate Method (DOM) is then used to solve numerically the angular integrals leading to a weighted sum:

$$\overrightarrow{q_r} = \int_{4\pi} I(\vec{r}, \hat{s})\hat{s}d\boldsymbol{\Omega} \approx \sum_{\boldsymbol{m=1}}^{\boldsymbol{M}} \boldsymbol{I_{mP}}\hat{s}w_m \quad \text{Eq. 1-34}$$

$T(\vec{r}, \hat{s})$ standing for the radiation intensity in the direction $\hat{s}$.

The combined LBM-DOM model was used to study the melting of fatty acids filled in glass bricks of the INERTRANS wall in presence of both natural convection and radiation for a total simulation time of 24 minutes (Figure 1-14, b). Figure 1-14 shows the geometry and boundary conditions for the studied cases: (a) melting of octadecane (high Prandtl) and Tin (low Prandtl) in presence of natural convection in square cavity and (b) melting of fatty acids in presence of natural convection and radiation in a rectangular brick.

The results showed that natural convection plays an important role in the transitional behavior of the global heat transfer process and should not be neglected. The long wave radiation has limited impact on the melting process while the shortwave radiation increases heat transfer, however, this increase is not as important as that produced by convection for this kind of materials. Figure 1-15 shows that natural convection doubles the liquid fraction present in the enclosure whereas long wave radiation has marginal effects (<3%). In addition the consideration of shortwave radiation enhances the liquid fraction by 10% compared to the convection model.

Concerning the computational time, it was found 6 hours 21 minutes for LBM model, and 130 hours 20 minutes for the LBM-DOM model (20 times larger considering radiation). Finally, they stated that computional times are very high and simpler model for radiation should be used.

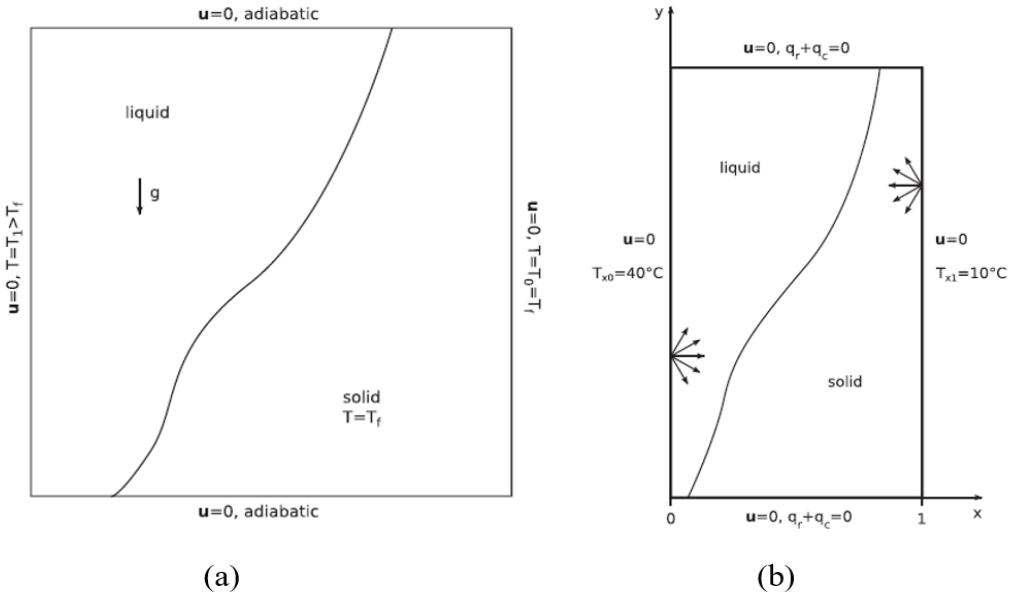

Figure 1-14: Thermal boundary conditions on the cavity for each case [63]

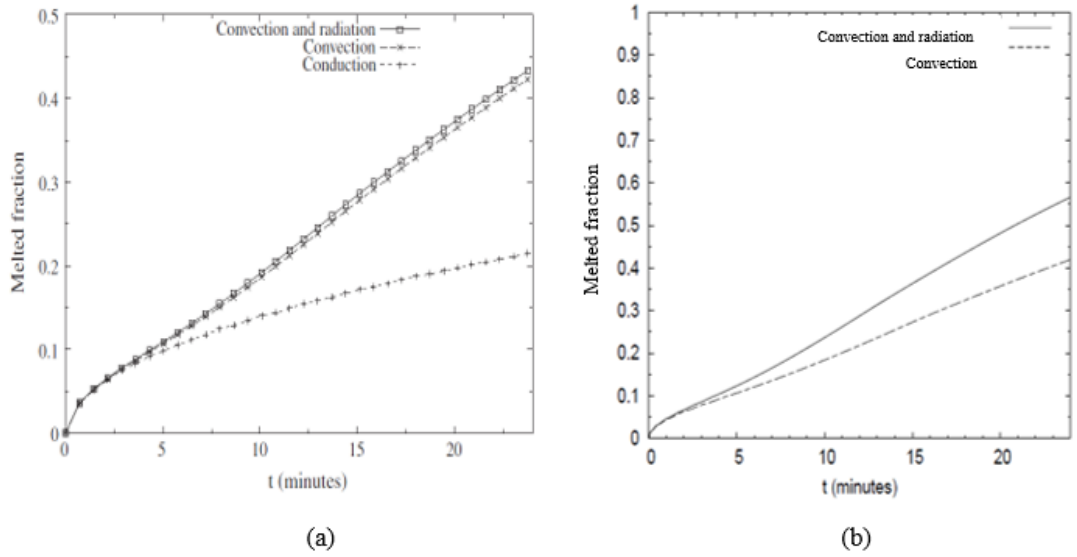

Figure 1-15: Melted fraction of the case of melting with convection and (a) long wave radiation, and (b) shortwave radiation

In the same context, another work was performed by Gong et al. [122]. They studied the melting of PCM (n-Octadecane) inside the rectangular transparent brick by both experimental and numerical approaches. This transparent brick, shown in Figure 1-16,a, was the same used to construct the TIM-PCM Trombe wall at the CETHIL's MINIBAT test cell. A non-intrusive experimental method was proposed (Figure 1-16, b). The two vertical surfaces of the enclosure were maintained with different but constant temperatures, the upper and front sides were kept available to record the inner process by a camera, and the bottom and back sides were insulated and kept adiabatic.

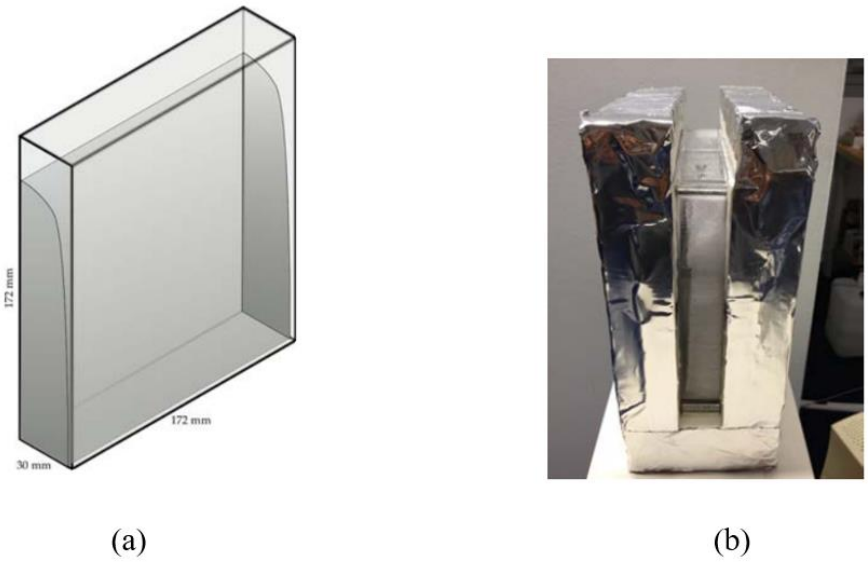

Figure 1-16: (a) Transparent brick filled with PCM, (b) experimental enclosure [122]

The experiments allowed to get enough data of the real physical melting process and showed that the heat transfer during melting process can be described as three stages: at the beginning, the pure conduction is the only form, then there is the competitive period of conduction and convection, and at the end, the convection prevails. In addition, the existence of natural convection dramatically influences the melting process. Numerically, the LBM with multiple-relaxation-time was used to solve the flow and the energy equation was used to solve the temperature distribution by finite difference scheme. Additionally, the enthalpy method was used to simulate the melting phase change. The simulation was specially designed to run on a CUDA enabled GPU to reduce the computational time. The simulation results demonstrated a good agreement with the experimental results (Figure 1-17).

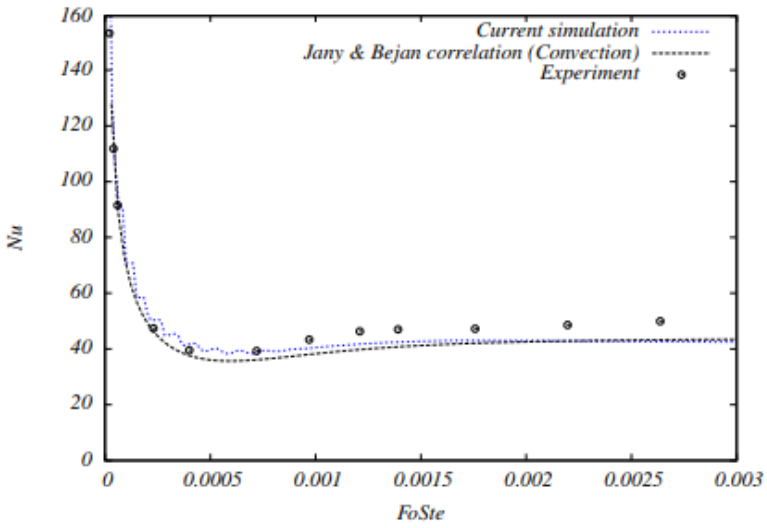

Figure 1-17: Comparison of Nusselt number of the 2D developed numerical model with the experimental results and Benchmark solution (Jany and Bejan)

However, for the computation efficiency, if was found that the performance decreases in three-dimensional simulation, and the CUDA programming pattern can't achieve ideal performance if there are many code divergences. Consequently, in the future, a more sophisticated approach should be devised in order to do this logic judgements in the code and to modify the solver to adapt to different or even more complex enclosures.

7. Discussion: Main limitations and thesis problematic and objectives

According to sections 2 and 3, we can state the following:

- Despite its importance, the effect of natural convection during melting process has been neglected in many studies. However, it is not sufficient to assume only conduction, and convection in the liquid phase should be taken into account.
- Convection heat transfer is less important than conduction during solidification process.
- The methods based on CFD, introducing Navier Stokes equations, and LBM models simulate the natural convection effect with more complexity and more realistic behavior. But these methods are time consuming and might require intensive computational power, even for a simple convection dominated phase change problem.
- The widely used enhanced conductivity approach, is fast and simple, however it has several shortages especially that it is unable to show the characteristics of phase change and cannot provide information about the melting front location. In addition, it is not recommended for high accuracy results.
- All numerical models for melting with natural convection collected have their own limitations, as the practical phase transformations in different applications are complicated, and the thermal conditions are not ideal. Various assumptions were set up for each numerical solution according to different numerical simulation purposes [18].
- The melting process consists mainly of three regimes: conduction-dominated regime, mixed conduction-convection regime and convection-dominated regime. These regimes are reflected by the average Nusselt number curve function of time. However, no consensuses were found on which one is the dominant heat transfer mechanism, which one can be ignored and how to combine these two transfer mechanisms in each modeling.
- The average Nusselt number is a key parameter in the convection dominated problem. To date, many correlations that have been developed in the literature are only suitable for a specific geometry and/or PCM.

According to section 4, we can state the follow:

- The integration of PCM in translucent facades increases the indoor thermal comfort of the building and consequently of occupant's satisfaction. It reduces the maximum indoor air temperature and increases the minimum indoor air temperature. It also increases the time lag between the imposed conditions and the internal conditions.
- Most previous works studying PCM-enhanced transparent components have been mainly developed for the heating season, and there is little quantification of their real advantages in terms of energy efficiency and indoor environmental comfort in summer season.
- Most studies on translucent facades have assumed one-dimensional transfers by conduction and radiation neglecting convection [98]–[100] and numerical models were specifically developed to take the interaction of PCM with solar radiation into account [12], [15], [123], [124].
- The interaction of convection and radiation has rarely been studied in the literature.
- In such walls as the INERTRANS wall, solidification is more likely to happen at night, in absence of solar radiation. Thus, the convection and radiation heat transfers are more important during melting process.

<u>According to section 6, we can state the follow:</u>

- The experimentations performed by Berthou et al. [121] showed that the performance of the TIM-PCM wall should be optimized, and solutions to overcome summer overheating and PCM cycling should be proposed. In their work, they were not able to properly present an experimentally validated numerical model to study the annual energy performance of the whole building, the reason is probably that the natural convection was not properly considered in the model. And thus, the question of an experimentally validated numerical model allowing the optimization of such a wall under different conditions is still open.
- Fuentes et al. [85] developed a LBM-DOM model to study the melting of fatty acids filled in glass bricks in presence of natural convection and radiation. The coupling of these phenomena was still not sufficiently studied in scientific literature. They emphasized on the importance of considering natural convection in the liquid PCM filled in glass bricks. However, the developed model requires a high computational time for a relatively small simulation time. Thus, it can't be used for yearly energy evaluation. Simpler model for radiation and natural convection during melting is still an open question.
- Gong et al. [122] focused in their work on the important issue of the melting process inside the brick. The radiation in the brick was not taken into account and the developed sophisticate model was not shown to be linkeable to energy simulation tool such as TRNSYS or Energy Plus for annual basis assessment.

Consequently, a lot of work needs to be done in the context of INERTRANS project, and principally the establishment of a numerical model that can represent the physics of the TIM-PCM wall, considering natural convection and radiation during PCM melting process. The model needs to be fast enough to be coupled with global energy simulation tool (such as TRNSYS) to perform annual energy assessment of a whole building integrating such a wall. Once the needed model is created and experimentally validated, the optimization of the TIM-PCM wall performance might be done under different conditions and configurations.

The objectives of this thesis can thus be written as follows:

1. To develop a 2D simplified numerical model for phase change in presence of natural convection (without recurring to the full solution of the Navier Stokes equations). In this work, the phase change is modelled using a fixed grid enthalpy method, the natural convection in the liquid PCM is accounted for using Bejan's scaling theory approach coupled with the enhanced conductivity method.
The simplified enhanced conductivity approach, used by many authors [26], [65], [67]–[69], [66], considers that the convection effect is prevalent in the whole liquid PCM, which is not true. The scaling theory proposed by Bejan [40] [37] allows to get a clear understanding of the role of natural convection in the liquid PCM through the sequence of mainly three regimes (pure conduction, mixed (transition) and convection regimes) and to adequately presenting the convection effect during melting process, especially the shape and the position of the melting front. That is why in this work these two approaches will be coupled. The equations are discretized using 2D implicit finite volume method and the code is written in MATLAB.
The model will be then validated using numerical and experimental benchmark solutions found in literature, in addition to a CFD model previously created in COMSOL for a test case: melting of Octadecane in square cavity; the computational simulations time are compared. Details and results are presented in chapter 2.

2. To develop a 2D simplified numerical model for phase change of fatty acids filled in glass bricks in presence of natural convection and shortwave radiation in the dynamic regime. The nodal absorptivity and transmissivity in the PCM are evaluated function of the liquid fraction, and the absorbed shortwave radiation is added to the energy equation as source term.
The model will be validated using the results of Fuentes et.al [85] of the LBM-DOM method (the only reference found in scientific literature for phase change in presence of natural convection and radiation). Details and results are presented in chapter 2.

3. To properly model the heat transfer through the TIM-PCM wall and then to couple the model with a global building energy simulation tool, TRNSYS, in order to study the energy performance of the whole building. The transmission of solar radiation through the wall layer is evaluated using Seigel equations. All details about the developed heat transfer model and the link MATLAB-TRNSYS are presented in chapter 3. To validate the coupled model, we have used the experimental cell present in PERSEE center of Mines ParisTech graduate school located in Sophia Antipolis. The experimental cell already exists and in the current thesis, we have just collected the data for summer and winter 2017 (see chapter 3).

4. Using the experimentally validated model, to propose passive solutions to optimize the wall behavior in summer conditions (see end of chapter 3).

5. To study the thermal behavior of an office building with integrated TIM-PCM wall under different climatic conditions and its impact on the indoor thermal comfort in summer conditions (more details in chapter 3), to compare its performance to that of the same building using a conventional double glazing, and to perform an economic analysis of the application of the wall. Details and results are presented in chapter 4.

In the above chapter, heat transfer mechanisms during the phase change were discussed. A literature review of the numerical models of phase change considering natural convection, as well as a state of the art of PCM integrated in transparent systems were presented. The TIM-PCM wall was described, in addition the problematic and the objectives of the thesis were identified. In the next chapter, a simplified model taking into account natural convection and radiation during phase change will be developed. The equations governing these phenomena as well as their simplifying assumptions, and the numerical methods adapted to their solution are presented.

References

[1] "OECD, World Energy Outlook 2012, Organisation for Economic Cooperation and Development, Paris, France, 2012." .

[2] "Directive 2010/31/EU of the European Parliament and of the Council of 19 May 2010 on the energy performance of buildings. Off J Eur Union, 2010; 53:13–35." .

[3] "Bosch J, Johnson FX, Clément E, Mertens R, Roubanis N. Panorama of energy – energy statistics to support EU policies and solutions. Luxembourg: Office for Official Publications of the European Communities; 2009." .

[4] "European Union. European Commission Energy Topics. 1995–2015." .

[5] "Cappelletti F, Prada A, Romagnoni P, Gasparella A. Passive performance of glazed components in heating and cooling of an open-space office under controlled indoor thermal comfort. Build Environ 2014;72:131–44."

[6] "Gomes MG, Santos AJ, Rodrigues AM. Solar and visible optical properties of glazing systems with venetian blinds: Numerical, experimental and blind control study. Build Environ 2014;71:47–59."

[7] "Peng J, Lu L, Yang H. An experimental study of the thermal performance of a novel photovoltaic double-skin facade in Hong Kong. Sol Energy 2013;97:293–304."

[8] "Ghoshal S, Neogi S. Advance glazing system – energy efficiency approach for buildings a review. Energy Procedia 2014;54:352–8."

[9] "Wang T-P, Wang L-B, Li B-Q. A model of the long-wave radiation heat transfer through a glazing. Energy Build 2013;59:50–61."

[10] "] Grynning S, Gustavsen A, Time B, Jelle BP. Windows in the buildings of tomorrow: energy losers or energy gainers? Energy Build 2013;61:185–92."

[11] "Grynning S, Goia F, Rognvik E, Time B. Possibilities for characterization of a PCM window system using large scale measurements. Int J Sustain Built Environ 2013;2:56–64."

[12] F. Goia, M. Perino, and M. Haase, "A numerical model to evaluate the thermal behaviour of PCM glazing system configurations," Energy Build., vol. 54, pp. 141–153, 2012.

[13] H. Manz, P. . Egolf, P. Suter, and A. Goetzberger, "TIM–PCM external wall system for solar space heating and daylighting," Sol. Energy, vol. 61, no. 6, pp. 369–379, Dec. 1997.

[14] K. A. R. Ismail, C. T. Salinas, and J. R. Henriquez, "Comparison between PCM filled glass windows and absorbing gas filled windows," Energy Build., vol. 40, no. 5, pp. 710–719, Jan. 2008.

[15] K. A. R. Ismail and J. R. Henrıquez, "Parametric study on composite and PCM glass systems," Energy Convers. Manag., vol. 43, no. 7, pp. 973–993, 2002.

[16] H. Weinläder, A. Beck, and J. Fricke, "PCM-facade-panel for daylighting and room heating," Sol. Energy, vol. 78, no. 2, pp. 177–186, Feb. 2005.

[17] "F. Goia, M. Perino, V. Serra, F. Zanghirella, Experimental assessment of the thermal behaviour of a PCM grazing, in: Proceedings of IAQVEC 2010, Syracuse, New York, USA, 15–18 August, 2010, pp. 1–8 (Paper Ref. 21–34)."

[18] S. Liu, Y. Li, and Y. Zhang, "Mathematical solutions and numerical models employed for the investigations of PCMs′ phase transformations," Renew. Sustain. Energy Rev., vol. 33, pp. 659–674, May 2014.

[19] E. Sparrow and S. Patankar, "Analysis of melting in the presence of natural convection in the melt region," ASME J Heat Transf, vol. 99:520–6, 1977.

[20] E. Sparrow and J. Ramsey, "Melting and natural convection due to a vertical embedded heater.," J Heat Transf, pp. 100:368–70, 1978.

[21] L. Yao and F. Chen, "Effects of natural convection in the melted region around a heated horizontal cylinder," ASME J Heat Transf, vol. 102:667–72, 1980.

[22] R. VISKANTA and N. Hale, "Photographic observation of the solid–liquid interface motion during melting of a solid heat from an isothermal vertical wall.," Lett Heat Mass Transf, vol. 5:329–37., 1978.

[23] A. Bathelt and R. VISKANTA, "An experimental investigation of natural convection in the melted region around a heated horizontal cylinder.," J Fluid Mech, pp. 1979;90:227–39.

[24] C. Harrison and F. Weinberg, "The influence of convection on heat transferin liquid tin.," Metall Trans B, pp. 1985;16:355–7.

[25] D. Buddhi and N. BANSAL, "Solar thermal storage systems using phase change materials," Int J Heat energy res, vol. 12:547–55., 1988.

[26] M. FARID and R. HUSIAN, “An electrical storage heater using the phase change method of heat storage.,” Energy Convers Manag, vol. 30(3):219–30, 1990.
[27] A. Hasan, “Phase change material energy storage system employing palmitic acid,” Sol Energy, vol. 52:143–54, 1994.
[28] M. Lacroix and T. Duong, “Experimental improvements of heat transfer in a latent heat thermal energy storage unit with embedded heat sources,” Energy Convers. Manag., vol. 39, no. 8, pp. 703–716, 1998.
[29] Y. Zhang and J. Yi, “A simple method, the T-history method of determining the heat of fusion specific heat and thermal conductivity of phase change materials,” Meas Sci Technol, 1999.
[30] R. Velraj and R. seeniraj, “Heat transfer enhancement in a latent heat storage system,” Sol Energy, 1999.
[31] A. SARI and K. KAYGUSUZ, “Thermal energy storage system using stearic acid as a phase change material,” Sol Energy, 2001.
[32] P. Lamberg, R. Lehtiniemi, and A.-M. Henell, “Numerical and experimental investigation of melting and freezing processes in phase change material storage,” Int. J. Therm. Sci., vol. 43, no. 3, pp. 277–287, Mar. 2004.
[33] X. Faure, “Enveloppe hybride pour bâtiment à haute performance énergétique,” Université Joseph-Fourier-Grenoble I, 2007.
[34] “Sasaguchi K, Viskanta R. Phase change heat transfer during melting and re-solidification of the melt area around cylindrical heat source (s)/sink(s). J Energy Resour Technol 1989;111:43–9.”
[35] Özisik MN. Heat conduction. New York: Wiley; 1980. .
[36] “Alexiades V. Mathematical modeling of melting and freezing processes. Washington: Hemisphere Publishing Corporation; 1993.”
[37] A. Bejan, Convection heat transfer, Fourth edition. Hoboken, New Jersey: Wiley, 2013.
[38] M. Lacroix and M. Benmadda, “Numerical simulation of natural convectiondominated melting and solidification from a finned vertical wall,” Numer. Heat Transfer, no. Part A Appl. 31, pp. 71–86, 1997.
[39] R. Velraj, R. seeniraj, B. Hafner, C. Faber, and K. Schwarzer, “HEAT TRANSFER ENHANCEMENT IN A LATENT HEAT STORAGE SYSTEM,” Solar Energy, vol. 65, no. No. 3, pp. 171–180, 1999.
[40] P. Jany and A. Bejan, “Scaling theory of melting with natural convection in an enclosure,” Int. J. Heat Mass Transf., vol. 31, no. 6, pp. 1221–1235, Jun. 1988.
[41] K. Morgan, “A numerical analysis of freezing and melting with convection,” Comp. Meth. App. Eng., vol. Vol. 28, pp. 275–84, 1981.
[42] J. Hsiao, “An efficient algorithm for finite difference analysis of heat transfer with melting and solidification,” ASME Paper No. WA/HT-42, 1984.
[43] A. . Brent and V. R. Voller, “Enthalpy-porosity technique for modeling convection-diffusion phase change: application to the melting of a pure metal,” Numerical Heat Transfer, vol. Vol. 13, pp. 297–318, 1988.
[44] B. Binet and M. Lacroix, “Melting from heat sources flush mounted on a conducting vertical wall,” Int. J. Num. Meth. Heat & Fluid Flow, vol. Vol. 10, pp. 286-306., 2000.
[45] Y. Cao and A. Faghri, “A numerical analysis of phase change problem including natural convection,” J HEAT TRANSFER, vol. 112, pp. 812–15, 1990.
[46] S. Wang, A. Faghri, and T. L. Bergman, “A comprehensive numerical model for melting with natural convection,” Int. J. Heat Mass Transf., vol. 53, no. 9–10, pp. 1986–2000, Apr. 2010.
[47] Z. Ma and Y. Zhang, “Solid velocity correction schemes for a temperature transforming model for convection phase change,” Int. J. Numer. Methods Heat Fluid Flow, vol. 16, no. 2, pp. 204–225, Feb. 2006.
[48] V. Voller and M. Cross, “An enthalpy method for convection/ diffusion phase change,” Int J Numer Methods Eng, vol. 24:271–84., 1987.
[49] V. Shatikian, G. Ziskind, and R. Letan, “Numerical investigation of a PCM-based heat sink with internal fins,” Int. J. Heat Mass Transf., vol. 48, no. 17, pp. 3689–3706, Aug. 2005.
[50] M. Faraji and H. El Qarnia, “Numerical study of melting in an enclosure with discrete protruding heat sources,” Appl. Math. Model., vol. 34, no. 5, pp. 1258–1275, May 2010.
[51] A. R. Archibold, M. M. Rahman, D. Y. Goswami, and E. K. Stefanakos, “Analysis of heat transfer and fluid flow during melting inside a spherical container for thermal energy storage,” Appl. Therm. Eng., vol. 64, no. 1–2, pp. 396–407, Mar. 2014.
[52] P. Wang, H. Yao, Z. Lan, Z. Peng, Y. Huang, and Y. Ding, “Numerical investigation of PCM melting process in sleeve tube with internal fins,” Energy Convers. Manag., vol. 110, pp. 428–435, Feb. 2016.

[53] Z. Liu, Y. Yao, and H. Wu, "Numerical modeling for solid–liquid phase change phenomena in porous media: Shell-and-tube type latent heat thermal energy storage," Appl. Energy, vol. 112, pp. 1222–1232, Dec. 2013.
[54] W.-B. Ye, D.-S. Zhu, and N. Wang, "Fluid flow and heat transfer in a latent thermal energy unit with different phase change material (PCM) cavity volume fractions," Appl. Therm. Eng., vol. 42, pp. 49–57, Sep. 2012.
[55] P. Goyal, A. Dutta, V. Verma, and I. T. R. Singh, "Enthalpy Porosity Method for CFD Simulation of Natural Convection Phenomenon for Phase Change Problems in the Molten Pool and its Importance during Melting of Solids."
[56] A. Faghri and Y. Cao, "Performance characteristics of a thermal energy storage module: a transient PCM/forced convection conjugate analysis," Int. J. HeatMass Transfer, pp. 93–101, 1991.
[57] P. Damronglerd and Zhang, "Modified temperature-transforming model for convection-controlled melting," AIAA J. Thermophy. Heat Transfer 21, pp. 203–208., 2007.
[58] x zeng and A. Faghri, "A temperature transforming model for binary solid–liquid phase change problems: Part I – mathematical modeling and numerical methodology," pp. 467–480, 1994.
[59] D. Groulx and P. H. Biwole, "Solar PV Passive Temperature Control Using Phase Change Materials," 2014.
[60] D. Chatterjee and S. Chakraborty, "An enthalpy-based lattice Boltzmann model for diffusion dominated solid–liquid phase transformation," Phys. Lett. A, vol. 341, no. 1–4, pp. 320–330, Jun. 2005.
[61] E. A. Semma, M. El Ganaoui, and R. Bennacer, "Lattice Boltzmann method for melting/solidification problems," Comptes Rendus Mécanique, vol. 335, no. 5–6, pp. 295–303, May 2007.
[62] C. Huber, A. Parmigiani, B. Chopard, M. Manga, and O. Bachmann, "Lattice Boltzmann model for melting with natural convection," Int. J. Heat Fluid Flow, vol. 29, no. 5, pp. 1469–1480, Oct. 2008.
[63] J. Miranda Fuentes, K. Johannes, F. Kuznik, M. Cosnier, and J. Virgone, "Melting with convection and radiation in a participating phase change material," Appl. Energy, vol. 109, pp. 454–461, Sep. 2013.
[64] M. M. Prieto and B. González, "Fluid flow and heat transfer in PCM panels arranged vertically and horizontally for application in heating systems," Renew. Energy, vol. 97, pp. 331–343, Nov. 2016.
[65] R. Kahraman, "A simplified model for melting of ice with natural convection," Int. Commun. Heat Mass Transfer, vol. 25, pp. 359–368, 1998.
[66] G. Vidalain, L. Gosselin, and M. Lacroix, "An enhanced thermal conduction model for the prediction of convection dominated solid–liquid phase change," Int. J. Heat Mass Transf., vol. 52, no. 7–8, pp. 1753–1760, Mar. 2009.
[67] P. Johansson, "Advanced Thermal Energy Storage Heat Transfer Study with Use of Comsol and Matlab," 2011.
[68] M. Costa and D. Buddhi, "Numerical simulation of a latent heat thermal energy storage system with enhanced heat conduction.," Energy Convers Manag, vol. 39:319–30., 1998.
[69] P. Dolado, A. Lazaro, J. M. Marin, and B. Zalba, "Characterization of melting and solidification in a real scale PCM-air heat exchanger: Numerical model and experimental validation," Energy Convers. Manag., vol. 52, no. 4, pp. 1890–1907, Apr. 2011.
[70] N. A. M. Amin, F. Bruno, and M. Belusko, "Effective thermal conductivity for melting in PCM encapsulated in a sphere," Appl. Energy, vol. 122, pp. 280–287, Jun. 2014.
[71] A. Castell and C. Solé, "An overview on design methodologies for liquid–solid PCM storage systems," Renew. Sustain. Energy Rev., vol. 52, pp. 289–307, Dec. 2015.
[72] B. W. Webb and R. VISKANTA, "On the characteristic length scale for correlating melting heat transfer data," Int. Commun. Heat Mass Transfer, vol. 12, pp. 637–646, 1985.
[73] C. Beckermann and R. Viskanta, "Effect of solid subcooling on natural convection melting of a pure metal," J. Heat Transf., vol. 111, no. 2, pp. 416–424, 1989.
[74] A. Brent, V. Voller, and K. Reid, "Enthalpy-porosity technique for modeling convection-diffusion phase change: application tothe melting of a pure metal.," Numer Heat Transfer, vol. 13:297–318., 1988.
[75] Y. Wang, A. Amiri, and K. Vafai, "An experimental investigation of the melting process in a rectangular enclosure," Int. J. Heat Mass Transf., vol. 42, no. 19, pp. 3659–3672, 1999.
[76] Z. Gong, S. Devahastin, and A. Mujumdar, "Enhanced heat transfer in free convection-dominated melting in a rectangular cavity with an isothermal vertical wall.," Appl Therm Eng, vol. 19:1237–51., 1999.
[77] Z. Younsi, A. Joulin, L. Zalewski, S. Lassue, and D. R. Rousse, "Phase change materials: a numerical method for the behavior predictions," in Proceedings of the Fourth International Conference on Thermal Engineering: Theory and Applications January, 2009, pp. 12–14.

[78] R. E. Murray and D. Groulx, "Modeling convection during melting of a phase change material," in Proceedings of the COMSOL Conference, 2011.
[79] D. Yanxia, Y. Yanping, J. Daiyong, C. Baoyi, and M. Jinfeng, "Experimental investigation on melting characteristics of ethanolamine–water binary mixture used as PCM," Int. Commun. Heat Mass Transf., vol. 34, no. 9–10, pp. 1056–1063, Nov. 2007.
[80] C.-J. Ho and R. Viskanta, "Heat Transfer During Melting From an Isothermal Vertical Wall," J. Heat Transf., vol. 106, no. 1, p. 12, 1984.
[81] "Yao LS, Cherney W. Transient phase-change around a horizontal cylinder. Int J Heat Mass Transf 1981;24:1971–81."
[82] "Rieger H, Projahn U, Beer H. Analysis of the heat transport mechanisms during melting around a horizontal circular cylinder. Int J Heat Mass Transf 1982;25:137–47."
[83] "Ismail KAR, da Silva MGE. Melting of PCM around a horizontal cylinder with constant surface temperature. Int J Therm Sci 2003;42:1145–52."
[84] "Furzerland RM. A comparative study of numerical methods for moving boundary problems. J Inst Math Appl 1980;26:411–29."
[85] J. M. Fuentes, "Développement d'un modèle de Boltzmann sur gaz réseau pour l'étude du changement de phase en présence de convection naturelle et de rayonnement," INSA de Lyon, 2013.
[86] N. Hannoun, V. Alexiades, and T. Z. Mai, "A reference solution for phase change with convection," Int J Numer Methods Fluids, vol. 48, pp. 1283–1308, 2005.
[87] N. Hannoun, V. Alexiades, and T. Z. Mai, "Resolving the controversy over tin and gallium melting in a rectangular cavity heated from the side," Numer Heat Transfer, vol. 44, pp. 253–276, 2003.
[88] A. Ghosh, B. Norton, and A. Duffy, "Measured thermal & daylight performance of an evacuated glazing using an outdoor test cell," Appl. Energy, vol. 177, pp. 196–203, Sep. 2016.
[89] F. Favoino, F. Fiorito, A. Cannavale, G. Ranzi, and M. Overend, "Optimal control and performance of photovoltachromic switchable glazing for building integration in temperate climates," Appl. Energy, vol. 178, pp. 943–961, Sep. 2016.
[90] N. DeForest, A. Shehabi, S. Selkowitz, and D. J. Milliron, "A comparative energy analysis of three electrochromic glazing technologies in commercial and residential buildings," Appl. Energy, vol. 192, pp. 95–109, Apr. 2017.
[91] D. Buddhi and S. D. Sharma, "Measurements of transmittance of solar radiation through stearic acid: a latent heat storage material," Energy Convers. Manag., vol. 40, no. 18, pp. 1979–1984, 1999.
[92] F. Goia, M. Perino, and V. Serra, "Experimental analysis of the energy performance of a full-scale PCM glazing prototype," Sol. Energy, vol. 100, pp. 217–233, 2014.
[93] B. L. Gowreesunker, S. B. Stankovic, S. A. Tassou, and P. A. Kyriacou, "Experimental and numerical investigations of the optical and thermal aspects of a PCM-glazed unit," Energy Build., vol. 61, pp. 239–249, Jun. 2013.
[94] S. Li, G. Sun, K. Zou, and X. Zhang, "Experimental research on the dynamic thermal performance of a novel triple-pane building window filled with PCM," Sustain. Cities Soc., vol. 27, pp. 15–22, Nov. 2016.
[95] S. Grynning, F. Goia, and B. Time, "Dynamic Thermal Performance of a PCM Window System: Characterization Using Large Scale Measurements," Energy Procedia, vol. 78, pp. 85–90, Nov. 2015.
[96] F. Goia, M. Perino, and V. Serra, "Improving thermal comfort conditions by means of PCM glazing systems," Energy Build., vol. 60, pp. 442–452, May 2013.
[97] C. Liu, Y. Wu, J. Bian, D. Li, and X. Liu, "Influence of PCM design parameters on thermal and optical performance of multi-layer glazed roof," Appl. Energy, vol. 212, pp. 151–161, Feb. 2018.
[98] F. Goia, "Thermo-physical behaviour and energy performance assessment of PCM glazing system configurations: A numerical analysis," Front. Archit. Res., vol. 1, no. 4, pp. 341–347, Dec. 2012.
[99] K. Zhong, S. Li, G. Sun, S. Li, and X. Zhang, "Simulation study on dynamic heat transfer performance of PCM-filled glass window with different thermophysical parameters of phase change material," Energy Build., vol. 106, pp. 87–95, 2015.
[100] K. A. R. Ismail, C. T. Salinas, and J. R. Henriquez, "Comparison between PCM filled glass windows and absorbing gas filled windows," Energy Build., vol. 40, no. 5, pp. 710–719, Jan. 2008.
[101] T. Silva, R. Vicente, and F. Rodrigues, "Literature review on the use of phase change materials in glazing and shading solutions," Renew. Sustain. Energy Rev., vol. 53, pp. 515–535, Jan. 2016.
[102] "L. A. Diaz and R. Viskanta, 'Experiments and analysis on the melting of a semitransparent material by radiation,' Heat Mass Transfer, vol. 20, pp. 311–321, 1986. 10.1007/BF01002422."

[103] G. Colomer Rey, Numerical methods for radiative heat transfer. Universitat Politècnica de Catalunya, 2006.
[104] F. Trombe, "Heating by solar radiation." CNRS Internal Report B-1- 73-100., 1973.
[105] P. Ohanessian and W. W. . Charters, "Thermal simulation of a passive solar house using a Trombe-Michel wall structure.," Sol. Energy 20, pp. 275–281, 1978.
[106] A. V. Sebald, J. R. Clinton, and F. Langenbacher, "Performance effects of Trombe wall control strategies.," Sol. Energy 23 (6), pp. 479–487, 1979.
[107] E. Kruger, E. Suzuki, and A. Matoski, "Evaluation of a Trombe wall system in a subtropical location.," Energy Build., vol. 66, pp. 364–372, 2013.
[108] M. Bojic, K. Johannes, and F. Alamdari, "Optimizing energy and environmental performance of passive Trombe wall," Energy Build, vol. 70, pp. 279–286, 2014.
[109] M. Telkes, "Trombe wall with phase change storage material," in Proceedings of the 2nd National Passive Solar Conference, Philadelphia, PA, USA., 1978.
[110] F. Fiorito, "Trombe walls for lightweight buildings in temperate and hot climates. exploring the use of phase-change materials for performances improvement.," Energy Procedia, vol. 30, pp. 1110–1119, 2012.
[111] L. Zalewski, A. Joulin, S. Lassue, and Y. Dutil, "Experimental study of small-scale solar wall integrating phase change material," Sol. Energy, no. 86, pp. 208–219, 2012.
[112] A. de Gracia, L. Navarro, A. Castell, A. Ruiz-Pardo, S. Alvarez, and L. F. Cabeza, "Experimental study of a ventilated facade with PCM during winter period," Energy Build., pp. 58, 324–332, 2013.
[113] L. Yongcai and L. Shuli, "Experimental study on thermal performance of a solar chimney combined with PCM," Appl. Energy 114, pp. 172–178, 2014.
[114] G. Diarce et al., "Ventilated active façades with PCM," Appl. Energy, vol. 109, pp. 530–537, Sep. 2013.
[115] Z. Hu, W. He, J. Ji, and S. Zhang, "A review on the application of Trombe wall system in buildings," Renew. Sustain. Energy Rev., vol. 70, pp. 976–987, Apr. 2017.
[116] Y. A. Kara and A. Kurnuç, "Performance of coupled novel triple glass unit and pcm wall," Appl. Therm. Eng., vol. 35, pp. 243–246, Mar. 2012.
[117] N. D. Kaushika and K. Sumathy, "Solar transparent insulation materials: a review," Renew. Sustain. Energy Rev., vol. 7, no. 4, pp. 317–351, Aug. 2003.
[118] I. L. Wong, P. C. Eames, and R. S. Perera, "A review of transparent insulation systems and the evaluation of payback period for building applications," Sol. Energy, vol. 81, no. 9, pp. 1058–1071, Sep. 2007.
[119] "Goetzberger A., Schmid J. andWittwer V. (1984) Transparent insulation system for passive solar energy utilization in buildings. In Proc. First E.C. Conference on Solar Heating. D. Reidel Publishing Company, Dordrecht, pp. 314–318."
[120] K. Johannes, F. Kuznik, F. Jay, P. Roquette, P. Achard, and Y. Berthou, "CRISTOPIA ENERGY SYSTEMS, SAVERBAT SAS,Elément d'enveloppe d'un bâtiment et ensemble comprenant un tel élément," Brevet Francais FR 1158194, 15-Mar-2013.
[121] Y. Berthou, P. H. Biwole, P. Achard, H. Sallée, M. Tantot-Neirac, and F. Jay, "Full scale experimentation on a new translucent passive solar wall combining silica aerogels and phase change materials," Sol. Energy, vol. 115, pp. 733–742, May 2015.
[122] W. Gong, "Heat storage of PCM inside a transparent building brick: Experimental study and LBM simulation on GPU," p. 186.
[123] C. Liu, Y. Zhou, D. Li, F. Meng, Y. Zheng, and X. Liu, "Numerical analysis on thermal performance of a PCM-filled double glazing roof," Energy Build., vol. 125, pp. 267–275, 2016.
[124] C. Liu, Y. Zheng, D. Li, H. Qi, and X. Liu, "A Model to Determine Thermal Performance of a Non-ventilated Double Glazing Unit with PCM and Experimental Validation," Procedia Eng., vol. 157, pp. 293–300, 2016.

CHAPTER 2

MELTING OF A PHASE CHANGE MATERIAL IN PRESENCE OF NATURAL CONVECTION AND RADIATION: A SIMPLIFIED MODEL

Chapter 2. Melting of a Phase Change Material in Presence of Natural Convection and Radiation: A Simplified Model

Résumé du chapitre en français :

Fusion d'un matériau à changement de phase en présence de convection naturelle et de rayonnement : un modèle simplifié

Un modèle simplifié pour modéliser la convection naturelle et le rayonnement courte longueur d'onde (CLO) pendant le processus de fusion d'un matériau à changement de phase est présenté dans ce chapitre. Pour modéliser le changement de phase, une méthode « enthalpique » modifiée a été utilisée. La convection naturelle qui apparaît dans le MCP liquide est prise en compte en utilisant l'approche de conductivité thermique efficace couplée avec la théorie d'échelle sans la résolution complète des équations de Navier-Stokes (N-S), tandis que le flux de rayonnement CLO absorbé est ajouté à l'équation d'énergie en tant que terme source en utilisant un algorithme simplifié. Le modèle mathématique est codé sous MATLAB en utilisant une méthode de volumes finis implicite en deux dimensions.

Ensuite, un modèle CFD complet est créé et mis en œuvre dans COMSOL Multiphysics en adoptant la méthode de capacité thermique modifiée. En particulier, une corrélation du nombre de Nusselt correspondant à notre cas d'étude est trouvée, sur la base du modèle CFD, et est ensuite implémentée dans le modèle simplifié pour calculer la conductivité efficace. Les résultats du modèle simplifié sont comparés à ceux du modèle CFD créé dans COMSOL, et aux résultats numériques et expérimentaux des benchmarks trouvés dans la littérature. Les résultats montrent que, pour un temps de calcul 45 fois plus court que celui de la CFD, les valeurs de fraction liquide moyenne, de la position du front de fusion à quatre instants différents, et de la position moyenne du front de fusion en fonction de temps sont acceptables avec des différences inférieures à 6%, 14% et 13% respectivement. D'autre part, les résultats du modèle simplifié montrent un très bon accord avec ceux des solutions des benchmarks. De plus, la modélisation de la convection naturelle pendant la fusion, modifie la fraction liquide moyenne d'environ 40% et la position du front de fusion d'environ 55% à l'instant adimensionnel SteFo = 0.01 par rapport à un modèle à conduction seule.

Puis, le modèle développé couplant la convection naturelle et le rayonnement courte longueur d'onde lors de la fusion est appliqué pour modéliser la fusion de l'acide gras intégré dans les briques de verre de la paroi INERTRANS. Les résultats obtenus sont en très bon accord avec les résultats d'un modèle de Boltzmann sur réseau et la méthode des ordonnées discrètes (LBM-DOM) trouvés dans la littérature, en termes de la fraction liquide moyenne. Il a été constaté que la convection naturelle fait

augmenter la fraction liquide d'environ 35% par rapport au modèle à conduction seule, tandis que le rayonnement CLO fait augmenter la fraction liquide d'environ 20% par rapport au modèle incluant la convection. En ce qui concerne le temps du calcul, les simulations du modèle simplifié sont beaucoup plus rapides par rapport au modèle LBM-DOM.

Le modèle proposé considérant à la fois la convection naturelle et le rayonnement pendant le processus de fusion est simple à mettre en œuvre et peut gérer efficacement les problèmes de changement de phase dominés par convection sans la résolution complète de l'écoulement dans un temps de calcul relativement court. Cependant, ce modèle simplifié est une représentation conceptuelle de la réalité, et il a été développé pour les applications pratiques de l'ingénierie thermique, où on cherche une évaluation annuelle de la performance énergétique. Dans le chapitre suivant, le modèle simplifié est utilisé pour simuler le comportement thermique de l'ensemble du mur INERTRANS sur une base annuelle, le processus de solidification étant également pris en compte. Le modèle simplifié pourrait également être intégré dans un outil de simulation d'énergie (par exemple TRNSYS ou EnergyPlus) pour évaluer le comportement thermique annuel d'un bâtiment.

Dans le chapitre suivant, le modèle simplifié sera utilisé pour simuler le comportement thermique du mur INERTRANS. Ensuite, il sera couplé à un outil de simulation énergétique globale (TRNSYS) pour évaluer le comportement thermique annuel de l'ensemble du bâtiment.

Abstract

In this chapter, a simplified model for melting of a phase change material (PCM) in presence of natural convection and radiation is presented. A modified enthalpy method is adopted to solve the phase change problem, the natural convection occurring in the liquid PCM is accounted for using the enhanced thermal conductivity approach coupled with the scaling theory, and the absorbed shortwave radiation flux is added into the energy equation as a source term using a simplified solution algorithm. Two-dimensional implicit finite volume method is used to solve the energy equation. First, the simplified model for melting with natural convection is validated using a CFD model, in addition to experimental and numerical benchmark solutions for a test case. Then, the simplified model for melting with combined natural convection and radiation is applied to the melting of a fatty acid eutectic filled in glass bricks, which will be used later to model the annual thermal behavior of a special translucent façade. This complete model is validated against the lattice Boltzmann-discrete ordinate method LBM-DOM. It was shown that (1) the proposed simplified model is simple to implement, and its simulations run significantly faster than those of CFD models and LBM-DOM model. Consequently, it can be easily integrated into an energy simulation tool for yearly performance evaluation, (2) during PCM melting process, natural convection has a noteworthy role as it enhances the average fraction of liquid and the position of the melting front, (3) shortwave radiation enhances the average liquid fraction.

Keywords: Phase Change Materials, natural convection, shortwave radiation, computational time, enhanced thermal conductivity, scaling theory, CFD.

Highlights:

- Simplified model for melting with natural convection and radiation.
- Enhanced thermal conductivity approach coupled with the scaling theory.
- During PCM melting, natural convection has a notable role.
- The simplified model runs much faster than CFD and LBM models.
- The model can be integrated into energy simulation tool for annual evaluation.

1. Introduction

A new kind of translucent storage wall has been proposed, in the French INERTRANS(1) project, composed of glass layer, a translucent insulation (silica aerogel) and fatty acid eutectic mixture filled in glass bricks [1], [2]. The solid PCM absorbs the solar radiation, thus increasing its temperature until the complete melting, while in liquid phase, the PCM transmits solar radiation. Then, the heat transfer is conducted by conduction, natural convection and radiation during the phase change. To optimize the energy performance of this type of storage walls, numerical modeling of the heat transfer mechanisms in the wall materials is required and especially the melting with combined natural convection and radiation.

In the last twenty years, convection dominated phase change problems have become the subject of numerous studies [3]–[11] and the natural convection was shown as a significant mechanism during melting process, whenever convection motion has enough space to develop [12]. This phenomenon was investigated using both experimental [13]–[16] and numerical approaches [17]–[20]. Even though the experimental studies show more accurately the real behavior of PCM, researchers prefer to study the phase change problems by mathematical solutions and numerical simulations due to the fact that numerous conditions can be carried out by changing the variables in a numerical model [21]. Numerically, various methods are currently explored and used to model phase change of a PCM accounting for natural convection, mainly the enthalpy-porosity approach [22]–[29], the temperature transforming model (TTM) [30]–[33], the equivalent thermal capacity method [34], the modified heat capacity method [35], in addition to the integral method, the boundary fixing method, the unstructured finite-element method, and the coordinate transformation method [21]. In these methods, the Navier-Stokes equations i.e. the energy equations in the solid and liquid phases coupled with the continuity and momentum equations in the liquid must be solved, hence the problem becomes strongly non-linear. In addition, Lattice Boltzmann Method (LBM) [2], [36]–[38] is used as well to model the fluid flow during phase change.

The computational time can be quite large, depending on the used method, the simulated problem and the spatial and temporal discretization [39]. The melting of Tin, filled in a square enclosure of height 0.1m, in presence of natural convection has been studied by different authors [39] [40] [41]. The computational time for the melting of Tin was found 450 hours for a total simulation time of 700 seconds with a mesh size of 400 × 400 in [40]; the simulations were conducted using a Compaq Alpha ES40 machine. While the computational time using the LBM in [39], for a simulation time of 1000 seconds is found 76 hours with a mesh size of 400 × 400, the simulations were conducted using an Intel Xeon X5472. Moreover, Hannoun et al. [41] reported 2400 hours of CPU to simulate 2500 seconds of the melting of Tin with a mesh size of 200 × 200, using Compaq Alpha ev67 machine. In

addition, the simulation of 5000 seconds of the melting of Octadecane, filled in square enclosure of height 0.1m, with natural convection took 34 hours with a mesh size of 225 × 225 [39].

Usually in thermal engineering applications, where yearly energy performance evaluation is sought, the building models with integrated PCM ignore the convection effect in the liquid region, due to the complexity of CFD models and the required high computational time. Therefore, the transient heat conduction term is only considered in the energy equation [42]. Because the assumption of conduction alone is not always adequate, a simplified model considering the effect of natural convection without the complete solution of the Navier–Stokes equations is needed. The natural convection effect could be accounted model using the enhanced thermal conductivity approach [5], [43]–[47]. Here, the average Nusselt number is considered as a main parameter, because it describes the convective heat transfer coefficient, and influences the procedure dynamics [48]. In this approach, the convection effect is considered in the whole liquid PCM. The scaling theory proposed by Bejan [49] [50] allows to get a clear understanding of the role of natural convection in the liquid PCM through the sequence of mainly three regimes (pure conduction, mixed (transition) and convection regimes) and to adequately presenting the convection effect during melting process, especially the shape and the position of the melting front.

In this chapter, we develop a simplified model for convection and radiation during PCM melting (section 2). Natural convection in the liquid PCM is modeled based on the enhanced thermal conductivity approach and the scaling theory (section 3.1). This model is validated using the results of a CFD model developed in COMSOL Multiphysics solver (section 3.2), in addition to numerical and experimental benchmark solutions from the literature for a test case: melting of Octadecane in a square enclosure heated from its left vertical wall (sections 3.3-3.5). Based on the numerical CFD results, a correlation for the Nusselt number is proposed (section 3.4). Then, the short-wave radiation is modeled in the PCM using a simplified solution algorithm (section 4). Later on, a simplified method coupling the natural convection and the shortwave radiation during melting is applied to the fatty acid filled in glass bricks used in the *INERTRANS* wall. The results are compared and validated against a lattice Boltzmann method coupled with Discrete Ordinate Method (DOM) to model natural convection and radiation respectively, during the melting of a fatty acid eutectic mixture (section 5). In this paper, only melting is modeled for three reasons: (i) the experimental and numerical benchmarking data on melting to compare our simplified model with, is abundant in the literature, (ii) according to many authors [51] [52], convection heat transfer is less important than conduction during solidification process (iii) in such walls as the INERTRANS wall solidification is more likely to happen at night, in absence of solar radiation.

(1) INERTRANS is acronym of Translucent Inertia, project funded by the French National Research Agency, PREBAT 2007).

2. Numerical methodology

The main challenge of the mathematical modeling of melting process is to properly represent the moving melting front. There are two approaches to solve this problem: fixed grid methods where the melting front is determined implicitly by the temperature/enthalpy distribution, and the deforming grid methods where the energy equation is formulated for each state, and then coupled by energy balance at the solid-liquid boundary (Stefan's condition), the mesh moves to track the phase interface position.

In this study, a fixed-grid modified "enthalpy" method is used, inspired by the work of Zivkovic et al. [53] which allows a separate calculation of the temperature and the liquid fraction. This method was previously used in several studies for different applications [54] [55] [56]. The main advantages of this method are that the moving melting front does not necessitate to be treated explicitly, the energy equation is analogous to the single-phase equation and a mushy region is allowed between the two phases. The energy equation, with natural convection and radiation, is given as:

$$\rho \frac{\partial H}{\partial t} = div(kgrad\ T) + \emptyset_{sol} \qquad \textbf{Eq. 2-1}$$

Where H is the total enthalpy:

$$H = h + L_H f_l \qquad \textbf{Eq. 2-2}$$

and h is the sensible heat

$$h = \int_{Tm}^{T} Cp\ dT \qquad \textbf{Eq. 2-3}$$

The fraction of the liquid is defined as:

$$f_l = 0\ , \quad if\ T < Tm\ (solid)$$

$$f_l =]0,1[\ , \quad if\ T = Tm\ (mushy\ region)$$

$$f_l = 1\ , \quad if\ T > Tm\ (liquid) \qquad \textbf{Eq. 2-4}$$

The thermal conductivity is defined as:

$$k = k_s\ , \quad if\ T < Tm$$

$$k = k_{enh} f_l + k_s(1 - f_l)\ , \quad if\ T = Tm$$

$$k = k_{enh}\ , \quad if\ T > Tm \qquad \textbf{Eq. 2-5}$$

The thermal conductivity is enhanced in the liquid phase using the enhanced conductivity method coupled with the scaling theory approach explained in section 3.1.

In the convective zone,

$$k_{enh} \sim k_l(1 + Nu_z) \quad \textbf{Eq. 2-6}$$

Otherwise

$$k_{enh} = k_l \quad \textbf{Eq. 2-7}$$

Nu_z is the Nusselt number defined function of z, the height of the convective zone.

And $\emptyset_{sol}$ is the radiative source term; the shortwave radiation through the PCM is modeled by means of a solution procedure proposed by Gowreesunker [57] detailed in section 4.

The two-dimensional Eq. 2-8, obtained from Eq. 2-1 is then used:

$$\rho Cp \frac{\partial h}{\partial t} = \frac{\partial}{\partial x}\left(k \frac{\partial T}{\partial x}\right) + \frac{\partial}{\partial y}\left(k \frac{\partial T}{\partial y}\right) - \rho L_H \frac{\partial f_l}{\partial t} + \emptyset_{sol} \quad \textbf{Eq. 2-8}$$

To solve the two-dimensional 2D phase change problem, the implicit finite volume method by Patankar 1980 [58] is used. The computational domain is divided into rectangular control volumes (CV) and the code is written in Matlab®.

The finite volume equations are derived by integrating Eq. 2-8 over a typical control volume. It is also necessary, in time-dependent problems, to integrate with respect to time *t* over a small interval *Δt* from *t* to *t* + *Δt*. After integration, we obtain the discretization equation as follows:

$$a_P T_P^{t+\Delta t} = a_W T_W^{t+\Delta t} + a_E T_E^{t+\Delta t} + a_S T_S^{t+\Delta t} + a_N T_N^{t+\Delta t} + b \quad \textbf{Eq. 2-9}$$

Where,

$$a_W = k_w \frac{\Delta y}{(\Delta x)_w}, a_E = k_e \frac{\Delta y}{(\Delta x)_e}, a_S = k_s \frac{\Delta x}{(\Delta y)_s}, a_N = k_n \frac{\Delta x}{(\Delta y)_n}$$

$$a_P = a_W + a_E + a_S + a_N + a_P^0$$

$$a_P^0 = \frac{\rho Cp \Delta x \Delta y}{\Delta t}$$

$$b = a_P^0 T_P^0 + \emptyset_{sol} \quad \textbf{Eq. 2-10}$$

Where, the product $\Delta x \Delta y$ defines the volume of each control volume, and the index "0" designates the previous time step. Note that for the boundary nodes, the boundary conditions will be included in the vector b. Deriving the discretization equation for each CV, we form a system of linear equations that is written in a matrix form as:

$$A * T = B \quad \textbf{Eq. 2-11}$$

When phase change occurs in the control volume P, the liquid fraction is calculated using Eq. 2-13 and it is strictly in the range]0,1[while the temperature is fixed to the melting temperature.

$$T_P \equiv T_m \quad \textbf{Eq. 2-12}$$

$$f_{l_P} = f_{l_P}^0 + \frac{k_e \Delta t}{\rho L_H \Delta x^2}(T_E - T_m) - \frac{k_w \Delta t}{\rho L_H \Delta x^2}(T_m - T_W) + \frac{k_n \Delta t}{\rho L_H \Delta y^2}(T_N - T_m) - \frac{k_s \Delta t}{\rho L_H \Delta y^2}(T_m - T_S) + \frac{\emptyset_{sol}}{\rho L_H} \quad \textbf{Eq. 2-13}$$

3. Melting with natural convection

3.1. Simplified model

The natural convection during melting process, is accounted for using the approach of scaling theory [49] [50] together with the enhanced conductivity method [59]. At first, the PCM melting is ruled by conduction, the convection effect starts in the melt when the criterion of distinct thermal boundary layers [47] [49] [50] [60] is respected:

$$\left(\frac{s}{H}\right)^4 Ra_H \geq 1 \quad \textbf{Eq. 2-14}$$

Where *s* is the position of the melting front, *H* is the height of the enclosure and Ra_H is given by:

$$Ra_H = \frac{g\beta H^3 (T_h - T_m)}{\alpha \nu} \quad \textbf{Eq. 2-15}$$

Hence, the PCM liquid thermal conductivity is enhanced (Eq. 2-6) and the enhancement is performed in a square shaped convective zone of surface (z x z) situated in the left superior corner of the enclosure. The height *z* of the convective zone is assumed to be equal to s_h, the thickness of the liquid zone assessed at the top of the enclosure [47].

$$z = s_h \quad \textbf{Eq. 2-16}$$

At each time-step, the value of the enhanced conductivity k_{enh} that depends on z, must be updated. Here, Rayleigh number is calculated in function of z:

$$Ra_z = \frac{g\beta z^3 (T_h - T_m)}{\alpha \nu} \quad \textbf{Eq. 2-17}$$

and the Nusselt number Nu_z is calculated function of the Rayleigh number. Many general Nusselt number correlations for the natural convection inside an enclosure are found in the literature based on the aspect ratio, *Ra* and *Pr* number restrictions. Some of them are listed in Table 2-1. Several authors have presented Nusselt number correlations during melting process as summarized in Table 2-2. Noting that, these correlations are based on numerical or experimental observations. Therefore, they are valid under some restrictions such as the geometry configurations, PCM used, thermal boundary conditions and variables under which the studies were performed [48]. It is also

worthy to mention that the selection of the characteristic length in the formulas of Ra and Nu is very critical; the average position of the melting front (s_{av}) or either the height of the enclosure (H) could be used [49][61].

Table 2-1: General Nusselt number correlations for natural convection problem in an enclosure

Ref.	Characteristic length	Correlations	Restrictions
Berkovsky and Polevikov [62]	Width L	$\mathrm{Nu_L} = 0.22\left(\frac{\mathrm{Pr}}{0.2+\mathrm{Pr}}\mathrm{Ra_L}\right)^{0.28}\left(\frac{\mathrm{H}}{\mathrm{L}}\right)^{-0.25}$	$2 \le \mathrm{H/L} \le 10$ $\mathrm{Pr} \le 10^5$ $10^3 < \mathrm{Ra_L} < 10^{10}$
		$\mathrm{Nu_L} = 0.18\left(\frac{\mathrm{Pr}}{0.2+\mathrm{Pr}}\mathrm{Ra_L}\right)^{0.29}$	$1 \le \mathrm{H/L} < 2$ $10^{-3} \le \mathrm{Pr} \le 10^5$ $\frac{\mathrm{Pr}}{0.2+\mathrm{pr}}\mathrm{Ra_L} > 10^3$
Berkovsky and Polevikov [50]	Height H	$\mathrm{Nu_H} = 0.18\left(\frac{\mathrm{Pr}}{0.2+\mathrm{Pr}}\mathrm{Ra_H}\right)^{0.29}\left(\frac{\mathrm{L}}{\mathrm{H}}\right)^{-0.13}$	$1 \le \mathrm{H/L} < 2$ $10^{-3} < \mathrm{Pr} < 10^5$ $\frac{\mathrm{Pr}}{0.2+\mathrm{pr}}\mathrm{Ra_H}\left(\frac{\mathrm{L}}{\mathrm{H}}\right)^3 > 10^3$
		$\mathrm{Nu_H} = 0.22\left(\frac{\mathrm{Pr}}{0.2+\mathrm{Pr}}\mathrm{Ra_H}\right)^{0.28}\left(\frac{\mathrm{L}}{\mathrm{H}}\right)^{0.09}$	$2 \le \mathrm{H/L} < 10$ $\mathrm{Pr} < 10^5$ $\mathrm{Ra_H} < 10^{13}$
Seki et al. [63]	Height H	$\mathrm{Nu_H} = 0.36\ \mathrm{Ra_H^{0.25}Pr^{0.051}}\left(\frac{\mathrm{H}}{\mathrm{L}}\right)^{-0.11}$	$5 < \mathrm{H/L} < 47.5$ $3 < \mathrm{Pr} < 40000$ $10^7 < \mathrm{Ra_H} < 4 \times 10^9$
Macgregor and Emery [64]	Width L	$\mathrm{Nu_L} = 0.42\ \mathrm{Ra_L^{0.25}Pr^{0.012}}\left(\frac{\mathrm{H}}{\mathrm{L}}\right)^{-0.3}$	$10^4 < \mathrm{Ra_L} < 10^7$ $10 \le \mathrm{H/L} \le 40$ $1 \le \mathrm{Pr} \le 2 \times 10^4$
		$\mathrm{Nu_L} = 0.046\ \mathrm{Ra_L^{1/3}}$	$10^6 < \mathrm{Ra_L} < 10^9$ $1 < \mathrm{H/L} < 40$ $1 < \mathrm{Pr} < 20$
Markatos and Pericleous [65]	Width L	$\mathrm{Nu_L} = 0.143\ \mathrm{Ra_L^{0.299}}$	$\mathrm{H/L} = 1$ $10^3 < \mathrm{Ra_L} < 10^6$
		$\mathrm{Nu_L} = 0.082\ \mathrm{Ra_L^{0.329}}$	$\mathrm{H/L} = 1$ $10^6 < \mathrm{Ra_L} < 10^{12}$

Table 2-2: Nusselt number correlations for different phase change materials with natural convection during melting process

Ref.	PCM / geometry	Correlations	Restrictions
Wang et al.[14]	-Polyethylene glycol 900 -Rectangular cavity heated from the side	$\overline{Nu} = 0.0219\ Ra^{0.387}Pr^{0.019}\left(\frac{H}{\delta}\right)^{0.0625}$	$2.02\text{x}10^6 \le \mathrm{Ra} \le 2.61 \times 10^7$ $Ste.Fo = 0.001 - 0.125$ $Pr = 804 - 1055$

Yanxia et al. [39]	- Ethanolamine–water binary mixture - Rectangular enclosure heated from its vertical wall	$\overline{Nu} = 0.198\, Ste^{-0.122}\, Ra^{0.258} Pr^{0.018}$	The valid range of the correlation is 0.04Nu value.
Ho and Viskanta [66]	- n-Octadecane - Rectangular cavity with conducting vertical walls.	$\overline{Nu} = 0.189\, Ra^{0.319}$	$10^3 \leq \mathrm{Ra} \leq 4.1 \times 10^5$
Gau and Viskanta [67]	- Gallium - Rectangular test cell	$\overline{\mathrm{Nu}} = 0.0631\left(\frac{\mathrm{Ra}}{\mathrm{Ste}}\right)^{0.274}$	Valid for conduction, mixed and convection regimes.
Pal and Joshi [68]	-n-triacontane - A side heated tall enclosure under constant heat flux boundary conditions	$\overline{\mathrm{Nu}} = 0.01559\left(\frac{\mathrm{Ra}^{1/5}}{\mathrm{Ste.\,Fo}}\right)^{0.4}$	$\frac{Ra^{1/5}}{Ste.Fo} < 0.0003$
Bejan [49]	-	$Nu = (2\theta)^{-\frac{1}{2}} + \left[0.35Ra^{\frac{1}{4}} - (2\theta)^{-\frac{1}{2}}\right]\left[1 + \left(0.0175Ra^{\frac{3}{4}}\theta^{\frac{3}{2}}\right)^{-2}\right]^{-\frac{1}{2}}$	$0 \leq \mathrm{Ra} \leq 10^8$ $0 \leq \mathrm{Ste.\,Fo} \leq 0.2$ Pr=50 $\mathrm{H}/\mathrm{L} = 1$ $\theta = Ste.Fo$
		$\mathrm{Nu}_\infty = 0.35\mathrm{Ra}^{1/4}$	At later times Nusselt number has an asymptotic shape Pr>1
Lim and Bejan [69]	-	$\overline{Nu} = \frac{0.35\, Ra^{1/4}}{[1 + (0.143/Pr)^{9/16}]^{4/9}}$	covering small and large Pr numbers RaH

Therefore, at each time step, the start of natural convection effect is tested, the height of the convective zone z is evaluated, Ra_z and Nu_z numbers are calculated and the thermal conductivity of liquid PCM is enhanced in the convective zone. So as a condition, when the ordinate of the PCM node y is greater than H-z (the PCM node is in the upper region), the enhanced conductivity method is applied. This enhancement scheme of the thermal conductivity is presented in Figure 2-1.

Noting that the calculations in the present work are done in the mixed regime, i.e., the bottom part of the enclosure is always ruled by conduction.

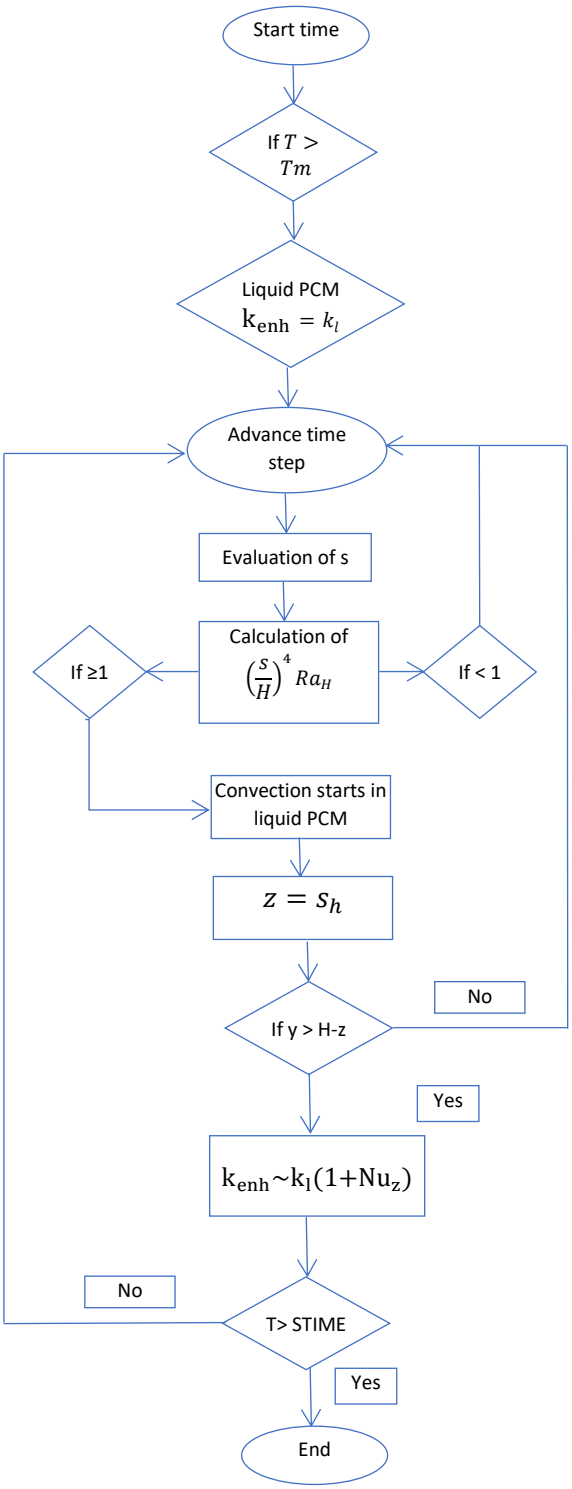

Figure 2-1: strategy retained to enhance the liquid thermal conductivity in the enclosure

3.2. CFD model

In this study, a CFD model is created and implemented in COMSOL Multiphysics 4.4 solver. The modified heat capacity method is employed. This method is well adapted for commercial finite

element solvers [70], and has been validated both numerically [71] and experimentally [72]. The heat diffusion equation is given as:

$$\rho C_p \frac{\partial T}{\partial t} + \nabla(-k\nabla T) + \rho C_p \vec{u}\nabla T = 0 \quad \textbf{Eq. 2-18}$$

The natural convection in the liquid PCM is taken into account for by means of the momentum equation as follows:

$$\rho \frac{\partial \vec{u}}{\partial t} + \rho(\vec{u}\nabla)\vec{u} = -\nabla P + \mu_l \nabla^2 \vec{u} + \vec{F}_b + \vec{F}_a \quad \textbf{Eq. 2-19}$$

Where $\vec{F}_b$ is the buoyancy force given by the Boussinesq approximation:

$$\vec{F}_b = -\rho_l\big(1 - \beta(T - T_m)\big)\vec{g} \quad \textbf{Eq. 2-20}$$

And $\vec{F}_a$ is the Darcy damping term [73]

$$\vec{F}_a = -A(T).\vec{u} \quad \textbf{Eq. 2-21}$$

The parameter A(T), defined in the momentum equation to ensure zero velocities in solid region (Carman–Koseny relation), is given as:

$$A(T) = \frac{C\big(1 - B_1(T)\big)^2}{B_1(T)^3 + q} \quad \textbf{Eq. 2-22}$$

Where C is a very large number and q is a very small number to evade the division by zero. Our model used the values C = 1.6e+06 kg/ (m^3. s) and q = 1e-03.

The function $B_1(T)$ is the continuous and twice-derivable liquid fraction function defined from function $B_0(T)$:

$$B_0(T) = \begin{cases} 0 & T < (T_m - \Delta T/2) \\ \frac{T - T_m + \Delta T/2}{\Delta T} & \left(T_m - \frac{\Delta T}{2}\right) < T < (T_m + \frac{\Delta T}{2}) \\ 1 & T > (T_m + \Delta T/2) \end{cases} \quad \textbf{Eq. 2-23}$$

The changing in the PCM thermo-physical properties are given function of temperature using the following equations:

$$\mu(T) = \mu_l\left(1 + \frac{\mathrm{C}\big(1 - \mathrm{B}_1(\mathrm{T})\big)^2}{C_0(\mathrm{B}_1(\mathrm{T})^3 + \mathrm{q})}\right) \quad \textbf{Eq. 2-24}$$

$$\rho(T) = \rho_s + (\rho_l - \rho_s)\mathrm{B}_1(\mathrm{T}) \quad \textbf{Eq. 2-25}$$

$$k(T) = k_s + (k_l - k_s)\mathrm{B}_1(\mathrm{T}) \quad \textbf{Eq. 2-26}$$

Where μ is the dynamic viscosity, ρ is the density and k the thermal conductivity of the PCM, for both the liquid and solid phase of the PCM and C_0=1 kg/ (m^3. s).

The modified heat capacity is given as:

$$C_p(T) = C_{ps} + \left(C_{ps} - C_{pl}\right)\mathrm{B}_1(\mathrm{T}) + L_H D(T) \qquad \textbf{Eq. 2-27}$$

Where

$$D(T) = \frac{e^{\frac{-(T-T_m)^2}{\left(\Delta T/4\right)^2}}}{\sqrt{\pi.\left(\Delta T/4\right)^2}} \qquad \textbf{Eq. 2-28}$$

The use of a Gaussian function for $D(T)$ ensures that the latent heat is conserved through the process since the integral of such function over the entire range melting temperature interval ΔT is always equal to 1 and C_0. For this study, a ΔT = 1 K is used.

3.3. Test case of melting with natural convection

Natural convection during the melting of Octadecane filled in a 2D square cavity of height H =0.1m is investigated. The initial temperature is equal to the melting temperature T_0=Tm=303.15K, and the PCM is initially at solid state. The left heated vertical wall temperature is T_h=313.15K, while the horizontal walls are adiabatic. The cold right wall temperature is T_c=T_0. When natural convection begins developing in the liquid PCM, a non-uniform displacement of the melting front is obtained as well as a non-uniform distribution of the heat flux at the solid-liquid interface. Table 2-3 summarizes the thermo-physical properties of Octadecane. Approximate values of the thermo-physical properties of Octadecane were used to estimate the governing parameters [74].

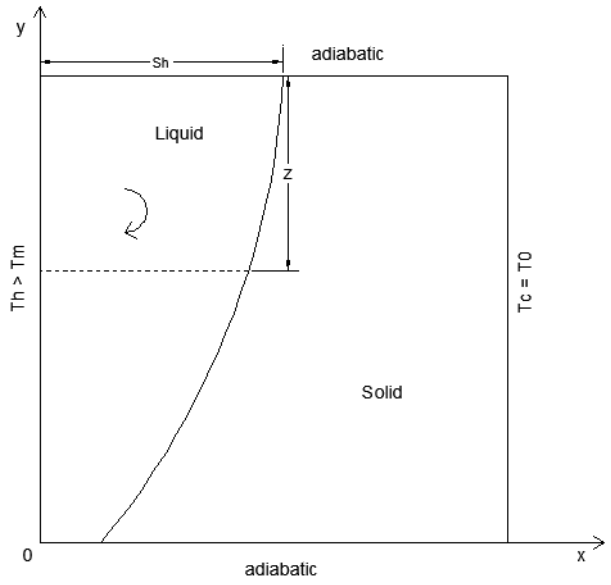

Figure 2-2: Schematic of the test case cavity filled with PCM.

Table 2-3: Thermo-physical properties of Octadecane [74]

Property	value
k (W/mK)	0.2
$Cp_s = Cp_l$ (J/kgK)	1250
$\rho_s = \rho_l$ (kg/m^3)	800
α (m^2/s)	2.10^{-7}
ν (m^2/s)	10^{-5}
L_H (J/kg)	$1.25.10^5$
Tm (K)	303.15
ΔT (K)	10
β (1/K)	2.10^{-3}
g (m/s^2)	10

The problem is characterized by the following dimensionless numbers:

Stefan number of $Ste = \frac{Cp(T_h - T_m)}{L_H} = 0.1$

Rayleigh number of $Ra_H = 10^8$

Prandtl number of $\mathrm{pr} = \frac{\nu}{\alpha} = 50$

To simplify the numerical model, we assume the follow: 1) the PCM is isotropic and homogenous, 2) the thermo-physical properties of the PCM are constant, 3) the Boussinesq approximation is applicable, 4) the density change, and hence the volume change, of the PCM during melting is neglected; 5) the flow in the liquid PCM is incompressible, laminar and Newtonian, 6) radiation and viscous dissipation are neglected.

3.4. Comparison between simplified model and CFD model simulations

The simulations for a time range of 5000s ($\theta = \mathrm{SteFo} = 0.01$) for both CFD model and simplified model are performed on a Dell Precision Tower 5810 using an Intel Xeon CPU E5-1650 v3 of speed 3.5 GHz, six cores (12 CPUs) and 16 GB of RAM.

A grid sensitivity analysis was performed to investigate the exactitude of the calculations. For the simplified model, the simulations in Matlab are lastly executed with a grid size containing 225 control volumes. The dimensionless time step is taken $\Delta\theta = 2\mathrm{x}10^{-5}$ for a total simulation dimensionless time of $\theta = \mathrm{SteFo} = 0.01$. While for the CFD model, the simulations in COMSOL are finally performed with 15268 triangular elements of maximum size 1.3e-3m and minimum size 1.5e-5m. The computer simulations of the simplified model run much faster than those of the CFD model (at least 45 times faster). The computation time for different mesh sizes is presented in Table 2-4.

Table 2-4: Comparison of the computation time between CFD and simplified models for different mesh sizes

	COMSOL		Matlab	
Mesh type	**Number of Triangular elements**	**Computation time (s)**	**Number of control volumes**	**Computation time (s)**
Normal	1284	184	25	2
Fine	2244	510	100	10
Finer	6626	1438	225	70
User defined	15268	3200	400	405
Extra fine	15866	3600	625	1906

According to the average Nusselt number curve at the left heated wall derived from the CFD model, a correlation for the average Nusselt number is proposed in Eq. 2-29. The correlation is found for a specific case (Ra=10^8, Ste=0.1 and Pr=50), the aim is to demonstrate the compatibility between both models. Least square fitting is used to correlate Nu_H (R^2=0.99):

$$\mathrm{Nu_H} = 23.073\ \mathrm{Ra_H^{0.0175}} \left(\frac{\mathrm{S_{av}}}{\mathrm{H}}\right)^{0.0525} \quad \textbf{Eq. 2-29}$$

Cases for different Nusselt number correlation and enhanced conductivity configurations are presented in Table 2-5.

Table 2-5: Cases to be conducted in the simplified model

cases	Nusselt number correlation	Enhanced conductivity
1	$Nu_z = 1$ (conduction only)	$k_{enh} = k_l$
2	$Nu_z = 0.18\left(\frac{Pr}{0.2+Pr}Ra_z\right)^{0.29}$ [50]	$k_{enh} \sim k_l(1+\overline{Nu_z})$
3	Correlation from CFD	$k_{enh} \sim k_l(1+\overline{Nu_z})$

3.5. Validation of the simplified model for convection during melting

To test the numerical solutions conducted on Matlab using the simplified method, the transient average value of the liquid fraction, the average position and the form of the melting front at four distinct times were compared to the CFD model results in addition to numerical and experimental results obtained by other researchers.

The first validation has been done by comparing the results of the average fraction of liquid function of the dimensionless time (Figure 2-3) from the simplified model, to those of the CFD model and the numerical benchmark on convective melting by Bertrand et al. [74]. The comparison with numerical benchmark results was addressed by two participants: Lacroix and Le Quere. Different methods were

used in these works to model the convection effect during melting. To execute the simulations for the melting process of n-octadecane, an Eulerian-Lagrangian method was used by Lacroix, with a non-dimensional time step of $2x10^{-5}$ and a grid size comprising 25 x 35 non-uniformly distributed nodes. On the same benchmark, Le Quere solved the continuity and momentum equations written in velocity pressure formulation using the enthalpy formulation in the energy equation.

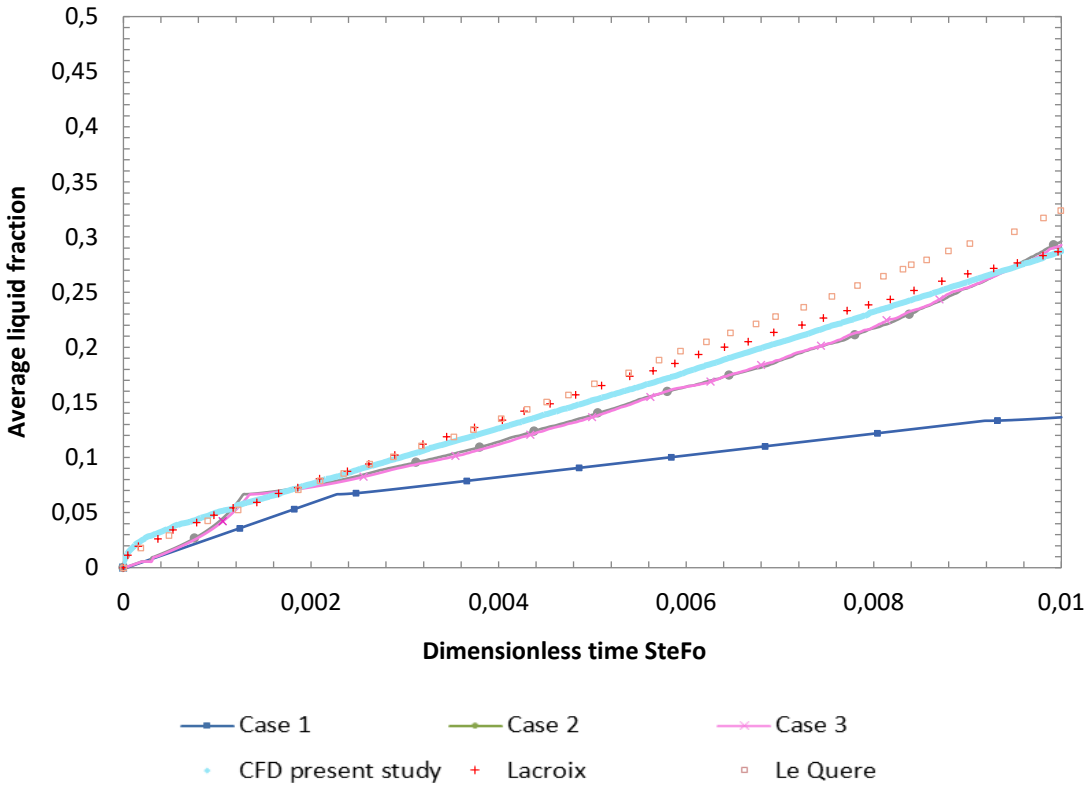

Figure 2-3: The average liquid fraction in function of dimensionless time from the model and the numerical benchmark [74]

Figure 2-3 shows a very good agreement between the proposed simplified model and the CFD model in terms of the average liquid fraction, the average difference found being less than 6%; the simplified model underestimates the value of the average liquid fraction compared to the CFD model. The results of case 2 and case 3 are very close; this shows the compatibility between the proposed correlation for Nusselt number extracted from the CFD model and the general correlation proposed by Berkovsky and Polevikov [50], so the model can be generalized using a general Nusselt number correlation. The results of the simplified model are then compared to those of Lacroix, the average difference is found about 5%, and an average dispersion is found about 10% comparing with the results of Le Quere. The results of the conduction-only model (case 1) show the importance of taking into account the convection effect during melting, where the average fraction of liquid is enhanced by about 40%.

Another validation for the simplified model can be carried out by the examination, at four different dimensionless times, of the melting front position (Figure 2-4 (a-d)).

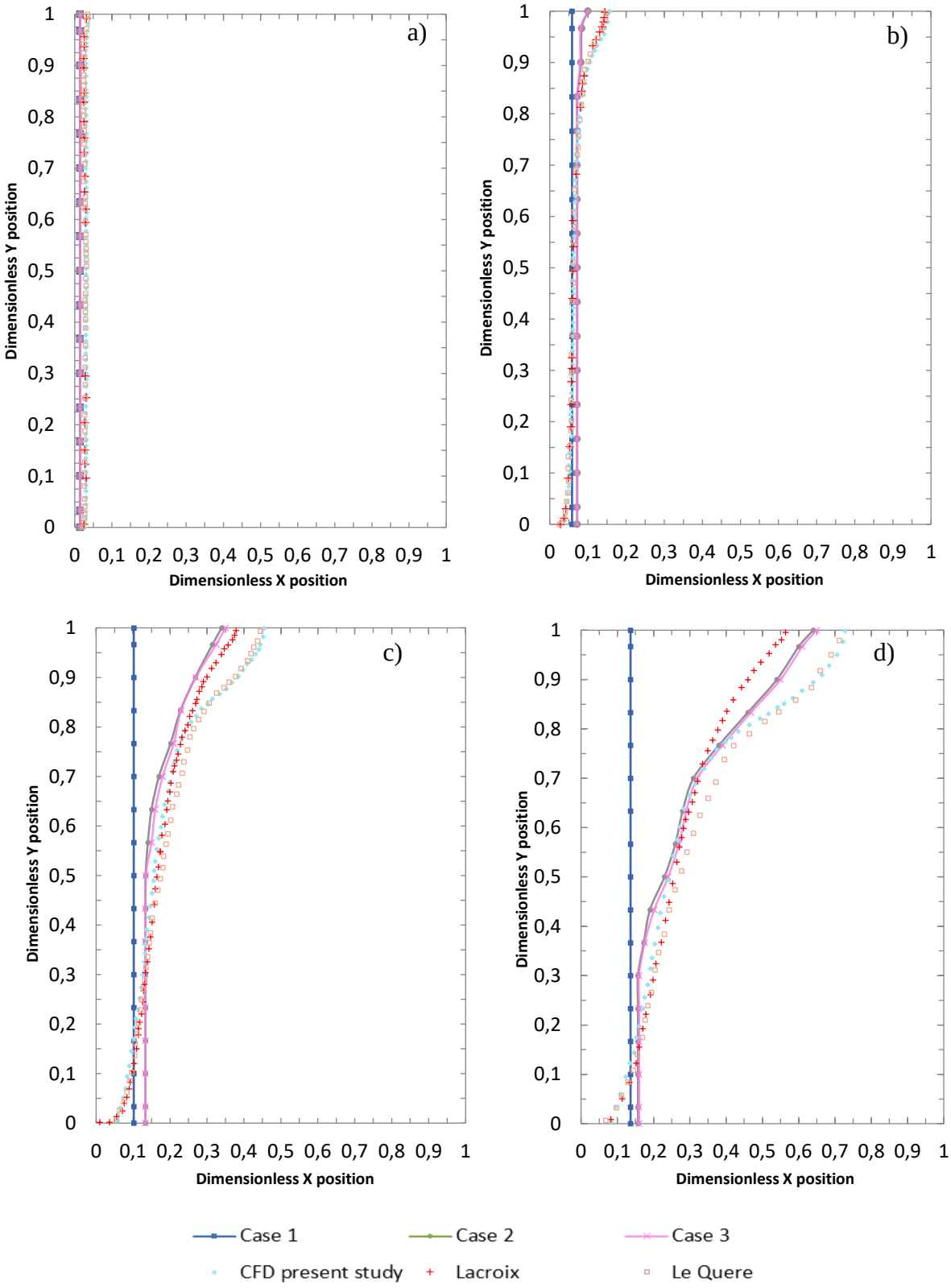

Figure 2-4: Comparison of melting front positions from the model and the numerical benchmark [74] at a) SteFo = 0.0005. b) SteFo = 0.002. c) SteFo = 0.006. d) SteFo = 0.01

Examination of the melting front positions (Figure 2-4 (a-d)) shows that the results of the enhanced conductivity model are close to those of the CFD model and are in good agreement for the overall shape of the melting front. At SteFo = 0.0005, the position of the melting front for all cases is almost

the same and is parallel to the left heated wall; here, heat transfer is dominated by conduction. At SteFo = 0.002, the average difference between the simplified model and the CFD model is within 1-5% range. In addition, the average differences are within 5-9% and 2-3.5% range compared with the results of Lacroix and Le Quere respectively. At SteFo = 0.006, the dispersions at the bottom half of the cavity are within 5-9% while at the top they are around 15% comparing the present model with the CFD model. The average difference is found about 8% and 14% compared with the results of Lacroix and Le Quere respectively. At SteFo = 0.01 the dispersions at the bottom half of the cavity are within 3-4%, while at the top half of the enclosure are within 8-11% range compared to CFD model. One can notice that the melting front extends faster to the right at the top of the cavity in the CFD model compared to the simplified one, the PCM melts quicker. Also, the differences, at the bottom half of the enclosure, are within 3-4% and 1-2% range while at the top half of the enclosure are within 6-8% and 7-11% range compared with the results of Lacroix and Le Quere respectively. Noting that the enhanced conductivity approach does not apply at the bottom of the enclosure, a difference in the shape of melting front can be observed at all times. The melting front corresponding to the conduction-only model moves parallel to the heated left wall because of the constant liquid thermal conductivity at the whole height of the enclosure; considering convection during melting enhances the average melting front position by about at 40% at SteFo = 0.006 and about 55% at SteFo = 0.01.

Figure 2-5 shows the results of the average position of the solid-liquid interface in the relatively short-time interval $0 < \mathrm{SteFo} < 0.006$. Here, the comparison is made between the proposed model and the CFD model on the one hand, and experimental benchmark solutions found in the reference [49] on the other hand. The figure displays a good agreement between the results of the simplified model and those of CFD; the average difference is found around 13%, also the value of the average position of the melting front is underestimated compared to CFD model. In addition, the experimental results obtained by Bareiss and Beer [75] and Ho and Viskanta [16] are fairly close to those of the present model, the average difference is found about 9%. The average position of the melting front is enhanced by about 40% taking the convection effect into consideration.

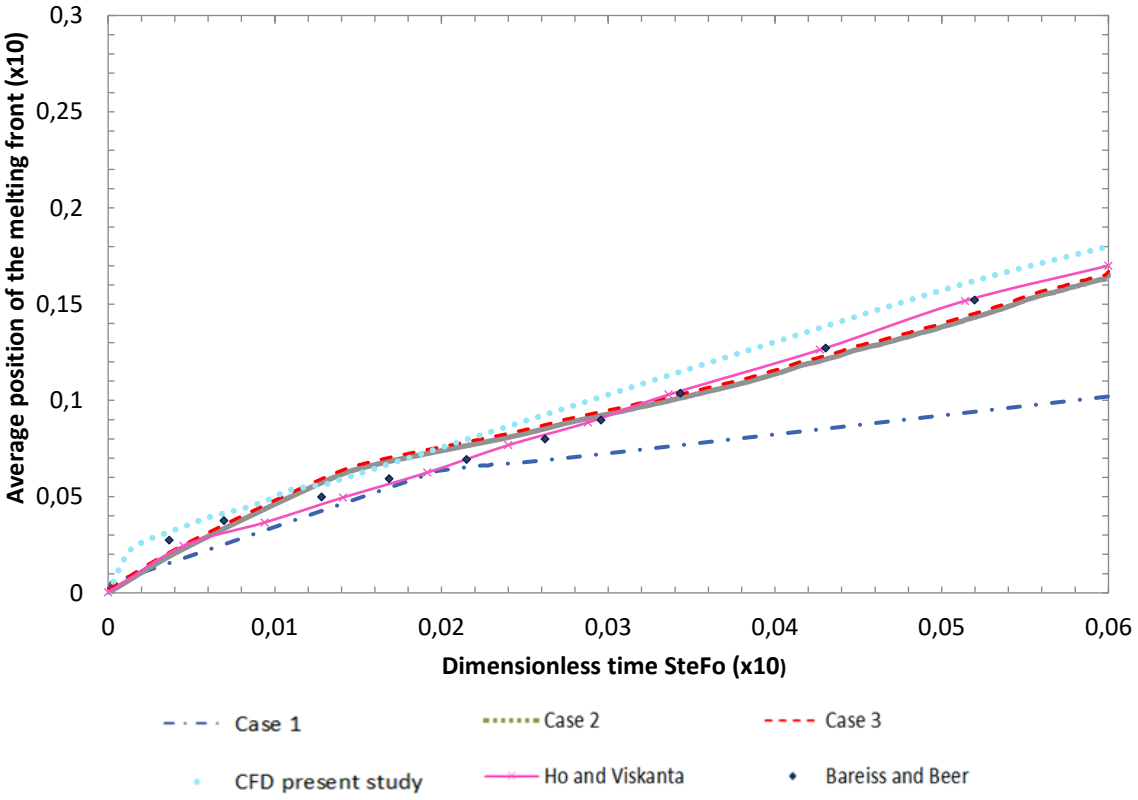

Figure 2-5: Comparison of the average position of the melting front

4. Shortwave radiation through PCM

Phase change materials have variable optical characteristics that depends on their physical state, thus investigating the short-wave radiation within the PCM is not quite simple. Gowreesunker [57] evaluated the nodal optical properties such as the transmissivity and absorptivity in function of the transient liquid fraction f_l.

When PCM changes from the fully solid to fully liquid, the fractional change in PCM transmittance is given as:

$$\delta = \frac{\tau_l - \tau_s}{1 - \tau_s} \qquad \textbf{Eq. 2-30}$$

The relation between the extinction coefficient σ and the liquid fraction is written as:

$$\sigma = f_l \sigma_l + (1 - f_l)\sigma_s \qquad \textbf{Eq. 2-31}$$

The advantage of this relation is that, during phase change, the extinction coefficient can be easily found from the liquid fraction and the liquid and solid extinction coefficients.

The transmittance of the PCM is:

$$\tau_{PCM} = 10^{-d} \qquad \textbf{Eq. 2-32}$$

Where d is the optical thickness:

$$d = \sigma . S$$ **Eq. 2-33**

Where *S* stands for the physical thickness

The absorptivity of the PCM evaluated at each node is given as:

$$\alpha_{PCM} = [\delta f_l + (1 - d)](1 - \tau_{PCM})$$ **Eq. 2-34**

To model combined phase change and radiation problems, the previous equations can be used. In addition, according to Elarga et al. [76], the absorption solar radiation is divided equally between the nodes representing each layer. Considering $N=N_x x N_y$ nodes in the PCM cavity, the absorbed solar radiation to be added as a source term to the energy equation at the node P is then given as:

$$\emptyset_{sol} = \frac{Q_{sol}\, \alpha_{PCM}}{N}$$ **Eq. 2-35**

Where α_{PCM} is calculated using Eq. 2-34.

One can notice that modeling of the longwave radiation is neglected, because it has a marginal effect on the melting process [77].

5. Application to the melting of fatty acid with natural convection and radiation

In this section, the simplified models for natural convection during melting process and for short wave radiation presented in the above sections are applied to the fatty acid eutectic filling the glass brick of the INERTRANS wall of total thickness 9.6 cm (Figure 2-6). The brick containing the PCM is 32 mm wide and 191 mm height (aspect ratio H/L≈6). The temperature of the left heated vertical wall is Th=40ºC, whereas the horizontal walls are adiabatic. The cold right wall temperature is equal to the initial temperature Tc=T0=10ºC (Figure 2-7). The problem is characterized by the following dimensionless numbers: Ste=0.257, Ra_H=3.72.109 and Pr=111.67. The PCM thermo-physical and optical properties are summarized in Table 2-6 and

Table 2-7 respectively. The total incident solar radiation flux is assumed Qsol=500 W/m2 and the material is considered to be absorbent and non-diffusing. The extinction coefficient for solid and liquid PCM are $\sigma_s = 200\ (1/\mathrm{m})$ and $\sigma_l = 2\ (1/\mathrm{m})$ respectively [78]. Here, only the fatty acid layer is considered and the heat transfer in the glass and other wall layers is not modeled.

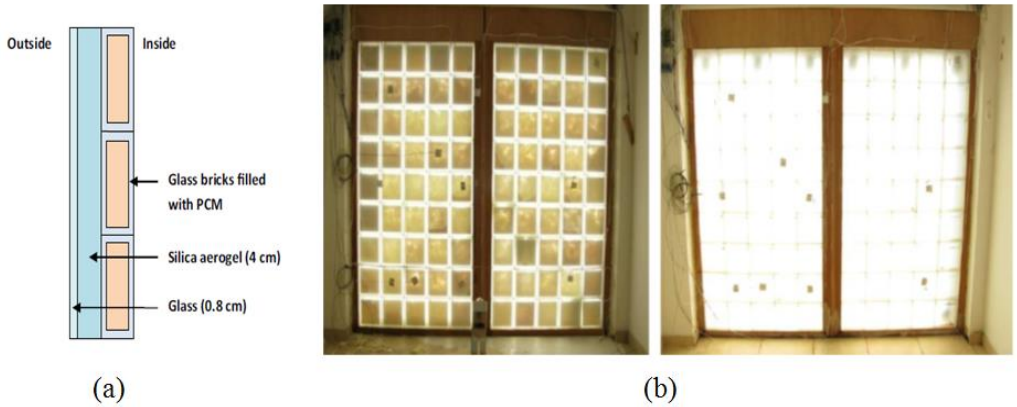

Figure 2-6: (a) Layout of the *INERTRANS* wall, (b) PCM filled in glass bricks [1]

Table 2-6: Thermo-physical properties of the fatty acid eutectic [1]

Property	value
k_s (W/mK)	0.182 (at 5.4 °C)
k_l (W/mK)	0.182 (at 39 °C)
L_H (J/kg)	152000
Cp_s (J/kgK)	1670
Cp_l (J/kgK)	2090
ρ_s (kg/m^3)	960 (at 35 °C)
ρ_l (kg/m^3)	884 (at 13 °C)
Tm (°C)	21.3
α (m^2/s)	$9{,}85.10^{-8}$
ν (m^2/s)	11.10^{-6}
β (1/K)	$3.1.10^{-3}$

Table 2-7: Optical properties of the fatty acid eutectic [1]

		τ%	ρ%
Liquid state	Energetic	90	5
	Optical	78	6
Solid state	Energetic	≈ 0	53
	Optical	≈ 0	56

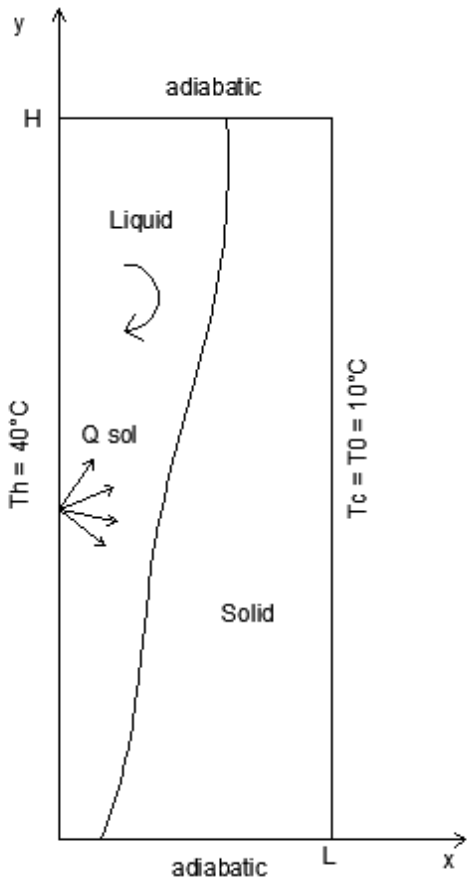

Figure 2-7: Schematic of fatty acid filled in glass bricks.

The accuracy of the calculations of the simplified model for combined natural convection and radiation during melting is investigated by performing grid sensitivity analysis. Simulations are done using 300 control volumes. To validate the model, the results are compared to those found by Fuentes et al. [77][78] for a total simulation time of 24 minutes. For melting problem, they have used the enthalpy method, to solve the radiative heat transfer they have used the discrete ordinate method (DOM) and the lattice Boltzmann method (LBM) was used to solve fluid flow equations.

The results of the simplified model in terms of the average liquid fraction in Figure 2-8 are in very good agreement compared to those of LBM-DOM model. Moreover, the natural convection enhances the liquid fraction by around 35% compared to the conduction only model and the shortwave radiation raises the liquid fraction by around 20% compared to the convection model.

Concerning the computational time, the simplified model simulations, performed on a Toshiba x64 based Processor using an Intel (R) core (TM) CPU M330 of speed 2.13 GHz, three cores and 4 GB of RAM, run significantly faster (about five minutes) than those conducted using LBM-convection model (6 hours 21 minutes) for natural convection during melting, and LBM-DOM model (130 hours 20 minutes) [78] for both natural convection and shortwave radiation during melting.

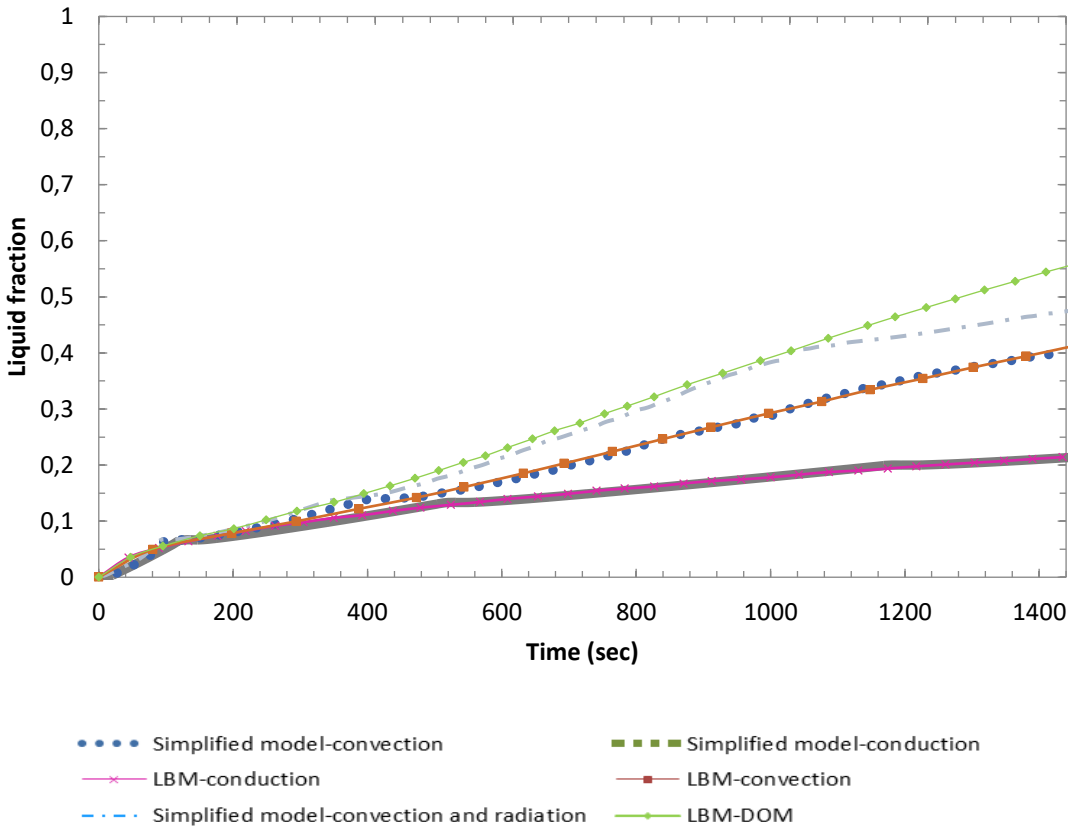

Figure 2-8: Comparison of the average liquid fraction

6. Conclusion

A simplified model for melting of a phase change material with combined natural convection and radiation is presented in this chapter. First, a simplified model for melting with natural convection is developed without the full solution of N-S equations. This model is based on the scaling theory and the enhanced thermal conductivity approach. Then, a full CFD model is created using COMSOL Multiphysics adopting the modified heat capacity method, and a correlation for the Nusselt number at the left heated wall is proposed based on CFD results, to calculate the enhanced conductivity.

The simplified model for natural convection during melting is validated against the CFD model, as well as numerical and experimental benchmarks. Comparing the results to those of CFD model, the difference is found less than 6%, in terms of the average liquid fraction, less than 14% in terms of the position of the melting front at four different times, and around 13% in terms of the average position of the melting front. On the other hand, the results of the simplified model show very good agreement with those of the benchmark solutions. Accordingly, the results are enhanced by about 40% to 55% when taking the natural convection effect into consideration compared to a conduction only model.

Then, a simplified method coupling the natural convection and the shortwave radiation during melting is applied to model the melting of the fatty acid filled in glass bricks of the *INERTRANS* wall. The

obtained results are in very good agreement to LBM-DOM results, in terms of the average liquid fraction. It is found that natural convection increases the liquid fraction by about 35% compared to the conduction only model, while the radiation increases the liquid fraction by about 20% compared to the convection model. Concerning the computational time, the simplified model simulations run significantly faster than those using the LBM-DOM model.

The simplified model considering both natural convection and radiation during melting process is simple to implement and can manage efficiently convection-controlled phase change problems without the full solution of the flow in a very small computational time. This simplified model is a conceptual representation of reality, and it is developed for practical thermal engineering applications, where yearly energy performance evaluation is sought, that cannot rely on highly computational time needed in CFD simulations. Accordingly, it is suitable to control a real-time phase change process that takes place in residential, commercial, and industrial latent heat thermal energy systems. As future work, the simplified model will be used to simulate the thermal behavior of the whole INERTRANS wall in a yearly basis where solidification process will have to be considered too. The simplified model could also be integrated in an energy simulation tool (e.g. TRNSYS or EnergyPlus) to evaluate the annual thermal behavior of a building

In the next chapter, the simplified model will be used to simulate the thermal behavior of the whole INERTRANS wall. Then, it will be coupled with a global energy simulation tool (TRNSYS) to evaluate the annual thermal behavior of a building.

References

[1] Y. Berthou, P. H. Biwole, P. Achard, H. Sallée, M. Tantot-Neirac, and F. Jay, "Full scale experimentation on a new translucent passive solar wall combining silica aerogels and phase change materials," *Sol. Energy*, vol. 115, pp. 733–742, May 2015.

[2] J. M. Fuentes, F. Kuznik, K. Johannes, and J. Virgone, "Development and validation of a new LBM-MRT hybrid model with enthalpy formulation for melting with natural convection," *Phys. Lett. A*, vol. 378, no. 4, pp. 374–381, 2014.

[3] E. Sparrow and J. Ramsey, "Melting and natural convection due to a vertical embedded heater.," *J Heat Transf*, pp. 100:368–70, 1978.

[4] E. Sparrow and S. Patankar, "Analysis of melting in the presence of natural convection in the melt region," *ASME J Heat Transf*, vol. 99:520–6, 1977.

[5] M. FARID and R. HUSIAN, "An electrical storage heater using the phase change method of heat storage.," *Energy Convers Manag*, vol. 30(3):219–30, 1990.

[6] A. Hasan, "Phase change material energy storage system employing palmitic acid," *Sol Energy*, vol. 52:143–54, 1994.

[7] M. Lacroix and T. Duong, "Experimental improvements of heat transfer in a latent heat thermal energy storage unit with embedded heat sources," *Energy Convers. Manag.*, vol. 39, no. 8, pp. 703–716, 1998.

[8] Y. Zhang and J. Yi, "A simple method, the T-history method of determining the heat of fusion specific heat and thermal conductivity of phase change materials," *Meas Sci Technol*, 1999.

[9] R. Velraj and R. seeniraj, "Heat transfer enhancement in a latent heat storage system," *Sol Energy*, 1999.

[10] A. SARI and K. KAYGUSUZ, "Thermal energy storage system using stearic acid as a phase change material," *Sol Energy*, 2001.

[11] P. Lamberg, R. Lehtiniemi, and A.-M. Henell, "Numerical and experimental investigation of melting and freezing processes in phase change material storage," *Int. J. Therm. Sci.*, vol. 43, no. 3, pp. 277–287, Mar. 2004.

[12] F. Souayfane, F. Fardoun, and P. H. Biwole, "Different mathematical models of convection during phase change," presented at the REDEC conference, NDU university Lebanon, 2016, pp. 1–8.

[13] C. Beckermann and R. Viskanta, "Effect of solid subcooling on natural convection melting of a pure metal," *J. Heat Transf.*, vol. 111, no. 2, pp. 416–424, 1989.

[14] Y. Wang, A. Amiri, and K. Vafai, "An experimental investigation of the melting process in a rectangular enclosure," *Int. J. Heat Mass Transf.*, vol. 42, no. 19, pp. 3659–3672, 1999.

[15] D. Yanxia, Y. Yanping, J. Daiyong, C. Baoyi, and M. Jinfeng, "Experimental investigation on melting characteristics of ethanolamine–water binary mixture used as PCM," *Int. Commun. Heat Mass Transf.*, vol. 34, no. 9–10, pp. 1056–1063, Nov. 2007.

[16] C.-J. Ho and R. Viskanta, "Heat Transfer During Melting From an Isothermal Vertical Wall," *J. Heat Transf.*, vol. 106, no. 1, p. 12, 1984.

[17] Z. Gong, S. Devahastin, and A. Mujumdar, "Enhanced heat transfer in free convection-dominated melting in a rectangular cavity with an isothermal vertical wall.," *Appl Therm Eng*, vol. 19:1237–51., 1999.

[18] Z. Younsi, A. Joulin, L. Zalewski, S. Lassue, and D. R. Rousse, "Phase change materials: a numerical method for the behavior predictions," in *Proceedings of the Fourth International Conference on Thermal Engineering: Theory and Applications January*, 2009, pp. 12–14.

[19] R. E. Murray and D. Groulx, "Modeling convection during melting of a phase change material," in *Proceedings of the COMSOL Conference*, 2011.

[20] A. Brent, V. Voller, and K. Reid, "Enthalpy-porosity technique for modeling convection-diffusion phase change: application tothe melting of a pure metal.," *Numer Heat Transfer*, vol. 13:297–318., 1988.

[21] S. Liu, Y. Li, and Y. Zhang, "Mathematical solutions and numerical models employed for the investigations of PCMs′ phase transformations," *Renew. Sustain. Energy Rev.*, vol. 33, pp. 659–674, May 2014.

[22] V. Voller and M. Cross, "An enthalpy method for convection/ diffusion phase change," *Int J Numer Methods Eng*, vol. 24:271–84., 1987.

[23] V. Shatikian, G. Ziskind, and R. Letan, "Numerical investigation of a PCM-based heat sink with internal fins," *Int. J. Heat Mass Transf.*, vol. 48, no. 17, pp. 3689–3706, Aug. 2005.
[24] M. Faraji and H. El Qarnia, "Numerical study of melting in an enclosure with discrete protruding heat sources," *Appl. Math. Model.*, vol. 34, no. 5, pp. 1258–1275, May 2010.
[25] A. R. Archibold, M. M. Rahman, D. Y. Goswami, and E. K. Stefanakos, "Analysis of heat transfer and fluid flow during melting inside a spherical container for thermal energy storage," *Appl. Therm. Eng.*, vol. 64, no. 1–2, pp. 396–407, Mar. 2014.
[26] P. Wang, H. Yao, Z. Lan, Z. Peng, Y. Huang, and Y. Ding, "Numerical investigation of PCM melting process in sleeve tube with internal fins," *Energy Convers. Manag.*, vol. 110, pp. 428–435, Feb. 2016.
[27] Z. Liu, Y. Yao, and H. Wu, "Numerical modeling for solid–liquid phase change phenomena in porous media: Shell-and-tube type latent heat thermal energy storage," *Appl. Energy*, vol. 112, pp. 1222–1232, Dec. 2013.
[28] W.-B. Ye, D.-S. Zhu, and N. Wang, "Fluid flow and heat transfer in a latent thermal energy unit with different phase change material (PCM) cavity volume fractions," *Appl. Therm. Eng.*, vol. 42, pp. 49–57, Sep. 2012.
[29] P. Goyal, A. Dutta, V. Verma, and I. T. R. Singh, "Enthalpy Porosity Method for CFD Simulation of Natural Convection Phenomenon for Phase Change Problems in the Molten Pool and its Importance during Melting of Solids."
[30] S. Wang, A. Faghri, and T. L. Bergman, "A comprehensive numerical model for melting with natural convection," *Int. J. Heat Mass Transf.*, vol. 53, no. 9–10, pp. 1986–2000, Apr. 2010.
[31] A. Faghri and Y. Cao, "Performance characteristics of a thermal energy storage module: a transient PCM/forced convection conjugate analysis," *Int. J. HeatMass Transfer*, pp. 93–101, 1991.
[32] P. Damronglerd and Zhang, "Modified temperature-transforming model for convection-controlled melting," *AIAA J. Thermophy. Heat Transfer 21*, pp. 203–208., 2007.
[33] x zeng and A. Faghri, "A temperature transforming model for binary solid–liquid phase change problems: Part I – mathematical modeling and numerical methodology," pp. 467–480, 1994.
[34] K. Morgan, "A numerical analysis of freezing and melting with convection," *Comp. Meth. App. Eng.*, vol. Vol. 28, pp. 275–84, 1981.
[35] D. Groulx and P. H. Biwole, "Solar PV Passive Temperature Control Using Phase Change Materials," 2014.
[36] D. Chatterjee and S. Chakraborty, "An enthalpy-based lattice Boltzmann model for diffusion dominated solid–liquid phase transformation," *Phys. Lett. A*, vol. 341, no. 1–4, pp. 320–330, Jun. 2005.
[37] E. A. Semma, M. El Ganaoui, and R. Bennacer, "Lattice Boltzmann method for melting/solidification problems," *Comptes Rendus Mécanique*, vol. 335, no. 5–6, pp. 295–303, May 2007.
[38] C. Huber, A. Parmigiani, B. Chopard, M. Manga, and O. Bachmann, "Lattice Boltzmann model for melting with natural convection," *Int. J. Heat Fluid Flow*, vol. 29, no. 5, pp. 1469–1480, Oct. 2008.
[39] J. M. Fuentes, "Développement d'un modèle de Boltzmann sur gaz réseau pour l'étude du changement de phase en présence de convection naturelle et de rayonnement," INSA de Lyon, 2013.
[40] N. Hannoun, V. Alexiades, and T. Z. Mai, "A reference solution for phase change with convection," *Int J Numer Methods Fluids*, vol. 48, pp. 1283–1308, 2005.
[41] N. Hannoun, V. Alexiades, and T. Z. Mai, "Resolving the controversy over tin and gallium melting in a rectangular cavity heated from the side," *Numer Heat Transfer*, vol. 44, pp. 253–276, 2003.
[42] M. M. Prieto and B. González, "Fluid flow and heat transfer in PCM panels arranged vertically and horizontally for application in heating systems," *Renew. Energy*, vol. 97, pp. 331–343, Nov. 2016.
[43] R. Kahraman, "A simplified model for melting of ice with natural convection," *Int. Commun. Heat Mass Transfer*, vol. 25, pp. 359–368, 1998.
[44] P. Johansson, "Advanced Thermal Energy Storage Heat Transfer Study with Use of Comsol and Matlab," 2011.
[45] M. Costa and D. Buddhi, "Numerical simulation of a latent heat thermal energy storage system with enhanced heat conduction.," *Energy Convers Manag*, vol. 39:319–30., 1998.
[46] P. Dolado, A. Lazaro, J. M. Marin, and B. Zalba, "Characterization of melting and solidification in a real scale PCM-air heat exchanger: Numerical model and experimental validation," *Energy Convers. Manag.*, vol. 52, no. 4, pp. 1890–1907, Apr. 2011.
[47] G. Vidalain, L. Gosselin, and M. Lacroix, "An enhanced thermal conduction model for the prediction of convection dominated solid–liquid phase change," *Int. J. Heat Mass Transf.*, vol. 52, no. 7–8, pp. 1753–1760, Mar. 2009.

[48] A. Castell and C. Solé, “An overview on design methodologies for liquid–solid PCM storage systems,” *Renew. Sustain. Energy Rev.*, vol. 52, pp. 289–307, Dec. 2015.
[49] P. Jany and A. Bejan, “Scaling theory of melting with natural convection in an enclosure,” *Int. J. Heat Mass Transf.*, vol. 31, no. 6, pp. 1221–1235, Jun. 1988.
[50] A. Bejan, *Convection heat transfer*, Fourth edition. Hoboken, New Jersey: Wiley, 2013.
[51] M. Lacroix and M. Benmadda, “Numerical simulation of natural convectiondominated melting and solidification from a finned vertical wall,” *Numer. Heat Transfer*, no. Part A Appl. 31, pp. 71–86, 1997.
[52] R. Velraj, R. seeniraj, B. Hafner, C. Faber, and K. Schwarzer, “HEAT TRANSFER ENHANCEMENT IN A LATENT HEAT STORAGE SYSTEM,” *Solar Energy*, vol. 65, no. No. 3, pp. 171–180, 1999.
[53] B. Zivkovic and I. Fujii, “An analysis of isothermal phase change of phase change material within rectangular and cylindrical containers,” *Sol. Energy*, vol. 70, no. 1, pp. 51–61, 2001.
[54] Z. Han, M. Zheng, F. Kong, F. Wang, and Z. Li, “Numerical simulation of solar assisted ground-source heat pump heating system with latent heat energy storage in severely cold area.,” *Applied Thermal Engineering*, vol. 28(11–12), 1427–1436, 2008.
[55] A. Najjar and A. Hasan, “Modeling of greenhouse with PCM energy storage,” *Energy Convers. Manag.*, vol. 49, no. 11, pp. 3338–3342, Nov. 2008.
[56] Q. Qi, S. Deng, and Y. Jiang, “A simulation study on a solar heat pump heating system with seasonal latent heat storage,” *Sol. Energy*, vol. 82, no. 8, pp. 669–675, Aug. 2008.
[57] B. L. Gowreesunker, S. B. Stankovic, S. A. Tassou, and P. A. Kyriacou, “Experimental and numerical investigations of the optical and thermal aspects of a PCM-glazed unit,” *Energy Build.*, vol. 61, pp. 239–249, Jun. 2013.
[58] S. V. Patankar, *Numerical heat transfer and fluid flow*. New York: McGraw-Hill., 1980.
[59] F. Souayfane, P. H. Biwole, and F. Fardoun, “MODELE SIMPLIFIE POUR LA PRISE EN COMPTE DE LA CONVECTION NATURELLE DANS LA MODELISATION DU CHANGEMENT DE PHASE SOLIDE-LIQUIDE.”
[60] M. Favre-Marinet and S. Tardu, *Convective heat transfer: solved problems*. London : Hoboken, NJ: ISTE ; Wiley, 2009.
[61] B. W. Webb and R. VISKANTA, “On the characteristic length scale for correlating melting heat transfer data,” *Int. Commun. Heat Mass Transfer*, vol. 12, pp. 637–646, 1985.
[62] I. Catton, *Natural convection in enclosures*, vol. 6. Toronto: in Proceedings of the 6th International Heat Transfer Conference, 1978.
[63] N. Seki, S. Fukusako, and H. Inaba, “Heat-Transfer of Natural-Convection in a Rectangular Cavity with Vertical Walls of Different Temperatures.,” *Bulletin of the Jsme-Japan Society of Mechanical Engineers*, vol. 21(152), pp. 246–253, 1978.
[64] R. K. Macgregor and A. P. Emery, “Free convection through vertical plane layers: moderate and high Prandtl number fluids,” *J. Heat Transfer*, vol. 91, 1969.
[65] N. C. Markatos and K. A. Pericleous, “Laminar and turbulent natural convection in an enclosed cavity,” *Int. J. Heat Mass Transf.*, vol. 27, no. 5, pp. 755–772, May 1984.
[66] C.-J. Ho and R. Viskanta, “Inward solid-liquid phase-change heat transfer in a rectangular cavity with conducting vertical walls,” *Int. J. Heat Mass Transf.*, vol. 27, no. 7, pp. 1055–1065, Jul. 1984.
[67] C. Gau and R. Viskanta, “Melting and Solidification of a Pure Metal on a Vertical Wall,” *J. Heat Transf.*, vol. 108, no. 1, p. 174, 1986.
[68] D. Pal and Y. K. Joshi, “Melting in a side heated tall enclosure by a uniformly dissipating heat source,” *Int. J. Heat Mass Transf.*, vol. 44, no. 2, pp. 375–387, 2001.
[69] J. S. Lim and A. Bejan, “The Prandtl Number Effect on Melting Dominated by Natural Convection,” *J. Heat Transf.*, vol. 114, no. 3, p. 784, 1992.
[70] S. K. Saha and P. Dutta, “Heat transfer correlations for PCM-based heat sinks with plate fins,” *Appl. Therm. Eng.*, vol. 30, no. 16, pp. 2485–2491, Nov. 2010.
[71] W. Ogoh and D. Groulx, “Stefan’s Problem: Validation of a One-Dimensional Solid-Liquid Phase Change Heat Transfer Process,” in *Comsol Conference 2010*, 2010.
[72] P. H. Biwole, P. Eclache, and F. Kuznik, “Phase-change materials to improve solar panel’s performance,” *Energy Build.*, vol. 62, pp. 59–67, Jul. 2013.
[73] V. R. Voller and C. Prakash, “A fixed grid numerical modelling methodology for convection-diffusion mushy region phase-change problems,” *Int. J. Heat Mass Transfer*, vol. 30 (8), pp. 1709-1719., 1987.

[74] O. Bertrand *et al.*, "Melting driven by natural convection A comparison exercise: first results," *International Journal of Thermal Sciences*, vol. 38 (1), pp. 5–26, 1999.
[75] M. Bareiss and H. Beer, "Experimental investigation of melting heat transfer with regard to different geometric arrangements," *Int. Commun. Heat Mass Transf.*, vol. 11, no. 4, pp. 323–333, 1984.
[76] H. Elarga, M. De Carli, and A. Zarrella, "A simplified mathematical model for transient simulation of thermal performance and energy assessment for active facades," *Energy Build.*, vol. 104, pp. 97–107, Oct. 2015.
[77] J. Miranda Fuentes, K. Johannes, F. Kuznik, M. Cosnier, and J. Virgone, "Melting with convection and radiation in a participating phase change material," *Appl. Energy*, vol. 109, pp. 454–461, Sep. 2013.
[78] J. M. Fuentes, "Développement d'un modèle de Boltzmann sur gaz réseau pour l'étude du changement de phase en présence de convection naturelle et de rayonnement," INSA de Lyon, 2013.

Complementary sections to chapter 2

A) Nusselt number correlation

Based on the average Nusselt number curve at the left heated wall derived from the CFD model, shown in Figure 1, a correlation was proposed in section 2.4.

The average Nusselt number is defined as:

$$Nu = \int_0^1 \frac{\partial T}{\partial x} dy \quad (1)$$

where, T is the temperature (K), x and y are the coordinates.

Or

$$Nu = \frac{h.H}{k_l} \quad (2)$$

where H is the height of the cavity, k_l is the thermal conductivity for the liquid PCM and h is the convective heat transfer calculated as:

$$h = \frac{Q}{\Delta T} \quad (3)$$

Q is the heat flux at the left heated wall (W/m^2) found in COMSOL, $\Delta T = T_h - T_m$ with Th (K) is the hot temperature at the left vertical wall and Tm (K) is the melting temperature

The correlation is found for a specific case, the aim is to demonstrate the compatibility between both models: the simplified developed model and the CFD model. This correlation was used to calculate the enhanced conductivity implemented in the simplified model.

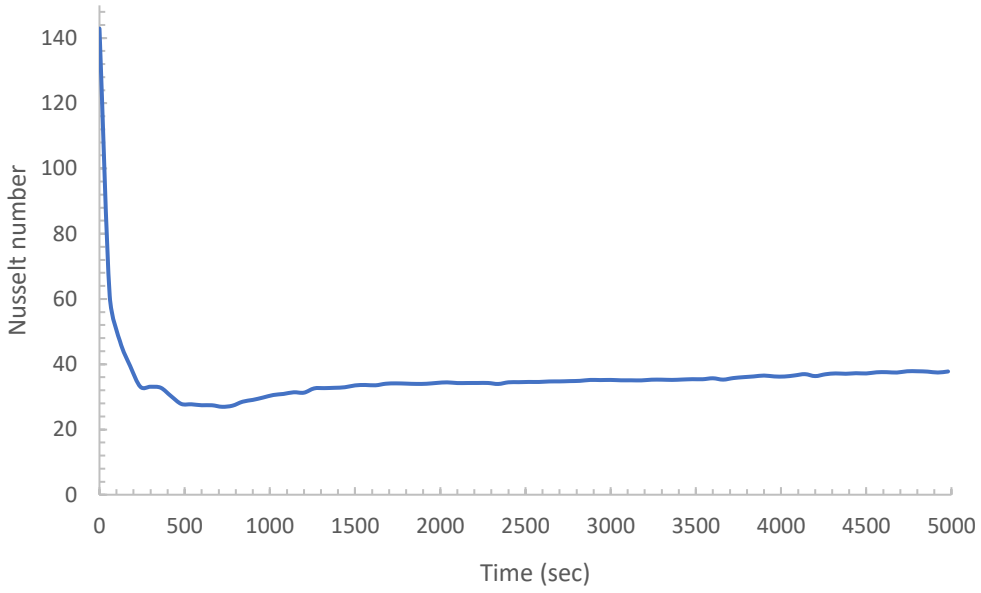

Figure 1: Average value for Nusselt number at the left hot vertical wall from Comsol software

The results of the simplified model for two different Nusselt number correlations (case 2 and case 3 in table 2-5), are found very close. This shows the compatibility between the proposed correlation for Nusselt number extracted from the CFD model and the general correlation proposed by Berkovsky and Polevikov [1]. So, the model can be generalized using a general Nusselt number correlation and the general correlation is used in the rest of our work.

Noting that in chapter 2, we have modeled natural convection and radiation only during melting process. According to many authors [2] [3], convection heat transfer is less important than conduction during solidification process and in such walls as the INERTRANS wall solidification is more likely to happen at night, in absence of solar radiation.

B) General concept of scaling theory proposed by Bejan

This section discusses the scaling laws adequate for two-dimensional natural convection in a rectangular enclosure filled with PCM, with two differentially heated sides and insulated top and bottom surfaces as illustrated in Figure 2.

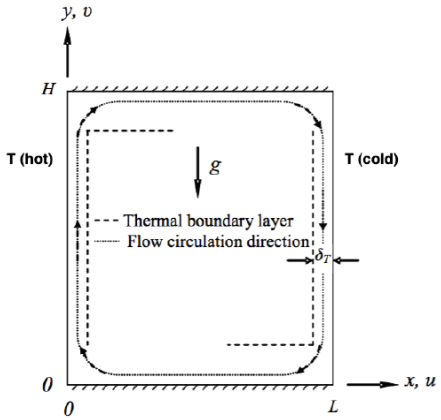

Figure 2: Two-dimensional natural convection in rectangular enclosure

The natural convection melting process can be analyzed as a sequence of four regimes labeled (a)–(d) in Figure 3. At first, when a small layer of liquid forms, the heat transfer is dominated by conduction and the melting front moves parallel to the left heated wall first regime (Figure 3-a). This regime is called the conduction limit regime, when the heat flux across the emerging vertical liquid film is balanced entirely by the enthalpy absorbed at the two-phase interface,

$$k\frac{T_h - T_m}{s} \sim \rho L_H \frac{ds}{dt} \quad (1)$$

In dimensionless terms, this yield

$$\frac{s}{H} \sim \theta^{1/2} \quad (2)$$

where, L_H is the latent heat of fusion; θ is the dimensionless time group

$$\theta = \frac{k(T_h - T_m)}{\rho L_H H^2} t = Ste\ Fo \tag{3}$$

and Ste and Fo are the Stefan and Fourier numbers respectively,

$$Ste = \frac{Cp(T_h - T_m)}{L_H} \tag{4}$$

$$Fo = \frac{\alpha t}{H^2} \tag{5}$$

The Nusselt number that corresponds to this conduction limit is

$$Nu = \frac{Q}{k(T_h - T_m)} \sim \frac{H}{s} \sim \theta^{-1/2} \tag{6}$$

where, Q is the total heat transfer rate through the left wall of the enclosure, per unit length in the direction perpendicular to the plane.

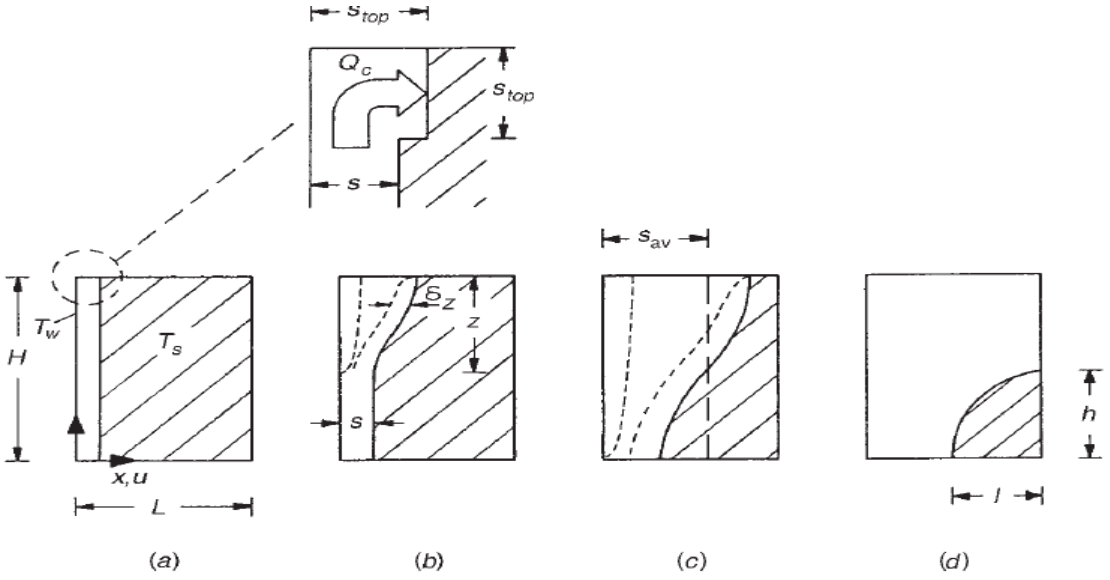

Figure 3: Regimes for melting in the presence of significant natural convection when the phase-change material is being heated from the side [4]

Secondly, because of the variation in density, the hot fluid rises and brings the heat to the solid via the interface between the two. This causes a non-uniform distribution of heat, and therefore a slight deformation of the melting front. The conduction process is gradually replaced by convection (Figure 3-b). This regime has been named the mixed regime (conduction + convection) and is characterized by an upper liquid region that has become wide enough to be ruled by convection (i.e., its lateral surfaces are lined by distinct boundary layers). Let the unknown dimension z be the height of this upper region. Heat transfer across the rest of the liquid space (height H-z) continues to be ruled by conduction. The convection in the upper region starts when the thermal boundary layer thickness δ_z becomes of the same order of magnitude as the thickness of the liquid layer s i.e., $\delta_z \sim s$ at the convection–conduction transition level: Considering that the liquid has a Prandtl number greater than

one, this yields to $\delta_z \sim z\, Ra_z^{-1/4}$ and the height z of the convective zone is then scaled as $z \sim H\, Ra_H \theta^2$. Where, Ra_z is the Rayleigh number based on *z*

$$Ra_z = \frac{g\beta z^3 (T_h - T_m)}{\alpha \nu} \quad (7)$$

And Ra_H is the Rayleigh number based on the enclosure height *H*

As the time increases, the convective zone expands downward. As mentioned, the heat transfer mechanism is convection over the height z and conduction over *(H- z)*; therefore, the total heat transfer rate through the heated wall, *Q*, is the sum:

$$Q \sim kz \frac{T_h - T_m}{\delta_z} + k(H - z) \frac{T_h - T_m}{s} \quad (8)$$

Thus, the Nusselt number is made up of two contributions, one due to conduction and the other to convection:

$$Nu \sim \theta^{-1/2} + Ra\theta^{3/2} \quad (9)$$

In conclusion, this heat transfer scaling law holds starting with $\theta = 0$ until the assumed convection zone (height *z*) extends all the way to the bottom of the liquid space, that is, until $z \sim H$. Let θ_1 be the time scale that corresponds to $z \sim H$, the mixed regime ends at a time of order: $\theta_1 \sim Ra^{-1/2}$. The Nusselt number scaling law for this regime distinguishes itself through the theoretical prediction of a Nu minimum of order $Nu \sim Ra^{1/4}$ at $\theta_{min} \sim Ra^{-1/2}$.

In the convection regime (Figure 3-c), also named quasi-steady regime, the convection fills the entire liquid space of height *H*. The overall Nusselt number scale is $Nu \sim Ra^{1/4}$ and the average melting front location is $s_{av} \sim HRa^{1/4}\theta$. In a system of finite horizontal extent L, this scenario holds until the liquid-solid interface reaches the right wall, i.e. $s_{av} \sim L$. Let $\theta_2 \sim \frac{L}{H} Ra^{-1/4}$ be the time scale associated with this event, the convection regime exists only if $\theta_2 > \theta_1$, that is if $Ra^{1/4} > \frac{H}{L}$. When this criterion is not satisfied (i.e., when $\theta_2 < \theta_1$), the mixed conduction plus convection regime ends at a time of order θ_2, that is, before the *Nu* (θ) curve has had time to reveal its minimum.

Finally, what happens after the melting front reaches the right wall constitutes a distinct heat transfer regime, the main features of which are sketched in Figure 3-d.

The Nusselt number curve function of time *Nu* (θ) has the features predicted by the scale analysis: first, the pure conduction ($\theta \ll \theta_1$) decay of order $\theta^{-1/2}$, here *Nu* (θ) starts with a maximum at the heated wall then decreases, followed by the mixed regime ($\theta \sim \theta_1$) with its *Nu* minimum, and finally, the pure convection regime ($\theta_1 < \theta < \theta_2$), *Nu* is time independent and plateau of order $Ra^{1/4}$. In fact, the convection aids in increasing the Nusselt number that eventually decays to an asymptotic value.

C) Enthalpy method for phase change problem in details

The enthalpy formulation is one of the most attractive and popular fixed-grid methods for solving the Stefan problem [5]. The main advantages of this method are that it does not require an explicit treatment of the moving solid-liquid interface [6], the governing equation is similar to the single phase equation and the enthalpy formulation allows a mushy zone between the two phases. As described by Voller [5], the equation of heat transfer for the phase change controlled by the conduction can be written as follows:

$$\frac{\partial H}{\partial t} = div\left(\frac{k}{\rho} grad\ T\right) \quad (1)$$

Where the total enthalpy H is the sum of sensible and latent heat:

$$H = h + L_H f_l \quad (2)$$

Where

$$h = \int_{Tm}^{T} Cp\ dT \quad (3)$$

Tm is the melting temperature of the PCM. In case of isothermal phase change, the fraction of the liquid is defined as:

$$f_l = \begin{cases} 0 & \text{if T} < \text{Tm (solid)} \\ 0-1 & \text{if T} = \text{Tm (mushy)} \\ 1 & \text{if T} > \text{Tm (liquid)} \end{cases} \quad (4)$$

Substituting equation (2) into equation (1) we get:

$$\frac{\partial h}{\partial t} = div\left(\frac{k}{\rho} grad\ T\right) - L_H \frac{\partial f_l}{\partial t} \quad (5)$$

Equation (5) combined with equations (3) and (4) together with the appropriate initial and boundary conditions constitute the mathematical model of conduction-controlled phase change. The two-dimensional equation (6), obtained directly from equation (5) is then used:

$$\frac{\partial h}{\partial t} = \frac{\partial}{\partial x}\left(\frac{k}{\rho}\frac{\partial T}{\partial x}\right) + \frac{\partial}{\partial y}\left(\frac{k}{\rho}\frac{\partial T}{\partial y}\right) - L_H \frac{\partial f_l}{\partial t} \quad (6)$$

the key feature of the used method [7] is to totally separate the calculation of the temperature of that of the liquid fraction. Thus, when a control volume reaches the melting temperature, its temperature is fixed and the energy that it gives or receives from its neighbors is considered through the liquid fraction.

At first, consider the case of control volume “i,j” which is fully solid or fully liquid. In this case, according to the definition of the sensible enthalpy (equation (3)) and the liquid fraction (equation (4)) it follows that:

$$\frac{\partial h_{i,j}}{\partial t} = Cp\ \frac{\partial T_{i,j}}{\partial t} \tag{7}$$

And

$$\frac{\partial f_l}{\partial t} \equiv 0 \tag{8}$$

Cp represents the specific heat of the solid or liquid phase, depending on the phase of the considered control volume. Therefore equation (6) becomes:

$$\rho Cp\ \frac{\partial T}{\partial t} = \frac{\partial}{\partial x}\left(k\ \frac{\partial T}{\partial x}\right) + \frac{\partial}{\partial y}\left(k\ \frac{\partial T}{\partial y}\right) \tag{9}$$

To solve the two-dimensional 2D phase change problem, the implicit finite volume method (Patankar 1980 [8]) is used, and the code is written in MATLAB®. The domain is divided into rectangular control volumes CV (see Figure 4).

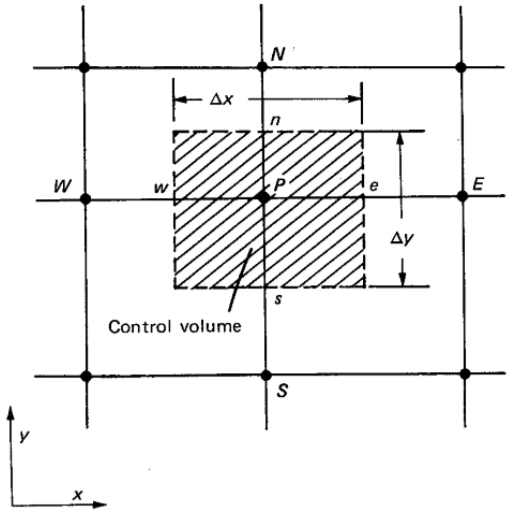

Figure 4: Typical control volume for the 2D situation

The finite volume equations are derived by integrating equation (9) over a typical control volume. It is also necessary, in time-dependent problems, to integrate with respect to time *t* over a small interval Δ*t* from, say, *t* until *t* + Δ*t* as following:

$$\rho Cp \int_t^{t+\Delta t}\int_w^e\int_s^n \frac{\partial T}{\partial t}\,dxdydt = \int_t^{t+\Delta t}\int_w^e\int_s^n \frac{\partial}{\partial x}\left(k\ \frac{\partial T}{\partial x}\right)dxdydt + \int_t^{t+\Delta t}\int_w^e\int_s^n \frac{\partial}{\partial y}\left(k\ \frac{\partial T}{\partial y}\right)dxdydt \tag{10}$$

After integration, we obtain the discretization equation as following:

$$a_P T_P^{t+\Delta t} = a_W T_W^{t+\Delta t} + a_E T_E^{t+\Delta t} + a_S T_S^{t+\Delta t} + a_N T_N^{t+\Delta t} + b \tag{11}$$

Or

$$a_{i,j} T_{i,j}^{t+\Delta t} = a_{i-1,j} T_{i-1,j}^{t+\Delta t} + a_{i+1,j} T_{i+1,j}^{t+\Delta t} + a_{i,j-1} T_{i,j-1}^{t+\Delta t} + a_{i,j+1} T_{i,j+1}^{t+\Delta t} + b \tag{12}$$

where,

$$a_W = a_{i-1,j} = k_w \frac{\Delta y}{(\Delta x)_w} \tag{13}$$

$$a_E = a_{i+1,j} = k_e \frac{\Delta y}{(\Delta x)_e}$$

$$a_S = a_{i,j-1} = k_s \frac{\Delta x}{(\Delta y)_s}$$

$$a_N = a_{i,j+1} = k_n \frac{\Delta x}{(\Delta y)_n}$$

$$a_P = a_W + a_E + a_S + a_N + a_P^0$$

$$a_P^0 = \frac{\rho Cp \Delta x \Delta y}{\Delta t}$$

$$b = a_P^0 T_P^0$$

where, the product $\Delta x \Delta y$ is the volume of control volume, and the index "0" designates the previous time step. Note that for the boundary nodes, the boundary conditions will be included in the vector b . Deriving the discretization equation for each control volume, we form a system of linear algebraic equations that is written in a matrix form as:

$$A * T = b \quad (14)$$

In the control volume adjacent to the volume control where phase change occurs, a discontinuity in the thermal properties occurs; a thermal conductivity at the interface must be used. The latter reflects this discontinuity and it is calculated as the harmonic average of thermal conductivities of neighboring control volumes.

The thermal conductivity of the control volume where the phase change occurs is approximated from the liquid fraction:

$$k_{pc} = k_l f_l + k_s (1 - f_l) \quad (15)$$

where, the index "pc" represents the control volume control where phase change occurs, indices l and s denote respectively the liquid and solid phases. Thus, for example, to calculate the thermal conductivity at the interface "north" of a control volume *P* directly to the "south" of the control volume *N* which changes phase, we use the following equation:

$$k_e = \frac{2 k_P k_N}{k_P + k_N} \quad (16)$$

Where, in this case:

$$k_N = k_{pc} \quad (17)$$

Since the control volume *N* (i.e., located above the considered control volume *P*) undergoes a phase change. A similar calculation is performed if the control volume undergoing phase change is below, before or after the considered control volume.

Secondly, the case of a node "i" where phase change occurs is considered. Therefore, the liquid fraction for this node is strictly in the range [0, 1] and the temperature for this node is equal to the melting temperature:

$$T_i \equiv T_m \tag{18}$$

From equation (3) we get:

$$\frac{\partial h}{\partial t} \equiv 0 \tag{19}$$

Equation (6) becomes:

$$L_H \frac{\partial f_l}{\partial t} = \frac{\partial}{\partial x}\left(\frac{k}{\rho}\frac{\partial T}{\partial x}\right) + \frac{\partial}{\partial y}\left(\frac{k}{\rho}\frac{\partial T}{\partial y}\right) \tag{20}$$

Integrating the above equation over a typical control volume and simultaneously averaging over a finite increment of time Δt we get:

$$f_{l_{i,j}} = f_{l_{i,j}}^{0} + \frac{k_e \Delta t}{\rho L \Delta x^2}(T_E - T_m) - \frac{k_w \Delta t}{\rho L \Delta x^2}(T_m - T_W) + \frac{k_n \Delta t}{\rho L \Delta y^2}(T_N - T_m) - \frac{k_s \Delta t}{\rho L \Delta y^2}(T_m - T_S) \tag{21}$$

This equation is used to adjust the liquid fraction in the control volume where the phase change occurs. It should be noted that when the material doesn't have the same density for the liquid and solid phases, an average density should be used in equation (21). The liquid fraction is calculated depending on the temperature distribution unlike other studies [5] [9] where the latter is adjusted depending on the enthalpy field. To the control volume undergoing a change phase, the coefficients of equation (11) take the following values:

$$a_W = a_E = a_S = a_N = a_P^0 = 0$$
$$a_P = 1$$
$$b = T_m \tag{22}$$

These coefficients allow isolating the CV where the phase change occurs fixing its temperature to the melting point and considering that the energy will be supplied or given to the neighboring CV through the variation of its liquid fraction. Thus, according to equation (21), all the heat supplied to the control volume which undergoes a phase change is used to change the amount of latent heat.

The implementation of the computational model can be described as follows:

1. The coefficients "a" of the equation (11) are formed depending on the properties of each node. If a node (or volume control) undergoes a phase change, coefficients (13) should be replaced by those of (22).
2. The temperature field is calculated solving the sets of equations (11).
3. The liquid fractions are updated from the temperature field using equation (21).
4. Check for the "beginning" and the "end" of melting is performed. If a node ends or starts phase change, some coefficients must be adjusted and the steps 1-3 must be repeated for the current time step.
    - Check the beginning of melting

For a given time step, if $T_{i,j} \geq T_m$ and $T_{i,j}^0 < T_m$ it indicates that the melting just started in the control volume. In this case, the node temperature $T_{i,j}$ is fixed to the melting temperature Tm, and the coefficients (13) must be replaced by coefficients (22). However, if the value $T_{i,j}$ is simply modified and set equal to Tm, a quantity of energy necessary for this CV to reach Tm is not considered. Therefore, equation (21) takes the following form:

$$f_{l_{i,j}} = f_{l_{i,j}}^0 + \frac{k_e \Delta t}{\rho L_H \Delta x^2}(T_E - T_m) - \frac{k_w \Delta t}{\rho L_H \Delta x^2}(T_m - T_W) + \frac{k_n \Delta t}{\rho L_H \Delta y^2}(T_N - T_m) - \frac{k_s \Delta t}{\rho L_H \Delta y^2}(T_m - T_S) - \frac{Cp_s}{L_H}\left(T_m - T_{i,j}^0\right) \quad (23)$$

The last term on the right-hand side of equation (23) represents the amount of sensible heat that is needed to raise the temperature of the control volume from the temperature in the previous time $T_{i,j}^0$ to the melting temperature T_m. Consequently, that amount of heat cannot be used for melting the PCM.

- Check the end of melting

For a given time step, if $f_{l_{i,j}} \geq 1$ and $f_{l_{i,j}}^0 < 1$ it indicates that within this time step, the control volume in question has melted completely. In this case, $f_{l_{i,j}}$ is set to 1, and the coefficients (22) in equation (11) are replaced by the coefficients (13) and the calculation is repeated for this time step. In the time step in which the phase change boundary moves from the control volume in question to the next one, the temperature of the volume control at the previous time is modified as follows:

$$T_{i,j\,modified}^0 = T_{i,j}^0 - \frac{L_H}{Cp_l}\left(1 - fl_{i,j}^0\right) \quad (24)$$

This modified temperature for the previous time is used to recalculate the temperature distribution in the PCM.

Where the last term on the right-hand side can be described as the amount of heat needed to completely melt the control volume in question within the time step and which consequently cannot be used to raise the temperature of the PCM.

D) CFD model numerical and experimental validation

In this study, the CFD model (chapter 2, section 3.2.) used to validate the proposed simplified model is based on the modified heat capacity method. This method is well adapted for commercial finite element solvers [10], and has been already validated both numerically in the references [11] [12] and experimentally in [8] [13].

P.H. Biwole et al. [13] proposed a detailed mathematical and numerical modeling of heat and mass transfers in coupled solar panel/phase change material architectures. A volume force was added to the buoyancy term in the Navier–Stokes' momentum conservation equation in order to force the

velocity field to be zero when the PCM is solid. In order to simulate both conduction and convection, the transient heat transfer diffusion equation was numerically solved simultaneously with the Navier–Stokes equations using a finite elements method. To validate the model, the experimental and simulated moving solid–liquid boundary was compared as well as the velocity field inside the PCM container through a PIV apparatus.

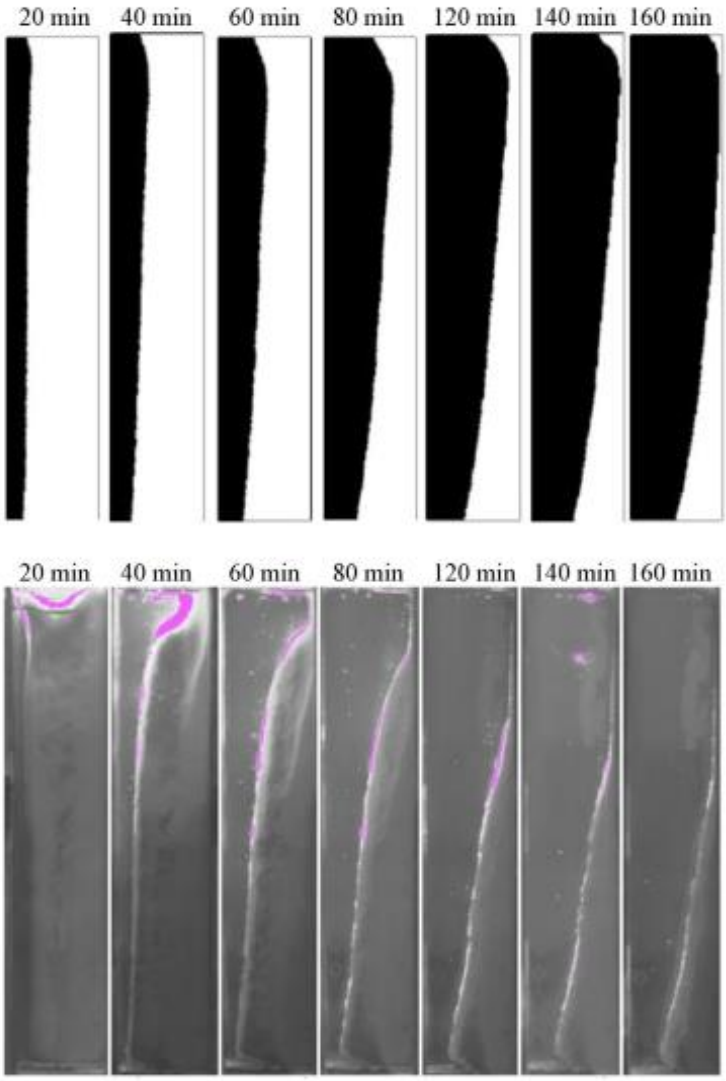

Figure 5: Transient comparison of the simulated and actual liquid–solid moving boundary location.

The transient comparison of the simulated and actual liquid–solid moving boundary location was carried out. On this first experiment, a fixed temperature of 40 ºC was imposed on the left side of the PCM tank and 20 ºC was imposed on the right side. A photograph of the boundary was taken every 20 min. This comparison showed a good agreement between simulation and measurement except on the top of the PCM domain as visible in Figure 5. The difference here is probably due to the air layer which was not simulated.

E) Thermal expansion

Experimentally, to prevent breaking from thermal expansion of the PCM, the bricks were initially filled with the PCM at a temperature of 50 ºC and an air gap of 2 cm was left on top of the liquid surface inside each brick.

Numerically, the geometry deformation due to volume expansion of the PCM was not modeled. This may cause a numerical loss of mass. However, the lower density of the liquid phase of the Fatty Acids (about 7.9 % lower than the solid density) means that a lower percentage of the mass in the system may numerically disappear between the initial fully solid phase and the final fully liquid one. This in turn may affect energy in the system, specifically the sensible energy.

In the numerical model, the ratio of sensible heat to latent heat is given by the Stefan number:

$$Ste = \frac{Cp(T_h - T_m)}{L_H} = 0.257$$

Thus, sensible energy represents about 20.44 % of the total energy stored, latent energy being the rest, which is not affected by the density change since it enters the system at melting. Therefore, the numerical loss of mass, and resulting energy difference in sensible heat represents approximately 7.9 % of the sensible amount, i.e. about 1.6 % of the total energy, which is an acceptable trade-off between precision and easy implementation for engineering applications.

For octadecane there is no problem since $\rho_s = \rho_l$.

References

[1] A. Bejan, *Convection heat transfer*, Fourth edition. Hoboken, New Jersey: Wiley, 2013.

[2] M. Lacroix and M. Benmadda, "Numerical simulation of natural convectiondominated melting and solidification from a finned vertical wall," *Numer. Heat Transfer*, no. Part A Appl. 31, pp. 71–86, 1997.

[3] R. Velraj, R. seeniraj, B. Hafner, C. Faber, and K. Schwarzer, "HEAT TRANSFER ENHANCEMENT IN A LATENT HEAT STORAGE SYSTEM," *Solar Energy*, vol. 65, no. No. 3, pp. 171–180, 1999.

[4] P. Jany and A. Bejan, "Scaling theory of melting with natural convection in an enclosure," *Int. J. Heat Mass Transf.*, vol. 31, no. 6, pp. 1221–1235, Jun. 1988.

[5] V. Voller, "Fast implicit finite-difference method for the analysis of phase change problems," *Numer Heat Transfer Part B*, pp. 17:155–69, 1990.

[6] H. S. Carslaw and J. C. Jaeger, *Conduction of heat in solids*. Oxford, UK: Oxford University Press, 1947.

[7] B. Zivkovic and I. Fujii, "An analysis of isothermal phase change of phase change material within rectangular and cylindrical containers," *Sol. Energy*, vol. 70, no. 1, pp. 51–61, 2001.

[8] S. V. Patankar, *Numerical heat transfer and fluid flow*. New York: McGraw-Hill., 1980.

[9] M. Lacroix, "Numerical simulation of a shell-and-tube latent heat thermal energy storage unit," *Sol. Energy*, vol. 50, no. 4, pp. 357–367, 1993.

[10] S. K. Saha and P. Dutta, "Heat transfer correlations for PCM-based heat sinks with plate fins," *Appl. Therm. Eng.*, vol. 30, no. 16, pp. 2485–2491, Nov. 2010.

[11] P. H. Biwole, D. Groulx, F. Souayfane, and T. Chiu, "Influence of fin size and distribution on solid-liquid phase change in a rectangular enclosure," *Int. J. Therm. Sci.*, vol. 124, pp. 433–446, Feb. 2018.

[12] W. Ogoh and D. Groulx, "Stefan's Problem: Validation of a One-Dimensional Solid-Liquid Phase Change Heat Transfer Process," in *Comsol Conference 2010*, 2010.

[13] P. H. Biwole, P. Eclache, and F. Kuznik, "Phase-change materials to improve solar panel's performance," *Energy Build.*, vol. 62, pp. 59–67, Jul. 2013.

CHAPTER 3

THERMAL BEHAVIOR OF A TRANSLUCENT SUPERINSULATED LATENT HEAT ENERGY STORAGE WALL IN SUMMERTIME

Chapter 3. Thermal Behavior of a Translucent Superinsulated Latent Heat Energy Storage Wall in Summertime

Résumé du chapitre en français

Comportement thermique estival d'un mur de stockage d'énergie translucide et super-isolé

Ce chapitre étudie le comportement thermique d'un mur solaire passif super isolant et translucide composé d'un vitrage, d'aérogel de silice (matériau d'isolation transparent), et du MCP (acide gras) contenu dans des briques de verre. L'objectif du mur MCP-Aérogel est de fournir stockage et restitution d'énergie, éclairage naturel et super isolation thermique / acoustique. Ce mur a été caractérisé expérimentalement en ambiance contrôlée et in situ sur un bâtiment grandeur nature situé au sein du laboratoire PERSEE de l'Ecole des Mines de Paris à Sophia Antipolis, dans le sud de la France. Les résultats expérimentaux ont montré que la performance thermique du mur est très élevée en hiver, tandis qu'en été les gains de chaleur à travers le mur provoquent un problème de surchauffe et le MCP n'arrive pas à se solidifier. Pour optimiser la performance du mur en été, un modèle numérique simplifié décrivant les mécanismes de transfert de chaleur à travers le mur en tenant compte de la convection naturelle dans le MCP liquide et de l'absorption et transmission du rayonnement courte longueur d'onde a été développé sous MATLAB. Le modèle numérique structuré est simple à mettre en œuvre et assez rapide pour être couplé avec TRNSYS afin d'évaluer la performance thermique annuelle de l'ensemble du bâtiment.

Le modèle MATLAB-TRSNYS est ensuite validé en utilisant des résultats expérimentaux pendant sept jours consécutifs en été et en hiver ; un bon accord est obtenu entre la température de surface interne du mur simulée et mesurée expérimentalement, ainsi qu'en comparant la température de l'air intérieur. L'erreur quadratique moyenne (EQM) et le pourcentage de l'erreur quadratique moyenne (PEQM) correspondants sont calculés et se situent entre 0,57 ºC - 1,43 ºC et 1,87% - 6,99% respectivement. La température dans la couche MCP calculée est également validée expérimentalement en été et les EQM et PEQM trouvés sont respectivement de 1,92 ° C et de 5,33%. Des solutions pour le problème de la surchauffe estivale parmi lesquelles des dispositifs d'ombrage, la ventilation naturelle nocturne et l'utilisation d'un type de verre spécial qui présente des propriétés de rayonnement solaire sélectif en fonction de la saison (Prisma Solar glass) ont été proposées. Ensuite, le mur a été appliqué dans des différentes conditions climatiques et le confort thermique ainsi que le cyclage du MCP ont été étudiés.

Les conclusions suivantes peuvent être tirées de ce chapitre : (1) le modèle numérique développé représente un bon point de départ pour des simulations sur différentes configurations du mur et permet d'étudier pleinement ses capacités et ses inconvénients sous différentes conditions opératoires, orientations, géométries et différents climats sans avoir besoin d'effectuer des analyses expérimentales coûteuses ; (2) pour être plus réaliste, la convection naturelle dans le MCP liquide ne doit pas être négligée lors de la modélisation du changement de phase ; (3) l'utilisation du vitrage Prisma Solar glass à la place du verre ordinaire dans la composition de la paroi étudiée s'avère être une technologie efficace pour résoudre le problème de surchauffe rencontré en été, tout en préservant les avantages du mur pendant l'hiver ; (4) le confort thermique ainsi que le cyclage de MCP en été dépendent des conditions climatiques. Dans le climat méditerranéen (classification Koppen Geiger Csa), les stores vénitiens à lattes tournées à 45 degrés combinés avec un surplomb de 1 m de projection peuvent assurer le confort thermique. Dans les climats océaniques (Cfb) et continentaux humides (Dfb), le confort thermique peut être assuré par l'utilisation exclusive d'un surplomb de projection 1 m et des stores vénitiens respectivement. Dans le climat subarctique (Dfc), le MCP réalise un cycle diurne complet et le confort thermique peut être atteint en fournissant une ventilation naturelle nocturne.

Dans le chapitre suivant, le coût global durant le cycle de vie (CCV) et du temps de retour sur investissement (TRI) et l'optimisation du mur MCP-aérogel dans différentes conditions climatiques seront étudiées en utilisant le modèle numérique validé.

Abstract

This paper investigates the thermal performance of a translucent solar wall providing, concurrently, storage and restitution of heat, super thermal-acoustic insulation and daylighting to the interior environment. The wall is composed of glazing, silica aerogel used as a transparent insulation material (TIM) and glass bricks filled with fatty acid, a eutectic phase change material (PCM). To assess the TIM–PCM wall thermal behavior, experimentations were conducted in-situ in a full-sized test cell located in Sophia Antipolis, southern France. Experimental data shows that the tested wall is more effective in winter and might cause overheating during the summer mainly due to solar gains and un-cycling behavior of PCM which remains in liquid state. To enhance the energy performance of the wall in summertime, a numerical model describing the heat transfer mechanisms occurring in the PCM layer in combination with the other transparent wall layers is developed. Then, the model of the wall is linked to TRNSYS software to assess the thermal performance of the whole building. The numerical model is validated experimentally, and a good agreement is shown comparing the simulated values with the measured data for seven consecutive days in summer and winter. The importance of considering the natural convection effect in the liquid PCM is also demonstrated. Moreover, it was shown that shading devices can effectively reduce overheating while natural night ventilation decreases the indoor temperature without affecting the PCM performance since the outdoor temperature is always higher than the phase change temperature. The use of a glass with selective solar reflection properties depending on the season instead of the ordinary glazing is shown also to be very effective way to overcome the overheating problem. Finally, the TIM-PCM wall is tested under different climate conditions and passive solutions are given to ensure thermal comfort in summer season.

Keywords: TIM-PCM wall, natural convection, radiation, experimental validation, overheating, thermal comfort.

Highlights:

- TIM-PCM wall provides heat storage/release, heat/sound insulation, and daylighting.
- Experimentations in-situ carried out in Sophia Antipolis, France.
- Numerical model of the heat transfer through the wall is developed.
- The model of the wall linked to TRNSYS is validated experimentally.
- Shading devices and nocturnal ventilation reduces overheating and discomfort.

1. Introduction

Buildings account for almost 41% of the world's energy consumption, which contributes to 30% of the annual greenhouse gas emissions [1]. Trombe wall integrating phase change materials (PCM) is a particular passive solar technique that has shown great potentialities and can reduce effectively the building energy consumption. Basically, traditional Trombe walls [2]–[6] consist of an external glazing, an air channel, and a high heat capacitance wall in contact with the indoor environment. To improve the Trombe wall heat storage performance, phase change materials were implemented in the wall composition and this technique has been investigated by numerous researchers [7]–[12]. During the day, this wall is heated due to the incident solar radiation, melting the PCM. While at night, when the outdoor temperature falls below the phase change temperature, the heat stored by the PCM is released warming the building. Fiorito (2012) [8] conducted a parametric study on the use of PCM in Trombe walls by varying the PCM position and the melting point temperature for five different climates. they found enhanced performances for the modified Trombe wall. Zalewski et al. [9] studied experimentally a Trombe wall with PCM components filled in the air channel and an insulating board replacing the high capacitance wall. They found that the heat storage capacity of the wall is increased. Also, an experimental Trombe wall (ventilated façade) with PCM was studied by De Gracia et al. [10] during winter season. They found that the use of the ventilated facade with PCM improves significantly the thermal behavior of the whole building. Kara and Kurnuç [13] investigated a PCM Trombe wall with a novel triple glass (NTG) to improve the performance of conventional Trombe wall system and overcome its main disadvantage: the overheating during the summer. However, in all these applications, the light transmission was still absent.

On the other hand, transparent envelope components are key elements in buildings, especially in offices and commercial buildings, that affect the energy performance and daylighting [14]–[16].

The integration of PCM in a transparent element of the building envelope enhances the ability of energy storage, since the PCM will be directly exposed to the solar radiation. This technology aims to smooth the indoor temperature, and decrease the energy fluctuations, providing daylighting at the same time.

Phase change materials were integrated within double [17] [18] or triple glazing units [19], within more complex glazing components [20] and within translucent solar walls [21]. The performance of glazing with integrated PCM was investigated both experimentally [17]–[19], [22], [23] and numerically [24]–[26]. Numerical models were specifically developed to take the interaction of PCM with solar radiation into account [27]–[30]. All numerical models developed in these studies neglected effect of natural convection in the liquid PCM. A literature review of the use of PCM in transparent and translucent building envelope components can be found in [31].

Manz et al. [21] studied a translucent wall for solar heating and daylighting composed of glass pan, air gap, a translucent PCM and a transparent insulation material (TIM). They investigated experimentally the optical PCM properties and a prototype of the TIM-PCM wall was constructed in 1994 in Swiss. Also, a one-dimensional numerical model (side effects were neglected) was developed considering only heat transfer by conduction and the optical properties were simulated using a Monte Carlo technique. The results show that the thermal and optical performance of the wall is very promising and that the chosen PCM in solid state reduces the heat and light gains, thus they proposed considering another PCM with a melting temperature of 21ºC instead of 26.5ºC. Weinläder et al. [32] investigated experimentally the thermal behaviour of three glazing systems incorporated with a plastic container filled with different PCM. However, in both studies the behavior of the system was not investigated in detail in the hot season and inferences on thermal comfort were not evaluated according to standards. To improve the poor thermal inertia of conventional glazing systems, Goa et al. [27] studied the implementation of a PCM layer in combination with glass panes. They developed a one-dimensional numerical model for heat and shortwave wave transmission, and the model was validated experimentally. They found that the numerical tool represents a good base for simulations on different configurations of PCM glazing systems.

Ismail et al. [28] investigated the thermal and optical properties of double-glazed units filled with PCM, through numerical and experimental analysis. For the numerical model, a one-dimensional formulation is developed, and a moving grid procedure is used within the PCM layer. They found that the PCM filled glass window system is practical and thermally effective.

Although the inclusion of PCM in glazing systems can have a positive effect on thermal comfort and contributes to improvements in the energy performance of buildings [22], the introduction of PCM in a double-glazing unit results in a reduced thermal resistance negatively affecting the thermal performance of the system. In addition, due to the complete melting of the PCM within the double-glazing unit during summer, the internal surface temperature of the glazing may increase to a level that may negatively affect thermal comfort [22].

In this chapter, a new kind of translucent storage wall proposed by the ANR INERTRANS [(1)] project is studied. It is composed of glazing, granular Silica Aerogel and PCM filled in glass bricks [33]. Many features, that are not found in a conventional Trombe wall, are combined by such wall: it provides heat gains from solar radiation, high thermal insulation, heat storage and release, natural daylighting and visual communication to the outside world.

The thermal performance of the TIM-PCM wall is tested in a full-sized test cell located in Sophia Antipolis, Southern France, within the center for Processes, Renewable Energies and Energy Systems (PERSEE) of Mines Paristech graduate school. In winter season, particularly in sunny cold days, the

PCM absorbs solar radiation, melts, and then releases the stored heat to the building at night by solidifying. While during the summer, an overheating problem is encountered mainly due to solar gains, the PCM remains in its liquid state and it is unable to release the stored heat at night [34]. Thus, to enhance the energy performance of the wall, numerical modeling of the heat transfer mechanisms in the wall materials is required and especially the melting with combined natural convection and radiation. Usually, the building models with integrated PCM ignore the convection effect in the liquid region, due to the complexity of CFD models and the required high computational time. It was proven that this assumption is not always adequate and convection effect must be considered in liquid PCM [35]–[43] [44].

Most previous works studying PCM-enhanced transparent components have been mainly developed for the heating season, and there is little quantification of their real advantages in terms of energy efficiency and indoor environmental comfort in summer season. Thus, the present paper focuses on the analysis of the summer performance of the innovative translucent TIM-PCM wall and on its effect on thermal comfort. The numerical model developed in this study aims to provide an easy tool to use and fast enough to be adopted as a design tool, to investigate the potentials and disadvantages of the novel TIM-PCM wall under different operative conditions and different climates and to propose solutions to optimize its performance in summer, without the need of performing extensive and expensive experimental analysis.

In this chapter, the TIM-PCM wall system is described in section 2, experimental data analysis is presented in section 3. A numerical model of the heat transfer mechanisms through the wall including natural convection and radiation during phase change is detailed in section 4, the code is written on MATLAB. The TIM-PCM wall model is linked to TRNSYS software to simulate the thermal behavior of the whole experimental cell in section 5. The MATLAB - TRNSYS model is validated in summer and winter season against the experimental results and the importance of considering natural convection in liquid PCM is demonstrated in section 6. Solutions for the overheating problem including shading devices and nocturnal natural ventilation are proposed in section 7. A special type of glass, Prisma solar glass, is used instead of the ordinary glazing in the TIM-PCM wall composition in section 7.2. The thermal behavior of the wall is tested using another PCM with higher melting temperature of 28ºC in section 7.4. Finally, the model is exploited, and the thermal comfort range is examined for three months in summer season under different climates conditions using ASHRAE Standard 55-2010 in section 8 and section 9.

2. System description

The TIM–PCM wall, proposed in the French INERTRANS [1] project, is shown in Figure 3-1 and Figure 3-2. It is composed, from outside to inside, of a glass pane having a thickness of 0.8 cm, a 4cm thick bed of granular silica aerogel (transparent insulation material), and eutectic of fatty acids as PCM filled in glass bricks of dimension 19cm × 19cm × 5cm. The Silica aerogel granulate bed provides super heat insulation, meaning that it has a thermal conductivity lower than that of still air (0.018 w/ (m K) for aerogel, 0.026 w/ (m K) for still air). The wall also provides sound insulation and solar and light transmission. This particular silica aerogel is chosen to meet the TIM–PCM wall transparency and insulation principles. The chosen PCM has a comfortable phase change temperature with long term stability. It provides solar absorption, energy storage and restitution, in addition to light transmission. It absorbs the solar radiation when being in solid state, thus increasing its temperature until the complete melting is achieved and transmits solar radiation when being in liquid phase.

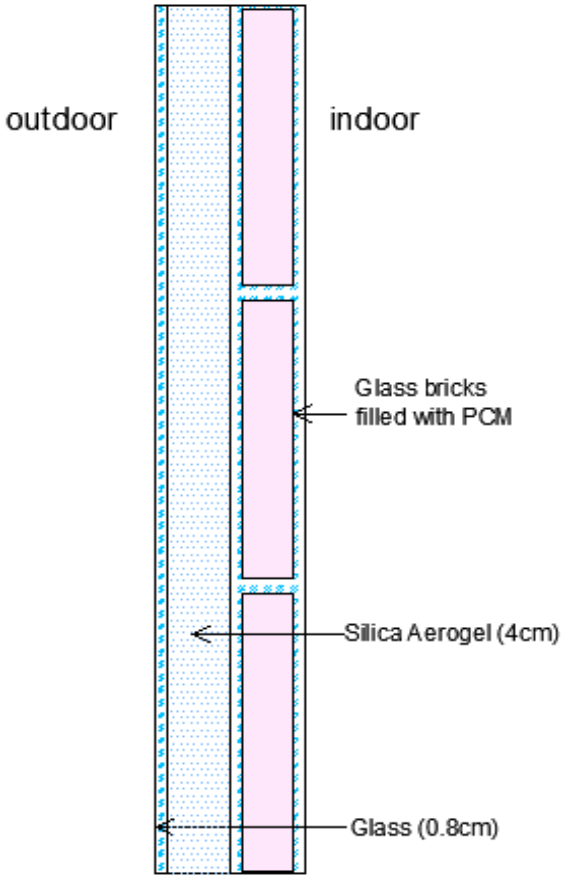

Figure 3-1: Schematic of the TIM–PCM wall.

(a) (b)

Figure 3-2: (a) TIM-PCM wall from the outside, (b) PCM in solid phase (left) and liquid phase (right), from the inside

The thermo-physical and optical properties of the used PCM, the silica aerogel and the glass are summarized in Table 3-1 to Table 3-4. Initially, at a temperature of 50ºC, the glass bricks are filled with the fatty acid and an air gap of 2 cm was left at the top of the liquid surface in each brick in order to avert breaking due to thermal expansion of the PCM [34] and the system is maintained by means of a wooden frame.

Table 3-1 Thermo-physical properties of the fatty acid eutectic [34]

Property	value
k_s (W/m.K)	0.182
k_l (W/m.K)	0.182
L_H (J/kg)	152000
Cp_s (J/kg.K)	1670
Cp_l (J/kg.K)	2090
ρ_s (kg/m^3)	960
ρ_l (kg/m^3)	884
Tm (°C)	21.3
α (m^2/s)	$9{,}85.10^{-8}$
ν (m^2/s)	11.10^{-6}
β (1/K)	$3.1.10^{-3}$

Table 3-2: Optical properties of the fatty acid eutectic CSTB [34]

		τ%	ρ%
Liquid state	Energetic	90	5
	Optical	78	6
Solid state	Energetic	≈ 0	53
	Optical	≈ 0	56

Table 3-3: Thermo-physical and optical properties of glass and Silica aerogel

properties/Materials	glass	Silica aerogel
Thickness (cm)	0.8	4
k (W/m.K)	1	0.018(at 25ºC)
Cp (J/kg.K)	840	1500
ρ (kg/m^3)	2700	100
τ%	80	57
α%	12	10

Table 3-4: Physical properties of the transparent insulation material silica aerogel (manufacturer' data)

Property	Value
Particle size	0.5-4.0 mm
Pore diameter	20 nm
Porosity	> 90%
Surface area	600-800 m^{2}g^{-1}

(1) INERTRANS is acronym of Translucent Inertia, project funded by the French National Research Agency (ANR), PREBAT program 2007).

3. Experimental data

To test the TIM–PCM wall behavior, experiments were conducted in situ in a full-sized test cell located in Sophia Antipolis, Alpes-Maritimes, southern France of latitude 43.61°, longitude 7.05° and elevation 164.23 meters.

The experimentations allow studying the influence of the TIM–PCM wall on the energy balance of the building in real conditions. The test cell is very well insulated with R-value varying from 4.7 to 6.8 (K.m²/W) depending on the PCM state and it is composed of three rooms (Figure 3-3). A reference room and a test room (9.29 m^2 floor area each), having the same walls properties except of their south-facing walls. The third room is used for data acquisition purpose (18.8 m^2). The south wall of the reference room (7.15 m^2) is opaque with high capacitance, composed from inside to outside, of plaster, glass wool thermal insulation, concrete and a 4cm layer of aerogel-based coating. The south wall of the test room (7.25 m^2) contains the translucent TIM–PCM of surface 4.41 m^2, this wall being an inset wall of 20 cm depth. The south-facing wall was isolated from the thermal effects of the test-cell other walls, i.e. the west wall of the test room, the partition walls, the ground and the roof are highly insulated. The walls construction materials in the test cell and the thermo-physical properties are summarized in Table 3-5 and Table 3-6 respectively.

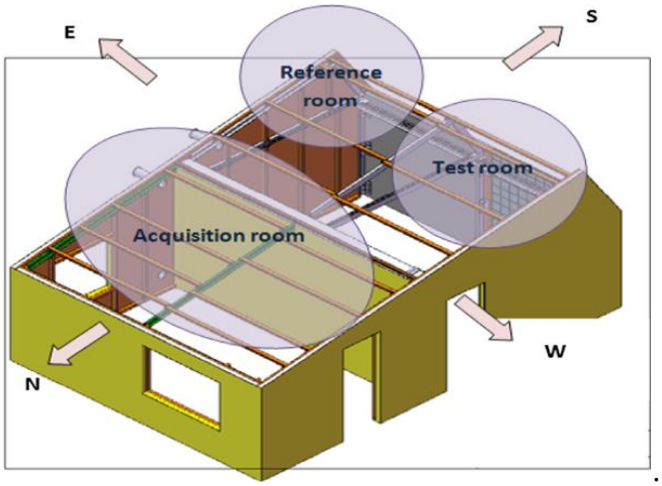

Figure 3-3 : Schematic presentation of the full-scale test cell.

Table 3-5: Test cell walls construction

Element	Area (m^2)	Construction	Thickness (m)
Test south wall	2.84	plasterboard	0.013
		Glass wool	0.16
		concrete	0.25
Reference south wall	7.15	plasterboard	0.013
		Glass wool	0.16
		concrete	0.25
		aerogel-based coating	0.04
Reference/test North wall	7.05/7.18	plasterboard	0.013
		Glass wool	0.16
		concrete	0.25
		Mousse phenol-formol	0.077
Reference west/ test east wall (partition)	11.7	plasterboard	0.013
		Glass wool	0.16
		plaster	0.013
Reference east/ test west wall	11.7	plasterboard	0.013
		Glass wool	0.16
		Wooden plate	0.019
		Expanded polystyrene	0.08
Reference/test floor	9.17/9.29	tiles	0.015
		concrete	0.15
		Expanded polystyrene	0.08
Reference/test south roof (slope 60º)	1.62/1.64	plasterboard	0.013
		Glass wool	0.16
		Wooden plate	0.018
Reference/test north roof (slope 12º)	8.27/8.38	plasterboard	0.013
		Glass wool	0.16
		Wooden plate	0.012
		Mousse phenol-formol	0.06
		Wooden plate	0.012
Acquisition room walls		Wooden plate	0.012

Table 3-6: Thermo-physical properties of the test room materials

Materials/properties	Thermal conductivity (W/m. K)	Specific heat (J/kg.K)	Density (kg/m^3)
plasterboard	0.32	800	790
Glass wool	0.041	840	12
concrete	2.1	800	2400
Aerogel-based coating	0.0268	990	156
Mousse phenol-formol	0.032	1255	32
Wooden plate	0.18	1700	780
Expanded polystyrene	0.04	1380	25
tiles	1	1000	2400

To measure the necessary data, a specific instrumentation is used:

- All-in one sensors (Prosensor HYGR0018 THAC, with added radiation protection) are used to measure the outdoor and the indoor air temperature (precision $\pm$0.4 ºC) and relative humidity (precision $\pm$3%).
- PT100 sensors, Prosensor Pt 100 DIN IEC 751 class B, are used to measure the surface temperatures with precision of $\pm$0.4ºC. And, PT100 sensors Prosensor SLM 250 PVC are used to measure the temperatures inside the TIM–PCM wall.
- A pyranometer (Littoclime 13S374, 320–1060 nm) of precision $\pm$7%, located at the east right-side of the TIM-PCM wall is used to measure the total radiation on the southern vertical plane, while a second pyranometer (Pulsonic, 400–1100 nm) of precision $\pm$4% is used to measure the total radiation on the horizontal plane.
- A wind vane and an anemometer (Pulsonic Aliza 147) of precision $\pm$0.5 m/s are used to measure the wind direction and velocity.
- Two sensors immersed in the PCM glass bricks are used to measure the temperature of the PCM.

The experimental cell is left in free floating mode, i.e. no mechanical HVAC system is installed, and no internal heat gains have been considered. The reference room is equipped with a cooling/heating system maintaining the room air temperature at 23°C in summer and winter.

The measured exterior and interior air temperatures and the incident solar radiation on the vertical plane for seven consecutive days in summer are shown in Figure 3-4. The average and maximum radiation on the south vertical plane, the maximum, minimum and average outdoor air temperature and the average indoor temperature from experimental data are summarized in Table 3-7.

Table 3-7: Summary of some experimental data measured for seven consecutive days in summer and winter season

	Average daily radiation on south vertical plane ($W.m^{-2}$)	Max radiation on vertical plane ($W.m^{-2}$)	Max outdoor temperature (ºC)	Min outdoor Temperature (ºC)	Average outdoor temperature (ºC)	Average indoor temperature (ºC)
30 July -5 August 2017	100.14	452.78	35.30	21.32	27.81	30.82
27 Januray-2 February 2017	41.63	719.26	16.63	5.22	10.65	18.38

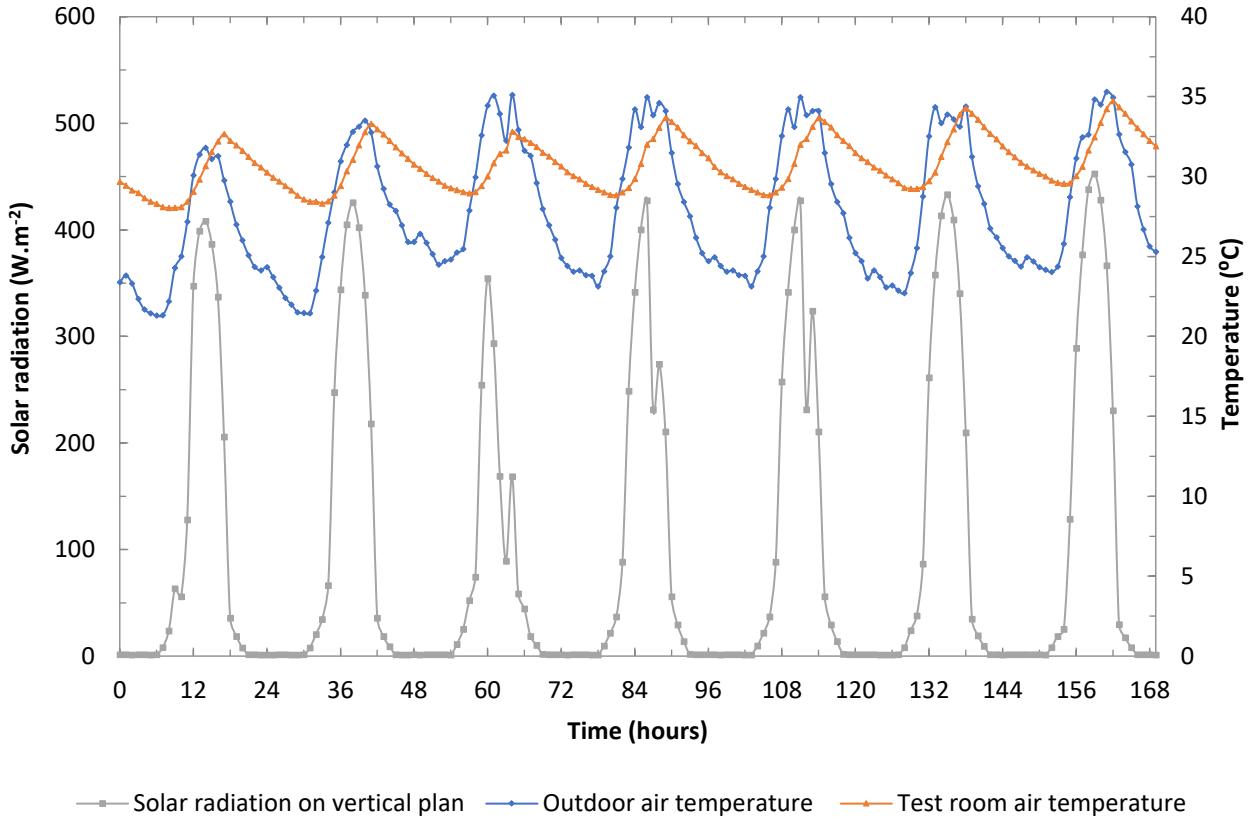

Figure 3-4: Temperatures and solar radiation for seven consecutive days in summer (30 July-5 August 2017)

The seven consecutive days in summer season (30 July-5 August 2017) are characterized by an outdoor air temperature varying from 21.32 ºC to 35.30 ºC, and a high solar radiation up to 452.78 $W.m^{-2}$ on the southern vertical plane. The high ambient temperature together with the solar radiation transmitted through the TIM-PCM wall, strongly increase the PCM temperature during the day (higher than 50ºC) and thus forbid even a partial solidification of the PCM at night (the PCM minimum temperature recorded at night is about 28ºC). This causes an overheating of the test room with an indoor air temperature going from 28.05 ºC to 34.73 ºC as shown in Figure 3-4. To avert this problem, and therefore attaining the thermal comfort range, shading devices (overhangs, blinds, shutters) or ventilation systems (natural night ventilation, mechanical ventilation) should be used.

The seven consecutive days in winter season (27January- 2 February) are characterized by a low outdoor temperature varying from 5.22 ºC to 16.63 ºC, with low (70.82 $W.m^{-2}$) and high (719.2 $W.m^{-2}$) solar radiation on the southern vertical plane. On January 27 and 28, the PCM does not melt staying in its solid state (PCM temperature lower than 21ºC) and the test room air temperature is about 17ºC. On January 29 and 30 and on February first, due the high incident solar radiation, the PCM melts during the day (PCM temperature up to 62ºC) and solidifies at night and the indoor temperature reaches more than 20ºC. The TIM-PCM wall is therefore very effective in the winter season (the average room air temperature is almost constant at18.38 ºC), keeping warm the indoor environment especially in sunny days. The measured PCM temperatures for seven consecutive days in winter and summer seasons respectively are shown in Figure 3-5.

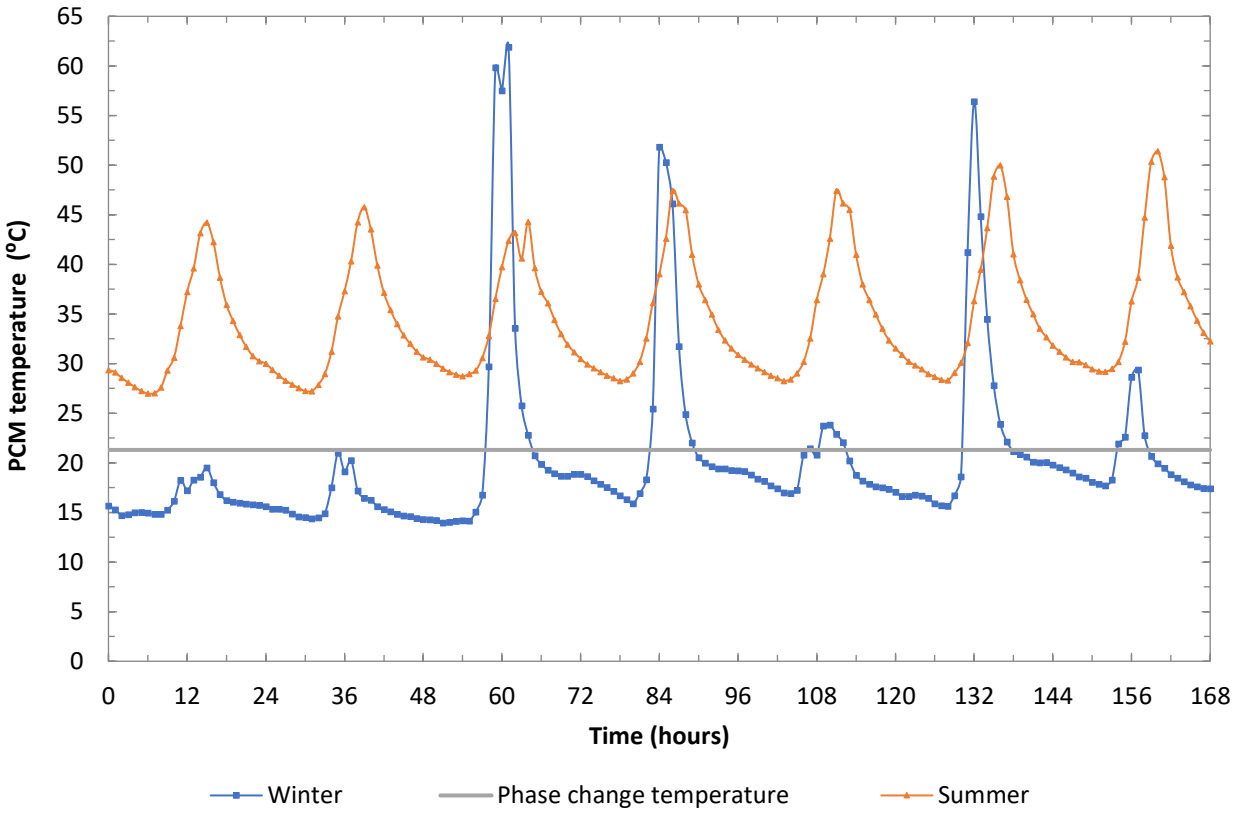

Figure 3-5: Measured PCM temperatures for seven consecutive days in summer (30 July-5 August 2017) and winter (27 January-2 February 2017).

4. Numerical model

The thermal study of a building and the validation of the associated numerical model require the knowledge of the different heat transfer mechanisms that take place: radiation, convection and conduction. To save computational time, most building energy simulation tools do not model the heat transfer in walls as two and three dimensional but rather consider it as one-dimensional approach.

Many researchers have conducted and experimentally validated one-dimensional transient numerical model for heat transfer in building envelopes integrating phase change materials [21], [27], [29], [45]–[48]. However, it was shown that the thermal bridge effects should not be neglected [49], and that the calculation of a thermal resistance of a wall, adopting the one-dimensional approach and neglecting the thermal bridge effects, could lead to an overestimation greater than 44% [50]. In addition, according to the French Scientific and Technical Center for Building Research (CSTB), thermal bridges can increase the thermal load of a house by 20% (CSTB, Réglementation thermique 2000).

The effective part of the TIM-PCM wall (without the frame) has only one element that causes a thermal bridge: the joints of the bricks. Modeling a portion of wall using software HEAT2, the conductive heat flux passing through the joints was estimated, and thus the thermal transmittance of the joints was found $Cj=1/Rj$ =16.54 W/(m^{2}K). The flow through the joints and the edges of the bricks is calculated as the difference between the flow through the glass bricks wall with the joints and the flow through a monoblock of glass brick.

In this study, a one-dimensional numerical model is developed considering the effect of thermal bridges caused by the joints of the bricks. Figure 3-6 shows the different modes of the heat transfer through the TIM-PCM wall and the representation of the node grid.

Mesh sensitivity analysis was carried out for the numerical model to make sure that the results are independent of the numerical domain. The number of nodes in each layer was increased and the solution was assumed grid independent when the difference between the calculated average indoor air temperatures for each grid size was less than 2%. The number of nodes in the PCM layer was augmented and a difference of about 1.2 % was found between the calculated average indoor temperatures for 5 nodes and 10 nodes.

Finally, a total of 16 nodes have been used, 2 for the glazing layer, 5 for the silica aerogel, 5 for PCM layer and 2 nodes for each glass brick. The chosen discretized scheme shows good accuracy within a satisfactory computational time, and it is well-matched with other works evaluating the annual thermal performance of PCM applications in facades [51]–[53].

The unsteady energy equation is written for each node and solved numerically (sections 4.1 to 4.6). The developed TIM-PCM wall model computes the temperature field and the solar radiation transmitted to the test cell through the wall at each time step, these outputs are then linked to TRNSYS to simulate the energy performance of the whole building.

4.1. Shortwave radiation

The shortwave solar radiation strongly affects the behavior of the translucent TIM-PCM wall, where the thermal energy storage in the PCM layer occurs mostly by dint of the interaction between the PCM and the solar radiation [51]. Phase change materials have variable optical characteristics that depend on their physical state; in the solid state, the PCM absorbs the solar radiation, thus increasing its temperature until the complete melting, while in liquid phase, the PCM transmits solar radiation, here the energetic and optical transmittance of TIM-PCM wall is significantly higher than that when PCM is in solid state [34]. The optical properties (transmission, reflection, and absorption coefficients) of the fatty acids eutectic are measured experimentally by the French scientific and technical center for building research CSTB (Table 3-2). The shortwave radiation through the PCM layer is modeled by means of a solution procedure proposed by Gowreesunker [18], where the nodal optical properties such as the transmissivity and absorptivity are evaluated in function of the transient liquid fraction f_l.

The solar radiation effect through a translucent wall can be accounted for using the radiative transfer equation (RTE). This equation can be solved using different methods such as Discrete Ordinates Model, Monte Carlo Model, Rosseland Model, Discrete Transfer Method, etc.; however, these methods are computationally expensive. On the other hand, the radiation can be taken into account without recurring to the full solution of the RTE, using the Radiosity - Irradiosity Method (RIM) [54]. In this paper, a simplified method proposed by Elarga et al. [55] is used, where the absorbed solar radiation is considered to be divided equally between the nodes representing each layer of the wall and the absorbed shortwave solar radiation flux is added into the energy equation as a source term.

Considering for example N nodes in the PCM layer, the absorbed solar radiation to be added to the energy equation at a node p is then given as:

$$\emptyset_{sol} = \frac{Q_{sol-trans}\,\alpha_P}{N} \qquad \textbf{Eq. 3-1}$$

where, $\emptyset_{sol}$ is the radiative source term, $Q_{sol-trans}$ is the transmitted solar radiation to the PCM layer (Eq. 3-10), α_P is the PCM absorption coefficient at the node p calculated using the equations proposed by Gowreesunker to model combined phase change and radiation problems [18].

The nodal optical properties such as the transmissivity and absorptivity in function of the transient liquid fraction f_l. When the PCM goes from the fully solid to fully liquid, the fractional change in PCM transmittance is given as:

$$\delta = \frac{\tau_l - \tau_s}{1 - \tau_s} \qquad \textbf{Eq. 3-2}$$

The relation between the extinction coefficient σ and the liquid fraction is written as:

$$\sigma = f_l\sigma_l + (1 - f_l)\sigma_s$$ **Eq. 3-3**

The transmittance of the PCM is:

$$\tau_P = 10^{-d}$$ **Eq. 3-4**

where d is the optical thickness:

$$d = \sigma.S$$ **Eq. 3-5**

where *S* stands for the physical thickness

The absorptivity of the PCM evaluated at each node is given as:

$$\alpha_P = [\delta f_l + (1 - d)](1 - \tau_{PCM})$$ **Eq. 3-6**

Moreover, the overall transmitted solar radiation through N=n+k layers is calculated using the following equations given by Siegel [56]:

$$\tau_s^{(n+k)} = \frac{\tau_s^{(n)}\tau_s^{(k)}}{1 - \rho_{s2}^{(n)}\rho_{s1}^{(k)}}$$ **Eq. 3-7**

$$\rho_{s1}^{(n+k)} = \rho_{s1}^{(n)} + {\tau_s^{(n)}}^2 \frac{\rho_{s1}^{(k)}}{1 - \rho_{s2}^{(n)}\rho_{s1}^{(k)}}$$ **Eq. 3-8**

$$\rho_{s2}^{(n+k)} = \rho_{s2}^{(k)} + {\tau_s^{(k)}}^2 \frac{\rho_{s2}^{(n)}}{1 - \rho_{s1}^{(k)}\rho_{s2}^{(n)}}$$ **Eq. 3-9**

where, $\tau_s^{(n+k)}$ is the transmittance for the entire system, $\tau_s^{(n)}$ and $\tau_s^{(k)}$ are the transmittances for n and k layers system respectively. $\rho_{s1}^{(k)}$ is the overall reflectance for a system of k layers for energy incident on the first (upper) surface of that entire system and $\rho_{s2}^{(n)}$ is the reflectance for a system of n layers for energy incident on the second (lower) surface of that entire n layer system.

The general characteristics of one layer are used to develop the overall behavior of a two-layer system, this procedure can be sustained and the behavior for one layer and two layers can be combined to build up the behavior for three layers, and so on.

For example, the transmitted solar radiation to the PCM layer is found using Eq. 3-7 to Eq. 3-9 as follow:

$$Q_{sol-trans} = \frac{\tau_1\tau_2\tau_3}{(1-\rho_2\rho_1)(1-\rho_2\rho_3)-\tau_2^2\rho_3\rho_1}.Q_{sol-total}$$ **Eq. 3-10**

where, τ_1, τ_2, τ_3 are the solar transmission coefficients and ρ_1, ρ_2, ρ_3 are the solar reflection coefficients of the glazing, silica aerogel and glass brick respectively.

The overall transmission of the solar radiation through the whole TIM-PCM wall calculated from Eq. 3-7 to Eq. 3-9 is found 27.36% in summer conditions when the PCM remains in liquid its state.

4.2. Longwave radiation exchange

Longwave radiative exchange takes place between the external surface of the wall and the outside environment, and among the internal surface of the wall and the indoor environment. The TIM-PCM wall is supposed to be opaque for the longwave radiation due to the presence of the silica aerogel layer.

The outdoor radiative heat exchange (W/m^2) is given as:

$$\emptyset_{\mathrm{LW,out}} = \varepsilon\sigma F_{\mathrm{grd}}\left(T_{\mathrm{grd}}^4 - T_{\mathrm{surf}}^4\right) + \varepsilon\sigma F_{\mathrm{sky}}\beta\left(T_{\mathrm{sky}}^4 - T_{\mathrm{surf}}^4\right) + \varepsilon\sigma F_{\mathrm{sky}}(1-\beta)\left(T_{\mathrm{air}}^4 - T_{\mathrm{surf}}^4\right) \quad \textbf{Eq. 3-11}$$

where, ε is the long-wave emittance of the surface and σ is the Stefan Boltzmann constant. The temperature of the ground surface is approximated to the ambient air temperature.

F_{grd} is the view factor of wall surface to ground surface temperature

$$F_{\mathrm{grd}} = (1 - \cos\delta)/2 \quad \textbf{Eq. 3-12}$$

F_{sky} is the view factor of wall surface to the sky

$$F_{\mathrm{sky}} = (1 + \cos\delta)/2 \quad \textbf{Eq. 3-13}$$

The view factor to the sky is divided between sky and air radiation by:

$$\beta = \sqrt{((1 + \cos\delta)/2)} \quad \textbf{Eq. 3-14}$$

where δ is the tilt angle of the surface, for vertical surface $\delta = 90°$.

The sum of the view factors to the ground, air, and sky is equal to 1. The view factor to the air will be often smaller than 0.15, since most surfaces lie somewhere between vertical and horizontal. So, air-surface interactions are not significant, so it will be neglected, the radiative heat exchange is linearized as follow:

$$\emptyset_{\mathrm{LW,out}} = h_{\mathrm{r,grd}} F_{\mathrm{grd}}\left(T_{\mathrm{grd}} - T_{\mathrm{surf}}\right) + h_{\mathrm{r,sky}} F_{\mathrm{sky}}\left(T_{\mathrm{sky}} - T_{\mathrm{surf}}\right) \quad \textbf{Eq. 3-15}$$

The sky temperature T_{sky} is given by Swinbank [57] function of the air temperature as follow, assuming a clear sky:

$$T_{\mathrm{sky}} = 0.0552 T_{\mathrm{air}}^{1.5} \quad \textbf{Eq. 3-16}$$

For a vertical wall, F_{grd} and F_{sky} are equal to 0.5. For usual sky and surface temperatures, the coefficients $h_{\mathrm{r,sky}}$ and $h_{\mathrm{r,grd}}$ vary around the values of 4.7 W/m^2. K and 5.7 W/m^2. K for buildings located in temperate regions.

The radiative flux received by the interior surface of the wall and emitted by other N surfaces of the test room, resulting from the linearization of the radiative transfers if all interior surfaces are black bodies ($\rho = \tau = 0$, $\varepsilon = 1$), is expressed by:

$$\emptyset_{LW,in} = \sum_{i=1}^{N} F_{is} h_{is} (T_i - T_{\mathrm{surf}}) \quad \textbf{Eq. 3-17}$$

where, F is the view factor, h_{is} is the radiative coefficient, T_{surf} is the internal surface temperature of the TIM-PCM wall and T_i is the temperature of each other surface of the room. The calculation of the indoor radiative exchange is complicated, since the computation of the view factors between the interior surface of the TIM-PCM wall and the other surfaces needs a specific detailed method [54]. For simplification, the temperatures of the other surfaces of the room are supposed to be equal to the indoor test room air temperature. Thus, the resulting radiative exchange (W/m^2) becomes:

$$\emptyset_{LW,in} = \mathrm{h_{is}}(\mathrm{T_{in}} - \mathrm{T_{surf}}) \quad \textbf{Eq. 3-18}$$

where $\mathrm{h_{is}}$ is the internal longwave radiative exchange coefficient, for standard building temperatures it varies very little around the value of 5 W/m^2. K

4.3. Convective heat exchange

The convective heat exchange occurs between the external surface of the TIM-PCM wall and the outside air, and between the internal surface of the wall and the inside air.

The general formulation of the convective heat flux (W/m^2) is given by:

$$\emptyset_{conv} = h_{conv}\,\Delta T \quad \textbf{Eq. 3-19}$$

Where, ΔT is the temperature difference between the surface and the surrounding air.

The Convective exchange with the external environment is generally calculated using a linear correlation function of the wind speed. The correlation in (W/ m^{2}K) used here is established by Sturrock [58]:

$$h_{out} = 5.7v + 11.4 \text{ (Windward)} \quad \textbf{Eq. 3-20}$$
$$h_{out} = 5.7v \text{ (Leeward)}$$

Where, v is the wind velocity (m/s)

The internal convection coefficient used to evaluate the convection heat transfer for the TIM-PCM wall with the interior is the one developed by Alamdari for vertical surfaces [51]:

$$h_{in} = \left\{ \left[1.5 \left(\frac{|\Delta T|}{H} \right)^{1/4} \right]^6 + [1.23(|\Delta T|)^{1/3}]^6 \right\}^{1/6} \quad \textbf{Eq. 3-21}$$

where ΔT is the temperature difference between the internal wall surface and the indoor air, and H is the height of the vertical surface.

4.4. Governing equations and boundary conditions

For the TIM-PCM wall, the heat transfer includes different regions, which are the outer glazing, insulation silica aerogel and the PCM filled in glass brick. A one-dimensional unsteady energy equation for glazing and insulation layer is given as

$$\rho C_p \frac{\partial T}{\partial t} = k \frac{\partial^2 T}{\partial x^2} + \emptyset_{sol} \quad \textbf{Eq. 3-22}$$

where ρ is the density (kg/m^3), C_p is the specific heat capacity (J/kg. K) and k is the thermal conductivity (W/m. K).

In the PCM layer, the heat transfer during phase change procedure is done by conduction, natural convection in the liquid phase and shortwave radiation. The unsteady energy equation for PCM regions is given as:

$$\rho C_p \frac{\partial T}{\partial t} = \frac{\partial}{\partial x}\left(k \frac{\partial T}{\partial x}\right) - \rho L_H \frac{\partial f_l}{\partial t} + \emptyset_{sol} \quad \textbf{Eq. 3-23}$$

where $\emptyset_{\mathrm{sol}}$ (W/m^2) is the absorbed solar radiation in the layer (section 4.1), L_H is the latent heat of fusion (J/kg) and f_l is the liquid fraction.

To solve the phase change problem a fixed-grid modified "enthalpy" method is used, inspired by the work of Zivkovic et al. [59]. The convection in the liquid PCM is accounted for using the enhanced thermal conductivity approach together with the scaling theory [60] [61] [62]. The convection effect is only considered in the upper part of the PCM layer of height z_1 and width z_2, while the zone $(\mathrm{z}_2.\mathrm{H}) - (\mathrm{z}_1.\mathrm{z}_2)$ is controlled by conduction. Therefore, an average enhanced conductivity for liquid nodes is used in the one-dimensional model expressed by:

$$k_{enh,p} = \frac{k_l[(\mathrm{z}_2.H) - (z_1.z_2)] + k_l.Nu_{z_1}(z_1.z_2).}{\mathrm{z}_2.H} \quad \textbf{Eq. 3-24}$$

where $k_{enh,p}$ is the liquid enhanced conductivity for the liquid PCM node p, H is the height of the glass brick filled with PCM and Nu_{z} is the Nusselt number correlation given by Berkovsky and Polevikov [63]. More details can be found in the reference [64].

4.5. Heat balance on a surface in contact with the external environment

The heat balance on the outside surface is given by:

$$\rho c_p \frac{\Delta x}{2} \frac{\partial T}{\partial t} = \emptyset_{cond}(t) + \emptyset_{\mathrm{LW,out}}(t) + \emptyset_{conv,out}(t) + \emptyset_{sol}(t) \quad \textbf{Eq. 3-25}$$

Where, $\emptyset_{cond}(t)$ is the conductive heat flux in (W/m^2) is given as:

$$\emptyset_{cond}(t) = \frac{k}{\Delta x}\left(T_{s+\Delta x} - T_{surf}\right) \quad \textbf{Eq. 3-26}$$

and $\emptyset_{sol}$ (W/m^2) is the solar absorption flux at the surface expressed by:

$$\emptyset_{sol}(t) = \alpha Q_{sol-total} \quad \textbf{Eq. 3-27}$$

$\emptyset_{\mathrm{LW,out}}(t)$ and $\emptyset_{conv,out}(t)$ are the radiative heat exchange (W/m^2) with the outdoor environment and the convective heat flux with the outside given in Eq. 3-15, Eq. 3-19 and Eq. 3-20 respectively.

4.6. Heat balance on a surface in contact with the internal environment

The heat balance on the internal surface is given by:

$$\rho c_p \frac{\Delta x}{2}\frac{\partial T}{\partial t} = \emptyset_{cond}(t) + \emptyset_{\mathrm{LW,in}}(t) + \emptyset_{conv,in}(t) + \emptyset_{sol}(t) \quad \textbf{Eq. 3-28}$$

Conduction flux through the wall (W/m^2) is given as:

$$\emptyset_{cond}(t) = \frac{k}{\Delta x}\left(T_{s-\Delta x} - T_{surf}\right) \quad \textbf{Eq. 3-29}$$

The transmitted solar radiation flux absorbed at the internal wall surface reads:

$$\emptyset_{sol}(t) = \alpha Q_{sol-trans} \quad \textbf{Eq. 3-30}$$

where $\emptyset_{\mathrm{LW,in}}(t)$ and $\emptyset_{conv,in}(t)$ are the net longwave radiant exchange flux between zone surfaces (W/m^2) and the convective heat flux with the indoor air given in Eq. 3-18, Eq. 3-19 and Eq. 3-21, respectively.

A one dimensional implicit finite volume method established by Patankar 1980 [65] is used to estimate the heat transfer mechanism through the TIM-PCM wall. The computational domain is divided into control volumes, the discretized equation over a typical control volume is written as follow:

$$a_P T_P^{t+\Delta t} = a_W T_W^{t+\Delta t} + a_E T_E^{t+\Delta t} + b \quad \textbf{Eq. 3-31}$$

where,

$$a_W = k_w \frac{\Delta y}{(\Delta x)_w}, a_E = k_e \frac{\Delta y}{(\Delta x)_e}$$

$$a_P = a_W + a_E + a_P^t$$

$$a_P^t = \frac{\rho Cp \Delta x}{\Delta t}$$

$$b = a_P^t T_P^t + \emptyset_{sol} \quad \textbf{Eq. 3-32}$$

The superscript *t* indicates the values at the previous time step, $t + \Delta t$ indicates the values at the current time step. k_w and k_e are the thermal conductivities calculated at the interface.

A system of linear equations is formed from the discretized equations and can be written in a matrix form as:

$$A * T = B \quad \textbf{Eq. 3-33}$$

where A is the matrix of coefficients (tri-diagonal sparse matrix), T is the vector of unknown temperatures and B is the vector of known terms including the values at the previous time step. The current temperature values $T_P^{t+\Delta t}$ are obtained from the previously solved time step temperatures values T_P^t. The system is solved using a direct non-iterative method, the Gaussian elimination algorithm, which produces the solution without explicitly forming the inverse. The Gaussian

elimination algorithm is a sequential process of removing unknowns from equations using forward elimination followed by back substitution [66]. This function is built in MATLAB.

5. MATLAB-TRNSYS link

The model of the heat transfer through the TIM-PCM wall is linked to TRNSYS via Type 155, whose function is to enable the use of MATLAB program in TRNSYS (Figure 3-6). This link enables to simulate the thermal performance of the test cell.

The inputs for Type 155 are: the outdoor air temperature, the sky temperature (Eq. 3-16 and Eq. 3-11), the incident solar radiation on vertical plan and the wind velocity from experimental data, in addition to the indoor air temperature, calculated at each time step, from Type 56 (TRNbuild), also the thermo-physical and optical properties of PCM, glass and silica aerogel (Table 3-1 to Table 3-4).

In TRNbuild Type 56 we define the building geometry, the wall constructions, the materials properties and the zones regimes (cooling, heating, infiltration, ventilation…). The solar radiation is processed to the building using Type 16 that needs the incident radiation on horizontal plan as input, while the outdoor air temperature and the outdoor relative humidity are linked to the building using Type 9 from experimental measured data. A part of the radiation is reflected from the ground, the reflectance of the ground above which the surface is located, concrete in our case, is taken 0.22.

Type 155 provides as output data the internal surface temperature. This boundary temperature is taken as an input to the Type 56, and the shortwave solar radiation transmitted into the test room through the translucent wall is defined as internal radiative heat gain. Type 75 is used to calculate the infiltration rate (ACH). The inputs for this type are: wind speed, outdoor and indoor air temperatures, outdoor and indoor relative humidity, outdoor and indoor air pressures and the leakage area (the leakage area was estimated 100 cm^2). And, the ground temperature is approximated to the ambient temperature. In addition, the internal convection coefficient used for horizontal surfaces are those developed by Glück [67].

For Type 155, A non-iterative component is called at the end of each time step, the outputs are calculated for one-time step based on the converged values of previous time step.

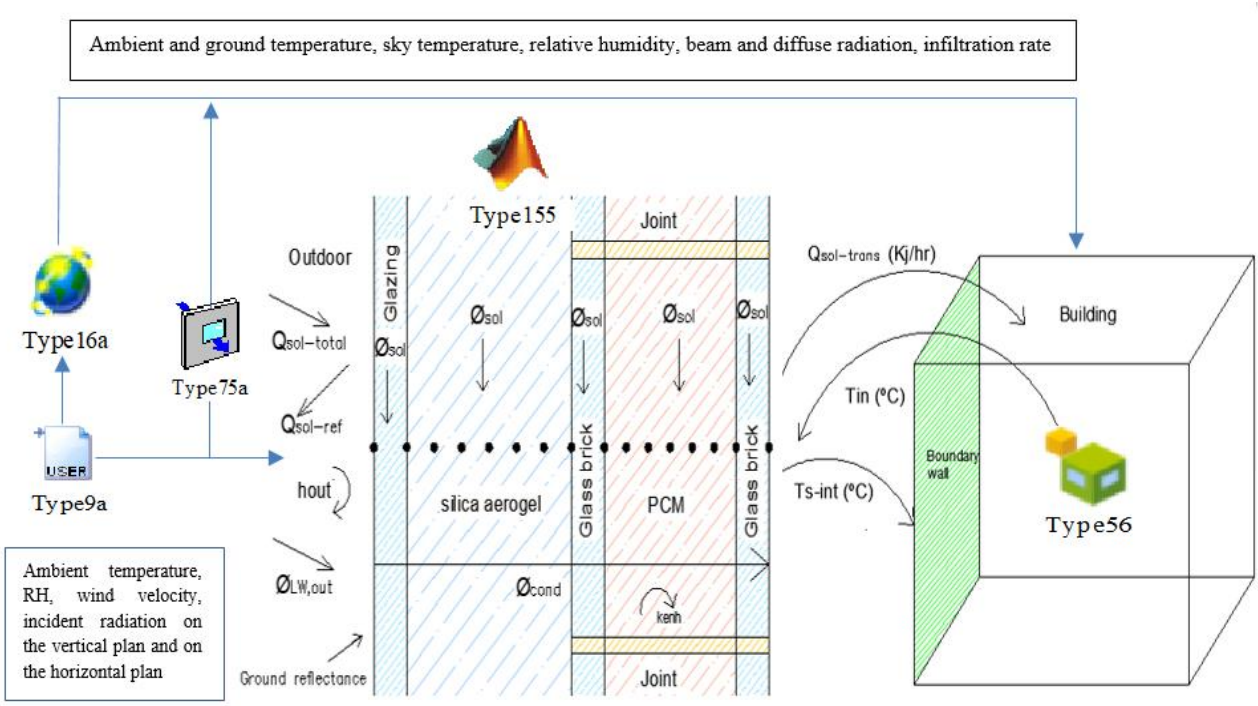

Figure 3-6: Integration mechanism of the TIM-PCM wall in TRNSYS and different heat transfer phenomena through the TIM-PCM wall and the computational grid

6. Model validation

To validate the numerical model, the hourly profile of the measured data and simulated results of the internal surface temperature and the indoor test room air temperature are compared for seven consecutive days in summer and winter seasons. The agreement between experimental data and simulated results is estimated using the root mean square error (RMSE) and the percentage root mean square error (PRMSE) shown in Eq. 3-34 and Eq. 3-35 respectively.

$$RMSE = \sqrt{\frac{1}{n}\sum_{i=1}^{n}(s_i - e_i)^2} \qquad \textbf{Eq. 3-34}$$

$$PRMSE = \sqrt{\frac{1}{n}\sum_{i=1}^{n}\left(\frac{s_i - e_i}{e_i}\right)^2} \qquad \textbf{Eq. 3-35}$$

The comparison between the measured and the simulated internal surface temperature of the TIM-PCM wall and the indoor test room air temperature in summer season is shown in Figure 3-7. The effect of natural convection in liquid PCM is also studied in summer and winter and the comparison is done between the experimental data and the simulated values from the model with and without natural convection in the liquid PCM. The PCM temperature filled in glass bricks is also compared in summer season, as shown in Figure 3-8.

Concerning the internal surface temperature of the TIM-PCM wall, it was measured experimentally using seven sensors (section 3). The simulated results are compared with a temperature measured at the middle of the left side of the wall. This measured temperature is very close to the average temperature of all the measured temperatures (maximum dispersion 1.1˚C, average difference 0.9 ˚C).

Despite the assumptions that have been made, the numerical model is found to be able to simulate the heat transfer phenomena through the TIM-PCM wall. A good agreement is observed comparing the experimental measured data and the simulated results. The model predicts properly the minimum and maximum peak values of the internal surface temperature, the indoor air temperature and the PCM temperature especially in the summer season, with a slight over-estimation of the uppermost values in summer and an underestimation of the lowermost values in winter.

The model, considering natural convection effect, estimates the internal surface temperature of the TIM-PCM wall in summer better than winter, where a maximum difference of 2.9 ºC is observed when the temperature in the PCM layer is inferior to the phase change temperature in February first after 6 p.m., while a very good agreement is observed when the PCM is in its solid state in January 27 and 28. The peak values in all days are in good agreement. The little over-estimation of the surface temperature of the TIM-PCM during summer is observed when the temperature of the PCM layer is relatively high, and the slight underestimation of the indoor temperatures occurs at night. In addition, the PRMSE and RSME demonstrate the good agreement between the experimental and the simulated results. The PRMSE of the indoor air temperature is 1.87% in summer and 4.05% in winter, and that of the internal surface temperature is 3.28 % in summer and increases to 6.99% when the winter season is examined as summarized in Table 3-8. While the RMSE is 0.76 ºC and 1.43 ºC for the indoor air temperature and the internal surface temperature respectively in winter season.

It was also shown that without natural convection, the model underestimates the temperature values compared to experimental results especially the highest peak values. If the natural convection effect is not considered in the summer season, the RSME of the PCM temperature increases from 1.92 ºC to 4.07 ºC and the PRMSE reaches 9.94 %, the difference between the maximum peaks reaches up to 11 ºC (Figure 3-8). For the surface temperature, the RMSE is 1.47 ºC and the PRMSE attains 4.12 % while a maximum difference of about 4.5 ºC is observed at the peaks. For the indoor air temperature, the RMSE is 0.84 ºC compared to 0.57 ºC considering the natural convection effect. Same for winter season, the values of RMSE and PRMSE increase when natural convection in liquid PCM is not considered (Table 3-8). Therefore, to get a good agreement between simulation results and experimental data, it is not always adequate to assume only conduction heat transfer inside the PCM and the natural convection effect must be considered in the liquid PCM.

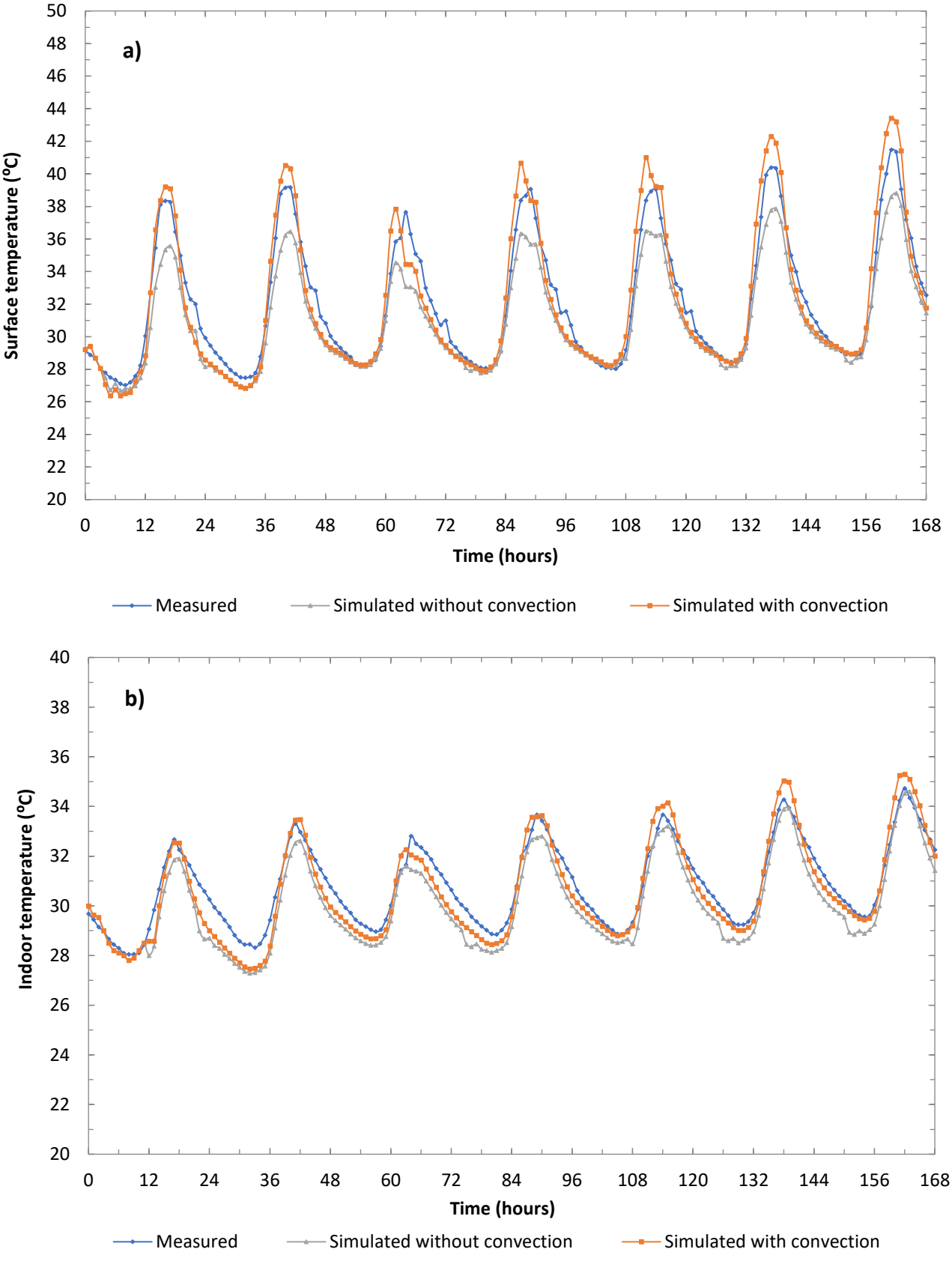

Figure 3-7: Simulated and measured a) internal surface temperature of the TIM-PCM wall and b) indoor test room air temperature for seven consecutive days in summer (30 July - 5 August 2017).

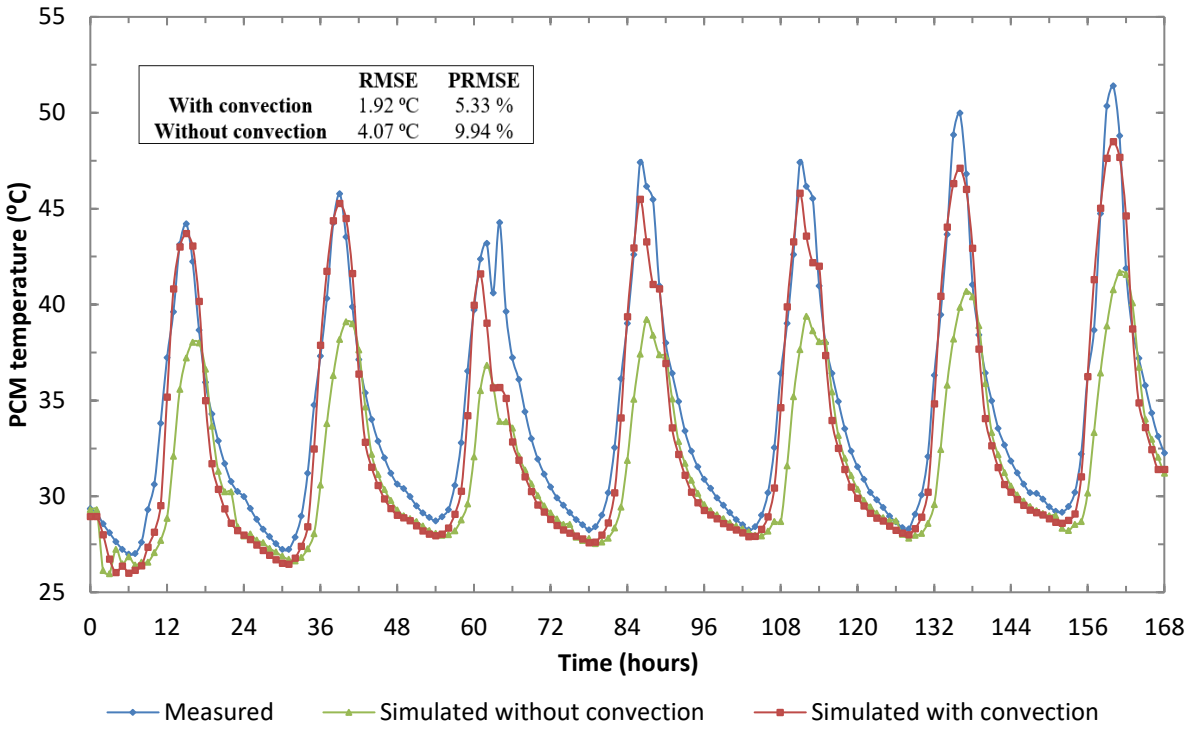

Figure 3-8: Simulated and measured PCM temperature for seven consecutive days in summer (30 July-5 August 2017).

Table 3-8: RMSE and PRMSE for the hourly profile of the surface and indoor temperature in summer and winter season

Season	Physical quantity	Model	RMSE	PRMSE
Winter	Surface temperature	With convection	1.43°C	6.99%
		Without convection	1.50°C	7.11%
	Indoor air temperature	With convection	0.76°C	4.05%
		Without convection	0.93°C	4.91%
Summer	Surface temperature	with convection	1.13 °C	3.28 %
		without convection	1.47 °C	4.12 %
	Indoor air temperature	with convection	0.57 °C	1.87 %
		without convection	0.84 °C	2.74 %

7. Proposed solutions for the PCM cycling and the overheating

As mentioned in section 3, the PCM in summer season remains in its liquid state and is unable to solidify by releasing the stored heat, which causes an overheating in the test cell. In this section, many solutions will be proposed to obtain, if it is possible, cycling of the PCM and to avoid the overheating problem. First, passive systems are suggested, such as the use of shading devices or natural night ventilation that offers cold from the outside. These applications are easy to implement, do not use active mechanical equipment and thus no extra energy is required. Then, the thermal behavior of the TIM-PCM is tested using another PCM having a higher phase change temperature.

7.1. Shading devices

Overheating due to solar radiation transmitted to the test cell through the translucent TIM-PCM wall can be reduced using shading devices. The most important motive of the use of shading devices is to prevent the direct solar radiation to enter into the building in summer season, and to allow the solar gains to enter the building when it is needed in the cold season [68], [69]. Shading devices can be either interior or exterior; the exterior devices are more effective than the interior ones, since more significant amount of solar radiation can be rejected to the outdoor environment. They include overhangs, awnings, louvers, venetian blinds and roller shades. Numerous studies have been done on shading devices showing their importance in reducing the cooling loads especially in hot climates [70].

7.1.1. Overhangs

The overhangs at the southern façade are a widely used method that provides external shading. Overhangs need to be designed properly to block the solar radiation during summer and permit its penetration during winter. In TRNSYS, overhangs can be defined using Type 34 and Type 67 is used to consider shading from far away objects. The defined dimensions of the overhang are mainly the overhang gap fixed at 20cm, the overhang extensions limited to 30 cm at each side and the overhang projection which value is increased from 0.5m to 2.5m.

The use of overhang decreases the maximum room air temperature by about 6ºC from 35.30ºC to 29.29 ºC for a projection of 1 m, and the minimum air temperature is decreased from 28.80 ºC to 25.84ºC at night. Increasing the overhang projection above 1 m has a minor effect on the maximum and minimum indoor air temperature as shown in Table 3-9.

Table 3-9: Values of maximum, minimum and average indoor test room air temperature for different overhang projections

Projection of the overhang (OP)	Base case	0.5m	1m	1.5m	2m	2.5m
Maximum indoor air temperature	35.30	30.56	29.29	29.11	29.06	28.91
Minimum indoor air temperature	28.80	26.61	25.84	25.68	25.80	25.56
Average indoor air temperature	31.34	28.09	27.27	27.15	27.11	27.06

7.1.2. Venetian blinds

Exterior venetian blinds are installed on the outside of the TIM-PCM wall; these blinds offer a high level of protection against solar radiation due to the reduction of light and heat. They consist of separate, equally-spaced horizontal slats. The venetian blinds have various thermal and optical properties which depend on the slat characteristics (rotation angle, shape, size, and colors) and the angle of incidence of solar radiation. The used blinds in this section are products from ISOTRA

[71][72], the solar and light transmittances are determined according to the standard CSN EN 13363-1+A1 [73] for the selected products of ISOTRA. The blinds slat angles were determined by two angles 45º (slats half closed) with solar reduction factor of 0.25 and 0º (totally closed, i.e. opaque) with solar reduction factor of 0.069. Different cases listed in Table 3-10 are studied to find an optimal solution for the overheating problem. Figure 3-9 shows the transmitted solar radiation through the TIM-PCM wall for each case, it is obvious that the use of venetian blinds reduces significantly the transmitted solar radiation into the test room cell, especially the opaque ones. Noting that, the blinds are down and set to their utilization angle when the total incident radiation is significant, i.e. from 9 a.m. till 5 p.m.

Table 3-10: Different cases to be tested to choose the best solution

Cases	Shading scenario
Case 1	No overhang and no external blinds (base case)
Case 2	Overhang of projection 1 m (type 34 TRNSYS, section 7.1.1)
Case 3	Venetian External Blinds with rotatable slat and a slat angle of 45 degrees /reduction factor 0.25 (according to DIN 4108, EN 4108 [74])
Case 4	Exterior Venetian Blinds with rotatable slat at 0-degree, silver color, reduction factor 0.069 (according to EN 13363-1+A1)
Case 5	Overhang 1 m + blind 45º (case 2 + case3)
Case 6	Overhang 1 m + blind 0º (case 2 + case 4)

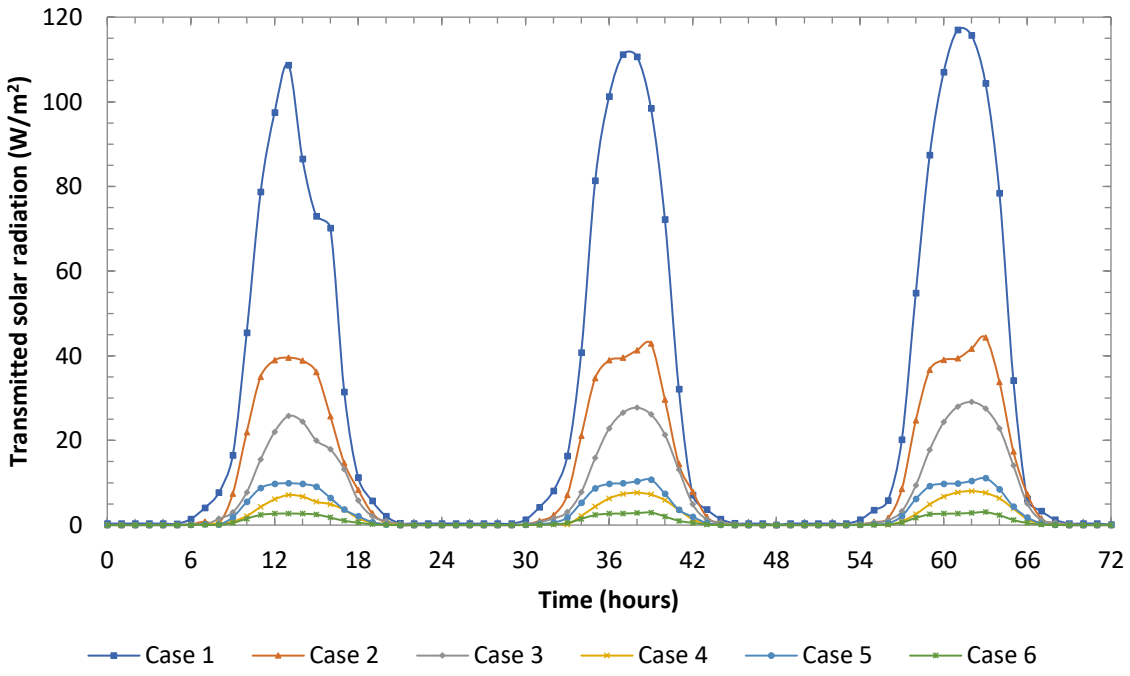

Figure 3-9: transmitted solar radiation through the TIM-PCM wall for the different cases in summer season (3, 4, 5 August)

Table 3-11: Values of minimum and maximum indoor test room air temperature for the different cases

	Case 1	Case 2	Case 3	Case 4	Case 5	Case 6
Maximum temperature	35.30	29.29	28.11	26.57	26.94	26.27
Minimum temperature	28.80	25.84	25.20	24.68	24.79	24.62

Table 3-12: Values of maximum and minimum PCM temperature for the different cases

	Case 1	Case 2	Case 3	Case 4	Case 5	Case 6
Maximum PCM temperature	51.41	35.34	32.22	28.34	29.11	27.54
Minimum PCM temperature	28.25	25.21	24.51	24.21	24.29	24.06

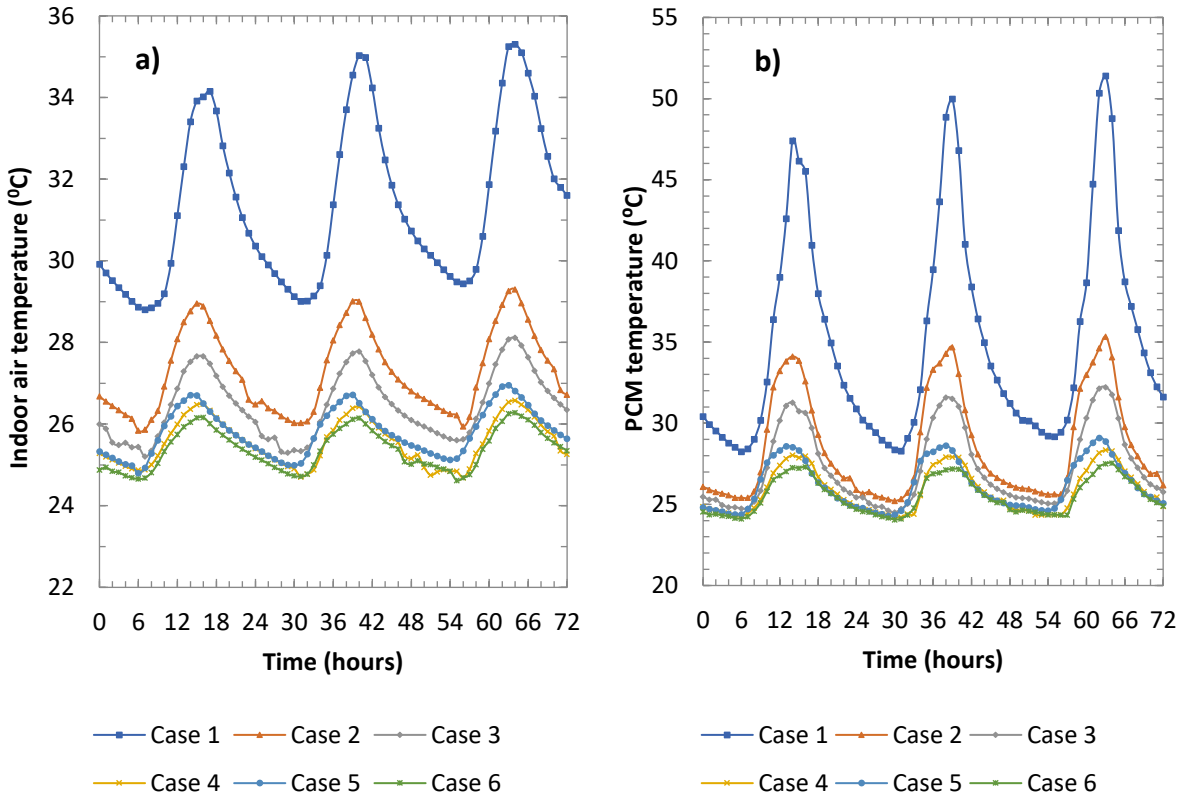

Figure 3-10: a) Indoor test room air temperature and b) PCM temperature for the different cases in summer season (3, 4, 5 August)

Figure 3-10 shows the indoor test room air temperature for the different cases. The venetian blinds with rotatable slat angle of 45° (case 3) reduce the maximum temperature from 35.30 ºC to 28.11ºC, while the opaque ones (case 4) reduce the peak temperature to 26.57 ºC with a minimum temperature of 24.68 ºC, solving the overheating problem. When combining the overhang with the venetian blinds of 45 degrees slat rotatable angle (case 5), the maximum indoor temperature reduces to 26.94 ºC and the minimum indoor temperature decreases to 24.79 ºC, in this case the light is fairly transmitted through the wall. When combining the overhang with the opaque blinds (case 6), the results are not significantly modified compared to case 4 as summarized in Table 3-11. The blinds can reduce the

peak temperature during the day more than 8 ºC and the minimum temperature at night up to 4 ºC. To benefit from the translucency of the TIM-PCM wall, case 5 can be considered as an optimal solution.

Figure 3-10 shows the temperature of the PCM layer for the different cases. Despite the significant reduction of the maximum PCM temperature, up to 23ºC, during the day for all cases, the PCM temperature at night does not drop below the phase change temperature (minimum temperature reached is 24.06 ºC, Table 3-12). Thus, the PCM will not be able to solidify and lower temperatures must be attained to solidify the PCM periodically in each diurnal cycle.

7.2. Prisma solar glass

Prisma solar glass is a special glazing developed by Lamberts Company which features selective solar radiation properties depending on the season. Due to its precisely-determined prismatic structure, it is possible for a large amount of the solar radiation in winter, having a lower angle of incidence, to pass through the glazing into the indoor environment. whereas, in summer season a large amount of the solar radiation, having a higher angle of incidence, is reflected to the outside. This type of glass is already applied in the construction of an office center in Fürstenfeldbruck, Germany.

Kara et al [13] have studied the performance of a coupled novel triple glass unit (TGU) and PCM wall, the mid layer of glass in the TGU being the Prisma solar glass. They have found that the solar transmittance of the TGU is reduced by 100% in summer (0.2 to 0.25) compared to winter (0.45 to 0.55) and no overheating for the PCM wall has been encountered in summer season.

The Prisma solar glass can be used instead of the ordinary glass in the external glazing of the TIM-PCM wall composition. As a result, most of the incident radiation on the wall is transmitted in winter and reflected in summer. Therefore, the heat storage in the PCM is maximal in winter and insignificant in summer, and therefore the overheating problem can be avoided. The Prisma solar glass was modeled by assuming a transmission and a reflection coefficient of value 10% and 78% respectively, for the external TIM-PCM glazing in summer season.

Figure 3-11 shows the indoor test room air temperature, and the PCM temperature for both glazing types for three consecutive days (3, 4, 5 August) in summer season. The results show that the lower solar transmittance during summer due to the use of Prisma solar glass can prevent the overheating problem. The peak indoor temperature is decreased by about 6.5 °C reaching a maximum value of 28.7 °C compared to 35.3°C using ordinary glazing. In addition, the maximum PCM temperatures are reduced up to 19 °C, while during the night the PCM temperature is still higher than the phase change temperature and the PCM remains in its liquid state. As a conclusion, the Prisma solar glass is shown to be an effective solution for the encountered overheating problem in summer.

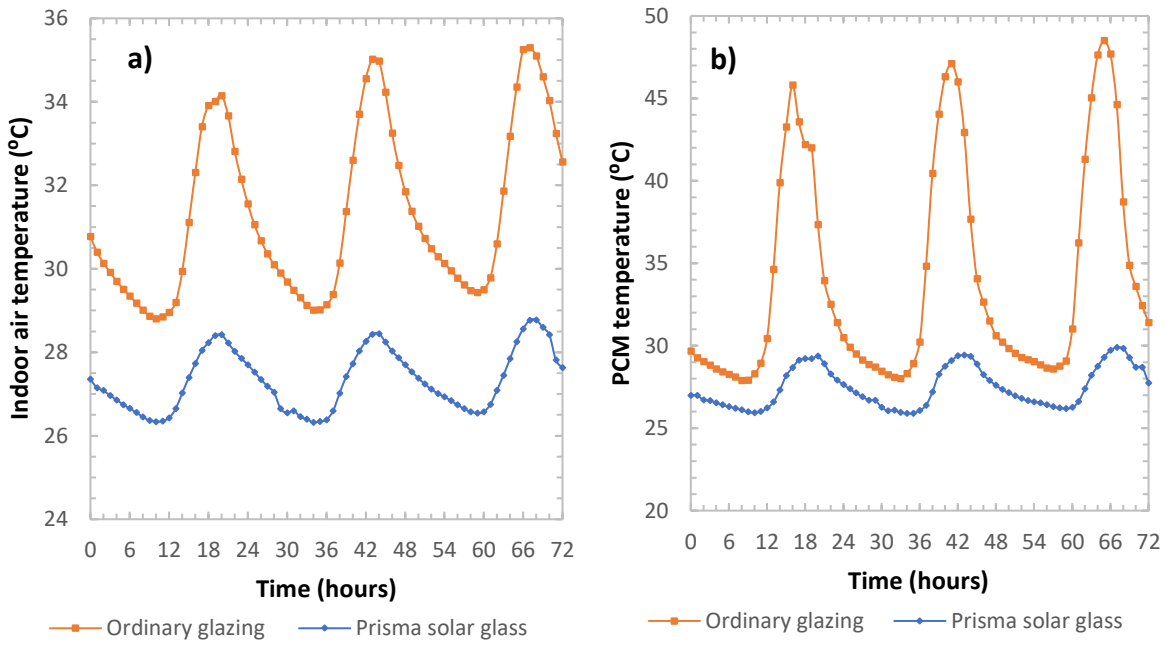

Figure 3-11: a) Indoor test room air temperature, and b) PCM temperature for both glazing type in summer season (3, 4, 5 August)

7.3. Natural night ventilation

Nocturnal ventilation is a passive cooling technique that uses the outdoor air at night to cool the building; the airflow is driven due to the temperature difference and the wind. The natural ventilation is considered in the aim of evacuating the extra heat at night, and to show its effect on the PCM performance and on the indoor air temperature during night and day.

A window of 1 m^2 located at the west wall is considered and scheduled to be open from 8 p.m. till 8 a.m. and closed during the day with opaque blinds to prevent the solar radiation from entering the room. The natural ventilation rate is calculated using the equations of Ghiaus and Roulet [75]. The flow rate (m^3/s) through the opening is calculated as:

$$\dot{V} = 0.5 A_w v_{eff} \quad \textbf{Eq. 3-36}$$

where A_w is the effective area of the open window and v_{eff} is found using an empirical model:

$$v_{eff} = (c_1 v_r^2 + c_2 H.\Delta T + c_3)^{1/2} \quad \textbf{Eq. 3-37}$$

where c_1 is a dimensionless coefficient depending upon window opening ($c_1 \sim 0.001$), c_2, c_3 are buoyancy and wind constant ($c_2 \sim 0.0035$, $c_3 = 0.01$), v_r (m/s) is the mean wind speed for the site, H is the height of the opening, and ΔT is the mean temperature difference between outdoor and indoor environment.

The flow in air changes per hour is given as follow:

$$ACH = \frac{3600}{V}\dot{V} \quad \textbf{Eq. 3-38}$$

where V is the volume of the room.

A flow rate between 6 ACH and 7 ACH is found for an opening area of 1 m^2, when the difference between outdoor and indoor air temperature is minimal and the mean wind velocity is about 0.1 m/s. A parametric study on the effect of different ventilation rates (otherwise different window opening proportion) is carried out. The recommended minimum ventilation rate by ASHRAE is 0.36 ACH [76]. For a ventilation rate of 2 ACH, the peak indoor temperature is reduced by 1ºC, above this ACH value the results are tardily changing where a ventilation rate of 6 ACH decreases the peak temperature by 1.5º C. The minimum temperature is reduced by about 2 ºC and 3.6ºC for a ventilation rate of 2 ACH and 6 ACH respectively, showing a higher effect of the natural ventilation at night. The natural night ventilation has almost (49.29°C → 48.16°C ~ 1 °C) no effect on the maximum PCM temperature, while at night this temperature is reduced by about 2.5 °C for 6 ACH. The nocturnal ventilation cannot improve the performance of PCM since the outdoor air temperature at night is relatively high in summer conditions.

Figure 3-12 shows that the natural night ventilation has insignificant effect on the indoor air temperature when blinds at 45° rotatable slat angle are used, and a ventilation rate of 2 ACH is sufficient in this case. As a conclusion, natural night ventilation alone cannot solve the overheating problem, and must be combined to shading devices.

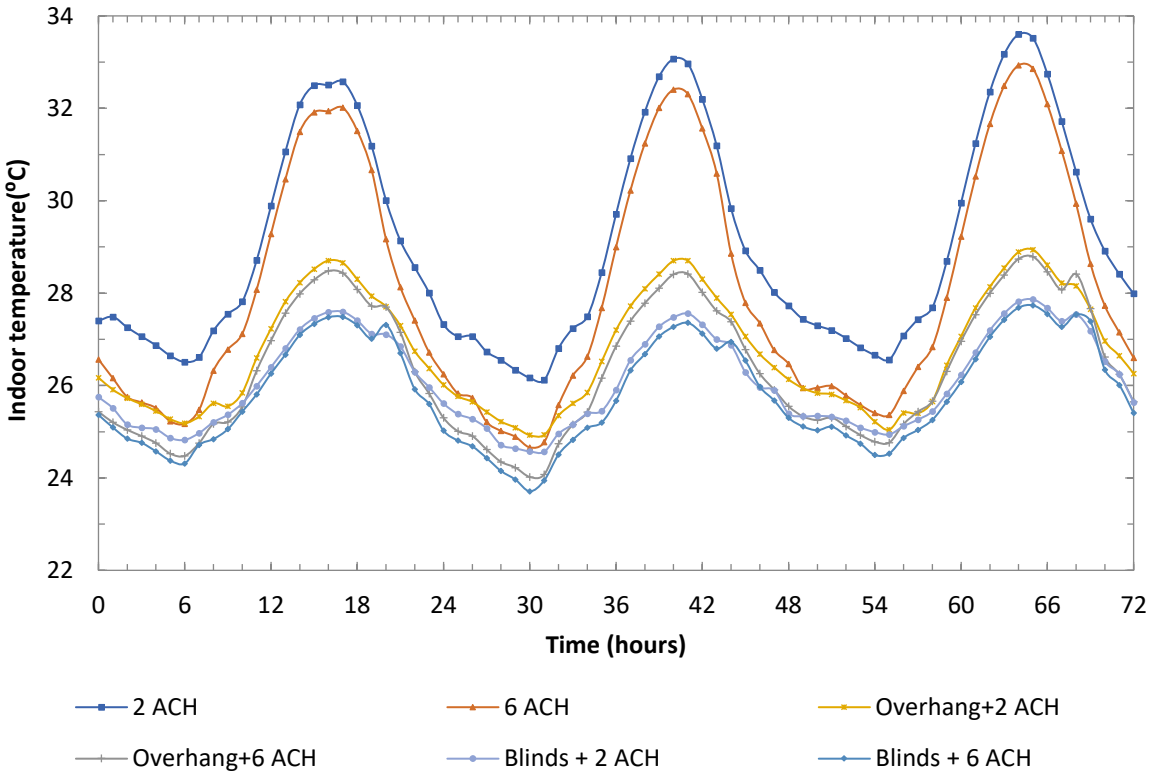

Figure 3-12: Indoor air temperature for different cases after applying natural night ventilation in summer season (3, 4, 5 August)

7.4. PCM RT28HC

It was noted that despite a better indoor temperature, due to shading devices and night ventilation, the PCM never solidifies in summer, due to its low melting temperature.

In this section another PCM, with a higher phase change temperature (chosen nearby the thermal comfort range [77]) is considered to be filled in the glass bricks instead of the fatty acid eutectic 21.3. The PCM is RT28HC, RUBITHERM® RT, a pure material, having similar optical properties of the fatty acid eutectic i.e. transparent in the liquid state and opaque in the solid state with phase change temperature of 28˚C. the thermo-physical properties can be found in [78].

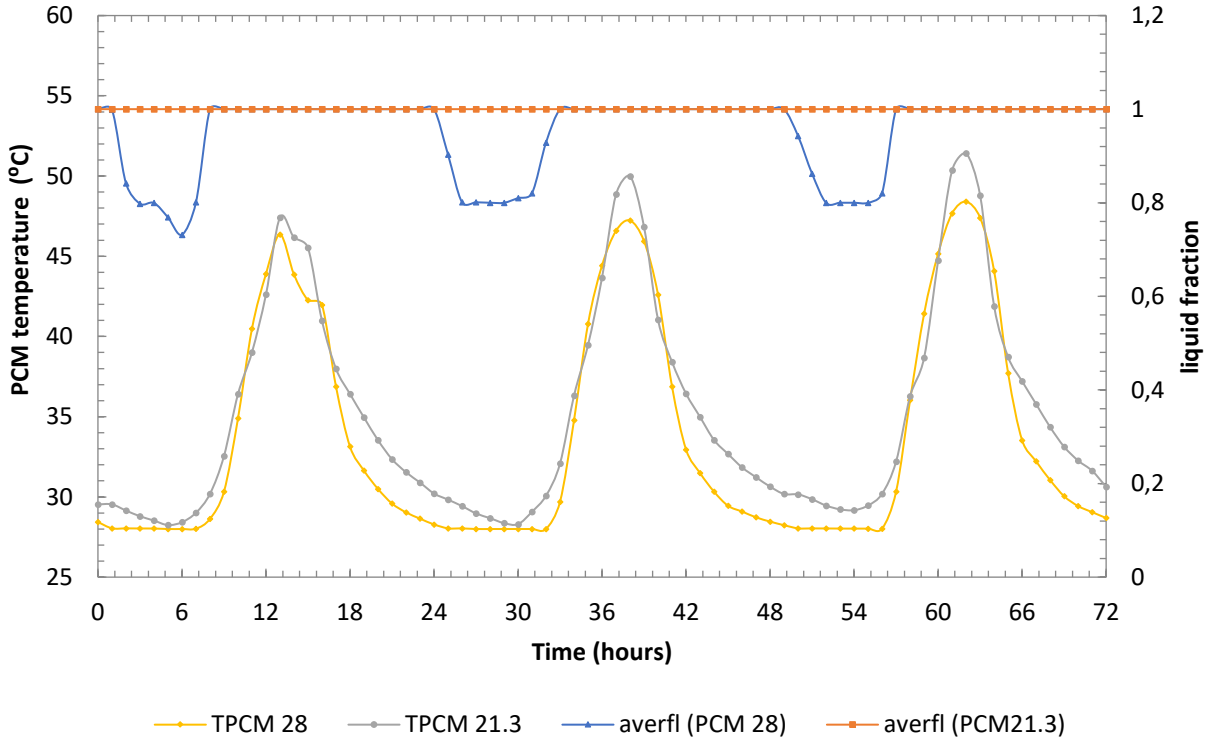

Figure 3-13: Average fraction of liquid and temperature in the PCM layer for both PCM in summer season (3, 4, 5 August)

Figure 3-13 shows the average liquid fraction of each PCM, the PCM having a phase change temperature of 21.3 ºC remains always in its liquid state during the whole day and night, while the other PCM with a phase change temperature of 28 ºC undergoes a partial freezing at night starting from 1 am solidifying by about 20% (fraction of liquid attains about 0.8) and then returns to its fully liquid state at 8 am with fraction of liquid equal to 1. During this partial solidification, a marginal portion of the stored heat during the day is released decreasing very slightly the maximum PCM temperature. Regarding the indoor air temperature, the difference is trivial using both PCM. Complete

cycling of the PCM28 can't be achieved in this summer conditions and the previous solutions (7.1.1, 7.1.2, 7.3) are recommended to avoid the overheating.

8. Thermal comfort evaluation

Considering that the test room cell of 9.29 m^2 is an office room, with working hours from 9 a.m. till 5 p.m. A schedule for people occupancy and equipment use defining a real case has been modeled. One person is considered in the office with load taken as 100 W, and a computer is considered of load 20 W [76]. Daylight is provided to the inner environment by the translucent TIM–PCM wall. The simulations are conducted for three months of the hot season (June 1 till August 31); the weather data file is extracted from TRNSYS Meteonorm library since the measured weather data in Sophia are not available for all this period.

An adaptive comfort model based on ASHRAE standard 55-2010 [79] is used to examine the thermal comfort. The indoor comfort temperature is related to the mean monthly outdoor air temperature. It defines two acceptability ranges (80% and 90%) that correspond to the satisfaction of the occupants. The office is considered as uncomfortable when the operative temperature falls out of the comfort ranges in the case where the office is occupied.

The comfort temperature, and the 90% and 80% acceptability limits are calculated respectively using the following equations:

$$T_{op} = 0.31 * T_{a(out)} + 17.8 \quad \textbf{Eq. 3-39}$$

$$T_{op} = 0.31 * T_{a(out)} + 17.8 \pm 2.5 \quad \textbf{Eq. 3-40}$$

$$T_{op} = 0.31 * T_{a(out)} + 17.8 \pm 3.5 \quad \textbf{Eq. 3-41}$$

where:

T_{op} is the operative temperature (°C) and $T_{a(out)}$ is the monthly mean outdoor air temperature (°C) calculated as the arithmetic average of the mean monthly minimum and maximum daily air temperatures for the considered month.

Figure 3-14 shows the indoor operative temperature in summer season for different cases, the dashed lines representing the comfort temperature and the 80% acceptability limits. For the base case, the indoor operative temperature is above the comfort level most of time, showing the overheating problem. The use of shading devices, especially the blinds, with or without nocturnal ventilation can bring the operative temperature closer to the comfort range.

Figure 3-15 shows the percentage of occupied time when overheating will possibly occur according to ASHRAE 55 adaptive comfort model for two different levels of satisfaction. It is shown that the office without shading devices or nocturnal natural ventilation has a discomfort time percentage of 90.22 % and 84.02 % for 90% and 80% satisfaction level respectively. The natural night ventilation

of 6 ACH reduces the discomfort time percentage to 69.75 % and 57.25 % for 90% and 80% acceptability range respectively. Adding an overhang of 1 m projection decreases the discomfort time to approximately 53.62 % for 80% satisfaction level. Applying the natural night ventilation in presence of the overhang decreases the overheating time percentage to 40.58% and 19.56% for 2 ACH and 6 ACH respectively for 80% satisfaction level. For 90% satisfaction level, the discomfort is decreased to 58.33% and 34.24% for 2 ACH and 6 ACH respectively. Moreover, with Venetian blinds of slats rotated at 45 degrees, there is not so much risk of overheating where the discomfort percentage does not exceed 6 % for 80% satisfaction level. Combining natural night ventilation with blinds decreases the percentage of overheating time to 2.89% and 1.99% for 2 ACH and 6 ACH respectively for 80% acceptability range. No overheating is observed when Venetian blind are combined with overhangs for 80% acceptability range while 3.44% of overheating time is found for 90% acceptability level.

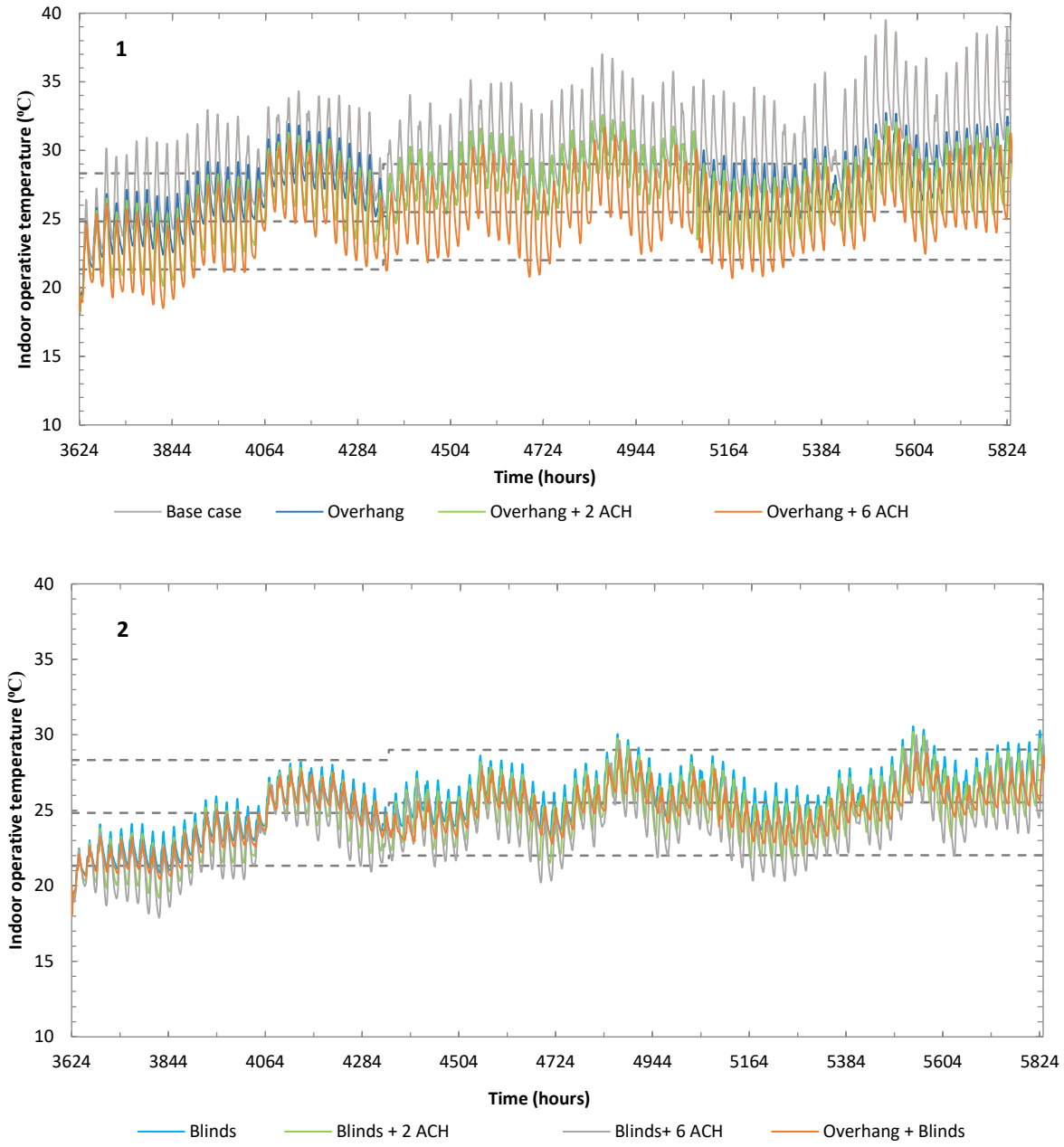

Figure 3-14: Indoor operative temperature in summer season for different cases

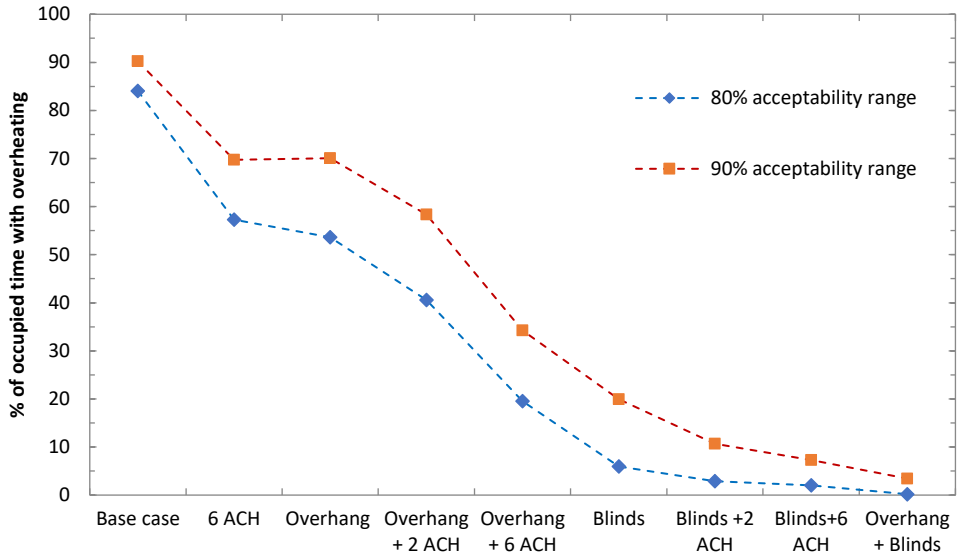

Figure 3-15: The percentage of occupied time where overheating occurs according to ASHRAE 55 adaptive comfort model for different levels of satisfaction

9. Application of the TIM-PCM wall under different climate conditions

In this section, the thermal comfort is studied for the same office room with same internal gains conditions, same orientation (south) but under different climates. Five different cities with different climates were chosen according to the Köppen–Geiger classification [80]. Madrid, Spain Csa (Hot-summer Mediterranean climate), Paris, France Cfb (temperate oceanic climate), Chicago, USA Dfa (hot-summer humid continental climate), Ottawa, Canada Dfb (warm-summer humid continental climate) and Kiruna, Sweden Dfc (subarctic climate). Figure 3-16 shows the percentage of occupied time when overheating will possibly occur according to ASHRAE 55 adaptive comfort model (section 8) for two different levels of satisfaction for the different climates in three months of hot season.

In the hot-summer Mediterranean climate (Csa) and the hot-summer humid continental climate (Dfa), the percentage of discomfort time for the base case is around 90% for both acceptability ranges. The use of overhang of 1 m projection decreases the time of overheating percentage time to 75% for 90% acceptability range. The reduction of discomfort percentage time is more significant in Dfa climate using blinds. Natural night ventilation alone has not a significant effect on the discomfort percentage time. To overcome the overheating problem in such climates (Csa and Dfa), Venetian blinds of slats rotated at 45 degrees combined with overhang should be used.

For the Oceanic climate (Cfb) the discomfort time for the base case is about 35% and 45% for 80% and 90% of occupants satisfied, respectively. Adding an overhang of 1 m projection decreases the percentage of discomfort time to less than 5% and 10% for 80% and 90% occupants are satisfied, respectively. No overheating is observed using Venetian blinds. In the warm-summer humid

continental climate (Dfb) the use of venetian blinds is sufficient to eliminate the discomfort time percentage. Providing natural ventilation decreases the discomfort time percentage. For the subarctic climate (Dfc), the percentage of occupied time where thermal comfort is not met does not exceed 16% for 80% of occupants satisfied and no overheating is observed during the occupied hours using overhang of 1m projection or providing natural night ventilation of 6 ACH for both 80% and 90% of occupants satisfied.

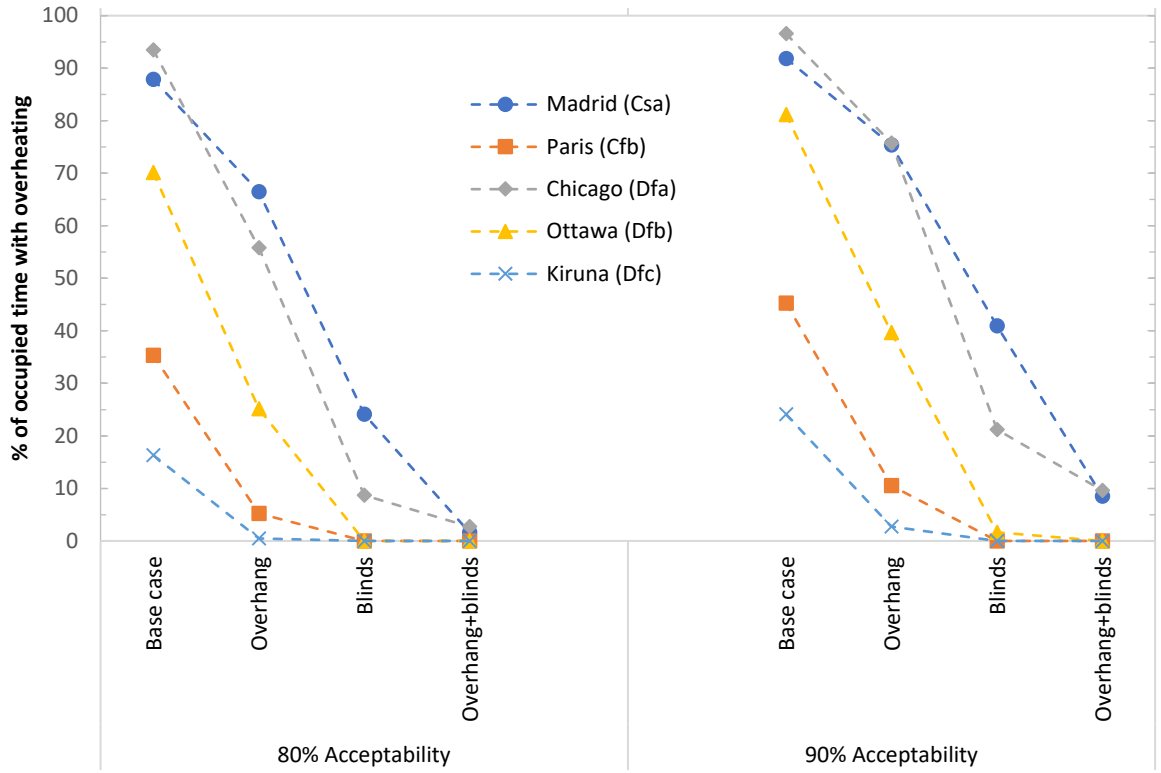

Figure 3-16: Percentage of occupied time where overheating occurs according to ASHRAE 55 adaptive comfort model for different levels of satisfaction for different climate conditions in summer season

Concerning the PCM cycling, in Csa and Dfa climates, the PCM remains in liquid state almost all the summertime for the base case. Using shading devices, the PCM solidifies or partially solidifies 20% of the summertime. In Paris, Cfb climate, the PCM remains in liquid state 75% of the time while in Ottawa, Dfb climate, the PCM remains liquid for 92% of the time. This can be explained by the lower outdoor ambient temperature at night in Paris allowing partial or complete solidification of the PCM. Using overhang, the PCM becomes liquid for 50% of the summertime, and the rest of the time changing phase or in solid state in Paris, Cfb climate. In subarctic climate (Dfc) the PCM achieves complete diurnal cycling and it is liquid for 40% of the summertime.

10. Conclusion

This paper investigates the thermal behavior of a novel special translucent superinsulated storage wall composed of glazing, silica aerogel and PCM filled in glass bricks. The aim of such wall is to provide energy storage and restitution, daylighting, and thermal/acoustic insulation. The TIM-PCM wall was tested in-situ in a full-sized test cell located at Sophia Antipolis, southern France. The experimental results showed that the wall is very efficient in winter season, while in summer the heat gains through the TIM-PCM wall cause an overheating problem and the PCM does not solidify. To optimize the wall's performance, a simplified numerical model for heat transfer through this composite wall considering natural convection in liquid PCM and short-wave radiation absorption and transmission has been developed. The structured numerical model is simple to implement and fast enough to be coupled with TRNSYS. The MATLAB-TRSNYS model is then validated using experimental results; a good agreement is obtained between the simulated and the experimentally measured internal surface temperature of the TIM-PCM wall and the indoor air temperature for seven consecutive days in summer and winter. Finally, the TIM-PCM wall has been applied in different cities under different climates in summertime and the thermal comfort and PCM cycling have been studied. The following general conclusions can be drawn:

- The developed numerical model represents a starting point for simulations on different configurations of the novel TIM-PCM wall and allows to fully investigate its abilities and drawbacks under different operative conditions, orientations, geometries and different climates without the need of performing expensive experimental analysis.
- To be more realistic, natural convection in the liquid PCM should not be neglected when modeling phase change in the wall.
- The use of Prisma solar glass instead of the ordinary glass in the TIM-PCM wall composition is shown to be an effective technology solving the encountered overheating problem in summer, while preserving the TIM-PCM advantages during winter.
- Thermal comfort and cycling of PCM in summertime depends on the climate conditions. In the hot-summer Mediterranean climate, Venetian blinds of slats rotated at 45 degrees combined with an overhang of 1 m projection can ensure thermal comfort with the TIM-PCM wall. In oceanic and warm-summer humid continental climates, thermal comfort can be ensured by the sole use of an overhang of 1 m projection and Venetian blinds respectively. In subarctic climate the PCM achieves complete diurnal cycling and thermal comfort can be attained providing natural night ventilation.

As future work, life cycle cost analysis, payback periods and optimization of TIM-PCM wall configuration under different climates conditions will be studied using the validated numerical model.

References

[1] C. Initiative, “Buildings and Climate Change http://admin.indiaenvironmentportal.org.in/files/SBCI-BCCSummary.pdf,” 2009.

[2] F. Trombe, “Heating by solar radiation.” CNRS Internal Report B-1- 73-100., 1973.

[3] P. Ohanessian and W. W. . Charters, “Thermal simulation of a passive solar house using a Trombe-Michel wall structure.,” *Sol. Energy 20*, pp. 275–281, 1978.

[4] A. V. Sebald, J. R. Clinton, and F. Langenbacher, “Performance effects of Trombe wall control strategies.,” *Sol. Energy 23 (6)*, pp. 479–487, 1979.

[5] E. Kruger, E. Suzuki, and A. Matoski, “Evaluation of a Trombe wall system in a subtropical location.,” *Energy Build.*, vol. 66, pp. 364–372, 2013.

[6] M. Bojic, K. Johannes, and F. Alamdari, “Optimizing energy and environmental performance of passive Trombe wall,” *Energy Build*, vol. 70, pp. 279–286, 2014.

[7] M. Telkes, “Trombe wall with phase change storage material,” in *Proceedings of the 2nd National Passive Solar Conference*, Philadelphia, PA, USA., 1978.

[8] F. Fiorito, “Trombe walls for lightweight buildings in temperate and hot climates. exploring the use of phase-change materials for performances improvement.,” *Energy Procedia*, vol. 30, pp. 1110–1119, 2012.

[9] L. Zalewski, A. Joulin, S. Lassue, and Y. Dutil, “Experimental study of small-scale solar wall integrating phase change material,” *Sol. Energy*, no. 86, pp. 208–219, 2012.

[10] A. de Gracia, L. Navarro, A. Castell, A. Ruiz-Pardo, S. Alvarez, and L. F. Cabeza, “Experimental study of a ventilated facade with PCM during winter period,” *Energy Build.*, pp. 58, 324–332, 2013.

[11] L. Yongcai and L. Shuli, “Experimental study on thermal performance of a solar chimney combined with PCM,” *Appl. Energy 114*, pp. 172–178, 2014.

[12] G. Diarce *et al.*, “Ventilated active façades with PCM,” *Appl. Energy*, vol. 109, pp. 530–537, Sep. 2013.

[13] Y. A. Kara and A. Kurnuç, “Performance of coupled novel triple glass unit and pcm wall,” *Appl. Therm. Eng.*, vol. 35, pp. 243–246, Mar. 2012.

[14] A. Ghosh, B. Norton, and A. Duffy, “Measured thermal & daylight performance of an evacuated glazing using an outdoor test cell,” *Appl. Energy*, vol. 177, pp. 196–203, Sep. 2016.

[15] F. Favoino, F. Fiorito, A. Cannavale, G. Ranzi, and M. Overend, “Optimal control and performance of photovoltachromic switchable glazing for building integration in temperate climates,” *Appl. Energy*, vol. 178, pp. 943–961, Sep. 2016.

[16] N. DeForest, A. Shehabi, S. Selkowitz, and D. J. Milliron, “A comparative energy analysis of three electrochromic glazing technologies in commercial and residential buildings,” *Appl. Energy*, vol. 192, pp. 95–109, Apr. 2017.

[17] F. Goia, M. Perino, and V. Serra, “Experimental analysis of the energy performance of a full-scale PCM glazing prototype,” *Sol. Energy*, vol. 100, pp. 217–233, 2014.

[18] B. L. Gowreesunker, S. B. Stankovic, S. A. Tassou, and P. A. Kyriacou, “Experimental and numerical investigations of the optical and thermal aspects of a PCM-glazed unit,” *Energy Build.*, vol. 61, pp. 239–249, Jun. 2013.

[19] S. Li, G. Sun, K. Zou, and X. Zhang, “Experimental research on the dynamic thermal performance of a novel triple-pane building window filled with PCM,” *Sustain. Cities Soc.*, vol. 27, pp. 15–22, Nov. 2016.

[20] S. Grynning, F. Goia, and B. Time, “Dynamic Thermal Performance of a PCM Window System: Characterization Using Large Scale Measurements,” *Energy Procedia*, vol. 78, pp. 85–90, Nov. 2015.

[21] H. Manz, P. . Egolf, P. Suter, and A. Goetzberger, “TIM–PCM external wall system for solar space heating and daylighting,” *Sol. Energy*, vol. 61, no. 6, pp. 369–379, Dec. 1997.

[22] F. Goia, M. Perino, and V. Serra, “Improving thermal comfort conditions by means of PCM glazing systems,” *Energy Build.*, vol. 60, pp. 442–452, May 2013.

[23] C. Liu, Y. Wu, J. Bian, D. Li, and X. Liu, “Influence of PCM design parameters on thermal and optical performance of multi-layer glazed roof,” *Appl. Energy*, vol. 212, pp. 151–161, Feb. 2018.

[24] F. Goia, “Thermo-physical behaviour and energy performance assessment of PCM glazing system configurations: A numerical analysis,” *Front. Archit. Res.*, vol. 1, no. 4, pp. 341–347, Dec. 2012.

[25] K. Zhong, S. Li, G. Sun, S. Li, and X. Zhang, “Simulation study on dynamic heat transfer performance of PCM-filled glass window with different thermophysical parameters of phase change material,” *Energy Build.*, vol. 106, pp. 87–95, 2015.

[26] K. A. R. Ismail, C. T. Salinas, and J. R. Henriquez, "Comparison between PCM filled glass windows and absorbing gas filled windows," *Energy Build.*, vol. 40, no. 5, pp. 710–719, Jan. 2008.
[27] F. Goia, M. Perino, and M. Haase, "A numerical model to evaluate the thermal behaviour of PCM glazing system configurations," *Energy Build.*, vol. 54, pp. 141–153, 2012.
[28] K. A. R. Ismail and J. R. Henrıquez, "Parametric study on composite and PCM glass systems," *Energy Convers. Manag.*, vol. 43, no. 7, pp. 973–993, 2002.
[29] C. Liu, Y. Zhou, D. Li, F. Meng, Y. Zheng, and X. Liu, "Numerical analysis on thermal performance of a PCM-filled double glazing roof," *Energy Build.*, vol. 125, pp. 267–275, 2016.
[30] C. Liu, Y. Zheng, D. Li, H. Qi, and X. Liu, "A Model to Determine Thermal Performance of a Non-ventilated Double Glazing Unit with PCM and Experimental Validation," *Procedia Eng.*, vol. 157, pp. 293–300, 2016.
[31] T. Silva, R. Vicente, and F. Rodrigues, "Literature review on the use of phase change materials in glazing and shading solutions," *Renew. Sustain. Energy Rev.*, vol. 53, pp. 515–535, Jan. 2016.
[32] H. Weinläder, A. Beck, and J. Fricke, "PCM-facade-panel for daylighting and room heating," *Sol. Energy*, vol. 78, no. 2, pp. 177–186, Feb. 2005.
[33] K. Johannes, F. Kuznik, F. Jay, P. Roquette, P. Achard, and Y. Berthou, "CRISTOPIA ENERGY SYSTEMS, SAVERBAT SAS,Elément d'enveloppe d'un bâtiment et ensemble comprenant un tel élément," Brevet Francais FR 1158194, 15-Mar-2013.
[34] Y. Berthou, P. H. Biwole, P. Achard, H. Sallée, M. Tantot-Neirac, and F. Jay, "Full scale experimentation on a new translucent passive solar wall combining silica aerogels and phase change materials," *Sol. Energy*, vol. 115, pp. 733–742, May 2015.
[35] E. Sparrow and J. Ramsey, "Melting and natural convection due to a vertical embedded heater.," *J Heat Transf*, p. 100:368–70, 1978.
[36] E. Sparrow and S. Patankar, "Analysis of melting in the presence of natural convection in the melt region," *ASME J Heat Transf*, vol. 99:520–6, 1977.
[37] M. FARID and R. HUSIAN, "An electrical storage heater using the phase change method of heat storage.," *Energy Convers Manag*, vol. 30(3):219–30, 1990.
[38] A. Hasan, "Phase change material energy storage system employing palmitic acid," *Sol Energy*, vol. 52:143–54, 1994.
[39] M. Lacroix and T. Duong, "Experimental improvements of heat transfer in a latent heat thermal energy storage unit with embedded heat sources," *Energy Convers. Manag.*, vol. 39, no. 8, pp. 703–716, 1998.
[40] Y. Zhang and J. Yi, "A simple method, the T-history method of determining the heat of fusion specific heat and thermal conductivity of phase change materials," *Meas Sci Technol*, 1999.
[41] R. Velraj and R. seeniraj, "Heat transfer enhancement in a latent heat storage system," *Sol Energy*, 1999.
[42] A. SARI and K. KAYGUSUZ, "Thermal energy storage system using stearic acid as a phase change material," *Sol Energy*, 2001.
[43] P. Lamberg, R. Lehtiniemi, and A.-M. Henell, "Numerical and experimental investigation of melting and freezing processes in phase change material storage," *Int. J. Therm. Sci.*, vol. 43, no. 3, pp. 277–287, Mar. 2004.
[44] F. Souayfane, F. Fardoun, and P. H. Biwole, "Different mathematical models of convection during phase change," presented at the REDEC conference, NDU university Lebanon, 2016, pp. 1–8.
[45] H. Elarga, F. Goia, A. Zarrella, A. Dal Monte, and E. Benini, "Thermal and electrical performance of an integrated PV-PCM system in double skin façades: A numerical study," *Sol. Energy*, vol. 136, pp. 112–124, Oct. 2016.
[46] F. Zanghirella, M. Perino, and V. Serra, "A numerical model to evaluate the thermal behaviour of active transparent facades," *Energy Build.*, vol. 43, no. 5, pp. 1123–1138, 2011.
[47] D. Faggembauu, M. Costa, M. Soria, and A. Oliva, "Numerical analysis of the thermal behaviour of ventilated glazed facades in Mediterranean climates. Part I: development and validation of a numerical model," *Sol. Energy*, vol. 75, no. 3, pp. 217–228, 2003.
[48] O. G. Pop, L. Fechete Tutunaru, F. Bode, A. C. Abrudan, and M. C. Balan, "Energy efficiency of PCM integrated in fresh air cooling systems in different climatic conditions," *Appl. Energy*, vol. 212, pp. 976–996, Feb. 2018.
[49] M. Alam, H. Singh, and M. C. Limbachiya, "Vacuum Insulation Panels (VIPs) for building construction industry–A review of the contemporary developments and future directions," *Appl. Energy*, vol. 88, no. 11, pp. 3592–3602, 2011.

[50] J. Kosny and E. Kossecka, "Multi-dimensional heat transfer through complex buildings envelope assemblies in hourly energy simulation programs," *Energy and Buildings*, p. 34:445-54, 2002.
[51] F. Goia, M. Perino, and M. Haase, "A numerical model to evaluate the thermal behaviour of PCM glazing system configurations," *Energy Build.*, vol. 54, pp. 141–153, Nov. 2012.
[52] H. Elarga, F. Goia, A. Zarrella, A. Dal Monte, and E. Benini, "Thermal and electrical performance of an integrated PV-PCM system in double skin façades: A numerical study," *Sol. Energy*, vol. 136, pp. 112–124, 2016.
[53] G. Fraisse, "Development of a simplified and accurate building model based on electrical analogy," *Energy & Buildings*, vol. 34, pp. 1017–1031, 2002.
[54] G. Colomer Rey, *Numerical methods for radiative heat transfer*. Universitat Politècnica de Catalunya, 2006.
[55] H. Elarga, M. De Carli, and A. Zarrella, "A simplified mathematical model for transient simulation of thermal performance and energy assessment for active facades," *Energy Build.*, vol. 104, pp. 97–107, Oct. 2015.
[56] R. Siegel, "Net radiation method for enclosure systems involving partially transparent walls," 1973.
[57] W. Swinbank, "Long-wave radiation from clear skies," *Q. J. R. Meteoro. Soc*, p. 89:339, 1963.
[58] F. Miranville, "Contribution à l'étude des parois complexes en physique du bâtiment: modélisation, expérimentation et validation expérimentale de complexes de toitures incluant des produits minces réfléchissants en climat tropical humide," Université de la Réunion, 2002.
[59] B. Zivkovic and I. Fujii, "An analysis of isothermal phase change of phase change material within rectangular and cylindrical containers," *Sol. Energy*, vol. 70, no. 1, pp. 51–61, 2001.
[60] F. Souayfane, P. H. Biwole, and F. Fardoun, "Modèle simplifié pour la prise en compte de la convection naturelle dans la modélisation du changement de phase solide-liquide," presented at the Colloque Inter-universitaire Franco-Québecois, Saint-lo, France, 2017.
[61] G. Vidalain, L. Gosselin, and M. Lacroix, "An enhanced thermal conduction model for the prediction of convection dominated solid–liquid phase change," *Int. J. Heat Mass Transf.*, vol. 52, no. 7–8, pp. 1753–1760, Mar. 2009.
[62] P. Jany and A. Bejan, "Scaling theory of melting with natural convection in an enclosure," *Int. J. Heat Mass Transf.*, vol. 31, no. 6, pp. 1221–1235, Jun. 1988.
[63] A. Bejan, *Convection heat transfer*, Fourth edition. Hoboken, New Jersey: Wiley, 2013.
[64] F. Souayfane, P. H. Biwole, and F. Fardoun, "Melting of a phase change material in presence of natural convection and radiation: A simplified model," *Appl. Therm. Eng.*, vol. 130, pp. 660–671, Feb. 2018.
[65] S. V. Patankar, *Numerical heat transfer and fluid flow*. New York: McGraw-Hill., 1980.
[66] S. S. Dhenakaran and E. R. Naganathan, "A new approach to multiple symmetric keys," *IJCSNS*, vol. 7, no. 6, pp. 254–259, 2007.
[67] B. Gluck, "Wärmetechnisches Raummodell: gekoppelte Berechungen und wärmephysiologische Untersuchung," *C.F. Müller Verlag*, pp. 66–67, 1997.
[68] T. E. Kuhn, C. Bühler, and W. J. Platzer, "Evaluation of overheating protection with sun-shading systems," *Sol. Energy*, vol. 69, pp. 59–74, 2001.
[69] A. I. Palmero-Marrero and A. C. Oliveira, "Effect of louver shading devices on building energy requirements," *Appl. Energy*, vol. 87, no. 6, pp. 2040–2049, Jun. 2010.
[70] A. Kirimtat, B. K. Koyunbaba, I. Chatzikonstantinou, and S. Sariyildiz, "Review of simulation modeling for shading devices in buildings," *Renew. Sustain. Energy Rev.*, vol. 53, pp. 23–49, Jan. 2016.
[71] "ISOTRA." [Online]. Available: http://www.isotra.com/calculation-of-solar-and-light-transmittance http://www.isotra.com/calculation-of-solar-and-light-transmittance.
[72] [Online]. Available: http://www.isotra.com/.
[73] "EN 13363-1 (2003) + A1 (2007): solar protection devices combined with glazing - Part 1: simplifies method Berlin, Beuth Verlaj GmbH." .
[74] "DIN 4108-2 Thermal protection and energy economy in buildings- Part2: Minimum requirements to thermal insulation, Berlin, Beuth Verlag GmbH." .
[75] C. Ghiaus and C.-A. Roulet, "Strategies for natural ventilation," *Nat. Vent. Urban Environ. Assess. Des.*, pp. 136–157, 2005.
[76] R. and A.-C. E. American Society of Heating, *ASHRAE handbook*. Atlanta: American Society of Heating, Refrigerating and Air-Conditioning Engineers, 2001.
[77] F. Souayfane, F. Fardoun, and P.-H. Biwole, "Phase change materials (PCM) for cooling applications in buildings: A review," *Energy Build.*, vol. 129, pp. 396–431, Oct. 2016.

[78] R. Hampus, *Performance improvement from single to multi phase change materials in a thermal energy storage system*. 2015.
[79] S. Ferrari and V. Zanotto, "Adaptive comfort: Analysis and application of the main indices," *Build. Environ.*, vol. 49, pp. 25–32, Mar. 2012.
[80] M. Kottek, J. Grieser, C. Beck, B. Rudolf, and F. Rubel, "World Map of the Köppen-Geiger climate classification updated," *Meteorol. Z.*, vol. 15, no. 3, pp. 259–263, Jun. 2006.

Complementary sections to chapter 3

A) Graphs for model validation in winter season

In summer season, the PCM remains in its liquid state and the model was validated for seven consecutive days (30 July-5 August 2017) comparing the simulated and the measured values for the internal surface temperature of the TIM-PCM wall, the indoor test room air temperature and the PCM temperature in section 6. The comparisons showed a very good agreement and that the natural convection in liquid PCM must be considered. In this section we will show the validation curves, for internal surface temperature and indoor temperature, for seven consecutive days in winter season (27 January-2 February 2017). In this period, phase change occurs, and the PCM melts during the day and solidifies at night.

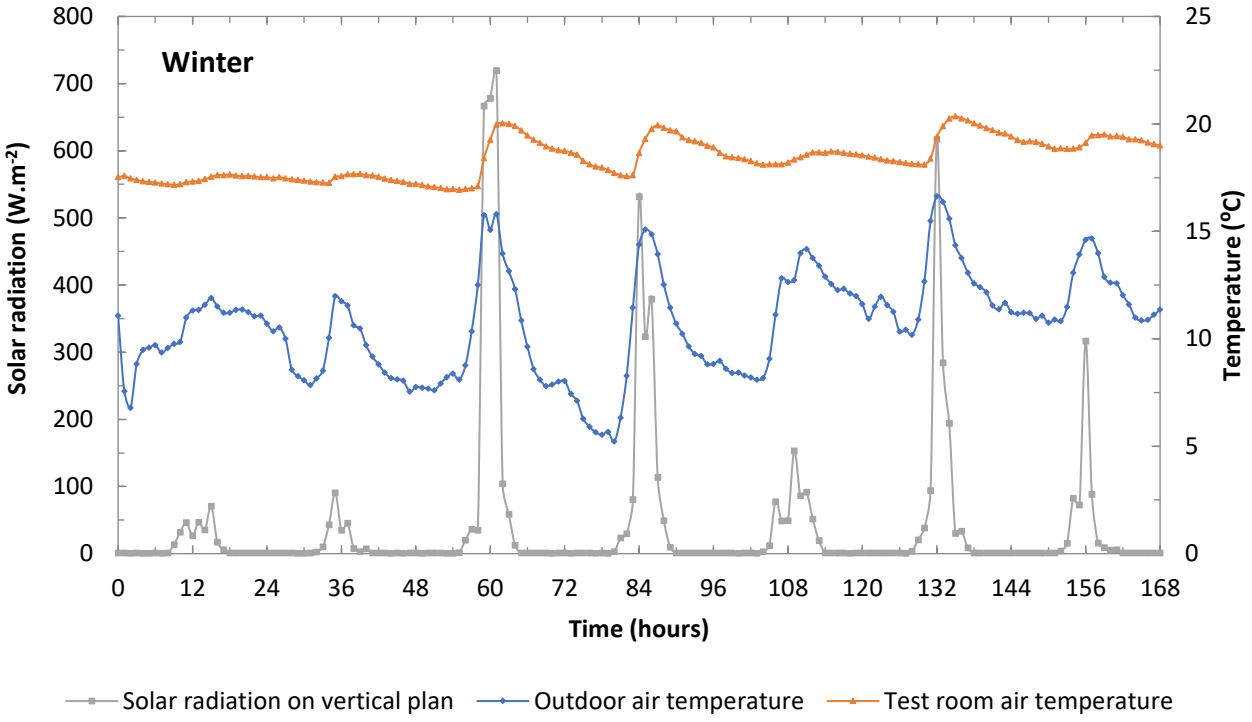

Figure 1: Temperatures and solar radiation for seven consecutive days in winter (27 January-2 February 2017).

The seven consecutive days in winter season (27January- 2 February) are characterized by a low outdoor temperature varying from 5.22 ºC to 16.63 ºC, with low (70.82 W.m^{-2}) and high (719.2 W.m^{-2}) solar radiation on the southern vertical plane (Figure 1). On January 27 and 28, the PCM does not melt staying in its solid state (PCM temperature lower than 21ºC) and the test room air temperature is about 17ºC. On January 29 and 30 and on February first, due the high incident solar radiation, the PCM melts during the day (PCM temperature up to 62ºC) and solidifies at night and the indoor temperature reaches more than 20ºC. The TIM-PCM wall is therefore very effective in the winter season (the average room air temperature is almost constant at18.38 ºC), keeping warm the indoor

environment especially in sunny days. The measured PCM temperatures for seven consecutive days in winter season are shown in Figure 2.

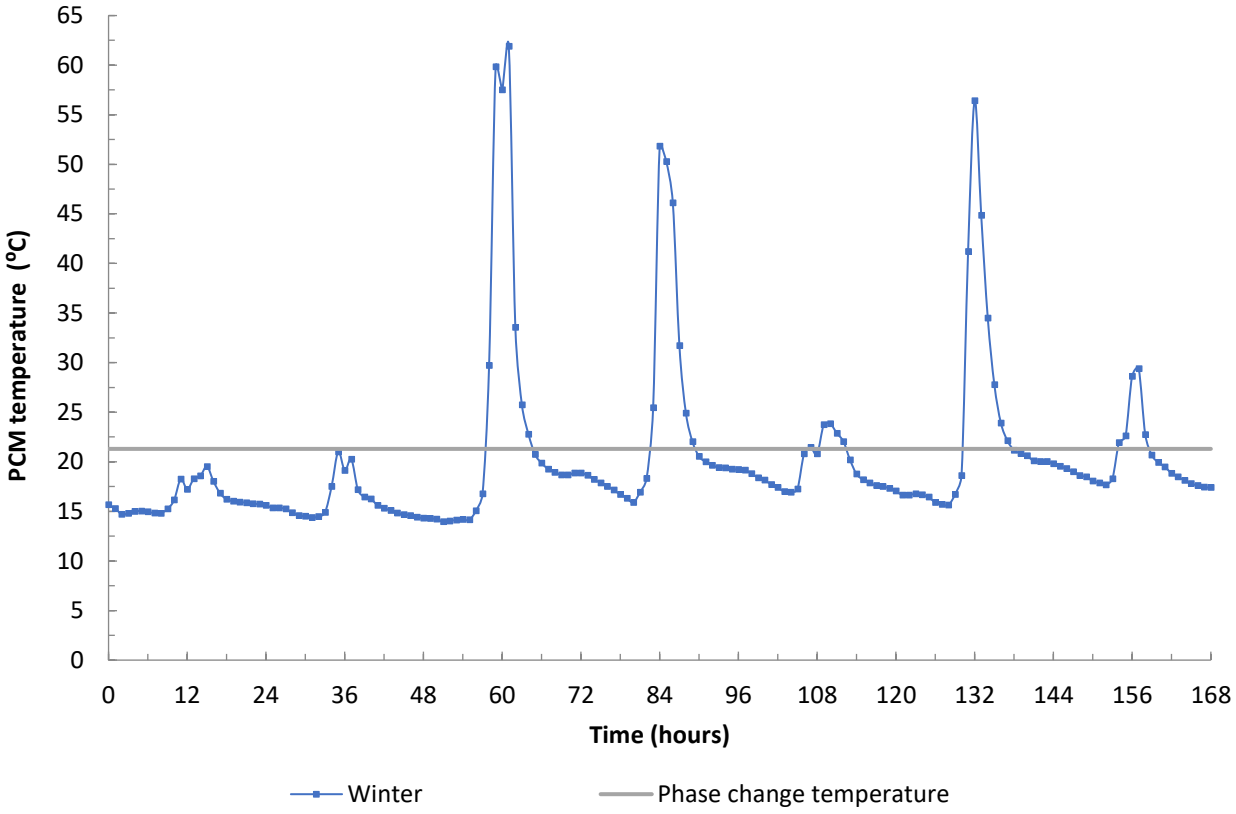

Figure 2: Measured PCM temperatures for seven consecutive days in winter (27 January-2 February 2017).

Noting that during solidification process, the convection heat transfer is less important than conduction [1,2]. In addition, in such walls as the INERTRANS wall solidification is more likely to happen at night, in absence of solar radiation. Thus, the equation of heat transfer for the phase change controlled by the conduction only is used to model solidification process (see Enthalpy method).

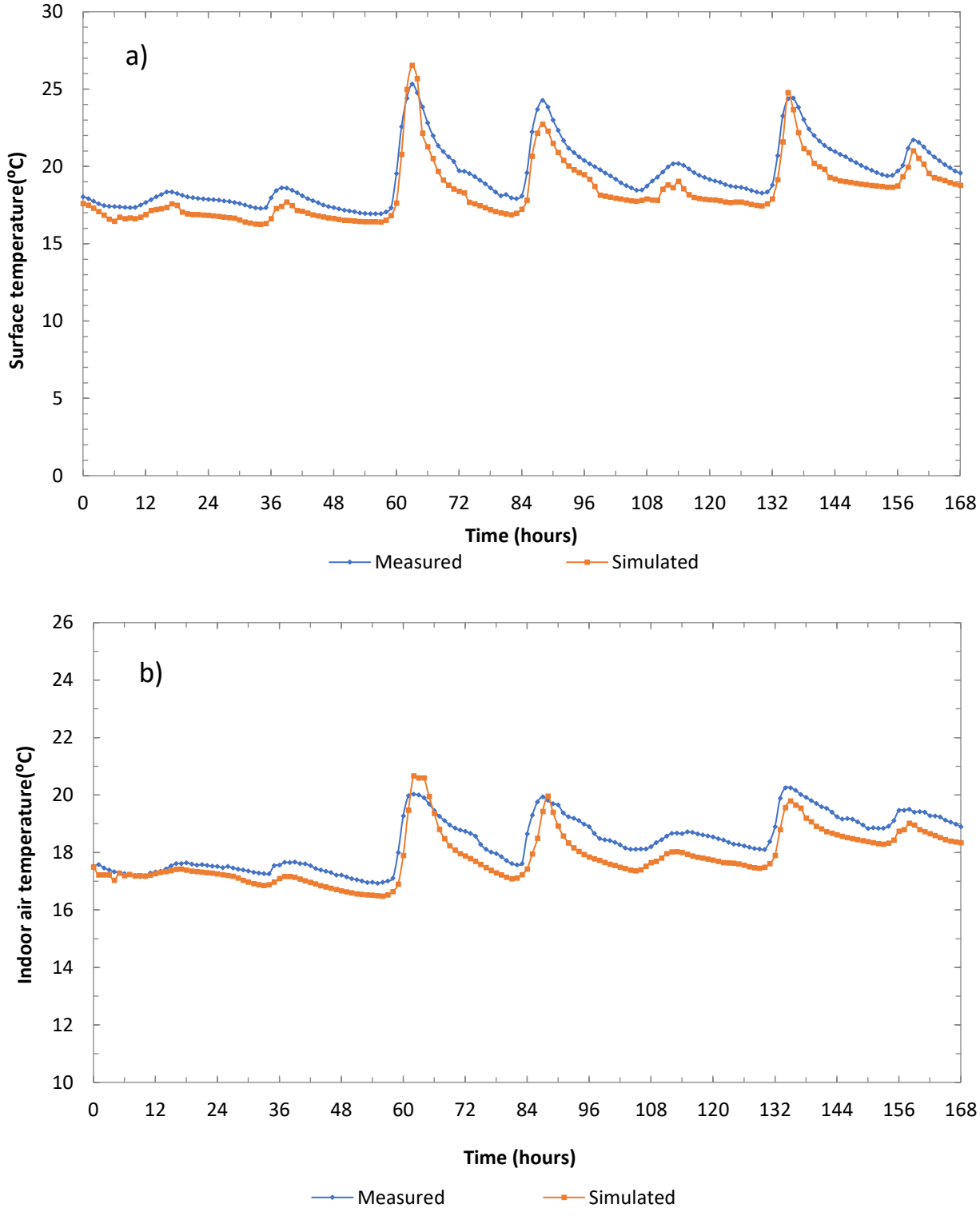

Figure 3: Simulated and measured a) internal surface temperature of the TIM-PCM wall and b) indoor test room air temperature for seven consecutive days in days in winter (27 January- 2 February 2017).

Figure 3 shows the simulated and measured internal surface temperature of the TIM-PCM wall and indoor test room air temperature for seven consecutive days in days in winter (27 January- 2 February 2017). The numerical model is found to be able to simulate the heat transfer phenomena through the TIM-PCM wall in winter. The model predicts properly the maximum and minimum peak values of

the hourly profile of the internal surface temperature and the indoor air temperature with a slight underestimation of the lowest values. The peak values in all days are in good agreement. For the indoor temperature a maximum difference between the simulated and experimental values is 1.3ºC. The PCM undergoes complete cycles in January 29, 30 and February first while the PCM is remains in its solid state in 27 and 28 January where a good agreement is found between experimental and simulated values.

In addition, the PRMSE and RSME demonstrate the good agreement between the experimental and the simulated results. The PRMSE of the indoor air temperature is 4.05%, and that of the internal surface temperature is 6.9 %. While the RMSE is 0.76ºC and 1.43ºC for the indoor air temperature and the internal surface temperature respectively. Here, the model considers convection during melting process.

These results are relatively acceptable, the model is validated in summer (when PCM is always in its liquid state) and in winter (when phase change occurs). Thus, the model can be used for annual thermal assessment.

B) Wind velocity and outdoor relative humidity in winter and summer seasons

The wind velocity is used to find the external convection heat transfer (correlation of Sturrock):

$h_{out} = 5.7v + 11.4$ (Windward)

$h_{out} = 5.7v$ (Leeward))

And, the outdoor relative humidity is linked to the building model (in TRNSYS).

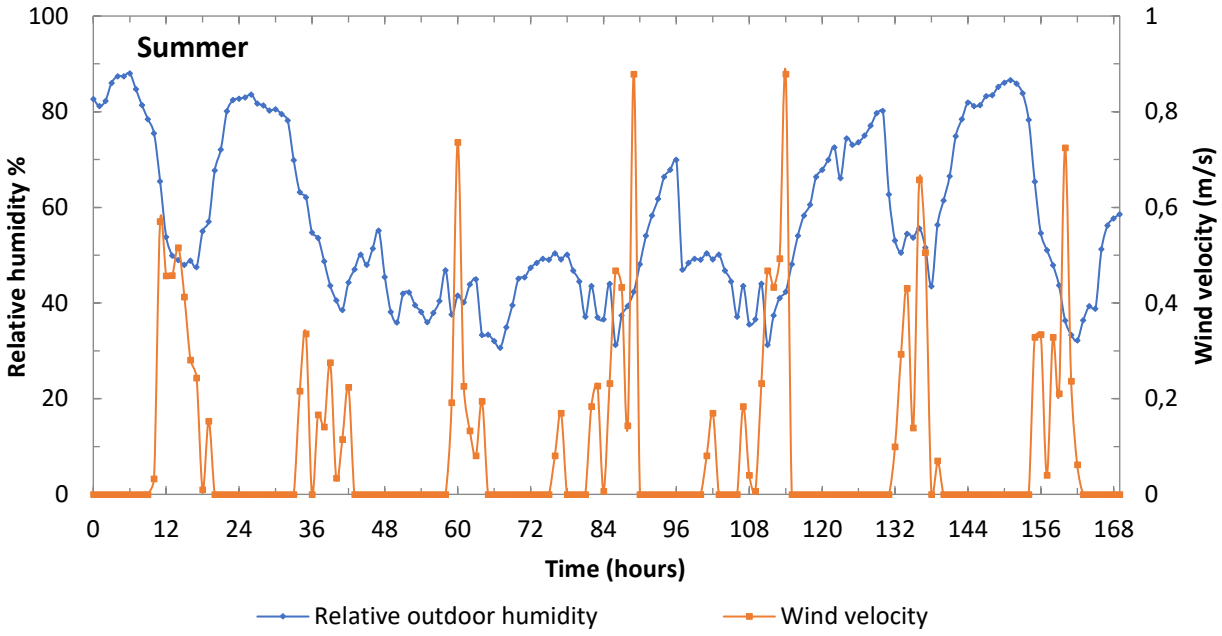

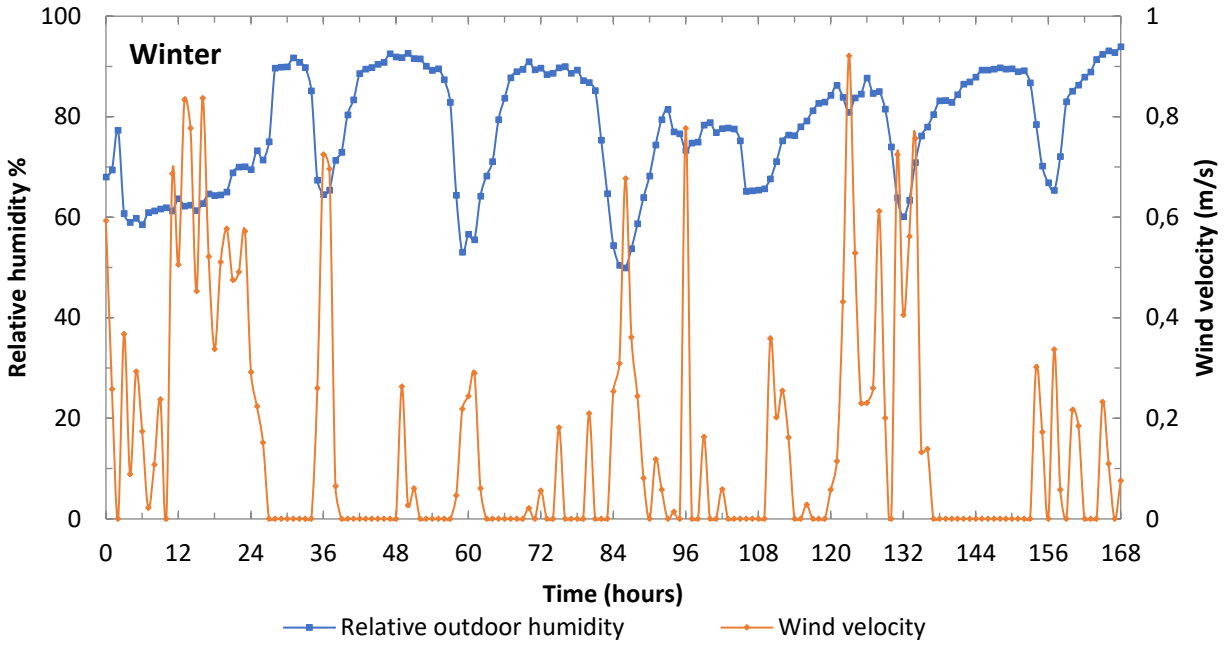

Figure 4: Measured wind velocity and outdoor relative humidity for seven consecutive days in summer (30 July-5 August 2017) and winter (27 January-2 February 2017).

References

[1] M. Lacroix and M. Benmadda, "Numerical simulation of natural convectiondominated melting and solidification from a finned vertical wall," *Numer. Heat Transfer*, no. Part A Appl. 31, pp. 71–86, 1997.

[2] R. Velraj, R. seeniraj, B. Hafner, C. Faber, and K. Schwarzer, "HEAT TRANSFER ENHANCEMENT IN A LATENT HEAT STORAGE SYSTEM," *Solar Energy*, vol. 65, no. No. 3, pp. 171–180, 1999.

CHAPTER 4

ENERGY PERFORMANCE AND ECONOMIC ANALYSIS OF A TIM-PCM WALL UNDER DIFFERENT CLIMATES

Chapter 4. Energy Performance and Economic Analysis of a TIM-PCM wall Under Different Climates

Résumé du chapitre en français

Performance énergétique et analyse économique liées à l'application du mur MCP-Aérogel sous différents climats

Dans un premier temps, ce chapitre étudie la performance énergétique d'un bureau typique suite à l'incorporation du mur MCP-aérogel dans son enveloppe, dans six climats différents considérés selon la classification de Köppen-Geiger. Le processus de simulation est réalisé pour une année entière à l'aide du modèle numérique TRNSY-MATLAB validé expérimentalement. Les charges énergétiques annuelles de chauffage et de refroidissement sont déterminées pour un bureau conventionnel équipé d'une fenêtre double vitrage, puis comparées à celles du bureau équipé d'un mur MCP-aérogel orienté sud. Les économies d'énergie dues à l'utilisation du mur MCP-aérogel sont aussi évaluées. La surface du double vitrage isolé et du mur MCP-aérogel varie de 0 m^2 à 7.532 m^2.

Dans tous les climats étudiés, la performance énergétique du bureau, en termes d'économies de chauffage et de refroidissement, est significativement améliorée avec l'incorporation de la paroi MCP-aérogel au lieu d'une fenêtre à double vitrage. De plus, les charges totales diminuent avec l'augmentation de la surface du mur sauf en climat méditerranéen (Csa). Ainsi, dans les villes ayant une saison estivale chaude, la surface du mur MCP-aérogel doit être limitée à une certaine valeur de manière à fournir des économies de chauffage significatives en hiver et des charges de refroidissement acceptables en été. Dans ce cas, la surface optimale du mur fournissant des charges énergétiques totales minimales est de 2,61 m^2 à Sacramento, USA (Csa). Cependant, les dispositifs d'ombrage peuvent être utilisés en été pour empêcher le problème de surchauffe et réduire les charges de refroidissement. Dans les autres climats étudiés, la surface de la paroi MCP-aérogel montrant la meilleure performance énergétique est de l'ordre de 7.5 m^2.

Dans un deuxième temps, la surface optimale du mur MCP-aérogel a été évaluée économiquement pour chaque climat grâce à une analyse portant sur le coût global durant le cycle de vie (CCV) et le temps de retour sur investissement (TRI). Deux critères ont été évalués : la surface optimale est celle qui assure le CCV minimal ou le TRI minimal. Il a été trouvé que lorsque le climat devient plus froid, la surface optimale du mur MCP-aérogel augmente. Dans les climats polaire (ET) et subarctique (Dfc), l'application de la paroi MCP-aérogel est trouvé économiquement faisable. Les économies de chauffage pour l'immeuble de bureaux situé à Dras, en Inde (Dsb, climat continental) ne sont pas suffisantes pour récupérer l'investissement en raison des faibles prix de l'énergie et du taux d'actualisation (discount rate) élevé. A Paris, France (Cfb, climats océanique), l'utilisation du mur

MCP-aérogel s'avère plus rentable que l'utilisation de la fenêtre double vitrage en termes de coût minimal du cycle de vie et de temps de retour sur investissement. A Sacramento, Usa (Csa, climat méditerranéen) et Toronto, Canada (Dfa, climat humide continental), l'application du mur n'est pas rentable aux prix actuels de l'énergie et de l'investissement. Les meilleurs candidats pour l'application du mur MCP-aérogel se trouvent là où le prix du gaz naturel est relativement élevé, rendant le coût d'investissement initial relativement insignifiant comparé aux économies de chauffage. La viabilité économique de l'application du mur MCP-aérogel dépend donc de différents facteurs : conditions climatiques, économies d'énergie, coûts énergétiques (prix du gaz naturel, prix de l'électricité ...), situation économique du pays (taux d'actualisation et facteur de valeur actuelle) et couts d'investissement.

Abstract

The application of an innovative translucent superinsulated latent heat storage wall, combining transparent insulation material and phase change materials (TIM-PCM wall), on the envelope of a typical office under different climates is evaluated. Energy and economic analysis related to this application are presented. The simulation process is carried out using an experimentally validated numerical model. The results show that the incorporation of the TIM-PCM wall, on the south orientation, is more efficient than the use of a double-glazed in all considered climates. Besides, increasing the TIM-PCM wall area increases the total energy savings in all climates except in the Mediterranean climate. The optimum TIM-PCM wall area is then evaluated economically through life-cycle cost and payback period analysis. The purpose is to ensure an effective performance of the wall in each climate and at the same time to ensure an economic viability. The results show that, in polar and subarctic climates, the application of the TIM-PCM wall has a high economic value and the investment appears to be attractive, the payback period being 10.5 years and 7.8 years respectively. In Paris (Oceanic climate), the use of the TIM-PCM wall is found more cost-effective than the use of double-glazed window showing lower total life-cycle cost and payback period. However, In Dras (continental climate), the use of the wall is found infeasible economically due to low energy prices and high discount rates. At current prices, the TIM-PCM wall investment in Sacramento (Mediterranean climate) and Toronto (Humid continental) does not offer economic benefits.

Keywords: TIM-PCM wall, energy performance, climatic zones, economic analysis, office building envelope.

Highlights:

- Application of the TIM-PCM wall under different climates.
- Energy and economic analysis related to the application of the TIM-PCM wall.
- Evaluation of the optimum TIM-PCM wall area in each climatic condition.
- Economic viability depends on climatic conditions, energy price and investment cost.

1. Introduction

Nowadays, reducing the total energy demand of the world is a crucial challenge, due to global warming, climate change effects, energy crisis, and environmental issues. Building sector contributes to a great part of the world's energy consumption [1], mainly due to the heating and cooling demands. Thus, one of the most important ways of reducing the total global energy consumption is to decrease the energy used in HVAC systems in buildings. One promising solution is the integration of latent thermal energy storage systems based on phase change materials in the building envelope. Phase change materials can store (during melting) and release (during solidification) large amounts of energy at an almost constant temperature. Consequently, they can enhance building energy performance, decrease building energy use, reduce peak heating and cooling loads and improve thermal comfort [2]–[6]. However, the workability of passive PCM application in buildings depends on the diurnal temperature variations that ensure the PCM cycling. Thus, an effective use of PCM in buildings requires an appropriate selection of thermo-physical properties, quantity, and position of the PCM. Many studies were conducted to find optimum PCM thickness, melting temperature, and location under different climate conditions [7]–[9]. However, in addition to energy-saving and thermally efficient materials, the ever-growing construction industries worldwide require environmentally friendly and inexpensive materials [10].

Trombe walls with integrated phase change materials are a passive solar technique that has shown great potentialities [11]–[15]. During the day, this wall is heated due to the incident solar radiation, melting the PCM. At night, when the outdoor temperature falls below the phase change temperature, the heat stored by the PCM is released, warming the building. However, this technique induces a loss of visual daylight comfort because it is opaque. Many studies focus on the integration of PCM into a transparent component [16] [17] [18] [19] [20] [21] so that the PCM is directly exposed to the solar radiation which improves the PCM charge process, providing daylighting at the same time. Although the integration of PCM in transparent or opaque building envelope has shown a positive impact on annual cooling and heating loads and indoor thermal comfort in various climate zones, there are still technical, environmental, and economic barriers to be addressed.

Kyriaki et al. [22] analyzed the state of the art of the existing research on the environmental and economic performance of the application of PCM in buildings by using life cycle analysis (LCA) and life cycle cost analysis (LCCA) methodologies. It was concluded that to minimize the overall environmental impact, the use of PCM and the useful life of the building should be maximized. In addition, they concluded that very few studies are found about the economic assessment of PCM, based on life-cycle cost analysis. And that the application of PCM does not seem to be economically viable because of their high initial investment cost. Baniassadi et al. [23] conducted an economic

optimization of the thickness of the insulation and the PCM layer of a residential building for different climatic regions of Iran using life-cycle cost analysis (LCCA). The results showed that with the current economic situation of the country and current energy prices, insulation layers are more cost-effective than phase change materials. This is due to the relatively high price of the BioPCM material which makes its use not economically viable. Akeiber et al. [10] evaluated the thermal performance and economy of a newly developed PCM extracted from Iraqi crude petroleum waste product. Experiments showed that the room without PCM encapsulation consumes higher energy to maintain the indoor temperature at 24ºC. The energy economy of the PCM incorporated room is simply evaluated by comparing the estimated electricity cost with the building that contains the traditional air conditioning system. They found that PCM encapsulation leads to a great amount of electrical energy saving and maintains better thermal comfort in hot and dry climate condition. Panayiotou et al. [24] evaluated the application of macroencapsulated PCM on the envelope of a typical dwelling in the Mediterranean region. The optimum case, achieving maximum energy savings, was combining the PCM with a common thermal insulation. The results showed that the maximum yearly energy savings obtained by the combined case are 66.2%. The results were also economically evaluated using life-cycle cost (LCC) analysis. It was shown that the use of PCM alone is not a very attractive solution in financial terms. This is due to the combination of high initial cost and low annual saving cost which results in a long payback time of 14 ½ years. When the PCM is combined with thermal insulation, the payback period is reduced to 7 ½ years. Kosny et al. [25] investigated a cost analysis of simple PCM-enhanced building envelopes in southern U.S. climates. They found that dispersed PCM in wall and attic applications can be cost-effective and payback periods for their building applications can be less than 10 years. Also, the best candidates for these applications are found where electricity cost is higher than $0.20/kWh and in U.S. locations with cooling degree days CDDs higher than 30000. Bland et al. [26] showed in their study the breakdown of the financial viability of installing a PCM system into a UK home. They found that an ideal PCM system installed into a residential building will need a service life of at least 25 years to make it viable. The PCM systems must provide significant energy savings before they become attractive to commercial purchasers. Chan [27] evaluated the thermal and the energy performance of a typical residential building with PCM integrated external walls in Hong Kong. They found that the building integrated with PCM is economically infeasible in Hong Kong, mainly due to the expensive capital cost of PCM wallboard with a payback period of 91 years. For economic analysis, Mi et al. [28] used the static and the dynamic payback period approach to evaluate the application of PCM in a typical office building in five different climates in China. They found that the energy savings resulting from PCM application were the best for the office building located in a severely cold climate, followed by cold region. From

the economic analysis, the application of PCM in cities having severe or cold winter showed high economic value and the investment appeared to be attractive. However, at current prices, the PCM investment in cities having a mild and warm climate, cannot be recovered and do not offer economic benefits. Wahid et al [29] highlighted the feasibility of PCM utilization in the households. They found that PCM could be extensively used in building structures to reduce the electricity demand. Sun et al. [30] presented an energy and economic analysis related to the application of phase change materials boards (PCMBs) in building enclosures during the cooling season. Following a simple payback period evaluation, they found that the use of PCMBs can be possibly cost-effective in occupied buildings for moderate temperature climates. Chaiyat [31] concluded that integration of PCM balls within the evaporator of the air-conditioner was more beneficial than the normal air-conditioner based on energy efficiency and economic results.

From all the above mentioned, it can be stated that: (1) the studies on economic analysis of building integrated with PCM are not comprehensive and more studies should be conducted to evaluate the economic performance of the use of PCM in buildings, (2) economic analyses related to the application of PCM in buildings are conducted based on a life-cycle cost evaluation or based on a payback period evaluation (3) the PCM systems must provide significant energy savings before they become attractive to commercial purchase, (4) the economic feasibility of PCM depends on climatic conditions, energy costs, country economic situation, (5) most previous studies found that the application of PCM is not economically viable mainly due to the expensive investment costs compared to the expected energy savings.

The present paper investigates an innovative passive solar wall, referred to as TIM-PCM wall, providing at the same time very high insulation, latent heat storage, and daylighting. The wall is composed of a glazing facing the outside, a gap filled with high insulation silica aerogels materials (transparent insulation material-TIM), and glass bricks filled with a eutectic PCM on the inside. The whole wall is translucent. The energy and economic performance of the incorporation of the TIM-PCM wall in an office room envelope are investigated under different climates via an experimentally validated numerical model for a whole year. The annual heating and cooling energy loads are determined for a conventional office room equipped with an insulated double-glazed window and then compared with those of the correspondent office room equipped with a TIM-PCM wall at the south orientation. Energy savings due to the use of TIM-PCM are evaluated. Then, the optimum TIM-PCM wall area is assessed economically for each climate through life-cycle cost and payback period analysis. The aim is to ensure a good functioning of the TIM-PCM wall in each climate and at the same time ensure economic feasibility. Noting that, The TIM-PCM wall is an innovative solar wall, its impact on the building thermal behavior has never been studied numerically under different

climates for an annual basis. Also, the feasibility of the wall application from an economic point of view has never been studied. The wall area was also optimized depending on the climate for the first time. In addition, in the literature, there is a lack of studies that evaluate the economic performance of the use of PCM in buildings. The effective PCM system, in terms of reducing heating or cooling loads, does not necessarily mean that this system can be applicable to real life constructions, it must provide significant energy savings before it becomes attractive to commercial purchase. The current study represents a starting point and should be continued in future, the purpose is not only to ensure an effective performance of the PCM application but also to ensure an economic viability.

2. Methodology

2.1. Description of simulated building

The energy performance of a single-story office building equipped with TIM-PCM wall is studied (Figure 4-1). The office has a height of 2.8 m and a total floor area of 32 m2 with a slab-on-grade foundation. The ground floor is highly insulated assuming a small heat exchange occurring between the office room and the ground. The walls construction composition and the thermo-physical properties of used materials are summarized in Table 4-1 and Table 4-2. The conventional office room is equipped with an insulated double-glazed window on the south wall of a total area of 11.2 m^2. The double glazing with krypton insulation of thickness 4/16/4 has a U value of 0.86 W/ m^2K and a g value of 0.598. The annual heating and cooling loads are determined for the conventional office room for different climate conditions and then compared through simulation with those of the correspondent PCM-enhanced office room, equipped with a TIM-PCM wall at the south orientation. The TIM-PCM wall shown in Figure 4-2 is composed, from outside to inside, of a glass pane having a thickness of 0.8 cm, a 4cm thick bed of granular silica aerogel, and a eutectic of fatty acids as PCM, filled in glass bricks of dimension 19cm × 19cm × 5cm. More details about the TIM-PCM wall can be found in [32], [33]. The thermo-physical and optical properties of the used PCM, the silica aerogel, and the glass are summarized in Table 4-1 to Table 4-5. In the simulation, the area of the insulated double-glazed window and the TIM-PCM wall is varied from 0 m^2 to 7.532 m^2. Otherwise, the ratio of the double-glazing area over the total south wall area varies between 0 % and 67 %, same for the TIM-PCM wall (Table 4-6).

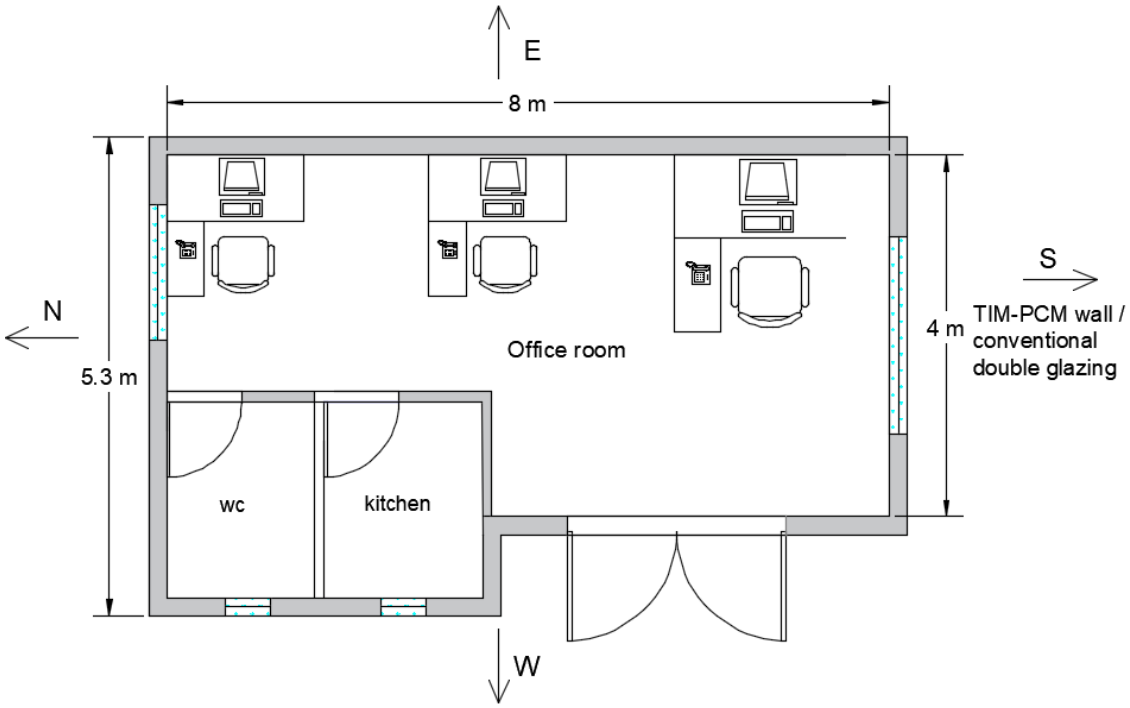

Figure 4-1: Typical plan of a simple office room.

Figure 4-2: TIM-PCM wall from the outside and Schematic of the TIM–PCM wall composition

Table 4-1: office room walls construction

Element	Construction (inside to outside)	Thickness (m)	U value (W/m^2K)
External walls	plasterboard	0.015	0.419
	Glass wool	0.085	
	concrete	0.20	
Partitions	plaster	0.013	0.241
	Glass wool	0.16	
	plaster	0.013	
Roof	plasterboard	0.013	0.163
	Glass wool	0.16	
	Wooden plate	0.012	
	Mousse phenol-formol	0.06	
	Wooden plate	0.012	
Floor	tiles	0.015	0.189
	concrete	0.15	
	Expanded polystyrene	0.08	

Table 4-2: Thermo-physical properties of the test room materials

Materials/properties	Thermal conductivity (W/m.K)	Specific heat (J/kg.K)	Density (kg/m^3)
plasterboard	0.32	800	790
Glass wool	0.041	840	12
concrete	2.1	800	2400
Mousse phenol-formol	0.032	1255	32
Wooden plate	0.18	1700	780
Expanded polystyrene	0.04	1380	25
tiles	1	1000	2400

Table 4-3: Thermo-physical properties of the fatty acids eutectic [32]

Property	value
k_s (W/m.K)	0.182
k_l (W/m.K)	0.182
L_H (J/kg)	152000
Cp_s (J/kg.K)	1670
Cp_l (J/kg.K)	2090
ρ_s (kg/m^3)	960
ρ_l (kg/m^3)	884
Tm (°C)	21.3
α (m^2/s)	$9.85x10^{-8}$
ν (m^2/s)	$11x10^{-6}$
β (1/K)	$3.1x10^{-3}$

Table 4-4: Optical properties of the fatty acids eutectic [32]

		τ%	ρ%
Liquid state	Energetic (0.1μm< λ <100μm)	90	5
	Optical (0.38μm<λ<0.78μm)	78	6
Solid state	Energetic (0.1μm< λ <100μm)	≈ 0	53
	Optical (0.38μm<λ<0.78μm)	≈ 0	56

Table 4-5: Thermo-physical and optical properties of glass and Silica aerogel

properties/Materials	glass	Silica aerogel
Thickness (cm)	0.8	4
k (W/m.K)	1	0.018(at 25ºC)
Cp (J/kg.K)	840	1500
ρ (kg/m^3)	2700	100
τ%	80	57
α%	12	10

Table 4-6: Different dimensions of the TIM-PCM wall to be studied

Bricks number	TIM-PCM wall area (m^2)	PCM volume (m^3)	Rest of wall area (m^2)	(TIM-PCM wall area / total wall area) (%)
0	0	0	11.2	0
40	1.5064	0.041344	8.65	13.5%
90	3.3894	0.093024	6.77	30%
140	5.2724	0.144704	4.89	47%
200	7.532	0.20672	2.63	67%

Regarding internal heat gains (Table 4-7), the office room is occupied by three persons in light work office activity with a constant metabolic rate of 115 W/person. To simulate a real-lifestyle, the office is considered occupied during the weekdays from 8 a.m. till 12 p.m. and from 2 p.m. till 6 p.m. and unoccupied during weekends.

The following scenario is adopted:

- The heating system is always available to maintain the indoor air temperature at a pre-defined setpoint level. The heating set-point schedule is the same as that of the French thermal regulations ‘‘RT 2012”, heating set-point is set at 19°C for occupied time and at 16°C for unoccupied times [34].
- The cooling set-point is set at 26°C for occupied time and off for unoccupied times.
- The infiltration rate is taken 0.4 ACH (ASHRAE Fundamentals Handbook [35])
- The European Lighting Standard EN12464-1 [36], requires an illuminance of 500 lux in working areas. The artificial lighting is not always ON since the TIM-PCM wall allows daylighting.

Table 4-7: Internal heat gains in the office room (ASHRAE Fundamentals Handbook (SI) [35])

Gains	Value
3 persons	115 W of which 45 W radiative 70 W convective
3 Computers	20 W of which 15% radiant and 85% convective
One printer	35 W of which 20% radiant and 80% convective
3 Phones / faxes	15 W of which 30% radiant and 65% convective
Microwave oven 28 L	400 W of convective gain
Small refrigerator	310 W of convective gain

2.2. Investigated climates

The main objective of this work is to evaluate the energy performance of the TIM-PCM wall and to find the optimum wall configuration in different places around the world. Therefore, six climates for different cities were considered according to the Köppen–Geiger classification [37]. Table 4-8 shows the description of the different selected climates for this study as well as the latitude, the longitude and the elevation for each city. Since the main purpose of the solar TIM-PCM wall is to provide heating to the indoor environment, most of the climates are chosen with mild, cold or severe winter season and the climate classifications A (tropical) and B (arid) are excluded from the study. The weather data files are extracted from TRNSYS Meteonorm library. Table 4-9 presents some major weather characteristics for each climate.

Table 4-8: Selected locations and climate characteristics according to Köppen-Geiger classification [37]

City	Climate	Latitude	Longitude	Elevation (m)
Sacramento, California, (USA)	Mediterranean climate (Csa)	38.5816° N	121.4944° W	9.1
Paris (France)	Oceanic climate (Cfb)	48.8566° N	2.3522° E	36
Toronto (Canada)	Humid Continental (Dfa)	43.6532° N	79.3832° W	76
Dras (India)	Continental (Dsb)	34.4330° N	75.7670° E	3066
Kiruna (Sweden)	Continental subarctic (Dfc)	67.8558° N,	20.2253° E	530
Barentsburg (Norway)	Polar climate (ET)	78.0648° N	14.2335° E	15

Table 4-9: Some main weather characteristics for each climate

City	Sacramento	Paris	Toronto	Dras	Kiruna	Barentsburg
Climate	**Csa**	**Cfb**	**Dfa**	**Dsb**	**Dfc**	**ET**
Max outdoor temperature (°C)	39.7	31.25	31.05	29.3	23.6	12.2
Min outdoor temperature (°C)	-0.8	-7.75	-21.75	-23.4	-32.75	-29.3
Max incident solar radiation on southern vertical plane (W/m^2)	833.08	844.97	881.84	963.86	837.01	890.74
Total yearly solar radiation on southern vertical plane (Kwh/m^2/ year)	1148.54	751.48	946.92	1044.83	686.27	601.23

In general, in cooling dominant climates (Köppen-Geiger classifications A and B) the optimum PCM melting temperature is closer to the maximum of 26ºC (melting range of 24ºC-28ºC), whereas in heating dominant climates (C and D) the optimum PCM melting is closer to the minimum of 20ºC (melting range of 18ºC-22ºC) [9]. The eutectic fatty acids integrated into the glass bricks of the TIM-PCM wall having a phase change temperature of 21.3˚C is appropriate for the chosen climates.

2.3. Numerical model

In this work, a one-dimensional numerical model is developed considering the effect of thermal bridges caused by the joints of the bricks. Mesh sensitivity analysis was carried out for the numerical model to make sure that the results are independent of the numerical domain. Finally, a total of 16 nodes were used, 2 for the glazing layer, 5 for the silica aerogel, 5 for PCM layer and 2 nodes for each glass brick. The chosen discretized scheme shows good accuracy within a satisfactory computational time, and it is well-matched with other works evaluating the annual thermal performance of PCM applications in facades [38]–[40]. The unsteady energy equation is written for each node and solved numerically. The developed TIM-PCM wall model computes the temperature field and the solar radiation transmitted to the test cell through the wall at each time step, these outputs are then linked to TRNSYS to simulate the energy performance of the whole building. More details about the development of the numerical model can be found in [41].

For the TIM-PCM wall, the heat transfer includes different regions, which are the outer glazing, the silica aerogel insulation and the PCM filled in glass brick. The one-dimensional unsteady energy equation for glazing and insulation layer is given as

$$\rho C_p \frac{\partial T}{\partial t} = k \frac{\partial^2 T}{\partial x^2} + \emptyset_{sol} \qquad \textbf{Eq. 4-1}$$

where ρ is the density (kg/m^3), C_p is the specific heat (J/kg. K), k is the thermal conductivity (W/m. K) and $\emptyset_{sol}$ (W/m^2) is the absorbed solar radiation at the surface of the layer.

In the PCM layer, the heat transfer during phase change is done by conduction, natural convection in the liquid phase and shortwave radiation. The unsteady energy equation for PCM regions is given as [42]:

$$\rho C_p \frac{\partial T}{\partial t} = \frac{\partial}{\partial x}\left(k \frac{\partial T}{\partial x} \right) - \rho L_H \frac{\partial f_l}{\partial t} + \emptyset_{sol} \qquad \textbf{Eq. 4-2}$$

where $\emptyset_{sol}$ (W/m^2) is the absorbed solar radiation, in the layer, L_H is the latent heat of fusion (J/kg) and f_l is the liquid fraction.

The absorbed solar radiation $\emptyset_{sol}$,at a node p in the PCM layer, is then given as [17]:

$$\emptyset_{sol} = \frac{Q_{sol-trans}\,\alpha_P}{N} \quad \textbf{Eq. 4-3}$$

$Q_{sol-trans}$ is the transmitted solar radiation to the PCM layer calculated using equations given by Siegel [43], α_P is the PCM absorption coefficient at the node p calculated using the equations proposed by Gowreesunker et al. to model combined phase change and radiation problems [17].

To solve the phase change problem, a fixed-grid modified "enthalpy" method is used, inspired by the work of Zivkovic et al. [44]. The convection in the liquid PCM is accounted for using the enhanced thermal conductivity approach together with the scaling theory [45] [46] [47]. The convection effect is only considered in the upper part of the PCM layer of height z_1 and width z_2, while the zone $(z_2.H_b) - (z_1.z_2)$ is controlled by conduction. Therefore, an average enhanced conductivity for liquid nodes is used in the one-dimensional model expressed by:

$$k_{enh,p} = \frac{k_l[(z_2.H_b) - (z_1.z_2)] + k_l.Nu_{z_1}(z_1.z_2).}{z_2.H_b} \quad \textbf{Eq. 4-4}$$

where $k_{enh,p}$ is the liquid enhanced conductivity for the liquid PCM node p, H_b is the height of the glass brick filled with PCM and Nu_z is the Nusselt number correlation given by Berkovsky and Polevikov [48]. More details can be found in the reference [33].

The heat balance on the outside surface is given by [49]:

$$\rho c_p \frac{\Delta x}{2}\frac{\partial T}{\partial t} = \emptyset_{cond}(t) + \emptyset_{LW,out}(t) + \emptyset_{conv,out}(t) + \emptyset_{sol}(t) \quad \textbf{Eq. 4-5}$$

where, $\emptyset_{cond}(t)$ is the conductive heat flux in (W/m^2) is given as:

$$\emptyset_{cond}(t) = \frac{k}{\Delta x}\left(T_{s+\Delta x} - T_{surf}\right) \quad \textbf{Eq. 4-6}$$

and $\emptyset_{sol}$ (W/m^2) is the solar absorption flux at the surface expressed by:

$$\emptyset_{sol}(t) = \alpha Q_{sol-total} \quad \textbf{Eq. 4-7}$$

$\emptyset_{LW,out}(t)$ and $\emptyset_{conv,out}(t)$ are respectively the radiative heat exchange (W/m^2) with the outdoor environment and the convective heat flux with the outside.

the radiative heat exchange with the outdoor environment is given as follow:

$$\emptyset_{LW,out} = h_{r,grd}F_{grd}\left(T_{grd} - T_{surf}\right) + h_{r,sky}F_{sky}\left(T_{sky} - T_{surf}\right) \quad \textbf{Eq. 4-8}$$

The sky temperature T_{sky} is given by Swinbank [50], function of the air temperature as follow, assuming a clear sky:

$$T_{sky} = 0.0552T_{air}^{1.5} \quad \textbf{Eq. 4-9}$$

For a vertical wall, F_{grd} and F_{sky} are equal to 0.5. For the usual sky and surface temperatures, the coefficients $h_{r,sky}$ and $h_{r,grd}$ range from 4.7 W/m^2. K to 5.7 W/m^2. K for buildings located in temperate regions.

The convective exchange with the external environment is generally calculated using a linear correlation function of the wind speed. The correlation in (W/ m^{2}K) used here is the one established by Sturrock [51]:

$$h_{out} = 5.7v + 11.4 \text{ (Windward)} \quad \text{Eq. 4-10}$$
$$h_{out} = 5.7v \text{ (Leeward)}$$

Where v is the wind velocity (m/s)

The heat balance on the internal surface is given by:

$$\rho c_p \frac{\Delta x}{2}\frac{\partial T}{\partial t} = \emptyset_{cond}(t) + \emptyset_{\mathrm{LW,in}}(t) + \emptyset_{conv,in}(t) + \emptyset_{sol}(t) \quad \text{Eq. 4-11}$$

Conduction flux through the wall (W/m^2) is given as:

$$\emptyset_{cond}(t) = \frac{k}{\Delta x}\left(T_{s-\Delta x} - T_{surf}\right) \quad \text{Eq. 4-12}$$

The transmitted solar radiation flux absorbed at the internal wall surface reads:

$$\emptyset_{sol}(t) = \alpha Q_{sol-trans} \quad \text{Eq. 4-13}$$

where $\emptyset_{\mathrm{LW,in}}(t)$ and $\emptyset_{conv,in}(t)$ are the net longwave radiant exchange flux between zone surfaces (W/m^2) and the convective heat flux with the indoor air.

The net longwave radiant exchange flux between zone surfaces is given by

$$\emptyset_{LW,in} = h_{is}(T_{in} - T_{surf}) \quad \text{Eq. 4-14}$$

where h_{is} is the internal longwave radiative exchange coefficient, for standard building temperatures it varies very little around the value 5 W/m^2. K

The internal convection coefficient used to evaluate the convection heat transfer for the TIM-PCM wall with the interior is the one developed by Alamdari for vertical surfaces [38]:

$$h_{in} = \left\{\left[1.5\left(\frac{|\Delta T|}{H}\right)^{1/4}\right]^6 + [1.23(|\Delta T|)^{1/3}]^6\right\}^{1/6} \quad \text{Eq. 4-15}$$

where ΔT is the temperature difference between the internal wall surface and the indoor air, and H is the height of the vertical surface.

A one-dimensional implicit finite volume method established by Patankar 1980 [52] is used to estimate the heat transfer mechanism through the TIM-PCM wall. The computational domain is divided into control volumes, the discretized equation over a typical control volume being written as follow:

$$a_P T_P^{t+\Delta t} = a_W T_W^{t+\Delta t} + a_E T_E^{t+\Delta t} + b \quad \textbf{Eq. 4-16}$$

where,

$$a_W = k_w \frac{\Delta y}{(\Delta x)_w}, a_E = k_e \frac{\Delta y}{(\Delta x)_e}$$

$$a_P = a_W + a_E + a_P^t$$

$$a_P^t = \frac{\rho Cp \Delta x}{\Delta t}$$

$$b = a_P^t T_P^t + \emptyset_{sol} \quad \textbf{Eq. 4-17}$$

The superscript *t* indicates the values at the previous time step, $t + \Delta t$ indicates the values at the current time step. k_w and k_e are the thermal conductivities calculated at the interface.

A system of linear equations is formed from the discretized equations and can be written in a matrix form as:

$$A * T = B \quad \textbf{Eq. 4-18}$$

where A is the matrix of coefficients (tri-diagonal sparse matrix), T is the vector of unknown temperatures and B is the vector of known terms including the values at the previous time step. The current temperature values $T_P^{t+\Delta t}$ are obtained from the previously solved time step temperatures values T_P^t. The system is solved using a direct non-iterative method, the Gaussian elimination algorithm, which produces the solution without explicitly forming the inverse. This function is built in MATLAB.

The model of the heat transfer through the TIM-PCM wall is then linked to TRNSYS via Type 155, whose function is to enable the use of MATLAB program in TRNSYS. This link enables to simulate the thermal performance of the test cell. The MATLAB-TRSNYS model is then validated using experimental results of a full-sized test cell located at Sophia Antipolis within the center for Processes, Renewable Energies and Energy Systems (PERSEE) of Mines Paris Tech graduate school [32]. A good agreement is obtained between the simulated and the experimentally measured internal surface temperature of the TIM-PCM wall and the indoor air temperature for seven consecutive days in summer and winter. Table 4-10 shows the root mean square error $RMSE = \sqrt{\frac{1}{n}\sum_{i=1}^{n}(s_i - e_i)^2}$ and the percentage of root mean square error $PRMSE = \sqrt{\frac{1}{n}\sum_{i=1}^{n}\left(\frac{s_i - e_i}{e_i}\right)^2}$ (where e_i and s_i are the experimental and the simulated values respectively) for the hourly profile of the surface and indoor temperature in summer and winter season. The validated numerical model allows to completely investigate the abilities and the drawbacks of the novel TIM-PCM wall under different conditions. More details on the model validation can be found in [41].

Table 4-10: RMSE and PRMSE for the hourly profile of the surface and indoor temperature in summer and winter season

Season	Physical quantity	RMSE	PRMSE
Winter	Surface temperature	1.43ºC	6.99%
	Indoor air temperature	0.76ºC	4.05%
Summer	Surface temperature	1.13 ºC	3.28 %
	Indoor air temperature	0.57 ºC	1.87 %

3. Energy Performance Analysis

In this section, the results of the annual heating and cooling loads are presented for (1) an office with an opaque wall at the south orientation, (2) conventional office equipped with double glazing with different areas on the south wall, and (3) an office equipped with TIM-PCM wall with different dimensions (shown in Table 4-6) at the south orientation. The energy savings due to the use of the TIM-PCM wall are evaluated compared to the two cases: office with opaque wall and office with of double-glazing on the south wall.

Figure 4-3 and Table 4-11 show the annual heating loads in kWh/m^2(floor area)/year in each climate, for different surface areas of the double-glazed window and the TIM-PCM wall (from 0 m^2 (opaque wall) to 7.532 m^2). The results show that, in all climates, the use of TIM-PCM wall at the south orientation instead of an opaque wall is very effective. In fact, the heating loads decrease with the increase of the area of the TIM-PCM wall (blue curve). This is due to the transmission of solar heat gains to the indoor environment (transmission of 90% when the PCM is liquid), the storage of the heat during the day and releasing it during the night (when the PCM works perfectly assuring diurnal cycling) and the superinsulation silica aerogel that prohibits the heat losses.

The first point on the curve (value at 0 m^2) designates the heating loads of the office with an opaque wall at the south orientation of U value 0.416 W/ m^2K. The integration of TIM-PCM wall of area 7.53 m^2 in the south wall instead of the opaque wall reduces the annual heating loads by 36.52% (from 228.54 kWh/m^2/year to 145.07 kWh/m^2/year) in Barentsburg (ET), by 38.90% (from 182.35 kWh/m^2/year to 111.44 kWh/m^2/year) in Kiruna (Dfc), by 51.69% (from 144.07 kWh/m^2/year to 69.60 kWh/m^2/year) in Dras (Dsb), by 54.12% (from 96.53 kWh/m^2/year to 44.29 kWh/m^2/year) in Toronto (Dfa), by 62.24% (from 61.54 kWh/m^2/year to 23.24 kWh/m^2/year) in Paris (Cfb) and by 90.04% (from 24.49 kWh/m^2/year to 2.44 kWh/m^2/year) in Sacramento (Csa). This means that when the climate gets warmer, the percentage of heating savings increase, and the passive solar wall can provide heating needs to the building.

Concerning the conventional office equipped with double glazing, although the insulation performance of the double glazing (U value 0.86 W/ m^2K) is inferior to that of the opaque external

wall (0.416 W/ m^2K), the heating loads decrease with the increase of the area of the double-glazing (orange curve). This reduction is due mainly to the solar heat gains provided by the transparent double glazing. However, the continuous reduction in heating loads is not always true especially in colder climates (Barentsburg (ET) and Kiruna (Dfc)), where the increase of the double-glazing area is not beneficial exceeding a certain area. The heating loads started to increase again using a double glazing of an area larger than 5.27 m^2. In this case, the impact of the U value reduction of the wall is more influential than the effect of solar heat gains.

The percentage of heating loads reduction due to the increase of glazing area depends mainly on the climate and the amount of the incident solar radiation, and this reduction is found less significant than that when the TIM-PCM wall is used. The integration of double glazing of area 7.53 m^2 in the south wall reduces the annual heating loads by 26.59% (from 144.07 kWh/m^2/year to 105.76 kWh/m^2/year) in Dras (Dsb), by 28.29% (from 96.53 kWh/m^2/year to 69.22 kWh/m^2/year) in Toronto (Dfa), by 32.43% (from 61.54 kWh/m^2/year to 41.58 kWh/m^2/year) in Paris (Cfb) and by 79.95% (from 24.49 kWh/m^2/year to 4.91 kWh/m^2/year) in Sacramento (Csa). Also, when the climate gets warmer, the percentage of heating reduction increase.

Table 4-11: Annual heating loads (kWh/m^2/year) for each city (climate) for an office equipped with double glazing and PCM enhanced office for different double glazing or TIM-PCM wall surfaces

Annual heating loads (kWh/m^2/year)									
	Office with opaque south wall	Office with double glazing (U value=0.86 W/ m^2K) on the south wall				Office with TIM-PCM wall at the south orientation			
Area of double glazing or TIM-PCM wall (m^2)	0	1.51	3.39	5.27	7.53	1.51	3.39	5.27	7.53
Barentsburg (ET)	228.54	225.71	222.94	221.52	221.87	213.41	188.84	167.31	145.07
Kiruna (Dfc)	182.35	177.39	173.77	172.28	172.38	167.16	146.47	129.23	111.44
Dras (Dsb)	144.07	133.92	122.86	113.88	105.76	127.34	105.22	87.18	69.60
Toronto (Dfa)	96.53	88.67	80.72	74.58	69.22	84.18	68.63	56.21	44.29
Paris(Cfb)	61.54	55.04	49.27	45.15	41.58	51.61	40.16	31.29	23.24
Sacramento (Csa)	24.49	16.81	10.83	7.23	4.91	16.03	8.48	4.73	2.44

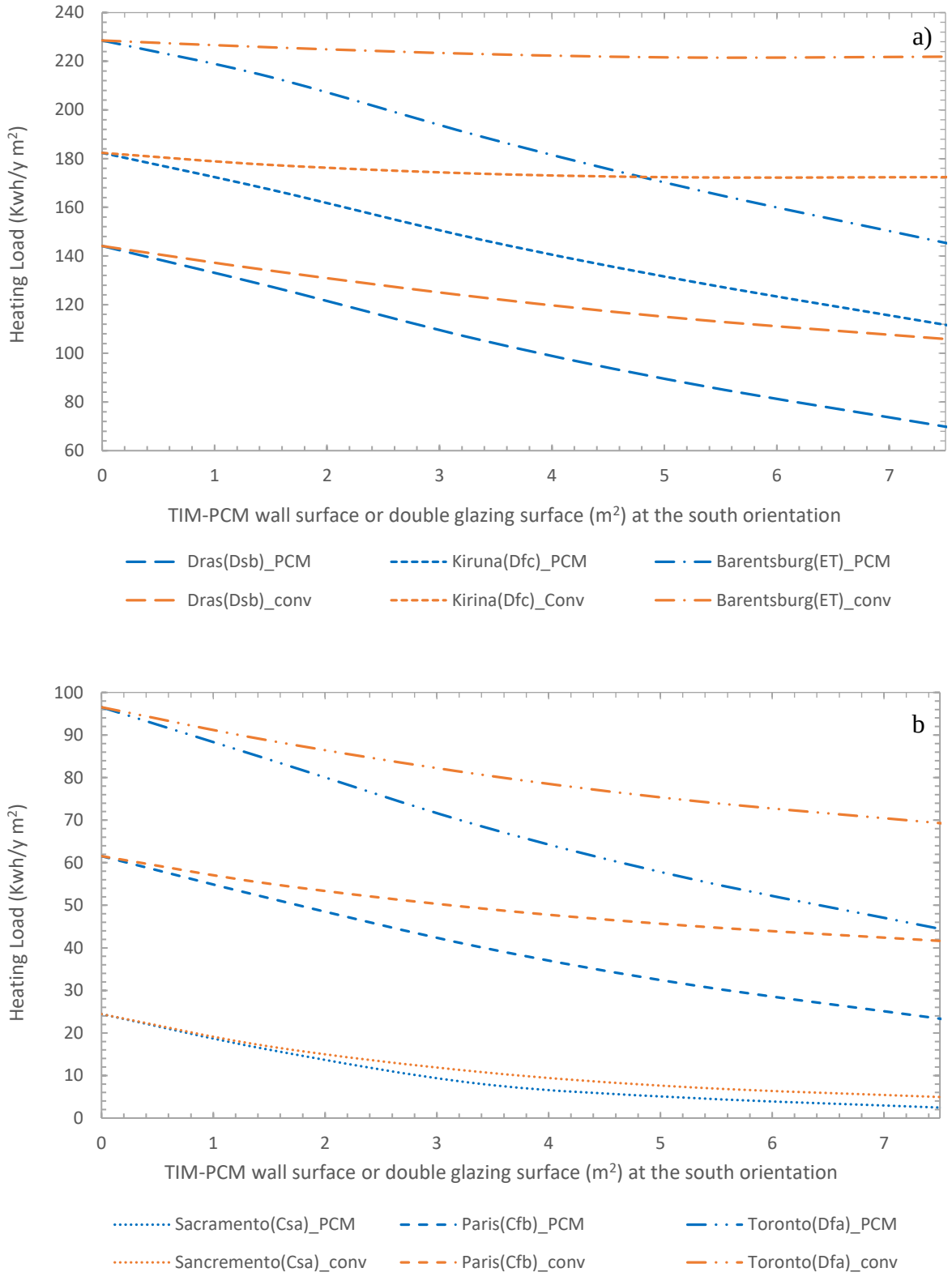

Figure 4-3: Annual heating load for (a) Dsb, Dfc, ET climates and (b) Csa, Cfb, Dfa climates function of the TIM-PCM wall or the double glazing (U value=0.86 W/ m²K) area.

Now, comparing the heating loads of the office with double glazing with those of the office with integrated TIM-PCM wall (comparing the orange curve with the blue curve at each area).

The energy performance of the office, in term of heating loads, can be significantly improved in all climates following the incorporation of the TIM-PCM wall instead of a conventional double glazing, especially for larger areas. This can be clearly shown in Figure 4-3 and Table 4-11, where the heating loads of PCM-enhanced office are always lower than those of the conventional office with double-glazing. For example, the integration of the TIM-PCM wall of 7.53m^2 instead of the double glazing of the same area decreases the heating loads from 221.87 kWh/m^2/year to 145.07 kWh/m^2/year in Barenstburg (ET) and from 105.76 kWh/m^2/year to 69.60 kWh/m^2/year in Dras (Dsb). This is mainly due to the energy storage provided by the PCM and the superinsulation of the silica aerogel that prohibits the heat losses, especially at night.

The annual heating savings in kWh/m^2/year and their associated percentages due to the integration of TIM-PCM wall instead of double glazing of different areas are shown in Table 4-12 and Figure 4-4. These heating savings always increase with the increase of the TIM-PCM wall area. For example, in Toronto, heating savings increase from 5.06% using a TIM-PCM wall of area 1.51 m^2 to 36.01% using a TIM-PCM wall of area 7.53 m^2. In all climates, the maximum heating savings following the integration of the TIM-PCM wall instead of the double glazing are reached when the surface area of the TIM-PCM wall is 7.53 m^2, and are found 34.62% (76.80 kWh/m^2/year) in Barentsburg, 35.35% (60.94 kWh/m^2/year) in Kiruna (Dfc), 34.18% (36.15 kWh/m^2/year) in Dras (Dsb), 36.01% (24.93 kWh/m^2/year) in Toronto (Dfa), 44.11% (18.33 kWh/m^2/year) in Paris (Cfb) and 50.32% (2.47 kWh/m^2/year) in Sacramento (Csa). We note that, although the PCM works better in Dras, the heating savings in Barentsburg are found higher (Table 4-12). This can be explained by the fact the performance of the office with double glazing is better in Dras due to higher solar heat gains, while in Braentsburg the heating loads of the office with double glazing barely decrease with the increase of its area. In addition, the percentage of heating savings is found more significant for warmer climates Csa and Cfb. The heating demand can be almost entirely met by the solar energy alone in Sacramento (Csa) using the TIM-PCM wall.

Table 4-12: Annual heating savings in (kWh/m²/year) by using TIM-PCM wall instead of double-glazed window (U value=0.86 W/ m²K) at south orientation

Area of double glazing or TIM-PCM wall (m²)	1.51		3.39		5.27		7.53	
Heating Savings	Δ_{HL} kWh/m²	%	Δ_{HL} kWh/m²	%	Δ_{HL} kWh/m²	%	Δ_{HL} kWh/m²	%
Barentsburg (ET)	12.30	5.45%	34.09	15.29%	54.21	24.47%	76.80	34.62%
Kiruna (Dfc)	10.22	5.76%	27.29	15.71%	43.04	24.98%	60.94	35.35%
Dras (Dsb)	6.58	4.91%	17.64	14.36%	26.70	23.44%	36.15	34.18%
Toronto (Dfa)	4.48	0.1%	12.08	14.97%	18.37	24.64%	24.93	36.01%
Paris(Cfb)	3.42	6.22%	9.11	18.49%	13.85	30.68%	18.33	44.11%
Sacramento (Csa)	0.78	4.64%	2.35	21.70%	2.49	34.51%	2.47	50.32%

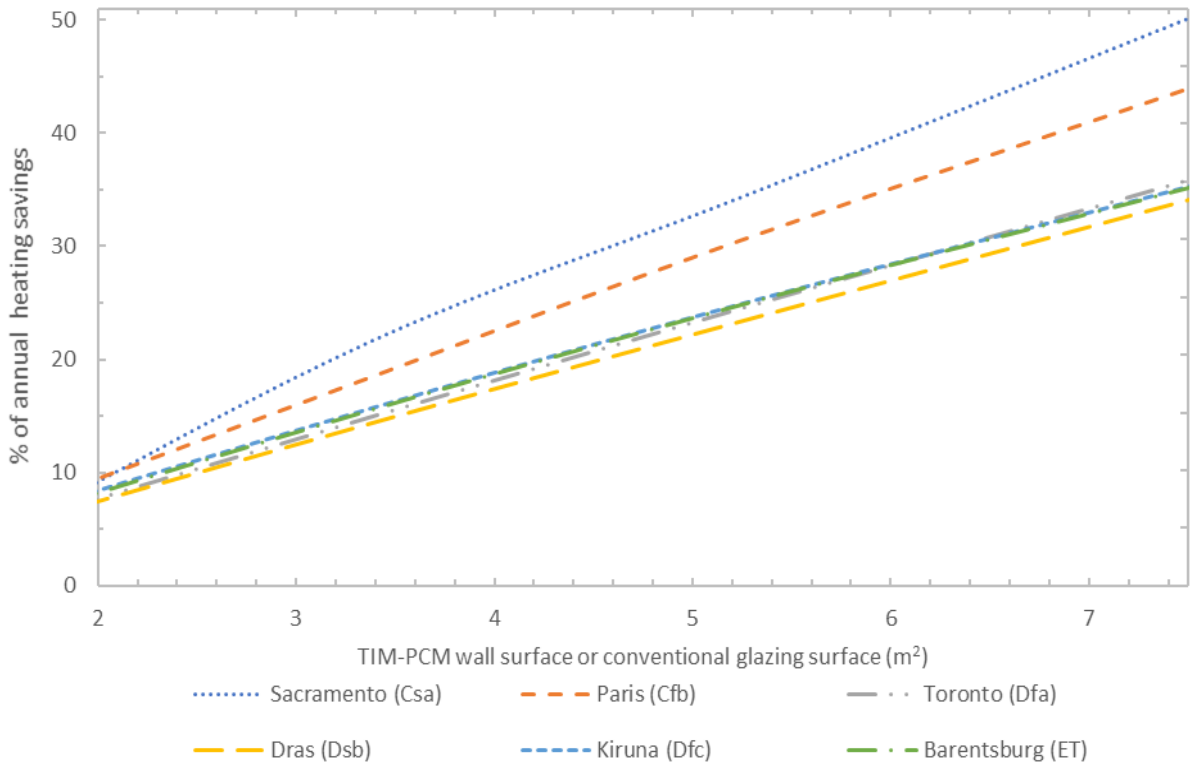

Figure 4-4: Percentage of annual heating savings with respect to conventional office with insulated double-glazed window (U value=0.86 W/ m²K) at south orientation

Figure 4-5 and Table 4-13 show the annual cooling loads in kWh/m²/year for each climate for different surface areas of the TIM-PCM wall or the double-glazed window (from 0 m² to 7.532m²).

Table 4-13: Annual cooling loads (kWh/m²/year) for each city (climate) for conventional office and PCM enhanced office for different surfaces

Cooling loads (Kwh/m²/year)									
	Office with Opaque wall	Office with double glazing U value 0.86				Office with TIM-PCM wall			
Area of window or TIM-PCM wall (m²)	0	1.51	3.39	5.27	7.53	1.51	3.39	5.27	7.53
Barentsburg (ET)	0	0	0	0.034	0.58	0	0	0	0.17
Kiruna (Dfc)	0	0	0	0.44	2.27	0	0	0.21	1.28
Dras (Dsb)	0	0.18	1.21	3.20	6.93	0.22	1.34	3.13	6.53
Toronto (Dfa)	0.82	3.45	7.14	11.86	19.08	3.24	6.51	10.40	15.82
Paris(Cfb)	0	0.54	2.39	5.58	11.44	0.46	2.13	4.65	8.87
Sacramento (Csa)	4.23	8.62	16.72	27.18	43.38	8.53	15.86	24.61	36.84

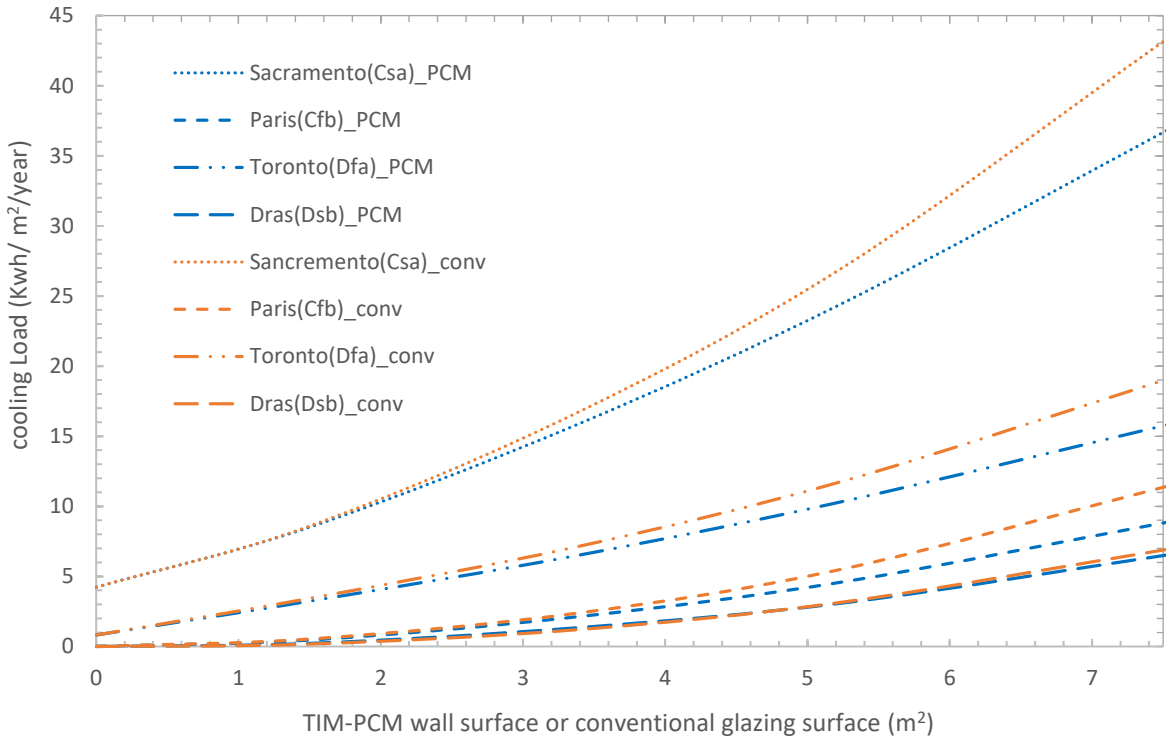

Figure 4-5: Annual cooling load for each city (climate) function of the TIM-PCM wall or the conventional glazing (U value=0.86 W/ m²K) surface

In polar climate and Continental subarctic climate, no cooling loads are found. In all other climates, the cooling loads increase for larger areas, this increase is more significant for the conventional office equipped with double glazing. For both cases, the increase of cooling loads in the hot summer season is due to higher solar heat gains. The maximum cooling savings following the integration of TIM-PCM wall instead of double glazing reach 17.07 % (3.26 kWh/m²/year) in Toronto (Dfa), 22.47 % (2.57 kWh/m²/year) in Paris (Cfb) and 15% (6.53 kWh/m²/year) in Sacramento (Csa) when the surface area of the TIM-PCM wall is 7.53 m². These results show that in a region with mild to hot

summer, the TIM-PCM wall is a better choice than a conventional double-glazed window to maintain a cool indoor temperature. In Dras (Dsb) the cooling savings are not significant as shown in Table 4-14 and no cooling savings are found when the area of the TIM-PCM wall is 1.51 m^2 and 3.39 m^2. However, the use of shading devices in summer can decrease the cooling loads. The use of Venetian blinds with rotatable slats of 45 degrees, allowing daylighting, reduce the cooling loads by 32% in Sacramento (Csa). The use Overhang of 1 m projection combined with the Venetian blinds can reduce this cooling loads by 38%. In Toronto (Dfa) the use of same blinds decreases the cooling loads by about 64%. This can be explained by the fact that the cooling loads in Sacramento (Csa) are not due only to the transmitted solar radiation but also to the high outdoor ambient temperature, reaching 40 ˚C, while in Toronto (Dfa) cooling loads are mainly due to the high solar radiation transmitted to the interior with a maximum outdoor temperature of 31˚C. The use of Venetian blinds in Paris (Cfb) and Dras (Dsb) reduces the cooling loads by about 71% and 78% respectively.

Table 4-14: Annual cooling savings in (KWh/m2/year) by using TIM-PCM wall instead of double-glazed window (U value=0.86 W/ m2K) at south orientation

Area of window or TIM-PCM wall (m^2)	1.51		3.39		5.27		7.53	
Heating Savings	Δ_{CL} Kwh/m^2	%	Δ_{CL} Kwh/m^2	%	Δ_{CL} Kwh/m^2	%	Δ_{CL} Kwh/m^2	%
Barentsburg (ET)	0	0%	0	0%	0.034	-	0.41	-
Kiruna (Dfc)	0	0%	0	0%	0.22	-	0.99	-%
Dras (Dsb)	-0.05	-28.3%	-0.14	-11.5%	0.07	2.14%	0.40	5.77%
Toronto (Dfa)	0.20	5.91%	0.63	8.79%	1.46	12.31%	3.26	17.07%
Paris(Cfb)	0.07	13.91%	0.26	10.83%	0.94	16.77%	2.57	22.47%
Sacramento (Csa)	0.08	0.94%	0.85	5.09%	2.57	9.45%	6.53	15%

Figure 4-6 shows the annual total energy loads for three different climates (Csa, Cfb, Dfa). Concerning other climates, the total energy loads are very close to the heating loads due to the respectively insignificant cooling loads.

In all considered climates, the total energy loads of the conventional office with double glazing and the PCM-enhanced office decrease with the increase of the area except in Sacramento (Csa) (because of high cooling loads). But still, the TIM-PCM wall performs better than the double glazing. The use TIM-PCM wall is more efficient than the use of a conventional insulated double-glazed window in terms of total energy loads in all considered climates, especially for larger areas where maximum total energy savings are reached. The total energy savings in kWh/m^2/year due to the integration of TIM-PCM wall instead of double glazing on the south orientation are shown in Figure 4-7-a.

On the other hand, comparing the results of total energy savings of the office with opaque wall at the south orientation with those of the office with integrated TIM-PCM wall shows that increasing the TIM-PCM wall area increases the total energy savings in all studied climates except in Mediterranean climate (Csa) where the maximum energy savings are reached at an area of 2.61 m^2 (Figure 4-7-b). The total energy savings following the integration of TIM-PCM wall instead of an opaque wall in kWh/m^2/year are shown in Figure 4-7-b.

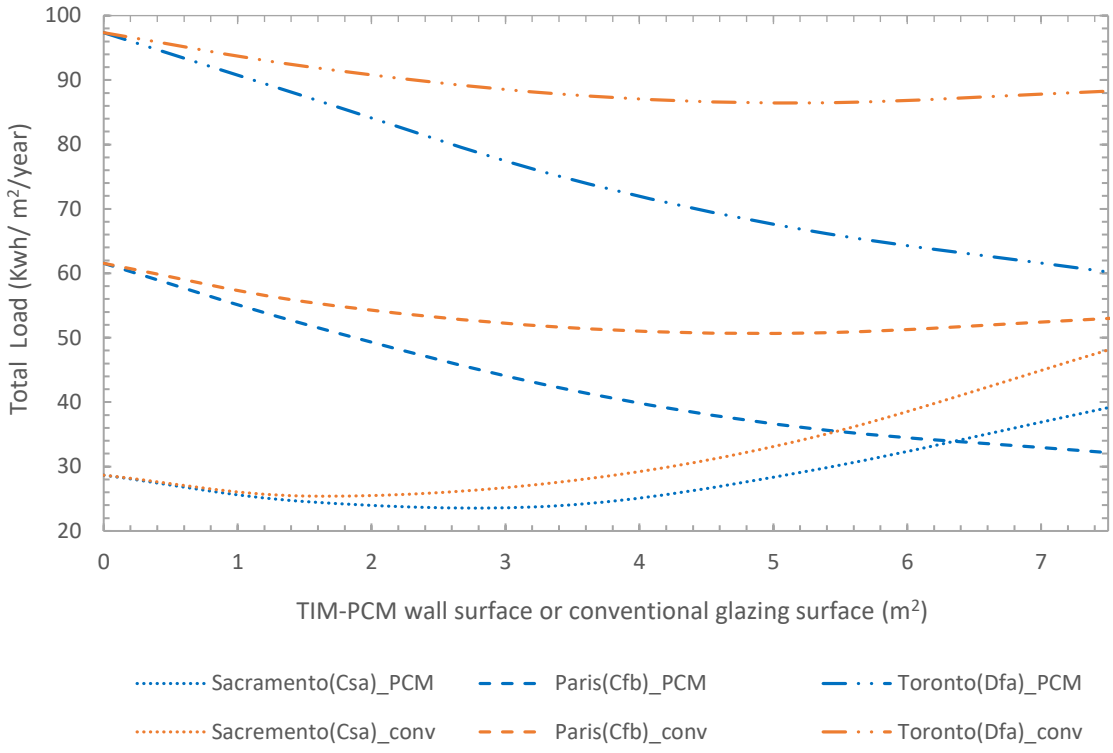

Figure 4-6: Annual total load for three different climates function of the TIM-PCM wall or the conventional glazing (U value=0.86 W/ m^2K) surface

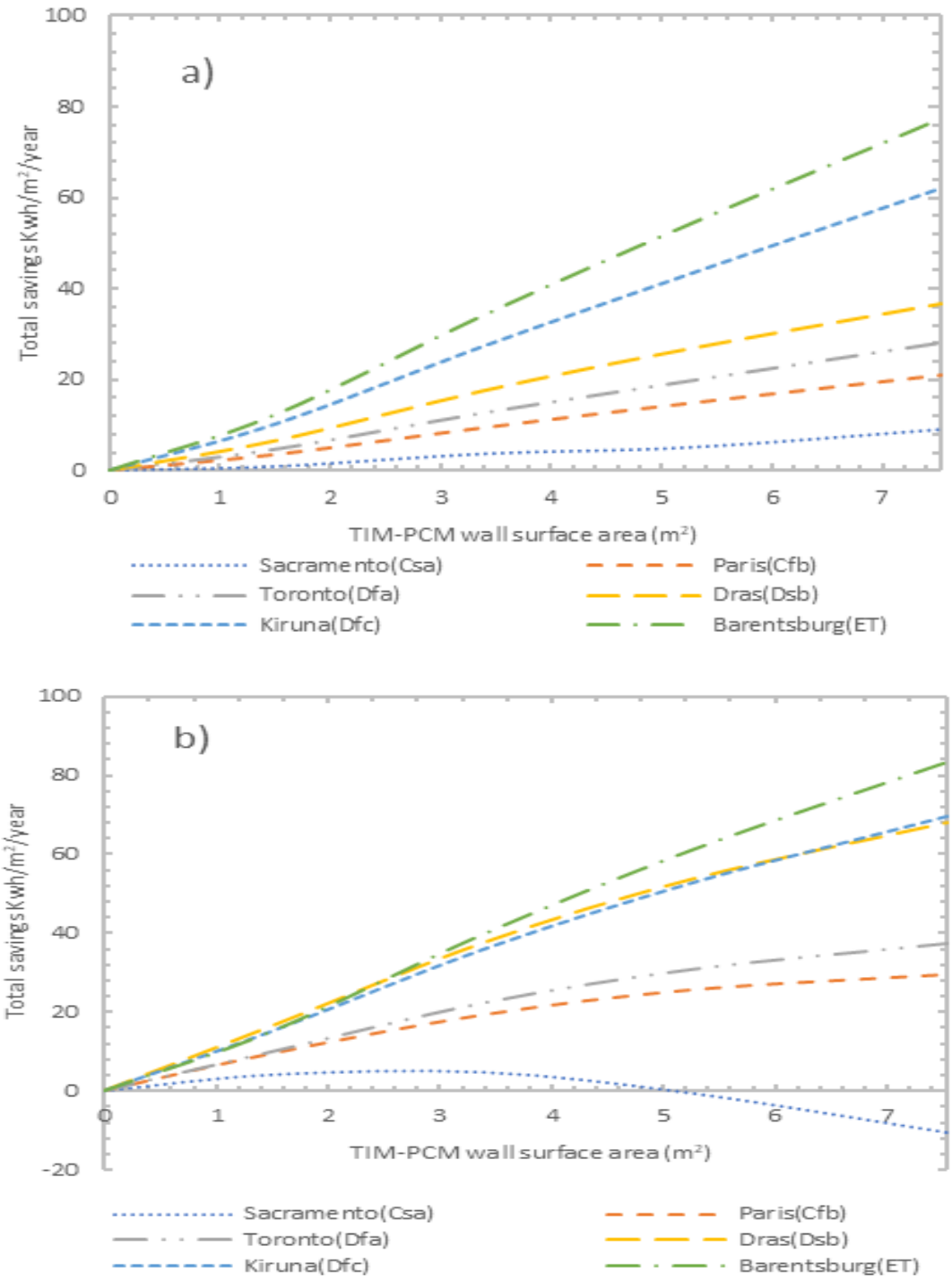

Figure 4-7: Annual total savings for each city (climate) as function of TIM-PCM wall surface with respect to a) conventional office with insulated double-glazed window and b) office with opaque wall at the south orientation

4. Economic Analysis

In addition to the investigation of the thermal and energy performance of the innovative TIM-PCM wall, an economic assessment is carried out for the applicability of this wall in buildings. In previous studies, economic analyses related to the application of PCM in buildings were conducted based on a life-cycle cost analysis [23] [24] or based on a payback period evaluation [28] [30]. The economic study in this work is based on the same concept of previous studies [23][24][53], and both life cycle cost analysis and payback period evaluation are conducted. Noting that the environmental impact of PCM incorporated in building envelopes can be assessed by employing a Life Cycle Assessment (LCA) approach. Many studies [54] have found that the PCM is more environmental friendly compared to other conventional thermal insulating material.

The life-cycle cost analysis involves the analysis of the costs of a system or a component over its entire lifetime. The optimum TIM-PCM wall area (otherwise PCM volume) corresponds to the value that provides a minimum total life-cycle cost. It depends mainly on the yearly heating and cooling loads, the costs of natural gas and electricity, the building lifetime, and the discount rate. The life cycle cost or LCC is defined by:

$$LCC = IC + \text{PWF}.EC \qquad \textbf{Eq. 4-19}$$

where IC is the initial cost for implementing the considered wall (materials prices + installation + labor cost), EC is the annual energy cost required to maintain indoor comfort within the office building for the selected design and operating features and PWF is the present worth factor. The heating and cooling costs over the lifetime of the building are evaluated as:

$$EC_h = \frac{Q_h}{\eta} * c_{ng} \qquad \textbf{Eq. 4-20}$$

$$EC_c = \frac{Q_c}{COP} * c_e \qquad \textbf{Eq. 4-21}$$

Where, EC_h and EC_c are the heating and cooling costs over the lifetime of the building. Q_h, Q_c, c_{ng}, c_e , η , COP respectively stand for the annual heating load, annual cooling load, natural gas cost, cost of electricity, heating system efficiency and the coefficient of performance of the cooling system.

The present worth factor PWF converts future recurrent expenses to present costs regarding the economic outlook of the country and depends on the discount rate ‘r’ and on the lifetime N. The discount rate is the general interest rate of the country. Therefore, when evaluating the present value of a certain investment via PWF, the discount rate should be considered in the formulation. The PWF is given by [55]:

$$PWF = \frac{1-(1+r)^{-N}}{r} \quad \textbf{Eq. 4-22}$$

In addition, the simple payback period PP for the TIM-PCM wall integrated into the building envelope is calculated by dividing the total initial cost by the energy savings cost [53]:

$$PP = IC/ESC \quad \textbf{Eq. 4-23}$$

where PP, IC, and ESC are respectively the payback period, the initial cost and the cost of energy savings including annual lighting savings cost in cities where its value is influential.

The initial investment cost was calculated considering only the material and installation costs (including labor cost) related to the building envelope (TIM-PCM wall). The installation cost of the HVAC systems and other design costs were not considered since their value was assumed to be the same for all the cases in the same location. For the same reason, only the energy costs were considered as annual costs. To evaluate the final value, the lifetime of the building is assumed to be 30 years.

In each country different electricity costs, natural gas prices, and different labor costs are considered. In most projects, labor costs represent approximately 25 to 35% of the total project costs [56]. The labor cost is estimated in each country between these two values (lower income countries have lower labor cost). Although the prices change according to the location, the material costs were assumed to be unvaried but later multiplied by the labor cost. The heating system is a natural gas boiler with an efficiency of 90% and the cooling system is an electrical vapor-compression heat pump of COP 2.9. The cost of electricity and the natural gas, the discount rate and the PWF are found for each country as summarized in Table 4-15.

Table 4-15: Cost of electricity, natural gas price and discount rate for each country

City	Electricity price **$ per kWh** [57], [58]	Natural Gas price **$ per kWh** [59]–[61]	Discount rate % [62], [63]	PWF
Barents burg (Norway)	0.1786	0.078	0.5	27.79
Kiruna (Sweden)	0.22	0.121	-0.5	32.45
Dras (India)	0.08	0.02	6	13.76
Toronto (Canada)	0.16	0.0113	1	25.81
Paris (France)	0.2	0.064	0.05	29.76
Sacramento (USA)	0.21	0.011	1.25	24.88

Table 4-16: Prices of materials

Materials	Prices
Concrete	100 \$ / m^3 [64]
Plasterboard	15\$ to 20\$ / m^2 [65]
Glass wool	60-100 \$ / m^3.[66]
Fatty acid PCM product	3.23 \$ /kg [67]
Silica aerogel	550\$/m^3 [53]
Single clear glazing	29.97\$/m^2 [55]
Insulated double glazing	102\$/m^2[55]

The prices of the used materials are summarized in Table 4-16. The price of PCM varies widely, according to their type, melting temperature and purity [25]. Unfortunately, it is impossible to take these factors into account to accurately estimate the price of PCM. Cascone et al. [68] estimated the price of PCM at about 40 €/m^2 for each cm of thickness. An additional 20% was considered for macroencapsulation [25]. The total estimated price of PCM was hence 48 €/ m^2 /cm, plus 4.36 €/m^2 for installation [69]. Baniassadi et al.[23] considered that finding an exact price for the PCM is a challenging task. They considered an average price of 22.53 (US \$/m^2) for the purchase, transport, and installation of BioPCM with an equivalent thickness of 2.01 cm. Saffari et al. [69] considered that the PCM cost is 0.62 €/kg based on previous purchase and the cost of the installation of PCM is approximated as 4.36 €/m^2. The cost of purchasing and installing PCM was estimated at USD 2/m^2 for a 10-mm thick layer of PCM in [27] and [28]. Table 4-17 summarizes the price of some PCM reported in the literature.

Table 4-17: Cost of some phase change materials (data source [25], [26], [68])

Material	Cost (US$/kg)
Paraffin Wax (organic)	1.88-2.00
Eicosane-technical grade (organic)	7.04
Eicosane-pure laboratory grade (organic)	53.9
Rubitherm (RT20)	16.31
Rubitherm (RT 23,25,27)	0.68
Stearic acid (fatty acid)	1.43-1.56
Palmitic acid (fatty acid)	1.61-1.72
Oleic acid (fatty acid)	1.67-1.76
Crude Glycerin (fatty acid)	0.22-0.29
M-27 (commercially available fatty acid)	14.26
M-51 (commercially available fatty acid)	11.13
Calcium chloride (inorganic-salt haydrates)	0.20
Latest^{TM}29T (commercially availabl²e salt hydrates)	4.95
BioPCM	1.30

In this study, following a discussion with 'PCM products Ltd' company [67], the price of the fatty acid product is approximated as 3.23 \$/kg. An additional 60% was considered for the integration of PCM in the glass bricks and for the installation, and 25-35% of the total cost is added for labor cost. The average total PCM cost is thus about 54 \$/m^2/cm in the investigated cities.

The lighting price is accounted for within the total life-cycle cost, when the artificial lighting is needed, and when its value is significant compared to heating and cooling loads prices. The European Lighting Standard EN12464-1 [36], requires an illuminance of 500 lux in working areas. In addition, according to IESNA Lighting Handbook [70] the recommended lighting level in offices is between 300 and 500 lux. Using a LED lamp, the illuminance of 300 - 500 lux corresponds to the power of 3.333 W/m^2 – 5.555 W/m^2 respectively, i.e. 90 - 150 W for the considered office. Accordingly, the

calculated total annual lighting load is 6.9 kWh/m^2/year to 11 kWh/m^2/year. The TIM-PCM wall provides at a certain time useful daylighting without the need for the artificial lighting, thus the annual lighting load decreases with the increase of the TIM-PCM wall area. The illuminance provided by the wall is approximated by the transmitted solar radiation and verified based on experimental measurements. For each climate, the number of occupied hours, where the daylighting is not sufficient (illuminance <500 Lux), is evaluated for each TIM-PCM wall surface area, and the cost of the needed artificial lighting is then calculated.

The life cycle cost and the payback period are evaluated for both cases, TIM-PCM wall and conventional insulated double-glazed window, and the recommendation for each climate from an economic point of view will be discussed. In section 3, the optimum TIM-PCM wall area showing the best energy performance in each climate was determined as 7.53 m^2 except in Sacramento (Csa). It's also necessary to find the optimum TIM-PCM wall area corresponding to minimum life cycle cost or minimum payback period in each climate. Figure 4-8 to Figure 4-12 show the initial cost, the heating and cooling consumption cost, the total cost, the energy savings cost, and the payback period for both cases for the different climates. From these figures, it can be noticed that the heating costs decrease, and cooling costs increase as the area of the TIM-PCM wall or the double-glazed window area increases. The initial cost varies almost linearly with the area. The total cost and payback period decrease to a certain minimum then start to increase in some cases. The optimum area is the one that ensures this minimum of the total cost or minimum payback period. For each climate, the optimum areas are presented in Table 4-18 and Table 4-19.

In colder climates (Figure 4-8 and Figure 4-9), Barentsburg (ET) and Kiruna (Dfc), the use of TIM-PCM wall is more cost-effective than the use of the double-glazed window, the optimum TIM-PCM wall area providing minimum LCC and minimum PP being 7.532 m^2. Due to the high heating loads in these climates and the relatively high natural gas prices and PWF, the total cost depends mainly on the heating costs and there is larger potential to reduce energy consumption costs through enlarging the TIM-PCM wall area. The minimum payback periods found are 10.5 years and 7.8 years in Barentsburg (ET) and Kiruna (Dfc) respectively, showing that the application of TIM-PCM wall is economically viable in these climates. In these cities, the cost of lighting is neglected since it is marginal compared to heating costs.

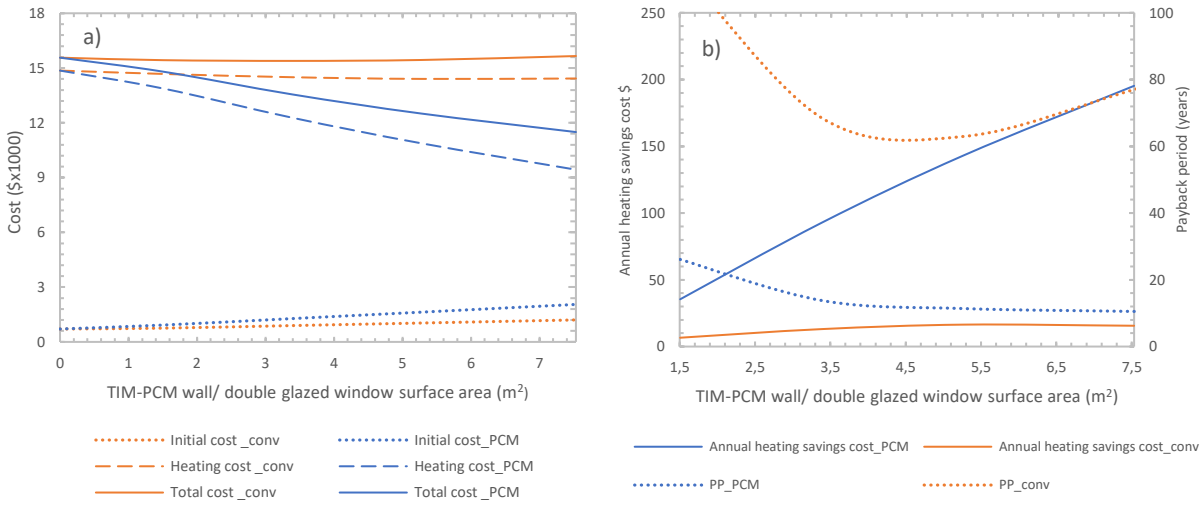

Figure 4-8: a) Life cycle cost and b) payback period for both cases for Barentsburg (ET)

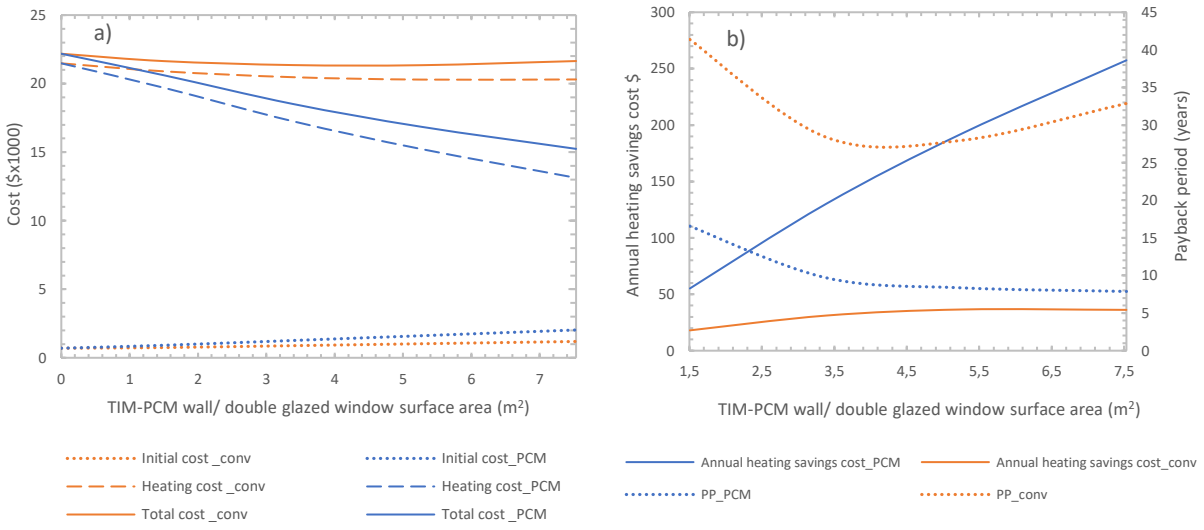

Figure 4-9: a) Life cycle cost and b) payback period for both cases for Kiruna (Dfc)

In Dras (Dsb), in spite of the high heating loads and energy savings due to the use of the TIM-PCM wall, the double-glazed window proves to be more cost-effective than the TIM-PCM wall (Figure 4-10-a). The initial cost controls the total life-cycle cost due to the very low energy prices (2 cents/kWh for natural gas) and relatively low PWF (high discount rate). The optimum TIM-PCM wall area is found 1.51 m^2 with a minimum LCC of 2002$ while the optimum double-glazed window area is 2.45 m^2 with a minimum LCC of 1892$ (Table 4-18). Concerning the minimum payback period, it is found about 35 years for an optimum TIM-PCM wall area of 4.57 m^2 (Table 4-19). The PP is relatively high because the cost of energy savings is insignificant compared to the initial cost, which makes the use of TIM-PCM wall infeasible economically. Higher natural gas prices and lower PCM investment costs are required in Dras (India).

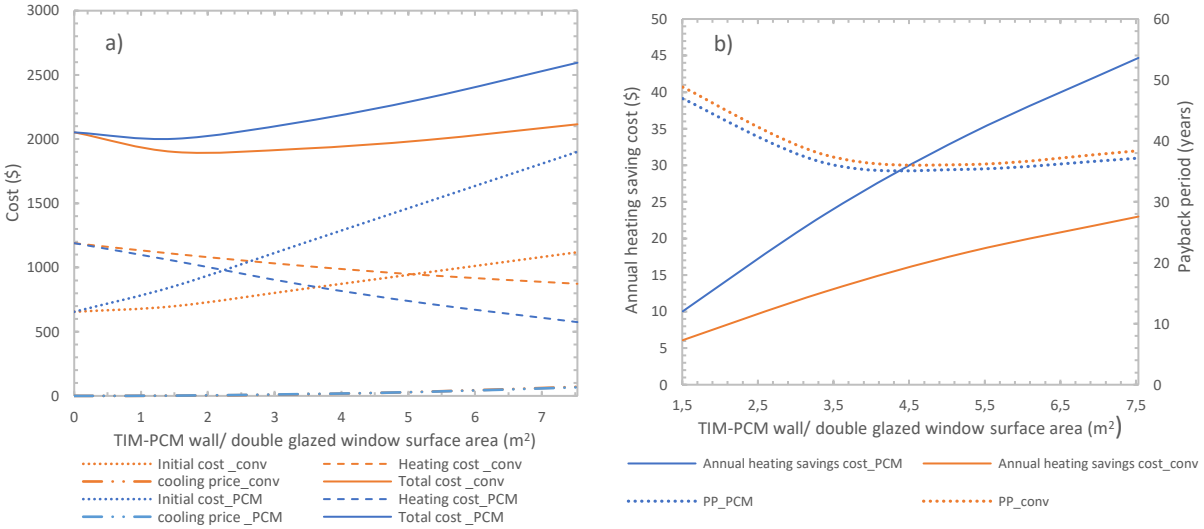

Figure 4-10: a) Life cycle cost and b) payback period for both cases for Dras (Dsb)

In Paris (Cfb), the use of TIM-PCM wall is more cost-effective than the use of the double-glazed window, giving lower LCC and PP (Figure 4-11). The optimum TIM-PCM wall area is found 5 m^2 with minimum LCC of 4145 $ (Table 4-18). Concerning the payback period, the minimum value is found 22 years corresponding to 3.87 m^2 (Table 4-19). To be more economically feasible, the reduction of the initial cost of the TIM-PCM wall is needed in Paris (France).

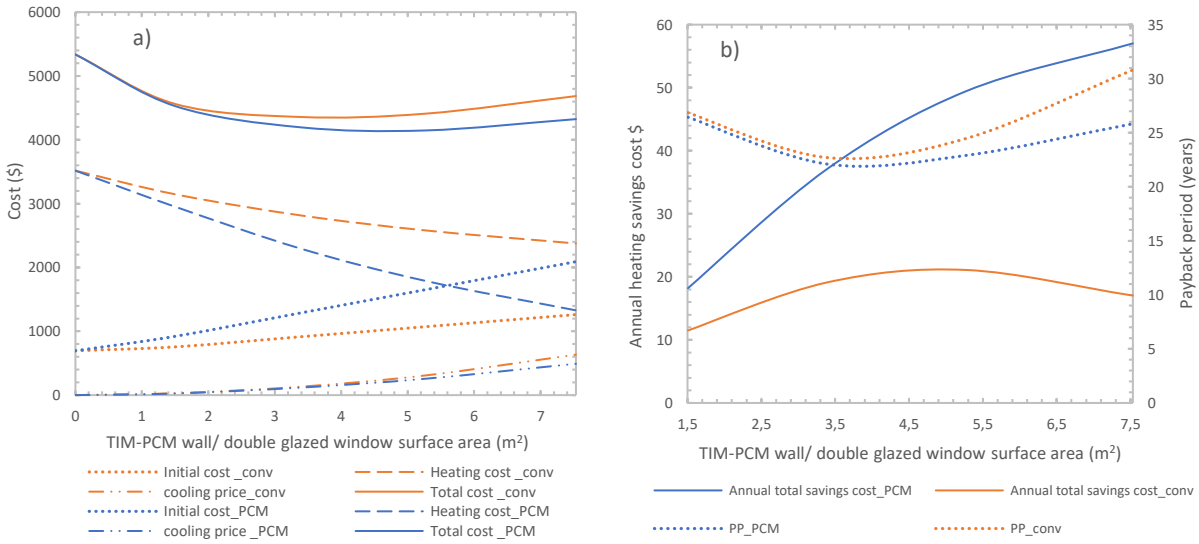

Figure 4-11: a) Life cycle cost and b) payback period for both cases for Paris (Cfb)

In Sacramento (Csa) and Toronto (Dfa) having a hot summer season (Figure 4-12), the use of double-glazed window is more efficient economically than the use of the TIM-PCM wall. In Sacramento (Csa), the optimum TIM-PCM wall area is found 1.4 m^2 with a minimum LCC of 1762$ while the optimum double-glazed window area is found 1.41 m^2 with a minimum LCC of 1610 $ (Table 4-18). In Toronto (Dfa), the heating savings cost is low due to the low natural gas prices in Canada (1.1

cents/ kWh), which makes the total cost depending mainly on the initial cost. The optimum TIM-PCM wall area is found 1.65 m^2 with a minimum LCC of 2143$ while the optimum double-glazed window area is 2.19 m^2 with a minimum LCC of 1999 $ (Table 4-18). Concerning the minimum payback period, the investment cost of the TIM-PCM wall can be recovered in Sacramento after 43 years and in Toronto after 51 years (Table 4-19) which makes the application of such a wall economically unviable.

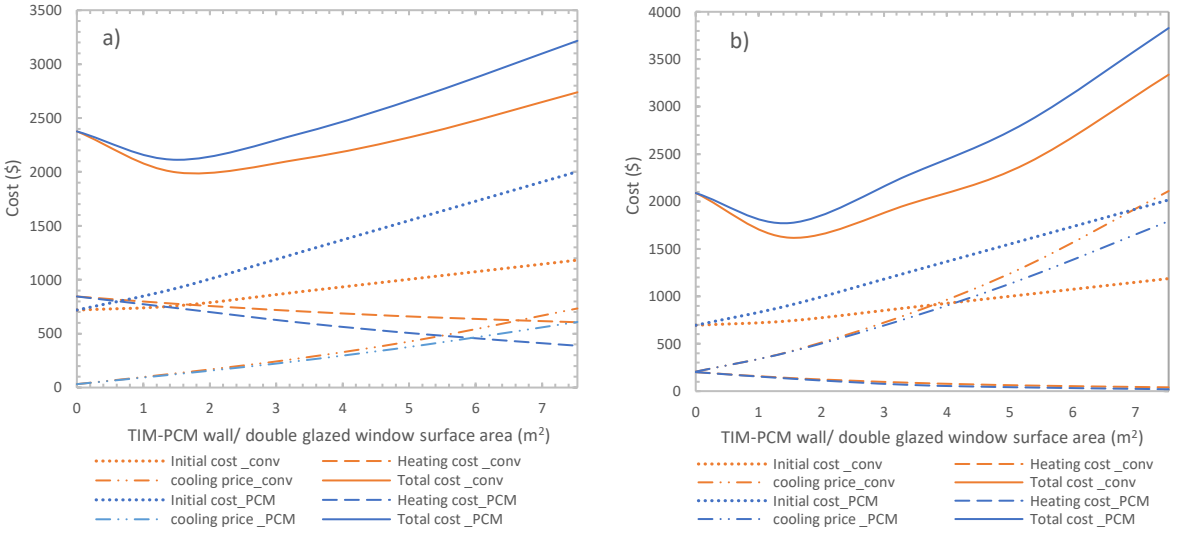

Figure 4-12: Life cycle cost for a) Toronto (Dfa) and b) Sacramento (Csa)

Table 4-18: Minimum life cycle cost and optimum area of the TIM-PCM wall and the double-glazed window in each climate

	Double-glazed window		TIM-PCM wall	
	Minimum LCC ($)	Optimum area (m^2)	Minimum LCC ($)	Optimum area (m^2)
Barentsburg (ET)	15384	3.28	11494	7.532
Kiruna (Dfc)	21317	4.22	15240	7.532
Dras (Dsb)	1892	2.45	2002	1.51
Toronto (Dfa)	1999	2.19	2143	1.65
Paris(Cfb)	4357	3.48	4145	5
Sacramento (Csa)	1610	1.41	1762	1.4

Table 4-19: Minimum payback period and optimum area of the TIM-PCM wall and the double-glazed window in each climate

	Double-glazed window		TIM-PCM wall	
	Minimum PP (years)	Optimum area (m^2)	Minimum PP (years)	Optimum area (m^2)
Barentsburg (ET)	61.72	4.63	10.51	7.532
Kiruna (Dfc)	27.11	4.34	7.87	7.532
Dras (Dsb)	35.95	4.75	35	4.57
Toronto (Dfa)	48.66	1.51	51.1	1.51
Paris(Cfb)	22.69	3.88	22	3.87
Sacramento (Csa)	31.3	1.51	43.26	1.51

Moreover, in Toronto (Dfa) and Sacramento (Csa), the use of external Venetian blinds with an estimated price of 40$/m^2 [71], [72] added to the initial cost, has no effect on the life cycle cost and slightly decreases the minimum payback period. In Sacramento (Csa), the use of double-glazed window still more cost-effective than the use of the TIM-PCM wall and do not offer economic benefits in such a climate.

5. Conclusion

In this work, energy and economic analysis of the application of a TIM-PCM wall on a typical office building envelope was investigated under different climates for a whole year. The results showed that, in all studied climates, the energy performance of the office, in terms of heating and cooling savings, can be significantly improved with the incorporation of the TIM-PCM wall instead of a conventional insulated double-glazed window. In addition, the total loads decrease with the increase of the area of the TIM-PCM wall except in Mediterranean climate. From an economic point of view, the following conclusions can be drawn:

- In ET and Dfc climates, the application of TIM-PCM wall is economically feasible.
- In general, when the climate gets colder, the optimum TIM-PCM wall area increases.
- The heating savings for the office building located in Dras (Dsb) are not sufficient to recover the investment, due to the low energy prices and high discount rates.
- In Paris (Cfb), the use of the TIM-PCM wall is found more cost effective than the use of double-glazed window in terms of minimum life-cycle cost and payback period.
- In Csa and Dfa climates, the TIM-PCM wall is not cost-effective at current energy and investment prices.
- The best candidates for the TIM-PCM wall application are found where energy prices for heating (natural gas in our study) are relatively high, making the initial capital cost relatively insignificant compared to the heating savings cost.
- The economic viability of the application of the TIM-PCM wall depends on different factors, mainly climatic conditions, energy savings, energy costs (natural gas prices, electricity prices, etc.), the economic situation of the country (discount rate) and investment costs.

Finally, further research should focus on the development of industrially scalable low-cost PCM, to decrease investment costs for buildings integrating such walls and as result make them economically viable.

References

[1] B. Hojjati and S. H. Wade, "US household energy consumption and intensity trends: a decomposition approach," *Energy Policy*, vol. 48, pp. 304–314, 2012.

[2] F. Kuznik, D. David, K. Johannes, and J.-J. Roux, "A review on phase change materials integrated in building walls," *Renew. Sustain. Energy Rev.*, vol. 15, no. 1, pp. 379–391, Jan. 2011.

[3] F. Ascione, N. Bianco, R. F. De Masi, F. de' Rossi, and G. P. Vanoli, "Energy refurbishment of existing buildings through the use of phase change materials: Energy savings and indoor comfort in the cooling season," *Appl. Energy*, vol. 113, pp. 990–1007, Jan. 2014.

[4] M. Alam, H. Jamil, J. Sanjayan, and J. Wilson, "Energy saving potential of phase change materials in major Australian cities," *Energy Build.*, vol. 78, pp. 192–201, Aug. 2014.

[5] F. Souayfane, F. Fardoun, and P.-H. Biwole, "Phase change materials (PCM) for cooling applications in buildings: A review," *Energy Build.*, vol. 129, pp. 396–431, Oct. 2016.

[6] R. Baetens, B. P. Jelle, and A. Gustavsen, "Phase change materials for building applications: A state-of-the-art review," *Energy Build.*, vol. 42, no. 9, pp. 1361–1368, Sep. 2010.

[7] F. Kuznik, J. Virgone, and J. Noel, "Optimization of a phase change material wallboard for building use," *Appl. Therm. Eng.*, vol. 28, no. 11–12, pp. 1291–1298, Aug. 2008.

[8] N. Soares, A. R. Gaspar, P. Santos, and J. J. Costa, "Multi-dimensional optimization of the incorporation of PCM-drywalls in lightweight steel-framed residential buildings in different climates," *Energy Build.*, vol. 70, pp. 411–421, Feb. 2014.

[9] M. Saffari, A. de Gracia, C. Fernández, and L. F. Cabeza, "Simulation-based optimization of PCM melting temperature to improve the energy performance in buildings," *Appl. Energy*, vol. 202, pp. 420–434, Sep. 2017.

[10] H. J. Akeiber, S. E. Hosseini, H. M. Hussen, M. A. Wahid, and A. T. Mohammad, "Thermal performance and economic evaluation of a newly developed phase change material for effective building encapsulation," *Energy Convers. Manag.*, vol. 150, pp. 48–61, Oct. 2017.

[11] M. Telkes, "Trombe wall with phase change storage material," in *Proceedings of the 2nd National Passive Solar Conference*, Philadelphia, PA, USA., 1978.

[12] F. Fiorito, "Trombe walls for lightweight buildings in temperate and hot climates. exploring the use of phase-change materials for performances improvement.," *Energy Procedia*, vol. 30, pp. 1110–1119, 2012.

[13] L. Zalewski, A. Joulin, S. Lassue, and Y. Dutil, "Experimental study of small-scale solar wall integrating phase change material," *Sol. Energy*, no. 86, pp. 208–219, 2012.

[14] A. de Gracia, L. Navarro, A. Castell, A. Ruiz-Pardo, S. Alvarez, and L. F. Cabeza, "Experimental study of a ventilated facade with PCM during winter period," *Energy Build.*, pp. 58, 324–332, 2013.

[15] L. Yongcai and L. Shuli, "Experimental study on thermal performance of a solar chimney combined with PCM," *Appl. Energy 114*, pp. 172–178, 2014.

[16] F. Goia, M. Perino, and V. Serra, "Experimental analysis of the energy performance of a full-scale PCM glazing prototype," *Sol. Energy*, vol. 100, pp. 217–233, 2014.

[17] B. L. Gowreesunker, S. B. Stankovic, S. A. Tassou, and P. A. Kyriacou, "Experimental and numerical investigations of the optical and thermal aspects of a PCM-glazed unit," *Energy Build.*, vol. 61, pp. 239–249, Jun. 2013.

[18] S. Li, G. Sun, K. Zou, and X. Zhang, "Experimental research on the dynamic thermal performance of a novel triple-pane building window filled with PCM," *Sustain. Cities Soc.*, vol. 27, pp. 15–22, Nov. 2016.

[19] S. Grynning, F. Goia, and B. Time, "Dynamic Thermal Performance of a PCM Window System: Characterization Using Large Scale Measurements," *Energy Procedia*, vol. 78, pp. 85–90, Nov. 2015.

[20] H. Manz, P. . Egolf, P. Suter, and A. Goetzberger, "TIM–PCM external wall system for solar space heating and daylighting," *Sol. Energy*, vol. 61, no. 6, pp. 369–379, Dec. 1997.

[21] T. Silva, R. Vicente, and F. Rodrigues, "Literature review on the use of phase change materials in glazing and shading solutions," *Renew. Sustain. Energy Rev.*, vol. 53, pp. 515–535, Jan. 2016.

[22] E. Kyriaki, C. Konstantinidou, E. Giama, and A. M. Papadopoulos, "Life cycle analysis (LCA) and life cycle cost analysis (LCCA) of phase change materials (PCM) for thermal applications: A review," *Int. J. Energy Res.*, Nov. 2017.

[23] A. Baniassadi, B. Sajadi, M. Amidpour, and N. Noori, "Economic optimization of PCM and insulation layer thickness in residential buildings," *Sustain. Energy Technol. Assess.*, vol. 14, pp. 92–99, Apr. 2016.

[24] G. P. Panayiotou, S. A. Kalogirou, and S. A. Tassou, "Evaluation of the application of Phase Change Materials (PCM) on the envelope of a typical dwelling in the Mediterranean region," *Renew. Energy*, vol. 97, pp. 24–32, Nov. 2016.
[25] J. Kosny, N. Shukla, and A. Fallahi, "Cost analysis of simple phase change material-enhanced building envelopes in southern U.S. climates," Fraunhofer CSE: U. S. Department of Energy, Tech. rep., 2013.
[26] Ashley Bland, Martin Khzouz, Thomas Statheros, and Evangelos Gkanas, "PCMs for Residential Building Applications: A Short Review Focused on Disadvantages and Proposals for Future Development," *Buildings*, vol. 7, no. 3, p. 78, Aug. 2017.
[27] A. L. S. Chan, "Energy and environmental performance of building façades integrated with phase change material in subtropical Hong Kong," *Energy Build.*, vol. 43, no. 10, pp. 2947–2955, Oct. 2011.
[28] X. Mi, R. Liu, H. Cui, S. A. Memon, F. Xing, and Y. Lo, "Energy and economic analysis of building integrated with PCM in different cities of China," *Appl. Energy*, vol. 175, pp. 324–336, Aug. 2016.
[29] M. A. Wahid, S. E. Hosseini, H. M. Hussen, H. J. Akeiber, S. N. Saud, and A. T. Mohammad, "An overview of phase change materials for construction architecture thermal management in hot and dry climate region," *Appl. Therm. Eng.*, vol. 112, pp. 1240–1259, Feb. 2017.
[30] X. Sun, Q. Zhang, M. A. Medina, and K. O. Lee, "Energy and economic analysis of a building enclosure outfitted with a phase change material board (PCMB)," *Energy Convers. Manag.*, vol. 83, pp. 73–78, Jul. 2014.
[31] N. Chaiyat, "Energy and economic analysis of a building air-conditioner with a phase change material (PCM)," *Energy Convers. Manag.*, vol. 94, pp. 150–158, Apr. 2015.
[32] Y. Berthou, P. H. Biwole, P. Achard, H. Sallée, M. Tantot-Neirac, and F. Jay, "Full scale experimentation on a new translucent passive solar wall combining silica aerogels and phase change materials," *Sol. Energy*, vol. 115, pp. 733–742, May 2015.
[33] F. Souayfane, P. H. Biwole, and F. Fardoun, "Melting of a phase change material in presence of natural convection and radiation: A simplified model," *Appl. Therm. Eng.*, vol. 130, pp. 660–671, Feb. 2018.
[34] *Patry, Pierre-Manuel, and Dimitri Molle. RT 2012 et RT existant: Réglementation thermique et efficacité énergétique. Editions Eyrolles, 2015. .*
[35] *Handbook, ASHRAE Fundamentals. "American society of heating, refrigerating and air-conditioning engineers." Inc.: Atlanta, GA, USA (2009). .*
[36] "European Lighting Standard EN12464-1." [Online]. Available: https://www.fagerhult.com/knowledge-hub/EN-12464-1/. [Accessed: 13-Feb-2018].
[37] M. Kottek, J. Grieser, C. Beck, B. Rudolf, and F. Rubel, "World Map of the Köppen-Geiger climate classification updated," *Meteorol. Z.*, vol. 15, no. 3, pp. 259–263, Jun. 2006.
[38] F. Goia, M. Perino, and M. Haase, "A numerical model to evaluate the thermal behaviour of PCM glazing system configurations," *Energy Build.*, vol. 54, pp. 141–153, Nov. 2012.
[39] H. Elarga, F. Goia, A. Zarrella, A. Dal Monte, and E. Benini, "Thermal and electrical performance of an integrated PV-PCM system in double skin façades: A numerical study," *Sol. Energy*, vol. 136, pp. 112–124, 2016.
[40] G. Fraisse, "Development of a simplified and accurate building model based on electrical analogy," *Energy & Buildings*, vol. 34, pp. 1017–1031, 2002.
[41] F. Souayfane, P. H. Biwole, and F. Fardoun, "Thermal behavior of a translucent superinsulated latent heat energy storage wall in summertime," *Appl. Energy*, vol. 217, pp. 390–408, May 2018.
[42] V. Voller, "Fast implicit finite-difference method for the analysis of phase change problems," *Numer Heat Transfer Part B*, pp. 17:155–69, 1990.
[43] R. Siegel, "Net radiation method for enclosure systems involving partially transparent walls," 1973.
[44] B. Zivkovic and I. Fujii, "An analysis of isothermal phase change of phase change material within rectangular and cylindrical containers," *Sol. Energy*, vol. 70, no. 1, pp. 51–61, 2001.
[45] F. Souayfane, P. H. Biwole, and F. Fardoun, "Modèle simplifié pour la prise en compte de la convection naturelle dans la modélisation du changement de phase solide-liquide," presented at the Colloque Inter-universitaire Franco-Québecois, Saint-lo, France, 2017.
[46] G. Vidalain, L. Gosselin, and M. Lacroix, "An enhanced thermal conduction model for the prediction of convection dominated solid–liquid phase change," *Int. J. Heat Mass Transf.*, vol. 52, no. 7–8, pp. 1753–1760, Mar. 2009.
[47] P. Jany and A. Bejan, "Scaling theory of melting with natural convection in an enclosure," *Int. J. Heat Mass Transf.*, vol. 31, no. 6, pp. 1221–1235, Jun. 1988.
[48] A. Bejan, *Convection heat transfer*, Fourth edition. Hoboken, New Jersey: Wiley, 2013.

[49] X. Faure, “Enveloppe hybride pour bâtiment à haute performance énergétique,” Université Joseph-Fourier-Grenoble I, 2007.
[50] W. Swinbank, “Long-wave radiation from clear skies,” *Q. J. R. Meteoro. Soc*, p. 89:339, 1963.
[51] F. Miranville, “Contribution à l’étude des parois complexes en physique du bâtiment: modélisation, expérimentation et validation expérimentale de complexes de toitures incluant des produits minces réfléchissants en climat tropical humide,” Université de la Réunion, 2002.
[52] S. V. Patankar, *Numerical heat transfer and fluid flow*. New York: McGraw-Hill., 1980.
[53] M. Ibrahim, P. H. Biwole, P. Achard, E. Wurtz, and G. Ansart, “Building envelope with a new aerogel-based insulating rendering: Experimental and numerical study, cost analysis, and thickness optimization,” *Appl. Energy*, vol. 159, pp. 490–501, Dec. 2015.
[54] A. Kylili and P. A. Fokaides, “Life Cycle Assessment (LCA) of Phase Change Materials (PCMs) for building applications: A review,” *J. Build. Eng.*, vol. 6, pp. 133–143, Jun. 2016.
[55] M. Krarti and P. Ihm, “Evaluation of net-zero energy residential buildings in the MENA region,” *Sustain. Cities Soc.*, vol. 22, pp. 116–125, Apr. 2016.
[56] “Percentage of cost breakdown between labour, materials and contractor profit in construction.” [Online]. Available: http://www.a4architect.com/2013/04/percentage-of-cost-breakdown-between-labour-materials-and-contractor-profit-in-construction/. [Accessed: 15-Jan-2018].
[57] “Global electricity prices by select countries in 2017 (in U.S. dollars per kilowatt hour).” [Online]. Available: https://www.statista.com/statistics/263492/electricity-prices-in-selected-countries/. [Accessed: 15-Jan-2018].
[58] “Electricity prices for households in Norway from 2010 to 2016, semi-annually (in euro cents per kilowatt-hour).” [Online]. Available: https://www.statista.com/statistics/643369/electricity-prices-for-households-in-norway/. [Accessed: 15-Jan-2018].
[59] Eurostat, “Electricity and natural gas price statistics.” [Online]. Available: http://ec.europa.eu/eurostat/documents/38154/41386/SEarticle2012S1.pdf/364a98b3-648f-4716-b95a-71484f430a9f. [Accessed: 15-Jan-2018].
[60] “Estimated landed prices of LNG worldwide as of May 2017, by select country (in U.S. dollars per million British thermal units).” [Online]. Available: https://www.statista.com/statistics/252984/landed-prices-of-liquefied-natural-gas-in-selected-regions-worldwide/. [Accessed: 15-Jan-2018].
[61] Eurostat, “Natural gas price statistics.” [Online]. Available: http://ec.europa.eu/eurostat/statistics-explained/index.php/Natural_gas_price_statistics. [Accessed: 15-Jan-2018].
[62] “Worldwide Central Bank Rates.” [Online]. Available: http://www.cbrates.com/. [Accessed: 15-Jan-2018].
[63] “Country comparison: Central Bank Discount Rate.” [Online]. Available: https://www.cia.gov/library/publications/the-world-factbook/rankorder/2207rank.html. [Accessed: 15-Jan-2018].
[64] “Concrete price considerations- cost of concrete.” [Online]. Available: https://www.concretenetwork.com/concrete-prices.html. [Accessed: 15-Jan-2018].
[65] “plasterboard installation.” [Online]. Available: https://www.ato.gov.au/Business/Small-business-benchmarks/In-detail/Benchmarks-A-Z/L-Q/Plastering-and-ceiling-services/?page=4. [Accessed: 15-Jan-2018].
[66] “glass wool price list.” [Online]. Available: https://www.alibaba.com/showroom/glass-wool-price-list.html. [Accessed: 15-Jan-2018].
[67] “PCM Products.” [Online]. Available: http://www.pcmproducts.net/Phase_Change_Material_Products.htm. [Accessed: 15-Jan-2018].
[68] Y. Cascone, A. Capozzoli, and M. Perino, “Optimisation analysis of PCM-enhanced opaque building envelope components for the energy retrofitting of office buildings in Mediterranean climates,” *Appl. Energy*, vol. 211, pp. 929–953, Feb. 2018.
[69] M. Saffari, A. de Gracia, S. Ushak, and L. F. Cabeza, “Economic impact of integrating PCM as passive system in buildings using Fanger comfort model,” *Energy Build.*, vol. 112, pp. 159–172, Jan. 2016.
[70] “Recommended Lighting Levels in Buildings- IESNA Lighting Handbook.” [Online]. Available: https://www.archtoolbox.com/materials-systems/electrical/recommended-lighting-levels-in-buildings.html. [Accessed: 13-Feb-2018].
[71] “Wholesale Pricing on Blinds and Shades.” [Online]. Available: http://www.blindsmax.com/blog/how-much-do-new-blinds-cost/. [Accessed: 13-Feb-2018].

[72]“wide venetian blinds prices.” [Online]. Available: http://wideblinds.co.uk/price_guide.html. [Accessed: 13-Feb-2018].

Complementary sections to chapter 4

A) Transient liquid fraction in each climate

The transient liquid fraction of the PCM during the simulated year can be found at each time step by the numerical model. The liquid fraction provides information about the state of the PCM: if fl = 0 the PCM is solid, if fl =1 the PCM is liquid, and if 0 < fl < 1 the PCM is changing phase. Also, the hourly profile of the liquid fraction can show if the PCM assure diurnal cycling in winter and summer seasons. The average liquid fraction in the PCM filled in glass bricks for a TIM-PCM wall of 7.532 m^2 function of the time is shown in the following figures. Noting that the year is 8760 hours, January starts from 0 to 744 hours, February from 744 to 1416 hours …. December from 8016 to 8760. June, July and August are from 3624 to 5832 hours.

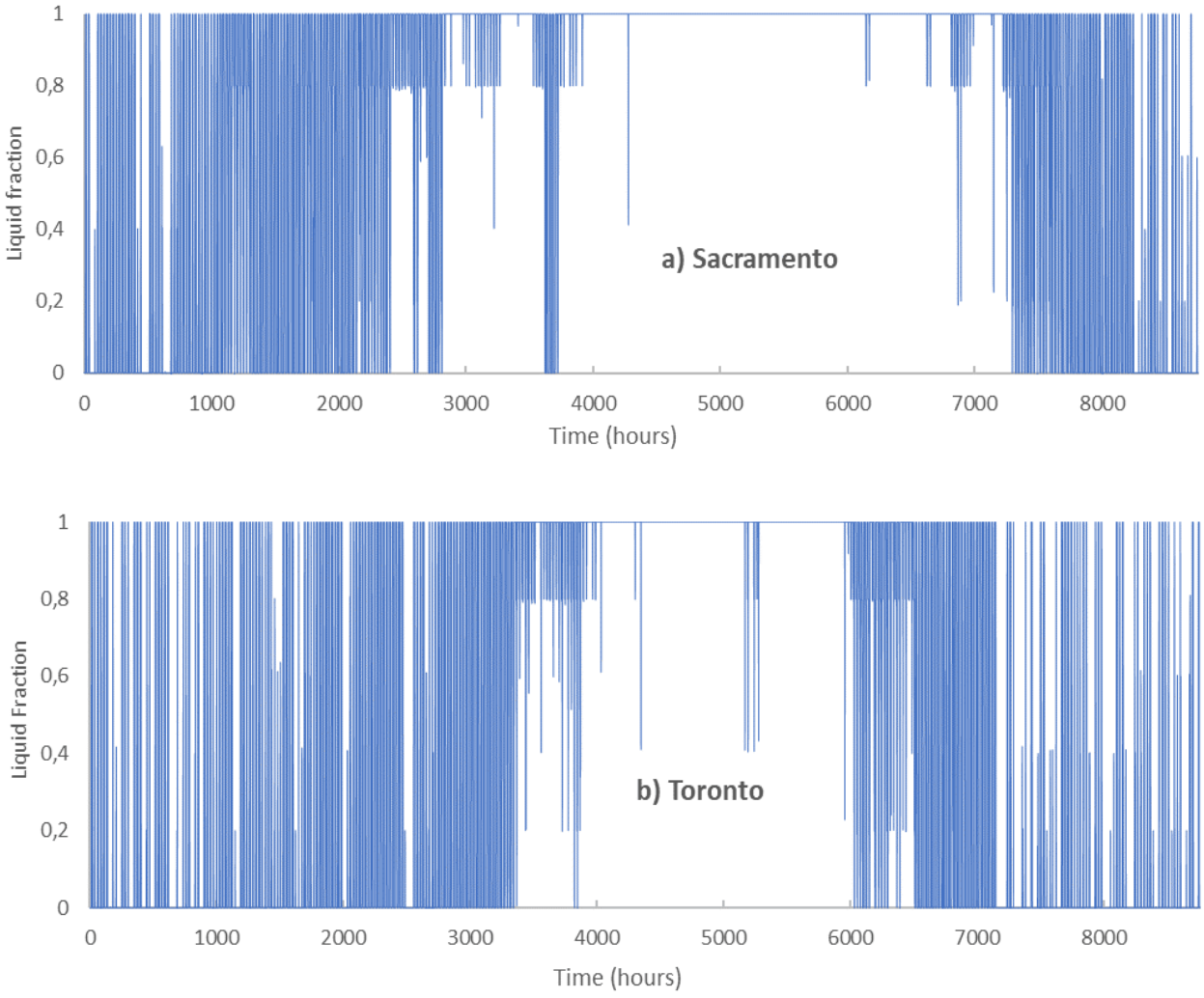

Figure 1: PCM liquid fraction function of time in a) Sacramento (Csa) and b) Toronto (Dfa)

Figure 1 shows that the PCM remains liquid almost all the summer in Sacramento (fl=1). This is due to the hot summer conditions and high solar gains during the day in addition to high external temperature during the night which prohibits PCM solidification. In winter, the PCM assure some

complete or partial diurnal cycles. In Toronto, the PCM seems to work better, where the PCM melts and solidifies for longer periods except in the period between 4000 hours and 6000 hours, here the PCM remains liquid with some partial solidifications.

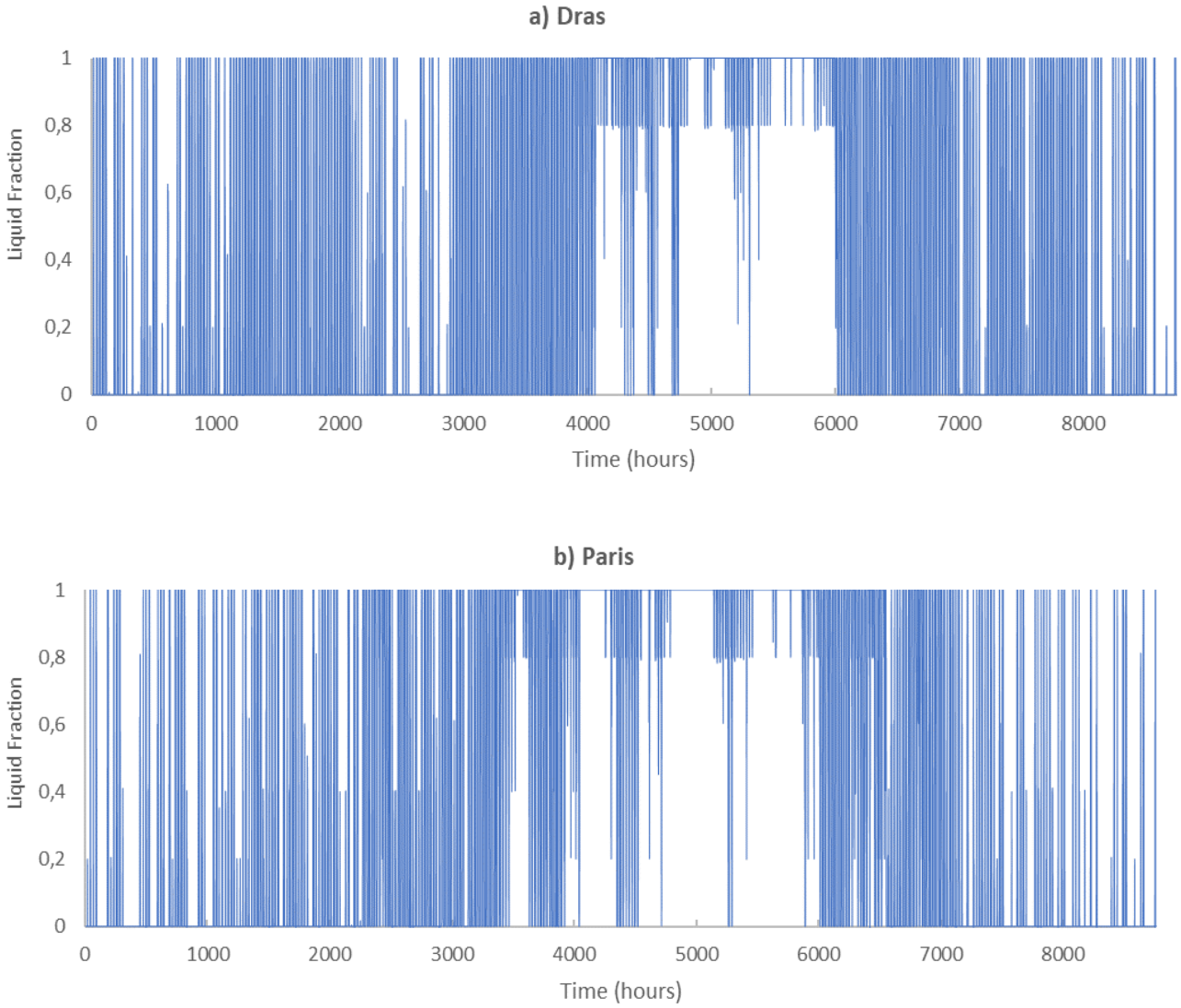

Figure 2: PCM liquid fraction function of time in a) Dras (Dsb) and b) Paris (Cfb)

The PCM assure partial and complete melting and solidification processes in Dras and Paris all the year (Figure 2). In winter season, the PCM can totally melt in Dras (liquid fraction reaches 1) more than Paris due to the higher solar radiation. In summer, the PCM is unable to completely solidify in hot periods.

Figure 3 shows that the PCM remains in solid state in Barentsburg for almost five months without melting (January, February, part of March, part of October, November, December). This is due to very low external temperatures and low incident solar radiation. In warm season, the PCM achieves complete diurnal cycling. In Kiruna the PCM can also achieves diurnal cycling except in the very cold months where it remains in its solid state (between 0 and 750 hours and 7710 and 8760 hours).

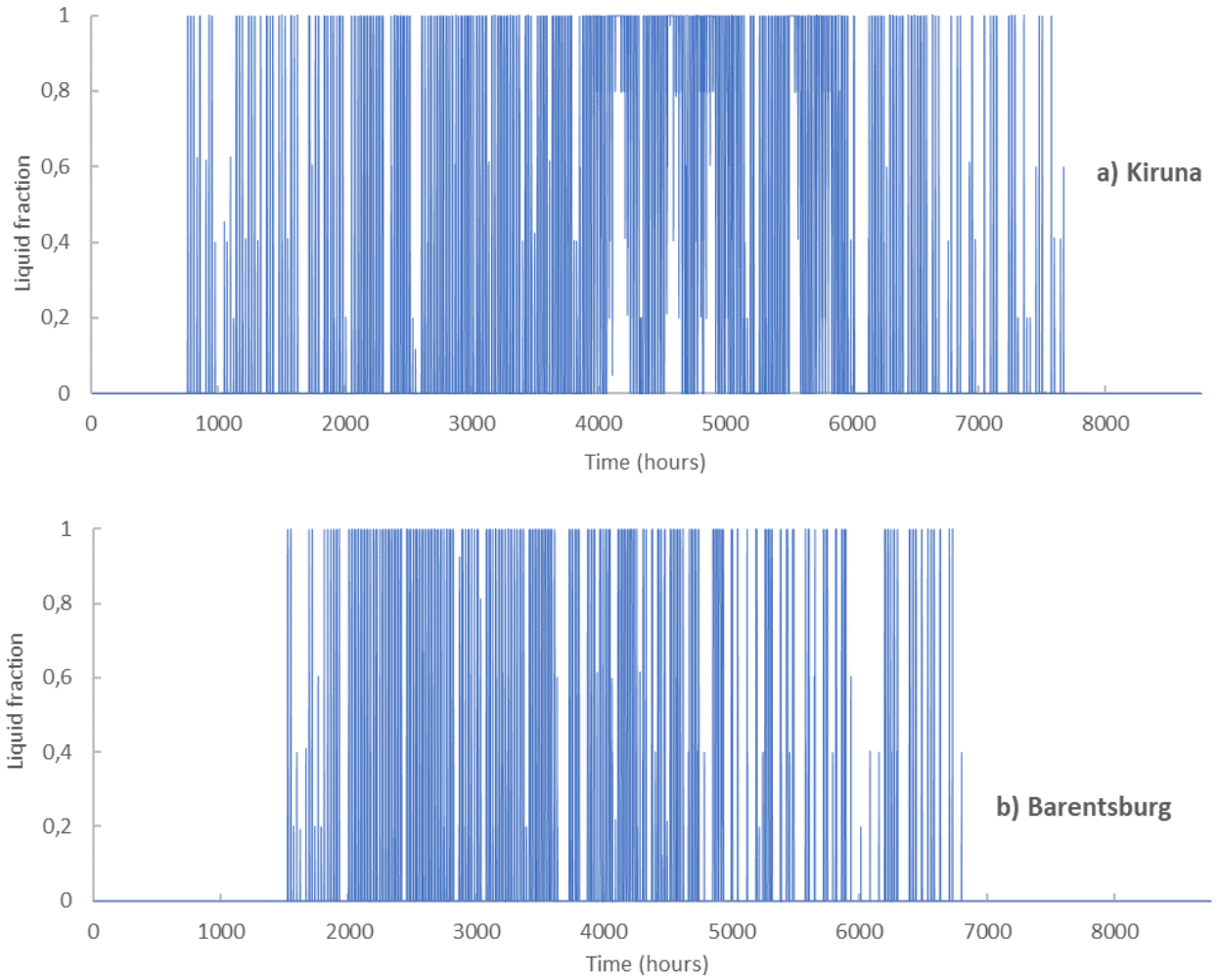

Figure 3: PCM liquid fraction function of time in a) Kiruna (Dfc) and b) Barentsburg (ET)

Figure 4 shows the percentage of time where the PCM is in solid state, liquid state or changing phase in each climate for different TIM-PCM wall areas. These graphs were found based on the hourly transient liquid fraction values calculated in the numerical model. When fl = 0, the PCM is solid, the number of hours where fl is equal to zero are counted and the percentage of time in the year is found, same for fl =1 (liquid PCM) and 0 < fl < 1 (PCM changing phase). For example, in Baretsburng, using a TIM-PCM wall of an area 7.532 m^2 (200 bricks filled with Fatty acids) the PCM remains solid 85% of the time. While in Dras the PCM is solid 52% of the time, liquid 37% of the time and changing phase the rest of the time. This means that in Dras the PCM works better and can assure cycling. In Sacramento, the PCM remains liquid about 65% of the time, due to the hot summer season where the PCM is unable to solidify.

It can be concluded that in the regions having a hot summer (Toronto and Sacramento) the PCM remains liquid in summer for long periods and can barely solidify, while in winter it can achieve diurnal complete or partial cycling. In climates having a warm summer season (Dras and Paris), the PCM works better in summer. In regions having a cold (continental or polar) winter, the PCM remains

solid for months without melting due to very low external temperature, while in the rest of the year, it can achieve diurnal cycling.

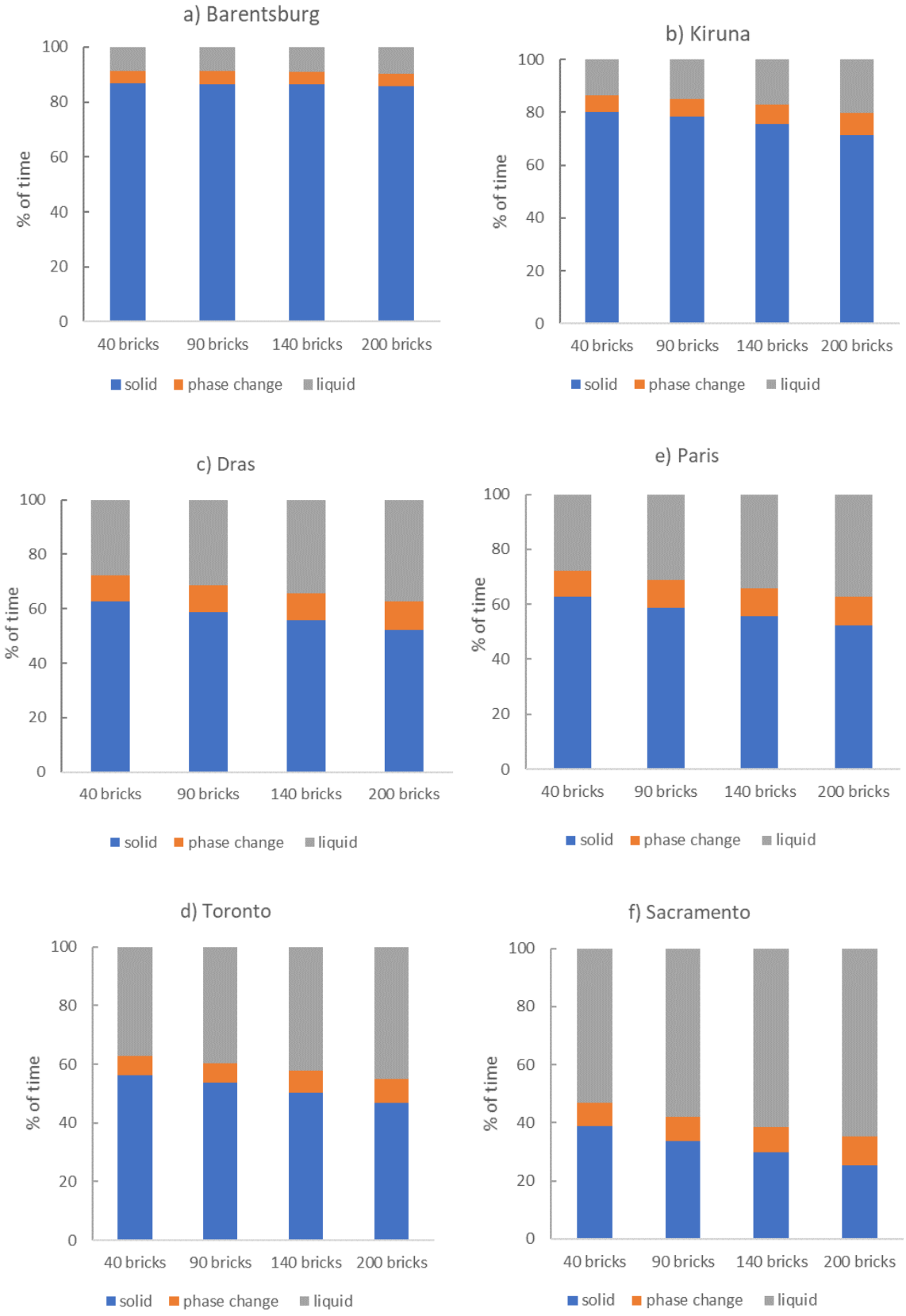

Figure 4: Percentage of time where the PCM is in solid state, liquid state or changing phase in each climate for different TIM-PCM wall dimensions.

B) Note

In this chapter, same construction of the building was assumed regardless of the climate. This was done in order to have a criterion of similarity between all the locations simulated, and to focus on the impact of the TIM-PCM wall on the building compared to a based case.

GENERAL CONCLUSION

General Conclusion

1. Overview of the achievements

During this thesis, we have developed a simplified model for melting with natural convection at first, and with both convection and short-wave radiation afterward. The simplified model for PCM melting with natural convection is based on the enhanced thermal conductivity approach coupled with the scaling theory. A modified enthalpy method is adopted to solve the phase change problem. Two-dimensional implicit finite volume method is used to solve the energy equation and the code is written on MATLAB. The results of the simplified model are validated using a complete CFD model, in addition to experimental and numerical benchmark solutions for a test case: melting of Octadecane in a square cavity. A correlation for the Nusselt number at the left heated wall is proposed based on CFD results, to calculate the enhanced conductivity. The shortwave radiation through the PCM is modeled by means of a simplified solution procedure and the radiative heat flux is added as a source term to the energy equation. A nodal evaluation of the PCM optical properties function of the liquid fraction was made. The absorbed solar radiation was equally divided between the nodes forming the PCM layer. The model was also developed on MATLAB using two-dimensional implicit finite volume method. It was validated against a LBM-DOM model found in the literature for the case of melting of Fatty acid filled in rectangular enclosure. Then, based on the two previous models, we have developed a numerical model describing the heat transfer mechanisms through the TIM-PCM wall. The latter is an innovative translucent passive solar wall proposed by INERTRANS project composed of glazing, silica aerogel for thermal insulation and PCM for absorption and storage of heat. The wall was experimentally tested in a full-scale test cell located in Sophia Antipolis, Southern France, within the PERSEE center of Mines ParisTech graduate school. The wall model was coupled with TRNSYS to evaluate the thermal performance of the entire building. The coupled MATLAB-TRNSYS model has been experimentally validated using the experimental cell located within the PERSEE center for seven consecutive days in summer and winter. Then, we have used the validated numerical model to optimize the thermal performance of the wall in summer season under different climatic conditions, in terms of thermal comfort. Finally, we have studied the annual energy performance of a typical office following the incorporation of the TIM-PCM wall into its south-facing envelope, under six different climates. The optimum TIM-PCM wall area is then evaluated economically for each climate through life-cycle cost (LCC) and payback period (PP) analysis.

The main conclusions issued from this work are:

- The developed simplified model for convection during phase change requires a computational time much shorter than that of the CFD model. The values of the average liquid fraction, the position of the melting front for four different instants, and the average position of the melting front function of time from the simplified model are found in good agreement with those of CFD model and Benchmark solutions.
- The modeling of natural convection during melting of Octadecane in square cavity enhances the position of the melting front by about 55% at dimensionless time SteFo = 0.01 and the average liquid fraction by about 40% compared to a conduction only model.
- Natural convection increases the liquid fraction by about 35% compared to the conduction only model, while the radiation increases the liquid fraction by about 20% compared to the convection model for the case of melting of Fatty acid filled in a rectangular enclosure.
- Concerning the computational time, the simplified model for both natural convection and radiation during melting run significantly faster than the LBM-DOM model.
- The developed simplified model considering both natural convection and radiation during melting process is simple to implement and can manage efficiently convection-controlled phase change problems without the full solution of the flow in a very small computational time. It is developed for practical thermal engineering applications, where yearly energy performance evaluation is sought, that cannot rely on highly computational time needed in CFD simulations.
- The coupled MATLAB-TRNSYS model, experimentally validated, represents a starting point for simulations on different configurations of the novel TIM-PCM wall and allows to fully investigate its abilities and drawbacks under different operative conditions, orientations, geometries and different climates without the need of performing expensive experimental analysis.
- To be more realistic, natural convection in the liquid PCM should not be neglected when modeling phase change in the wall.
- The use of Prisma solar glass instead of the ordinary glass in the TIM-PCM wall composition is shown to be an effective technology solving the encountered overheating problem in summer, while preserving the TIM-PCM advantages during winter.
- Cycling is not reached in summer conditions in most climates except in the subarctic climate (Dfc) where the PCM achieves complete diurnal cycles.
- Even if the PCM does not cycle in summertime, indoor thermal comfort can be ensured using shading devices.

- In all considered climates in chapter 4, the energy performance of the office, in terms of heating and cooling savings, can be significantly improved with the incorporation of the TIM-PCM wall instead of a double-glazed window.
- In regions having a hot summer (Toronto and Sacramento), the PCM remains liquid in summer for long periods and can barely partially solidify, while in winter it can achieve complete or partial diurnal cycling. In climates having a warm summer (Dras and Paris), the PCM works better in summer with more partial PCM solidifications. In regions having a cold (continental or polar) winter, the PCM remains solid for months without melting, while in the rest of the year, it can achieve diurnal cycling.
- From an economic point of view, we have found that when the climate gets colder, the optimal surface of the wall increases.
- In polar (ET) and subarctic (Dfc) climates, the application of the TIM-PCM wall is found economically feasible. In Mediterranean (Csa) and continental humid (Dfa) climates, the wall application is unprofitable at current energy and investment prices.
- The best candidates for TIM-PCM wall application are cities where the price of natural gas is relatively high, making the initial investment cost relatively insignificant compared to heating savings.
- The economic viability of applying the TIM-PCM wall depends mainly on climatic conditions, energy savings, energy costs, the country's economic situation and the investment cost.
- A Graphical User Interface GUI is created on MATLAB to model the phase change problem in rectangular cavity in presence of both natural convection and radiation.

2. Limitations and perspectives

Although this research has reached its aims, there were some limitations that may consist a starting point for future work. In the 2D numerical model for natural convection during melting process, the convective zone dimension was approximated to be equal to the position of the melting front at the top of the cavity. This assumption is not always accurate, and more research should be done concerning a better approximation of this zone. Moreover, the effect of thermal expansion in the cavity was neglected to simply the numerical model. In future works, this should be considered. The developed Nusselt number correlation was for a very specific case (specific PCM, geometry…). Although this developed correlation has not been used in the rest of the work (a general correlation of Berkovsky and Polikov has been used in the rest of numerical modeling, see chapter 2) more efforts

should be done to provide correlations that are appropriate for a wide range of realistic geometries and parameters.

In addition, in our work, we have not modified the construction of the TIM-PCM wall depending on each climate. As a future work the constructive solution can be changed, and a multidimensional optimization study can be performed by combining TRNSYS with an optimization tool such as GenOpt or Mobo. It would be a question to study the impact of various PCM (modification of the melting temperature, latent heat, thickness), and to vary the width of the silica aerogel bed as well as its optical characteristics in order to find an optimal solution suitable for each climate. It is also necessary to change the construction of the building depending on the climate zone. A ventilated air gap can be also added to the wall composition to ensure crystallization of the PCM at night. This could be the subject of a full-fledged study based on the modification of the TIM-PCM wall model.

In addition, the available components for modeling PCM (Type 1270, Type 260...) in TRNSYS only consider conduction heat transfer, so we suggest, as perspective, creating a new component for PCM considering all heat transfer modes occurring during phase change and in 2D if possible.

Moreover, concerning the economic study, there were some difficulties in estimating the prices of materials in each country, especially the PCM cost used in the TIM-PCM wall construction. To improve this study, exact prices of PCM product, installation, transport, encapsulation must be provided by the manufacturer.

Finally, although the incorporation of phase change materials into buildings seems to be very beneficial, it seems necessary that new studies are devoted to understanding the behavior of PCM and especially the study of supercooling, crystallization kinetics, phase segregation, containment as well as health and safety aspects, cost and lifespan of these materials. Such realistic features of PCM were not taken into account in our numerical model.

Conclusion Générale

1. Aperçu des réalisations

Au cours de cette thèse, nous avons développé un modèle simplifié pour la simulation de la fusion, avec convection naturelle dans un premier temps, et avec convection et rayonnement courte longueur d'onde (CLO) dans un deuxième temps. Le modèle simplifié pour la prise en compte de la convection naturelle lors de fusion du MCP utilise l'approche de la conductivité efficace et la théorie d'échelle. La méthode enthalpique a été utilisée pour modéliser le changement de phase. Le modèle mathématique est codé sous MATLAB en utilisant la méthode de volumes finis implicite en deux dimensions. Les résultats du modèle simplifié sont ensuite validés en utilisant un modèle CFD complet précédemment développé dans COMSOL Multiphysics, et des résultats numériques et expérimentaux des benchmarks trouvés dans la littérature pour le cas de fusion de l'Octadecane dans une enceinte carrée. En particulier, une corrélation du nombre de Nusselt correspondant à notre cas d'étude a été trouvée, sur la base du modèle CFD, et est ensuite implémentée dans le modèle simplifié. Le modèle simplifié de la fusion avec convection et rayonnement courte longueur d'onde utilise un algorithme simplifié pour trouver le flux de rayonnement CLO absorbé par le MCP. Ce flux est ensuite ajouté à l'équation d'énergie en tant que terme source. Une évaluation nodale des propriétés optiques du MCP en fonction de la fraction de liquide a été faite. De même, le rayonnement solaire absorbé a été divisé entre les nœuds formant le couche MCP. Le modèle mathématique est codé à nouveau sous MATLAB en utilisant la méthode des volumes finis en deux dimensions. Les résultats obtenus sont en très bon accord avec les résultats d'un modèle de Boltzmann sur réseau et la méthode des ordonnées discrètes (LBM-DOM) trouvés dans la littérature, en termes de la fraction liquide moyenne pour le cas de fusion de l'acide gras contenu dans une enceinte rectangulaire. Ensuite, se basant sur les deux modèles précédents, nous avons développé un modèle numérique décrivant les mécanismes de transfert de chaleur à travers le mur MCP-aérogel. Ce dernier est un mur solaire passif translucide innovant proposé par le projet INTERTRANS et composé d'un vitrage, de l'aérogel de silice pour l'isolation thermique et des matériaux à changement de phase (MCP) pour l'absorption et le stockage de la chaleur issue du rayonnement solaire. Ce mur a été caractérisé expérimentalement en ambiance contrôlée et in situ sur un bâtiment grandeur nature présent au sein du centre du centre Procédés, Energies Renouvelables et Systèmes Energétique (PERSEE) situé à l'Ecole des Mines à Sophia Antipolis. Le modèle du mur a été couplé au logiciel de simulation dynamique des systèmes thermiques TRNSYS, pour évaluer la performance thermique de l'ensemble du bâtiment. Ce modèle a été validé expérimentalement à l'aide de la cellule expérimentale du centre PERSEE pendant sept jours consécutifs en été et en hiver. Ensuite, nous avons utilisé le modèle validé pour optimiser la performance thermique du mur en été sous différentes conditions climatiques, en termes du confort

thermique. Enfin, nous avons conduit une évaluation énergétique annuelle ainsi qu'une étude économique pour l'application du mur MCP-aérogel dans l'enveloppe d'un bâtiment dans différents climats.

Les principales conclusions de ce travail sont :

- Le modèle simplifié développé pour la convection pendant le changement de phase nécessite un temps de calcul beaucoup plus court que celui du modèle CFD. Les valeurs de fraction liquide moyenne, de la position du front de fusion pour quatre instants différents, et de la position moyenne du front de fusion au cours du temps sont en bon accord avec celles du modèle CFD et des solutions Benchmark.
- La modélisation de la convection naturelle pendant la fusion de l'Octadécane dans une cavité carrée modifie la position du front de fusion d'environ 55% à l'instant SteFo = 0.01 et la fraction liquide moyenne d'environ 40% en comparaison avec un modèle à conduction seule.
- La convection naturelle fait augmenter la fraction liquide d'environ 35% par rapport au modèle à conduction seule, tandis que le rayonnement CLO fait augmenter la fraction liquide d'environ 20% par rapport au modèle tenant compte de la convection pour le cas de la fusion de l'acide gras contenu dans une enceinte rectangulaire.
- En ce qui concerne le temps du calcul, les simulations du modèle simplifié, tenant en compte la convection naturelle et le rayonnement CLO, sont beaucoup plus rapides que celles utilisant le modèle LBM-DOM.
- Le modèle proposé considérant à la fois la convection naturelle et le rayonnement pendant le processus de fusion est simple à mettre en œuvre et peut gérer efficacement les problèmes de changement de phase dominés par convection sans la résolution complète de l'écoulement dans un temps de calcul relativement court. Il a été développé pour les applications pratiques de l'ingénierie thermique, où on cherche une évaluation annuelle de la performance énergétique.
- Le modèle MATLAB-TRSNYS validé expérimentalement représente un bon point de départ pour des simulations sur différentes configurations du mur et permet d'étudier pleinement ses capacités et ses inconvénients sous différentes conditions opératoires, et dans différents climats.
- Pour être plus réaliste, la convection naturelle dans le MCP liquide ne doit pas être négligée lors de la modélisation du changement de phase.

- L'utilisation d'un type de verre spécial (Prisma Solar glass) au lieu du verre ordinaire dans la composition de la paroi MCP-aérogels se révèle être une technologie efficace pour résoudre le problème de surchauffe rencontré en été, tout en préservant les avantages du mur en hiver.
- Le confort thermique ainsi que le cyclage du MCP en été dépendent des conditions climatiques.
- Le cyclage n'est pas atteint l'été dans la plupart des climats sauf dans le climat subarctique (Dfc).
- Dans tous les climats étudiés, dans le chapitre 4, la performance énergétique du bureau, en termes d'économies de chauffage et de refroidissement, peut être significativement améliorée avec l'incorporation de la paroi MCP-aérogel à la place d'une fenêtre à double vitrage.
- Dans les régions ayant un été chaud (Toronto et Sacramento), le MCP reste liquide en été pendant de longues périodes et peut difficilement se solidifier même partiellement, tandis qu'en hiver, il peut effectuer un cycle diurne complet ou partiel. Dans les climats ayant un été tiède (Dras et Paris), le MCP fonctionne mieux en été réalisant des solidifications partielles. Dans les régions ayant un hiver froid (continental ou polaire), le MCP reste solide pendant des mois sans se fondre, tandis que pendant le reste de l'année, il est possible de faire des cycles diurnes.
- D'un point de vue économique, nous avons trouvé que lorsque le climat devient plus froid, la surface optimale du mur augmente.
- Dans les climats polaire (ET) et subarctique (Dfc), l'application de la paroi MCP-aérogel est économiquement faisable. Dans les climats méditerranéens (Csa) et humides continentaux (Dfa), l'application du mur n'est pas rentable aux prix actuels de l'énergie et de l'investissement.
- Les meilleurs candidats pour l'application du mur MCP-aérogel se trouvent là où le prix du gaz naturel est relativement élevé, rendant le coût d'investissement initial relativement insignifiant comparé aux économies de chauffage.
- La viabilité économique de l'application du mur MCP- aérogel dépend principalement des conditions climatiques, des économies d'énergie, des coûts de l'énergie, de la situation économique du pays et du coût d'investissement.
- Une interface graphique GUI est créée sur MATLAB pour modéliser le problème de changement de phase dans une cavité rectangulaire en présence de convection naturelle et de rayonnement.

2. Limitations et perspectives

Bien que cette recherche ait atteint ses objectifs, certaines limitations peuvent constituer un point de départ pour des travaux futurs. Dans le modèle numérique bidimensionnel pour la convection naturelle pendant la fusion, la dimension de la zone convective était approximativement considérée égale à la position du front de fusion au sommet de la cavité. Cette hypothèse n'est pas toujours exacte, et des recherches supplémentaires devraient être effectuées concernant une meilleure approximation de cette zone. De plus, l'effet de la dilatation thermique dans la cavité a été négligé pour simplifier le modèle numérique. Dans les travaux futurs, ceci doit être considéré. Au cours de cette thèse, la corrélation de nombre de Nusselt a été développée pour un cas très spécifique. Malgré que cette corrélation développée n'ait pas été utilisée dans le reste du travail (une corrélation générale de Berkovsky et Polikov a été utilisée dans le reste de la modélisation numérique, voir chapitre 2), des efforts supplémentaires devraient être déployés pour fournir des corrélations appropriées à une large gamme des géométries et des paramètres.

De plus, dans notre travail, nous n'avons pas modifié la construction du mur MCP-aérogel en fonction de chaque climat. Comme travail futur, la solution constructive peut être modifiée, et une étude d'optimisation multidimensionnelle peut être réalisée en combinant TRNSYS avec un outil d'optimisation tels que GenOpt ou Mobo. Il s'agirait d'étudier l'impact de divers MCP (modification de la température de fusion, de l'enthalpie, de l'épaisseur), de faire varier l'épaisseur du lit d'aérogel de silice et ses caractéristiques optiques afin de trouver une solution optimale convenable à chaque climat. Il est également nécessaire de modifier la construction du bâtiment en fonction de la zone climatique. En plus, une lame d'air ventilée peut être ajoutée à la composition du mur afin d'assurer la cristallisation du MCP la nuit. Cela pourrait faire l'objet d'une étude à part entière basée sur la modification du modèle de mur MCP-aérogel.

Les composants disponibles pour modéliser les MCP (Type 1270, Type 260 ...) dans TRNSYS ne prennent en compte que le transfert de chaleur par conduction. Nous proposons donc de créer un nouveau composant pour les MCP prenant en compte tous les modes de transfert de chaleur pendant le changement de phase et en 2D si possible.

En outre, bien que l'incorporation des matériaux à changement de phase dans les bâtiments semble être très bénéfique, il semble nécessaire que de nouvelles études se consacrent à la compréhension du comportement du MCP et notamment à l'étude de la surfusion, la cinétique de cristallisation, la ségrégation des phases, le confinement ainsi que les aspects sanitaires, sécuritaires, le coût et la durée de vie de ces matériaux. Ces caractéristiques réalistes des MCP n'ont pas été prises en compte dans notre modèle numérique.

ANNEXES

Annex A: Phase Change Materials (PCM) for Cooling Applications in Buildings: A Review

Abstract:

Cooling demand in the building sector is growing rapidly; thermal energy storage systems using phase change materials (PCM) can be a very useful way to improve the building thermal performance. The right use of PCM in the envelope can minimize peak cooling loads, allow the use of smaller HVAC technical equipment for cooling, and has the capability to keep the indoor temperature within the comfort range due to smaller indoor temperature fluctuations. This article presents an overview of different PCM applications in buildings for reducing cooling loads under different climate conditions, and the factors affecting the successful and the effective use of the PCM. Many drawbacks have been found in PCM applications, mainly the intense impact of summer weather conditions over the PCM performance, which prohibits its complete solidification during night, and thus, limiting its effectiveness during the day. Proposed solutions are reviewed in this article. Finally, a topology diagram is presented to summarize the steps leading to an effective use of PCM in building applications.

Keywords*:* Phase Change Materials, cooling applications, active systems, passive systems, PCM effectiveness, melting temperature.

Highlights:

- PCM for cooling applications (active and passive systems).
- Factors affecting PCM effectiveness.
- Topology diagram summarizing PCM application.

Nomenclature

Cp	specific heat	(J/kg·K)
E_{daily}	Average daily cooling load	(KW)
Hf	Latent heat of fusion	(J/kg)
k_l	thermal conductivity at liquid state	(W/m·K)
ks	thermal conductivity at solid state	(W/m·K)
Q_{cool}	Cooling load	(kW)

Tm	Melting temperature	(°C)
Ts	Solidification temperature	(°C)
ρ_{PCM}	Density of PCM	(kg/m^3)

Acronyms

AC	Air conditioning
ACH	Air change per hour
AHU	Air handling unit
ASEAN	Association of Southeast Asian Nations
CC	Cooled-ceiling
COP	Coefficient of performance
DRSS	Distributed Responsive System of Skins
E	Energy storage effectiveness
E*	Modified energy storage effectiveness
EIA	Ecodesign Impact Accounting (study)
EJ	Exajoules
HTF	heat transfer fluid
HVAC	heating, ventilating, and air conditioning
LHS	Latent heat storage
LHTES	Latent heat thermal energy storage
Mtoe	Million Tonnes of Oil Equivalent
MVS	Mechanical ventilation system
PCM	Phase change materials
RT	Rubitherm GmbH
SEER	Seasonal Energy Efficiency Ratio
SIP	Structural Insulation Panels
SPP	Simple payback period
SSPCM	Shape stabilized PCM
TES	Thermal energy storage
VDSF	Ventilated double skin facade

VF	Ventilated facade
WHS	Water heat storage

1. Introduction

An ever-increasing world population combined with a large increasing in energy demand has led to an important environmental crisis that already shows its clear beginning. The primary energy production, according to the International Energy Agency (IEA), has increased 49% and CO2 emissions 43% over the past 20 years [1]. Research findings have specified that buildings account for almost 41% of the world's energy consumption, which constitutes 30% of the annual greenhouse gas emissions [2]. It is expected that the energy demand in the building sector will rise by about 50% in 2050, and the space cooling demand will triple between 2010 and 2050. Hence, the building envelope should be optimized in order to minimize cooling loads in hot climates. In highly efficient-energy applications for cooling, the energy savings potential is estimated to be between 10% and 40% [3]. In the European Union (EU), the building sector is the main energy consumer and constitutes about 40% of the total energy usage; considerable parts of this energy usage are directly related to the heating and cooling of buildings [4]. In 2010, according to the EIA forecasts, the space cooling demand in the EU reached 220 TWh, and it is expected to increase to 305 TWh (+38%) in 2020 and 379 TWh (+72%) in 2030 [5].

Another study conducted by the European Technology Platform on Renewable Heating and Cooling (RHC) [6] showed that the cooling demand in the EU is expected to rise in both residential and service sectors as shown in Figure 0-1.

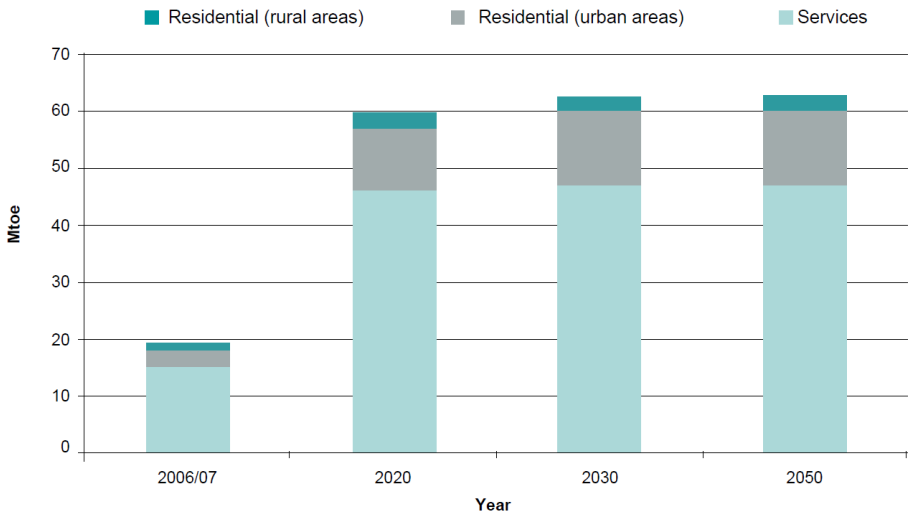

Figure 0-1: Predicted evolution of cooling demand in EU for residential and service sectors [6]

Additionally, in 2006 the building sector in the USA accounts for 38.9% of the total primary energy consumption; 18% for commercial buildings while 20.9% for residential buildings [7]. In 2009–2010, the energy consumption of residential building in Australia was around 25% of total energy consumptions [8]. Present predictions show that the energy use by nations with rising economies (Middle East ,Southeast Asia, South America and Africa) will increase to an average annual rate of 3.2% and will exceed by 2020 that for the developed countries (Western Europe, Japan, North America, New Zealand and Australia) at an average growing rate of 1.1% [9]. According to IEA [10], the cooling demand is expected to increase swiftly in areas where urbanization is promptly growing as shown in Figure 0-2.

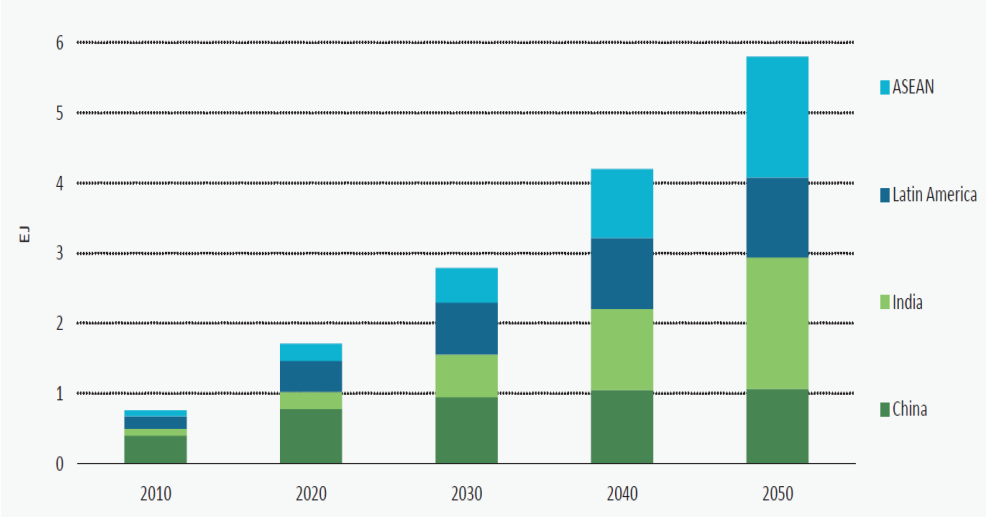

Figure 0-2: Predicted evolution of cooling demand (Exa-joule "EJ") in four different regions [10]

Since the energy consumption of heating and air conditioning systems is still rising with the increasing demand for thermal comfort, therefore there is large potential to ameliorate the building energy efficiency in the areas of heating and cooling technologies.

One of the interesting ways to reduce the energy demands is the use of thermal energy storage (TES). Depending on environmental circumstances, TES materials can absorb heat, store it and release it; improving the gap between energy supply and energy consumption [11]. The energy can be stored by TES materials in three ways namely sensible heat, latent heat or chemical reactions. The latent heat thermal energy storage (LHTES) is an attractive way and has taken much attention over the last decades for heating and cooling purposes in buildings. In residential buildings, a large variety of studies proved that the application of thermal mass in well-insulated structures provides cooling and heating energy savings between 5 and 30% [12].

Recently, Phase change materials (PCM), that utilize the principle of LHTES, have received a great interest and forms a promising technology. PCM have large thermal energy storage capacity in a temperature range near to their switch point and present a nearly isothermal behavior during the

charging and discharging process [13]. The right use of PCM can minimize the peak heating and cooling loads, and has the capability to keep the indoor temperature within the comfort range due to smaller temperature fluctuations. Consequently, reduce the dimensions and energy consumption of the corresponding technical equipment. The main advantage of the use of PCM is that it enhances the thermal storage potential with a minimum change of the existing building design [12]

Many studies have investigated the use of PCM in buildings and showed that PCM can remarkably improve the building energy performance. But a lot of difficulties were encountered especially concerning the efficient use of PCM and its practical application.

Al-Saadi and Zhai [14], Baetens et al. [15], Cabeza et al.[16], Khudhair and Farid [17], Kuznik et al [18] and others, have conducted several reviews on the use of PCM in buildings for thermal energy storage and indoor climate comfort purposes, clearly showing that the interest for PCM is increasing worldwide. It has been also proved by several authors that PCM provide energy benefits in the heating period while limited benefits were found during the cooling season.

This study presents an overview of different PCM applications in buildings for reducing mainly the cooling loads under different climate conditions. The difficulties related to the material selection and the factors affecting the successful and the effective use of the PCM are also discussed.

2. Phase change materials (PCM)

2.1. General

PCM can be used to store energy or to control the temperature swings within a specific range. Therefore, applications for heating and cooling in buildings are expected to have great potential for PCM use. When the temperature rises, PCM absorb heat in an endothermic process and changes phase from solid to liquid. As the temperature drops, PCM release heat in an exothermic process, and return to its solid phase.

Certain types of PCM do not satisfy the desired criteria for an appropriate storage medium. The PCM to be used for thermal energy storage purposes should meet desirable thermo-physical, kinetic and chemical requirements shown in Table 0-1[7] .

Table 0-1 thermo-physical, kinetic, chemical, economic and environmental requirements of PCM [7]

Thermo-physical Requirements	Kinetic Requirements	Chemical Requirements	Economic and environmental requirements
- Appropriate melting temperature in the required operating temperature range. - High latent heat of fusion.	-High nucleation rate to avoid super cooling of the liquid phase. - High rate of crystallization to satisfy demands of heat	- Long term chemical stability of the PCM. - No degradation after freeze/melt cycles.	- Low price and cost effective. - availability -Nonpolluting.

- High specific heat. - High thermal conductivity of solid and liquid phases. -High density. - Congruent melting of the PCM. -cycling stability. - Small vapor pressure. - Small volume changes. - Little or no sub-cooling during freezing. -no segregation.	recovery from the storage system.	- Complete reversible freeze/melt cycle. - No corrosiveness. -non-flammable, Non-toxic and non-explosive materials for safety.	- Low environmental impact. - Good recyclability. - Low embodied energy. - Facility of separation from other materials.

2.2. PCM classification

A considerable number of PCM is available in any desired temperature range. According to their chemical composition, PCM can be categorized as organic compounds, inorganic compounds and eutectic mixtures. Each group has its typical range of melting temperature and its range of melting enthalpy. The paraffin waxes, salt hydrates, fatty acids and eutectic organic /non-organic compounds are the most used since last 30 years. The relationship between the melting enthalpy (kJ/l) and the temperature of PCM is shown in Figure 0-3. These characteristics are considered very important especially for their application in building envelopes (i.e. PCM incorporated into finish materials, thermal insulation or structural components) [12].

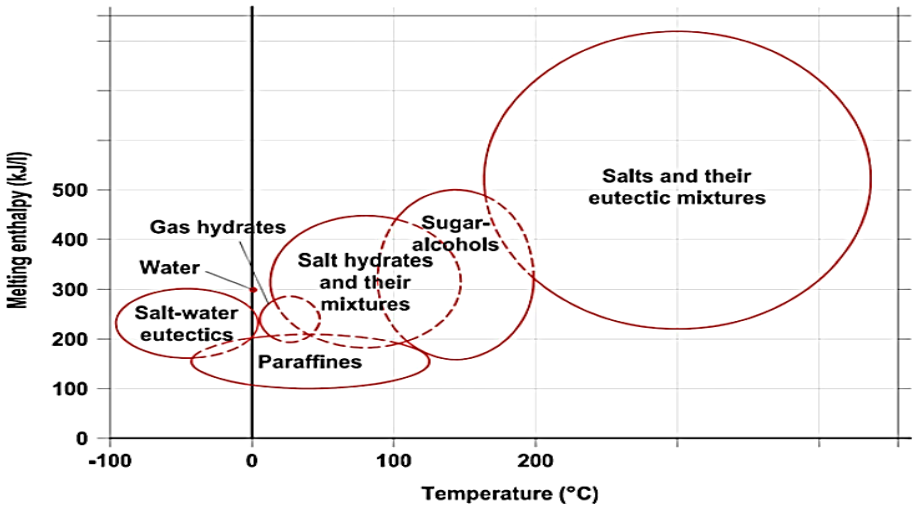

Figure 0-3: Relationship between PCM melting enthalpy and temperature for the different groups of PCM [15]

For a specific application, PCM for thermal energy storage in buildings do not meet all the above stated requirements and performance properties. Each material has its own specific poor characteristics, which can be enhanced by proposing different solutions. For example, using metallic fins can increase the thermal conductivity of PCM, introducing a nucleating agent may suppress

super-cooling and the use of suitable PCM thickness can prevent incongruent melting [7]. A classification of PCM is given Figure 0-4.

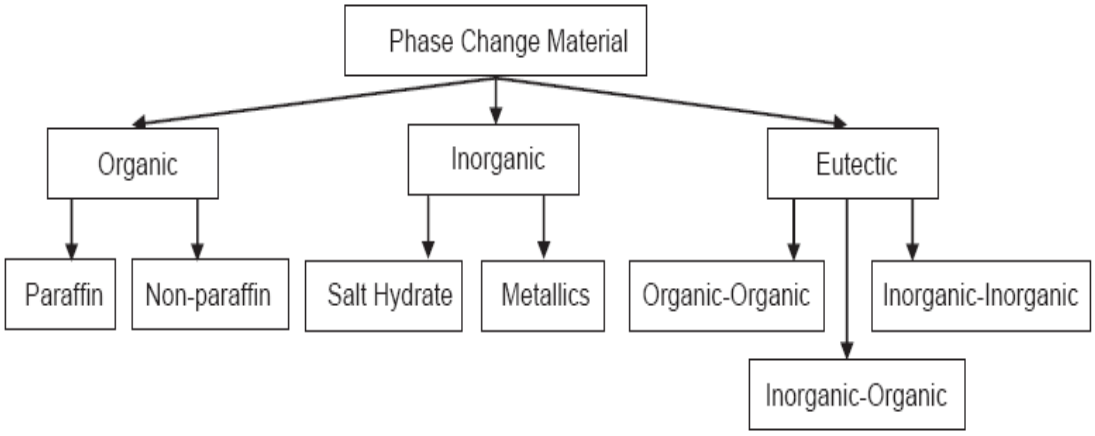

Figure 0-4: PCM classification [19]

2.2.1. Organic materials

Organic phase change materials are paraffin and non-paraffin, the latter including fatty acids, ester, alcohols, glycols, etc... They have some characteristics making them beneficial to latent heat storage in buildings. Generally, organic PCM are available in large temperature range, they are chemically stable, non-corrosive and non-toxic, they freeze with little or without super cooling, they present no segregation, and they have a high latent heat of fusion and good nucleation rate. However, Most of the organic PCM are not stable in higher temperatures due to covalent bonds [7] . Also, their density is low (usually less than 103 kg/m3), which is below the density of inorganic materials such as water and salt hydrates.

Paraffin are available in a large range of melting points from about 20°C up to 70 °C, however they have a low thermal conductivity (about 0.2W/ (m.K)) limiting their applications[17]. During the freezing cycle, when high heat transfer rates are desired, Paraffin present a problem. Moreover, they have a large volume change during the phase change [20]. In addition, they are available from many manufacturers, but they are expensive comparing to salt hydrates. Paraffin wax is the most used commercial organic PCM.

Fatty acids that are generally presented by the chemical formula CH3 (CH2)2nCOOH, have similar characteristics to paraffin and they are stable at cycling. The combination of different fatty acids to get melting temperatures range of 20–30°C with a precision of ± 0.5 °C can be promising [7].

2.2.2. Inorganic materials

Inorganic materials are salt hydrates and metallic. They have respectively good thermal conductivity and high latent heat of fusion; they are not expensive and non-flammable. Their main drawback is compatibility with metals, since in some combinations of PCM with metals corrosion can be developed [7]. They require containment; hence, they are inadequate for impregnation into porous building materials.

The most attractive and important TES materials are salt Hydrates, due to their relative high storage density of about 240 kJ/kg, their small volume change during phase transition, and their relative high thermal conductivity of about 0.5W/ (m.K). Salt hydrates have some disadvantages such as super-cooling, segregation, and corrosion [7]. Concerning Metallic PCMs, they are not within the desired temperature range for building applications.

2.2.3. Eutectics

Eutectics are a mixture of proportions of many solids, in order to get more desired properties mainly a higher latent heat and a more specific melting point. They almost melt and solidify without segregation, preventing the separation of components. Eutectics are divided into 3 groups according to their consisting materials: organic–organic, inorganic–organic and inorganic–inorganic eutectics.

3. PCM for cooling applications

Recently, it has been noticed that the cooling demand of the building sector is increasing rapidly, especially in developing countries, due to: 1) the high need of comfort of building occupants, 2) the rise of the internal heat gains of buildings, 3) the impact of urban heat island felt in overcrowded cities and 4) the reduced cost of cooling equipment [21][22][23]. Thus, Passive or efficient-energy solutions for space cooling have received much attention.

In space cooling, the objective is to keep a space cold, more precisely to avoid the temperature increasing above a certain level, which can be carried out in three ways: the reduction of heat input, the reduction of temperature fluctuations, and the improvement of heat rejection [7].

To meet the cooling requirements, PCM can be installed into the building in passive or active systems. Passive systems do not use active mechanical equipment and no additional energy is required i.e. the heat is charged or discharged only due to temperature fluctuations when the air temperature rises or falls beyond the PCM melting point and only natural ventilation provides cold from outside. Passive applications are easily implemented and can be integrated into the building envelope (walls, roofs, and floors).

On the contrary, Active systems need the help of mechanical equipment to achieve the PCM thermal energy charging or discharging. In this case PCM can be installed in storage units, in HVAC systems or it can be used as heat-cold storage tank in solar cooling technique.

Different PCM cooling system classifications have been suggested in different studies [24] [25]. In the current study the PCM cooling systems are divided into five categories: free cooling, solar cooling, air conditioning systems, evaporative and radiative cooling and PCM in building envelope. Active and passive cooling systems could be found together or each alone in these categories. Many PCM used for cooling applications is listed in Table 0-2.

Table 0-2: PCM used for cooling applications

Name of PCM	Melting point (°C)	Latent heat(KJ/Kg)	Reference
Emerest 2325 (butyl stearate + butyl palmitate 49/48)	17-21	138-140	[24]
Hexadecane	18	236	[26]
Heptadecane	18	214	[26]
KF, 4H2O	18.5	231	[24]
Butyl stearate	19	140	[29]
Paraffin C16–C18	20-22	152	[32]
Paraffin RT20	20-22	172	[34]
Paraffin FMC	20-23	130	[33]
Dimethyl sebacate	21	120-135	[32]
Eutectic E21	21	150	[34]
Capric-lauric 45/55	21	143	[27]
Salt hydrates Na_2SO_4,$10H_2O$	21	198	[33]
ClimSel C 21	21	122	[34]
Octadecane	22	244	[26]
Capric-palmitate 75.2/24.8	22.1	153	[30]
Paraffin RT25	24	164	[33]
CaCl2·6H2O	24-29	192	[31]
45% Ca(NO3)2_6H2O + 55% Zn(NO3)2_6H2O	25	130	[32]
66.6% CaCl2_6H2O + 33.3% Mgcl2_6H2O	25	127	[32]
Mn(NO3)2,6H2O	25.8	125.9	[28]
Paraffin R27	26–28	179	[32]

SP27	27	180	[33]
Eutectic E23	29	155	[34]

3.1. Free cooling

In free cooling technique, a separate storage unit is utilized in order to provide the cold into the room whenever it is required by circulating room air through the storage unit. The difference between the natural night ventilation and free cooling is that fans or other mechanical equipment (extra power) are used to charge or discharge the heat from the storage unit which improves the cooling potential, unlike the night ventilation where building envelope such as walls are used for thermal storage. The effectiveness of PCM-based free cooling application depends on the diurnal temperature range that should be between 12°C and 15°C [35]. If the air temperature swing between day and night is relatively small, then other parameters should be accurately considered in the design of free cooling system coupled with PCM i.e. selection of an appropriate PCM with suitable encapsulation [36].

The principle of a free cooling system with PCM, shown in Figure 0-5, consists of two operation modes:

- Solidification of PCM: occurs at night when the ambient temperature is lower than the indoor temperature. The outdoor cool air flows across the storage unit, by means of a fan, absorbing heat from PCM, which leads to the beginning of solidification process, which lasts until the outdoor temperature became nearly equal to the PCM solidification temperature.
- Melting of PCM: occurs during the day when the indoor temperature increases above the comfort range. Hot air of the room passes through the storage unit and the heat is absorbed by the solid PCM which leads to the beginning of melting process. Consequently, the room air temperature is reduced, and the cooled air is delivered to the interior of the building.

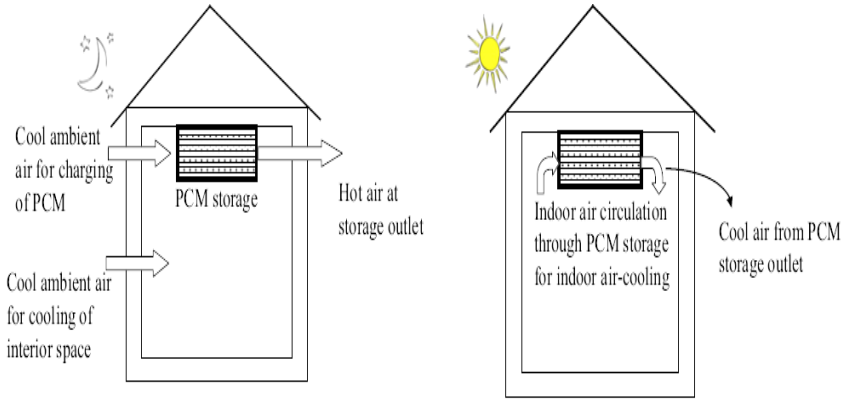

Figure 0-5: Principal function of PCM ‘‘free cooling system’’[25]

Many Parameters affect the thermal performance of a free cooling system during charging and discharging such as the air flow rate, the outlet air temperature and the inlet air temperature of the storage unit, in addition to the thermo-physical properties and encapsulation thickness of PCM, which

all affect the melting and the solidification processes. Moreover, PCM melting temperature is an important factor in the design of a free cooling system. The cooled air temperature in the room after the discharging of PCM should be within the comfort range (23–27°C), therefore the PCM melting temperature should be taken between 19°C and 24°C [34].

It is found that commercially available PCM having melting point between 20°C and 27°C, are often used in the application of free cooling system. In addition, most of the studies have used paraffin as PCM in the storage unit since they do not react with the encapsulated material (no leakage) and without sub cooling in contrast to salt hydrates which are rarely used.

Many Studies had discussed the efficiency of free cooling system in alleviating the building cooling loads during hot periods. An experimental installation was designed by Zalba et al. [36] to investigate the performance of PCM in free cooling system. The principal parameters affecting the melting and solidification processes were discussed. They concluded that the designed installation is technically and economically beneficial, considering further enhancements such as increasing the heat transfer coefficient and the use of more appropriate PCM. Mosaffa et al [37] studied numerically, using heat capacity method, the performance of multiple PCM TES unit for free cooling shown in Figure 0-6. They investigated the impact of some parameters mainly the thickness and the length of PCM slabs, and the thickness of air channels using energy-based optimization method. Another optimization method, based on energy storage effectiveness, was proposed by same authors [38] to enhance the performance of multiple PCM free cooling system (Figure 0-7), They concluded that the suggested method is not appropriate for free cooling system optimization, but the model may be advantageous to design an optimum free cooling system at different climates. Anisur et al. [39] aimed to validate experimentally a previous analytical work concerning a shell LHS system (Figure 0-8); they concluded that this method is beneficial to design an air cooling system forecasting different parameters.

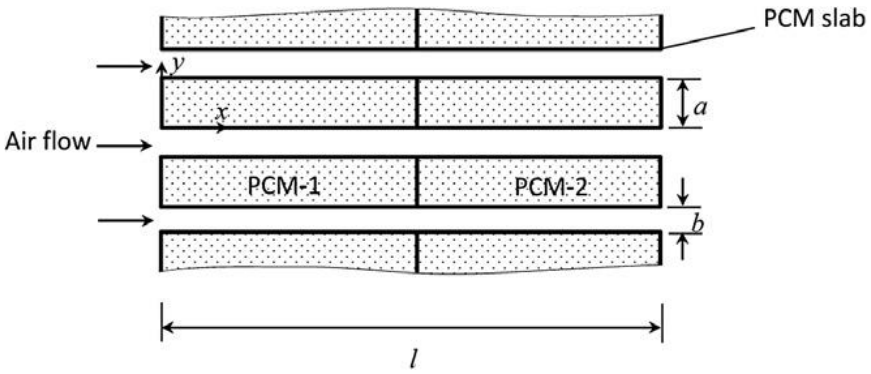

Figure 0-6: Schematic diagram of the TES unit [37]

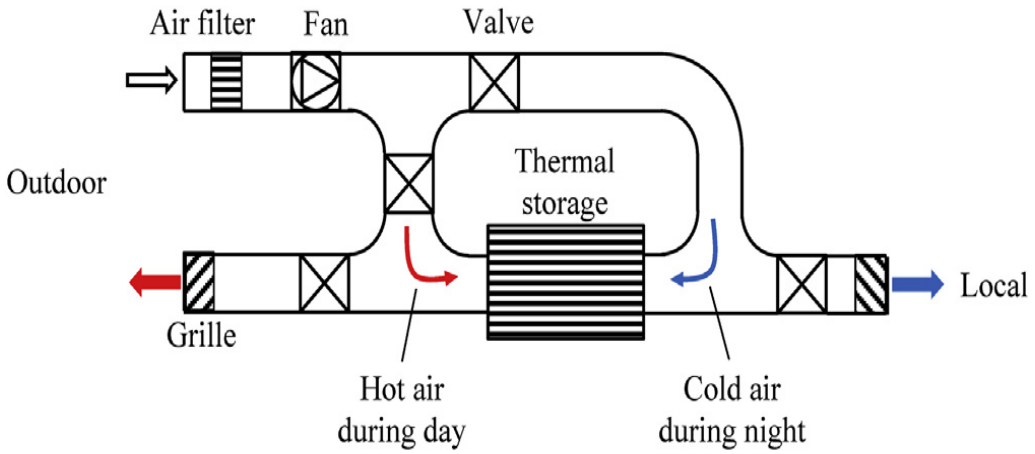

Figure 0-7: Installation of thermal storage for free cooling [38]

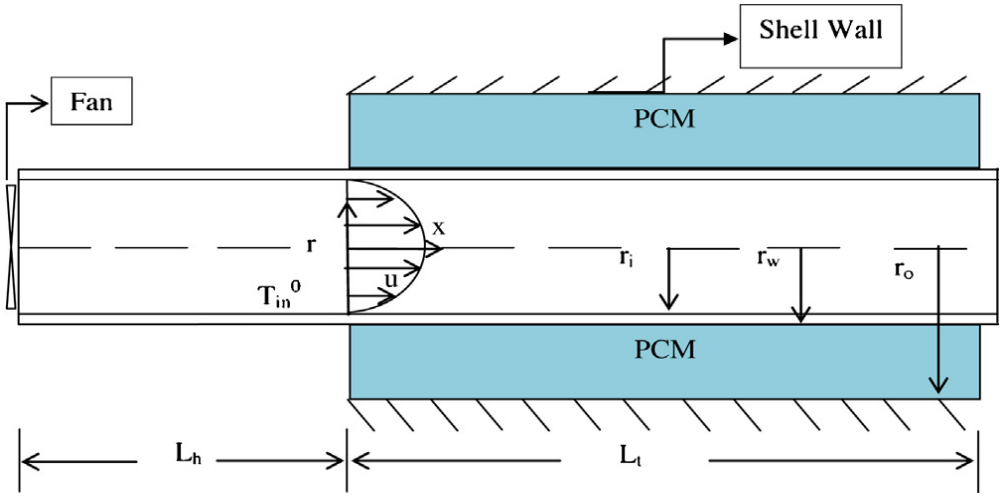

Figure 0-8:Schematic diagram of LHS System for air cooling through cylindrical tube [39]

Rouault et al [40] investigated numerically the effect of the geometry (shapes and arrangements), of rectangular tubes filled with PCM (Figure 0-9), on the LHTES unit performance. They finally suggested a future design support system principally considering the PCM solidification stage. Osterman et al [41] examined numerically, using Fluent software, and experimentally the performance of a proposed TES system (Figure 0-11) on a yearly basis, and they discussed its viability for space cooling and space heating. They concluded that the maximum quantity of cold is accumulated in August and July, due to larger diurnal temperature fluctuations. Darzi et al [42] investigated the influence of PCM plate thickness, inlet air temperature and mass flow rate on the efficiency of plate PCM storage unit (Figure 0-10). They found a linear relation between the PCM-plates thickness and the duration of melting process. Lazaro et al [43] tested experimentally two prototypes of PCM-air heat exchangers. They concluded that, for free cooling applications, the design of heat exchangers is more important than improving PCM thermal conductivity.

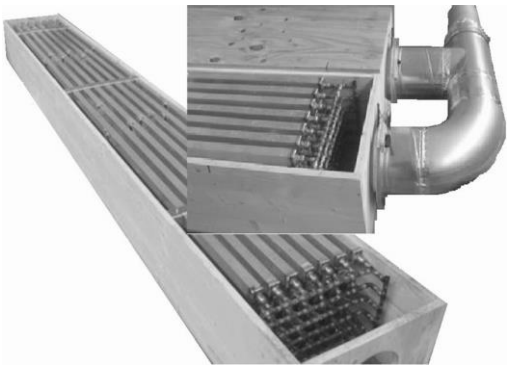

Figure 0-9: An energy storage unit and its airline connection [40]

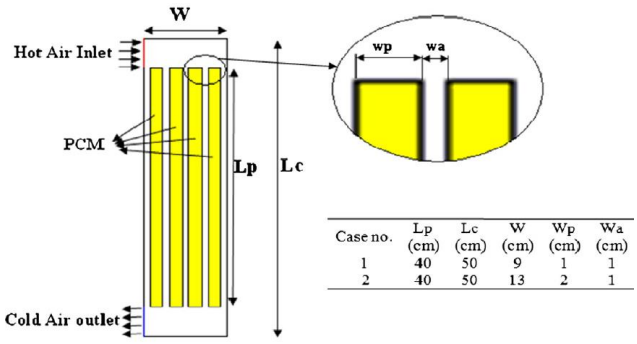

Case no.	Lp (cm)	Lc (cm)	W (cm)	Wp (cm)	Wa (cm)
1	40	50	9	1	1
2	40	50	13	2	1

Figure 0-10: Schematic diagram of heat exchanger with plate-type PCM [42]

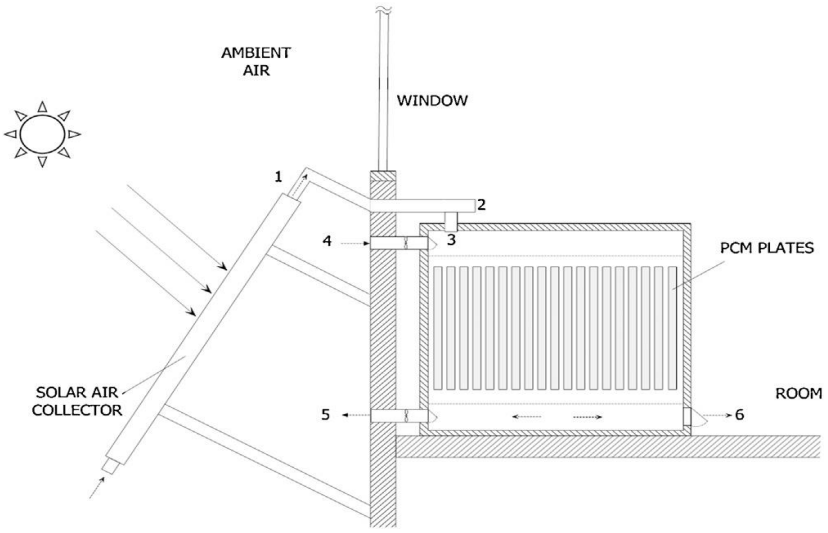

Figure 0-11: Conceptual design of a storage unit [41]

Tan and Zhao [44] investigated the performance of PCM storage unit (Figure 0-12) integrated in thermoelectric system using a mathematical model, and then validated it experimentally. They also recommended a guideline on the design of the combined system. They concluded that the selection of TEM depends significantly on three factors namely the COP, cost and cooling power. Yanbing et al. [45] investigated the performance of night Ventilation with PCM (NVP) storage system .They found that the NVP system is efficient and can decrease the room energy consumption. Takeda et al [46] investigated the potential of a PCM packed bed storage unit (positioned in the building ventilation system) in decreasing the ventilation load for different Japanese climates. They found that during discharging procedure, the outlet air temperature is always constant and in the range of phase change temperature. The use of PCM storage unit can decrease the building ventilation load up to 62% in the different considered Japanese cities. Waqas and Kumar [47] investigated experimentally the performance of free cooling system in hot and dry climate; the storage unit is shown in Figure 0-13. They found that a complete solidification of PCM can be achieved in short period when the air

flow rate is higher and the outdoor temperatures are lower at night. Moreover, the potential of free cooling principle was also investigated using other different systems: two cylindrical LHTES filled with PCM spheres [48] as shown in Figure 0-14, cold storage composed of a metal box [49] built in a ceiling board, with aluminum fins in order to increase its thermal power, heat pipes embedded in PCM [50], PCM packed bed storage [51] integrated under the floor as shown in Figure 0-15 and a bulk PCM tank with a finned-pipe heat exchanger [52] (TRNSYS component type 842) as shown in Figure 0-16. The free cooling system applications are summarized in Table 0-3.

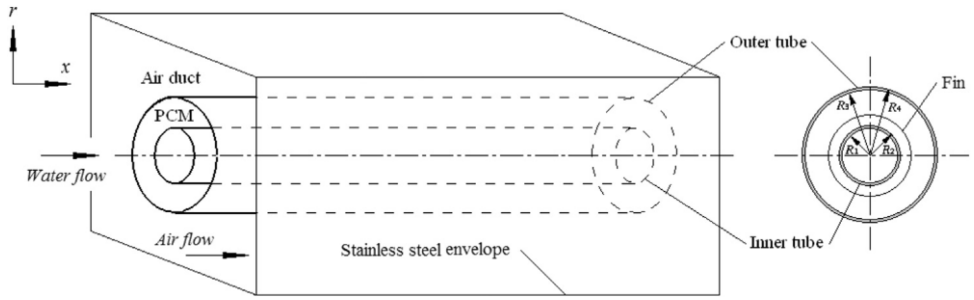

Figure 0-12: Schematic diagram and cross-section of the PCM heat storage unit [44]

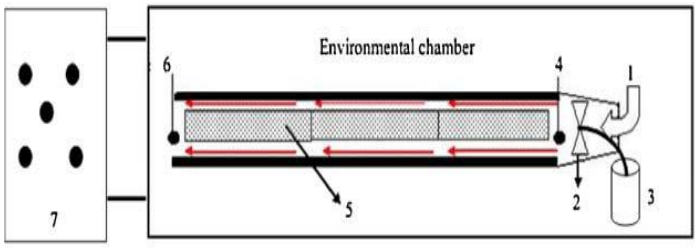

1: Air inlet to storage unit. 2: Fan. 3: Fan speed controller. 4: Air inlet temperature sensor. 5: storage material (PCM). 6: Air outlet temperature sensor. 7: Control panel for chamber AC, heater and fan.

Figure 0-13: The experimental PCM storage unit [47]

Figure 0-14: cylindrical LHES filled with PCM spheres [48]

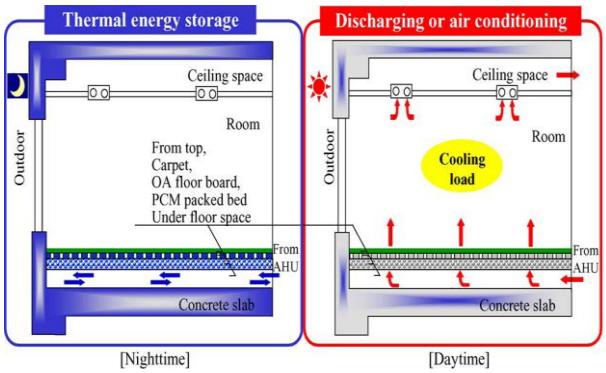

Figure 0-15: Concept of the PCM system packed bed storage integrated under the floor [51]

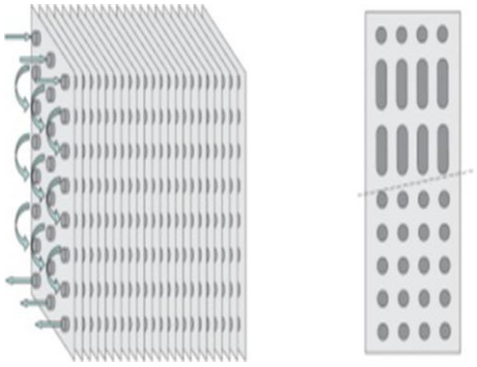

Figure 0-16: Heat exchanger considered in TRNSYS [52]

Table 0-3: PCM in active free cooling system applications

Ref/Type*	Location/ climate	Used PCM properties	Heat exchanger	Results
[36] E	Laboratory experiment-Spain	-encapsulated PCM RT25 -Tm=25°C - m_{total} PCM = 3 kg	flat plate heat exchanger	Main parameters affecting solidification and melting processes: - Thickness of PCM encapsulation, -air flow, - inlet air temperature --interaction between temperature and thickness
[37] E,S	Tabriz, Iran	-CaCl2_6H2O, Tm=29°C -Paraffin C18, Tm=27.5°C -RT25, Tm=26.6°C	Parallel rectangular air channels separated by PCM slabs	COP=7 realized by: -combination of RT25& CaCl2_6H2O - air channel thickness= 3.2 mm - PCM slab length= 1.3 m and thickness= 10 mm
[38] E,S	Eindhoven, south of Netherlands	-Climsel C24, Tm=24°C -KF4H2O, Tm=18.5°C	Layers of flat PCM slabs with HTF channels in between	- COP= 7.63 & Q_{cool}=4.38 kW - Air channel thickness=3.2 mm, length=1.3 mm, slab thickness= 9 mm.& maximum flow rate=1200 m3/h → T_{outlet} < 20 °C for 8 h & power consumption =4.6 kWh -Air flow rate<700 m^3/h→ optimum E*= 0.66 → COP<5.76 & Q_{cool}=2.96KW -Air channel thickness ↘↘ → E*= 0.54 → COP=6.22 & power consumption=5.8 kWh.

[39] E	Kuala Lumpur, Malaysia	-Heptadecane -Tm =22.33°C	shell and tube LHS filled with PCM	- $T_{inlet\ air}$ ↗↗→ Better (COP). - $T_{inlet\ air}$= 34.5°C , tube inner radius=5.35 mm and 1 mm thickness→ COP=4.16
[40] E,S	-	-RT28 HC paraffin -Tm=28°C	bundle of rectangular tubes filled with PCM	-Vertical flat plates marginally more effective than horizontal ones. - Improvement of heat exchange between tubes & air are required.
[41]E,S	Ljubljana, Slovenia	-paraffin RT22HC - m_{PCM} in the plate = 1003 g	30 CSM Plates filled with PCM & Air gap between plates=0.8 cm.	-Reduction of annual energy consumption =142 kWh. - In July and august: complete TES cycles & stored energy rises. -TES cost = 2*cost of a conventional system. -TES cost in the operation period is lower.
[42] S	different indoor temperature conditions	-PCM salt SP22A17 -Tm=22-24°C	PCM plates type storage	- Mass flow rate ↗↗ → cooling power ↗↗ - Stefan number↗↗→ cooling power & T_{outlet} ↗↗ -Lower mass flow rate & lower Stefan number → more efficient heat exchanger.
[43] E	Zaragoza, Spain	-inorganic PCM: Ks=0.7w/m.k Stored energy=31.584KJ -organic PCM: Ks=0.16w/m.k Stored energy=24.395KJ	2 prototypes: -aluminum pouches filled with inorganic PCM - aluminum panels filled with organic PCM	- Lower Ks and lower stored energy → cooling power↗↗ & shorter melting period -Prototype 2 more practical for free-cooling.
[44] E,S	Denver, Colorado, USA	-organic paraffin RT22 -Tm=19-23°C(main peak=22°C) - m_{total} PCM=15.4 kg.	Shell and tube PCM storage unit incorporated in thermoelectric cooling system	- PCM integration→ COP ↗↗ from 0.5 to 0.78 - determining PCM volume depends on system accumulated heat dissipation. - Necessity to evaluate the weather condition to ensure fully discharging of PCM at night.
[45] E,S	Beijing-China	-2000 capsules containing fatty acid - Tm = 22 °C - 26°C, - m_{total} PCM=150 kg.	PCM Packed Bed Storage (NVP)	-NVP reduces the room temperature and increase thermal comfort level. -during day, PCM discharged 300 w cold to the room -$COP_{overall}$ (Qdis/P fan) = 80.
[46] E,S	8 Japanese cities	-PCM granules (65% ceramic and 35% paraffinic hydrocarbon), -Tm =22.5-25°C - m_{total} PCM bed=4.59 kg	PCM packed bed fixed vertically in a supply air duct.	- Selection of PCM depends on climatic data particularly on the diurnal temperature variation. - Significant reduction in ventilation load in all cities, especially in Kyoto by about 62.8%.
[47] E	Islamabad-Pakistan/ dry and hot climate	-SP29 encapsulated in containers of galvanized steel -Tm =27-29°C - m_{total} PCM =13 kg	PCM storage unit: open air circuit type (flat plate heat exchanger)	- decreasing $T_{charging}$ from 22°C to 20°C →33% less time required to fully solidify the PCM - increasing $T_{charging}$ from 22°C to 24°C →52% more time required to fully solidify the PCM.

				- Increasing air flow rate from 4 m^3/hr to 5 m^3/hr → 16% reduction of solidification time period. -Tm of PCM affects the storage unit performance more than the air flow rates.
[48] E,S	Ljubljana-Slovenia/ latitude =46°C	- RT20 paraffin -Tm=20 °C	2 cylindrical LHTES units filled with PCM spheres, integrated into MVS	- Optimum PCM mass in both LHTES units: 6.75 kg/m^2 (heavyweight bldg.) and 13.5 kg/m^2 (lightweight bldg.) - mechanical ventilation size is reduced -more favorable temperatures are provided.
[49] E	Lab scale experiment Ljubljana-Slovenia	- RT 20 paraffin -Tm = 22 °C - m_{total} PCM =3.6 kg	metal box with external and internal fins filled with PCM	- $T_{outlet\ air}$ (when airflow =1.5 m s^{-1}) < $T_{outlet\ air}$ (when airflow = 2.4 m s^{-1}). -proper selection of PCM type depends on local climate conditions. - Inlet air temperature=26°C and airflow=1.5 m s^{-1}→ greater air cooling time by the buffer compared to other regimes
[50] E,S	Typical UK summer conditions	-Salt hydrate (Na2SO4 ,10H2O) -Tm =21 °C.	heat pipes embedded in PCM storage unit	- $\Delta T = Tm - T_{charging}$ ↗↗→ Better solidification: - higher air flow rates (→ full solidification -free cooling → prevents overheating in summer, and reduces CO2 emissions. - ΔT between air and PCM~15°C →PCM melting and solidification in practical time (7±10h). - Heat transfer <40 W when temperature difference is 5°C (more reasonable) and flow rates 0.18 m^3/s.
[51] E,S	Japan	PCM granules with diameter of some micrometers containing paraffin.	PCM packed bed storage	Each night, 89% of daily Qcool is stored using 30 mm thick packed bed of granular PCM.
[52] S	Stockholm/ Swedish climate excessive overheating in summer	-Commercially available salt based PCM -Tm~17 °C (close to the average summer temperature in Stockholm)	bulk PCM tank with a finned-pipe in an aluminum based heat exchanger	-Active free cooling keep the room temperature within indoor comfort range. - 75% of the cooling demands are met at half of electricity consumption. -free cooling is an economically and environmentally proper solution for a passive building.

*(E: experimental, S: simulation)

It could be noticed that the main component in the free cooling system is the PCM storage unit; moreover, suitable PCM with appropriate melting temperature should be carefully selected. PCM free cooling system technology is not yet commercialized and its initial cost is higher by about 10% than a traditional air-conditioner; keeping this cost competitive with other traditional cooling technologies requires more PCM commercialization [33]. However, it was shown that PCM solidification during the limited period at night is slow due to the low thermal conductivity of PCM; heat transfer improvements are needed. It is also found that free cooling systems are investigated numerically in

many studies, and barely any free cooling system was applied in experimental real case for building [25]. Also, the majority of studies investigated the PCM free cooling performance in summer conditions in European climates, however there is a need to evaluate the potential of PCM free cooling system for the desert climate with high diurnal temperature ranges [25].

3.2. Solar cooling systems with PCM

Solar cooling systems including adsorption and absorption cooling have been examined in the last few years, and it can be considered as alternatives to traditional air conditioning systems. Moreover, solar powered absorption cooling system can realize summer comfort conditions in buildings at low primary energy consumption. Solar cooling systems can reduce the cooling needs in buildings under hot climate [53]; they can also decrease the peak demand for electricity and consequently reduce the environmental pollution.

The use of PCM with solar absorption cooling, help significantly to meet cooling demand when the solar energy is not available.

Helm et al. [54] examined a solar-driven absorption cooling system coupled with PCM and a dry air cooler instead of a traditional wet cooling tower as shown in Figure 0-17. They concluded that by integrating PCM in heat rejection circuit of the chiller, a quantity of required power could be shifted to the off-peak hours with minor rise in total electric consumption of the absorption cooling system. A novel concept for a solar cooling system including dry cooler with PCM had been investigated [55] in order to improve the system efficiency. The operating costs and maintenance for the new developed system are lower, compared to the wet cooling tower. On hot days, PCM support the dry cooler to assure a low cooling water return temperature to the absorption chiller. At the University of Lleida, Gil et al.[56][57][58] developed a TES system for solar cooling application shown in Figure 0-18 (pilot plant at the laboratory), in order to be used later in real installation for cooling purposes on the roof of a building in Seville [58]. The storage tank implemented in real solar cooling installation is shown in Figure 0-19. In the experiment, a dry cooler was used to remove heat instead of the absorption chiller and an electrical boiler was used to provide heat instead of the solar collector. They also tested two PCM storage tanks (shell-and-tubes heat exchanger) one with fins and the other without fins [57]. They concluded that in the design of a real PCM storage tank, the dead PCM volumes must be avoided.

Belmonte et al [59] investigated the performance and the feasibility of an alternative solar cooling system where the open wet tower is replaced by a dry cooler combined with PCM TES system (Figure 0-20). Then, conventional and alternative configurations were simulated and compared for different climate conditions. They concluded that the conventional system is more efficient, at all locations, in terms of chiller's COP and produced cooling energy, but in terms of overall system COP, the system

efficiency is improved by 50% in the alternative configuration. Furthermore, Agyenim et al. [60] designed a tube heat exchanger with PCM in order to improve the COP of LiBr/H2O absorption cooling system. It has been found that the chosen PCM was appropriate to improve the COP of the solar cooling system. The solar cooling systems combined with PCM applications are summarized in Table 0-4.

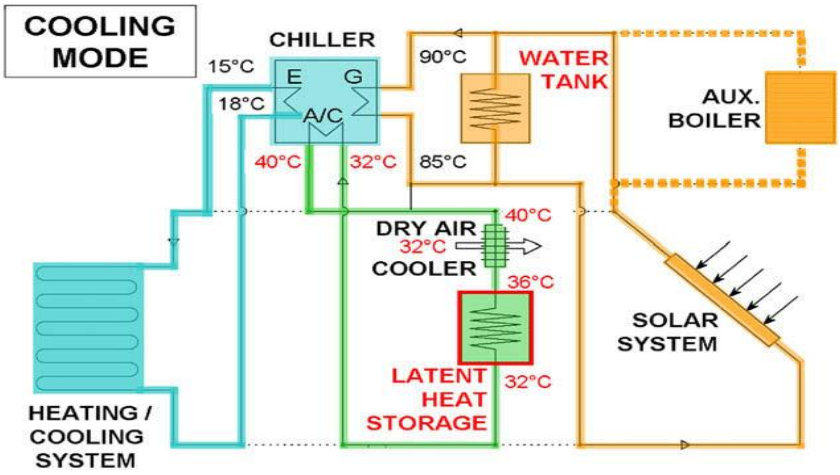

Figure 0-17: solar heating and cooling system with absorption chiller and latent heat storage in cooling mode [54]

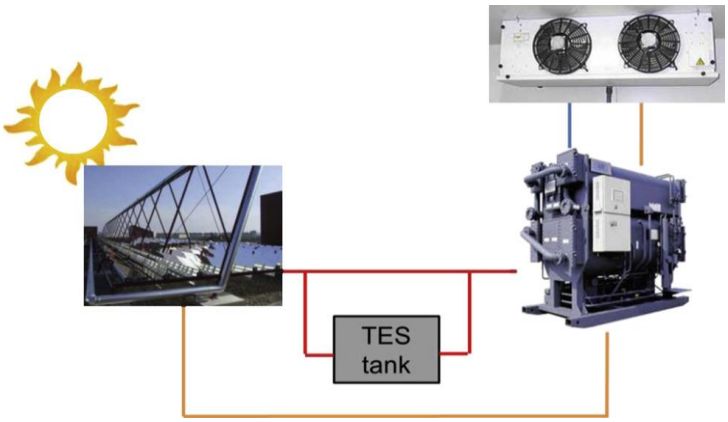

Figure 0-18: Location of PCM storage tank in the solar cooling application [58]

Figure 0-19: Storage tank implemented in a real solar cooling installation at the University of Sevilla (Spain) [58]

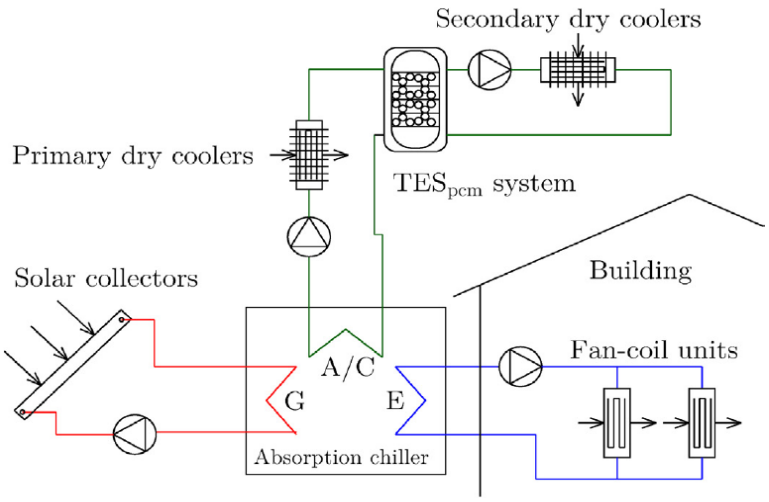

Figure 0-20: solar cooling system with dry coolers and a TES PCM [59]

Table 0-4: PCM combined with Solar cooling system applications

Ref/ Type*	Location/ climate	Used PCM properties	PCM-solar system	Results
[54] E	Munich, Germany	-calcium chloride hexahydrate (CaCl2,6H2O) -Tm= 27–29°C	-PCM & dry air cooler in solar-driven absorption system -PCM support heat rejection of absorption chiller	-PCM instead of conventional WHS→Volumetric storage density 10 times higher. -Reduction of over-sizing of the solar collector
[55]E, S	8 European climatic conditions	-Calcium chloride hexahydrate -Tm=29°C	-PCM with dry re-cooled sorption chiller -LHS module with inner heat exchanger containing 1 m³ of PCM	-In situ measurement→positive effect on SEER for cooling by 11.4. - Simulation→ efficiency ↗↗ up to 64% compared to system with only dry re-cooling (without PCM)
[58] E	Lleida & Seville, Spain	- PCM : Hydroquinone -Tm= 166 °C-173°C	PCM storage tank with absorption chiller and Fresnel collectors	-Tank with fins→shorter melting/solidification time, PCM conductivity↗↗, heat transfer rates↗↗, energy stored faster - fins→ money &time investment↗↗, PCM quantity& stored energy ↘↘ → rejection of using fins in real applications.
[59] S	52 provinces of Spain	- hydrated salts. -Tm=30°C	PCM in the heat rejection loops of absorption chillers	Alternative system with PCM TES: -In temperate & humid summers→ COPsys improved by one unit. - Reduction of total cooling energy in evaporator (21–38%) -worsening of mean performance coefficient of chiller (between 7&13%).
[60] E	Cardiff, Wales.	-Erythritol -Tm=117.7°C	PCM at the hot side of absorption chiller with solar collector	Erythritol suitable for the application, provide 4.4 hours of cooling at peak load

*(E: experimental, S: simulation)

3.3. PCM-air conditioning systems

Air conditioning systems control several changes such as weather conditions, residential, commercial and industrial activities. Thus, during the day, the electrical consumption varies considerably and reaches peak values. Integrating PCM in AC system could significantly reduce the cooling load, where AC with smaller power size could be used. Fang et al. [61] tested the performance of an AC system incorporated with PCM spherical capsules packed bed. They investigated different parameters mainly the cool storage rate and capacity, the condensation and the evaporation pressures of the refrigeration system, the COP of the system, the inlet and outlet coolant temperatures during charging and discharging periods and others. They concluded that the AC system incorporated with PCM showed better performances. Figure 0-21 shows their investigated experimental system. Chaiyat [62] installed a PCM bed in the return duct of an AC system (Figure 0-22) in order to reduce the air temperature that enters the evaporating coil and thus improving the cooling efficiency of the AC.

A tube-in-tank off-peak PCM storage system shown in

Figure 0-23 , incorporated in a domestic chiller, was modelled and simulated by Bruno et al [63] using ε-NTU technique (effectiveness-number of transfer units) to determine the instantaneous heat transfer. Zhao and Tan [64] aimed to increase the cooling COP of a conventional AC by integrating a shell-and-tube PCM thermal storage unit that uses water (for charging loop) and air (for discharging loop) as a HTF. Figure 0-24 shows the AC integrated with PCM and a cross-section of PCM thermal storage unit. They investigated the impact of HTF mass flow rate, inlet temperature and fin height on PCM system performance. Results showed that optimization should be carried out, depending on the cooling load profile, in order to design HTF mass flow rate and fin height. The air-conditioning systems combined with PCM applications are summarized in Table 0-5.

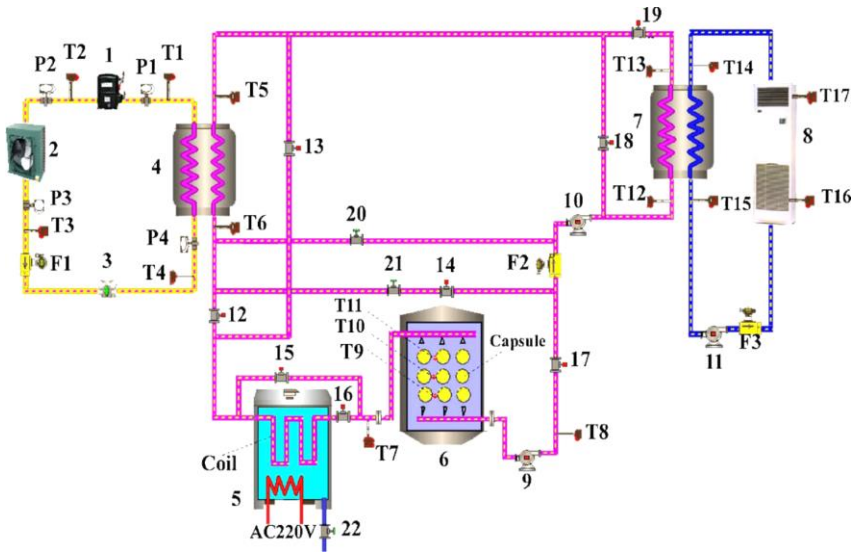

Figure 0-21: Schematic diagram of the AC experimental system with PCM [61]

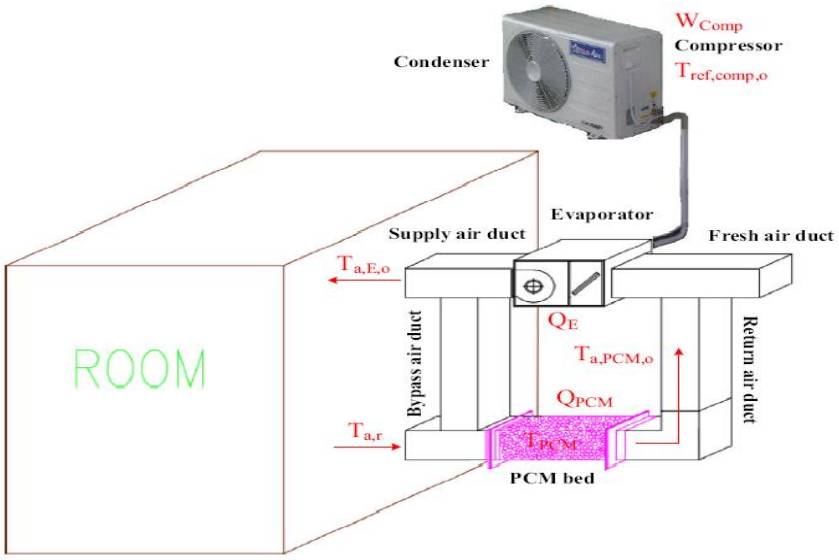

Figure 0-22: prototype of the air-conditioner integrated with the PCM bed [62]

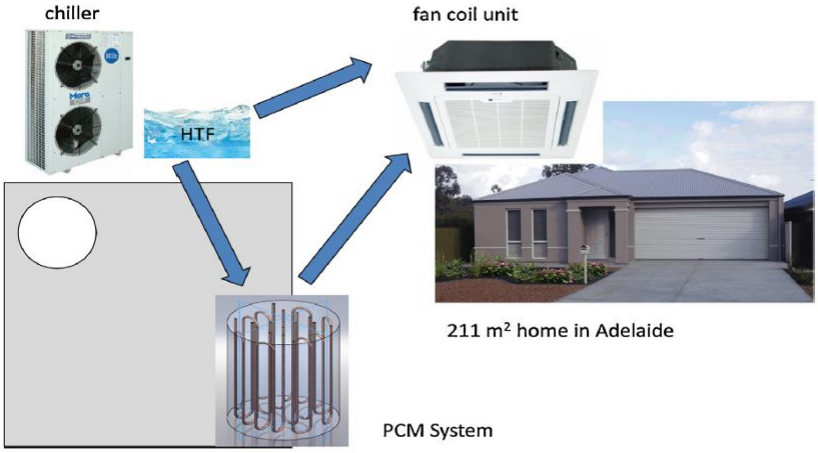

Figure 0-23: schematic diagram of domestic cooling system with PCM storage unit [63]

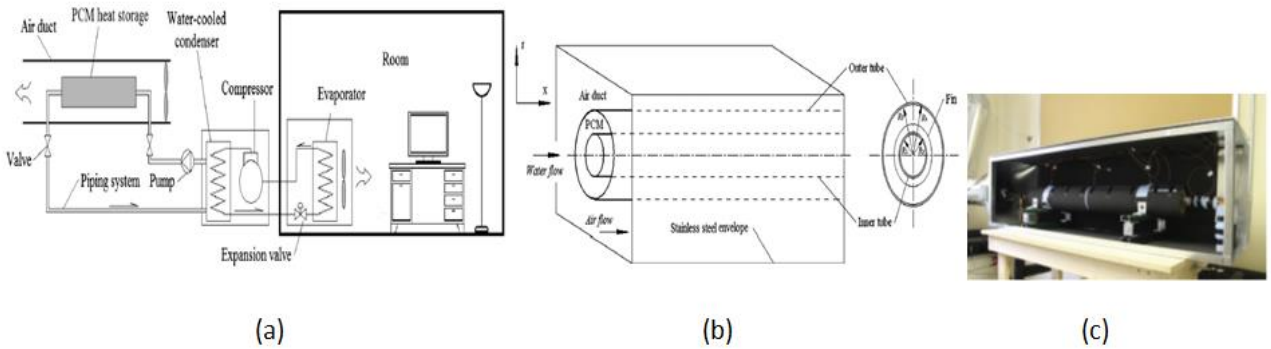

Figure 0-24: (a) Schematic diagram of AC integrated with PCM thermal storage, (b) cross-section of the PCM thermal storage unit, (c) photo of PCM thermal storage unit during heat charging process [64]

Table 0-5: PCM-air conditioning system applications

Ref./ Type*	Location/climate	Used PCM	PCM-AC system	Results
[61] E	Lab experiment in china	Water used as PCM (183 spherical capsules)	cold storage AC system with spherical PCM capsules packed bed, consisting of refrigeration & charging and discharging circulation systems	- In case of charging: cold storage rate ↘↘ from 12.3 kW to 2.2 kW & cold storage capacity= 59.7 MJ - In case of discharging: cold discharge rate ↘↘ from 8.5 kW to 3.4 kW & cold storage capacity = 45 MJ - Outlet air temperatures remained between 20.7 °C & 24.4°C.
[62] E,S	Chiang Mai, Thailand	-RT20 - Tm~19–22°C	-PCM in group of plastic balls kept in packed bed with thickness 40cm.	- Use of packed ball bed of PCM → significant reduction in energy consumption of air-conditioner for air cooling. - Electrical power of PCM-air conditioner system could be saved~9%. - The payback period of PCM~4.12 y. - PCM ball integrated with air-conditioner seemed beneficial &highly effective.
[63] S	Adelaide, Australia / semi Mediterranean climate	-Hf= 220 kJ/kg, ρ= 1200 kg/m^3 , ks= 1.5 W/m K. & kl= 1.2 W/m K -Different Tm = 0,4,7,10°C	PCM thermal storage unit coupled to chiller with an inverter driven scroll compressor	- 85% of energy consumption for cooling shifted to off-peak period. -Tm & Ts ↗↗ → energy consumption ↘↘ - PCM with Tm= 4°C→ possibility to attain an energy saving for cooling. - PCM with Tm=10°C → energy savings~ 13.5% -Energy usage ↗↗ with a more efficient PCM storage system. - Optimal charging during coldest time at night → energy consumption ↘↘ - kl ↗↗ → amount of discharging at daytime ↗↗ & significant load shifting
[64] E,S	Laramie, Wyoming, USA	- PCM RT22 -Tm=19–23°C (main peak: 22) - m_{total} PCM~ 6.3 kg	-AC integrated with shell-and-tube PCM thermal storage system - Function of PCM: heat sink to the AC during day cooling period.	- In heat charging process: T_{inlet} HTF (water), mass flow rate & fin height ↗↗ →PCM heat charging rate↗↗ & total charging time is shorter. - In heat charging process: HTF (air) mass flow rate↘↘ → save fan energy consumption. - Effectiveness of PCM storage system > 0.5. - PCM storage system instead of conventional cooling tower for a water-cooled AC → COP ↗↗ by 25.6%.

[65] S	Nagoya- Japan	PCM mixtures of paraffin waxes	Air distribution system (AC) equipped with a PCM storage tank for peak shaving	-In Nagoya, 400 kg of PCM for 73.8 m2 of room surface (5.4 kg/m2) are optimum values to maintain a constant room temperature without the need of cold source operation. - Appropriate PCM melting temperature was about 19°C.

*(E: experimental, S: simulation)

3.4. Evaporative and radiative cooling systems

Direct Evaporative cooling strategy is a way to cool the air by evaporation of water. More precisely, evaporation of water allows the absorption of the heat and thus the air is cooled. After evaporation, the water vapor transfers the absorbed heat to the air as latent heat. Thus the humidification of air occurs and the total enthalpy of air barely changes. The cooled and the humidified air are therefore used for cooling purposes in building especially under dry and hot climates. Indirect evaporative cooling is more suitable for humid climates, due to the humidity added to the air by separating air and water. The evaporative cooling system is investigated in the Darmstadt house (2009) [66]. Other attractive cooling strategy is the night radiative cooling (losing heat by thermal radiation), suggested by the Technical University of Madrid in 2007 and used by Hegger et al.[67] [66] in the Darmstadt house (2007). Moreover, Zhang and Niu [68] investigated a hybrid system (Figure 0-25) which is a combination of a nocturnal radiative cooling coupled with microencapsulated PCM slurry storage tank (Tm=18°C) in order to evaluate its cooling performance in buildings. The investigations were carried out under different climatic conditions in five cities in China (from north to south: Urumqi, Beijing, Lanzhou, Shanghai and Hong Kong). The results showed that the energy savings in Lanzhou and Urumqi are up to 77% and 62% for low-rise buildings respectively, and Hong Kong under hot and humid climate showed the weakest performance. Authors recommended using this hybrid system in cities where the temperature is low at night and the weather is dry (north and central china).

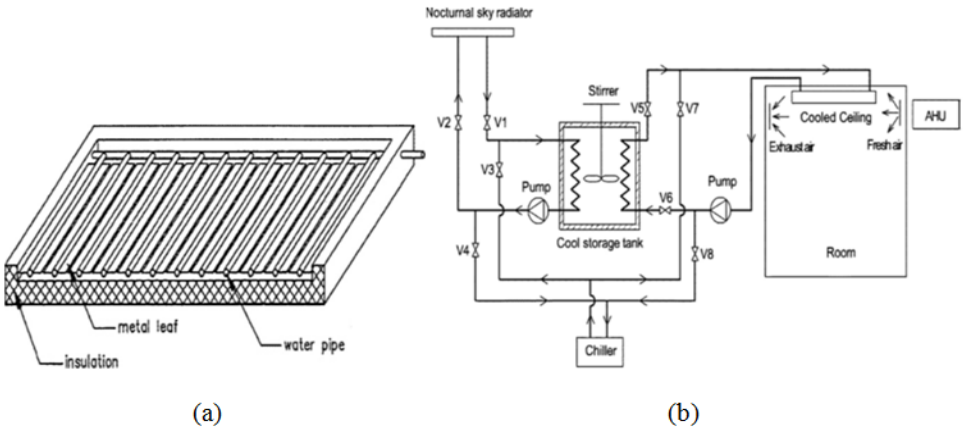

Figure 0-25: (a) Construction of the nocturnal sky radiator, (b) Schematic diagram of the hybrid system [68]

Ansuini et al. [69] developed radiant floor panels with granulated PCM showed in Figure 0-26 (Ts=24°C and Tm =29°C) with incorporated pipes for heating and cooling. The primary results showed that the PCM panels could be useful in summer but their performance was unhelpful in winter. The increased resistance between pipes and the melted granulated PCM is the cause of the bad performance of PCM panels during the heating season. With the aim to decrease the thermal resistance of granulated PCM, a special steel matrix (act as thermal diffuser) was designed to optimize the internal structure of the radiant floor. A numerical simulation was carried out after this optimization in winter, mid-season and summer season. It was concluded that in summer season, the quantity of cooling water to keep the temperature in comfort range was reduced by 25%, however in winter season there is no effect. In the mid-season, the floor temperature peak was reduced by about 3.5°C. This system is effectively beneficial to maintain the room temperature comfortable without any extra energy source.

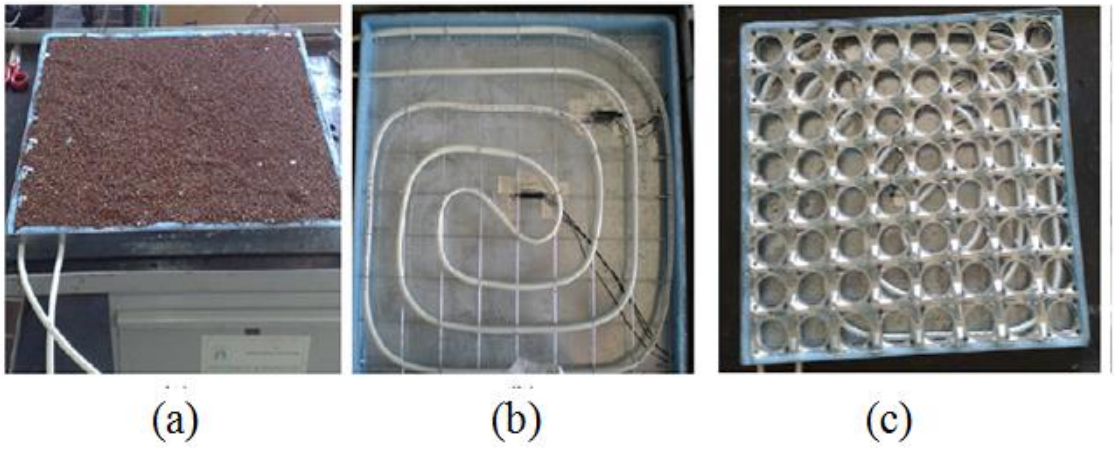

Figure 0-26: (a) metal container with pipes and supporting metal net, (b) specimen filled with the granular PCM (c) optimized specimen with the steel matrix [69]

Wang et al. [70] proposed a hybrid system consisting of cooled ceiling , microencapsulated PCM slurry storage (hexadecane C16H34 particles and pure water, Tm=18.1°C) and evaporative cooling technique shown in Figure 0-27. They evaluated the system in five cities in China under different climatic conditions. The cooling energy produced by the evaporative cooling system is stored by the MPCM slurry storage. The results showed that energy savings reached 80% under northwestern Chinese climate (Urumqi), about 10% under southeastern Chinese climate (Hong Kong) and between these two values for the other three cities (Shanghai, Beijing, Lanzhou). This hybrid system is suitable for cities under dry climate with high diurnal temperature difference.

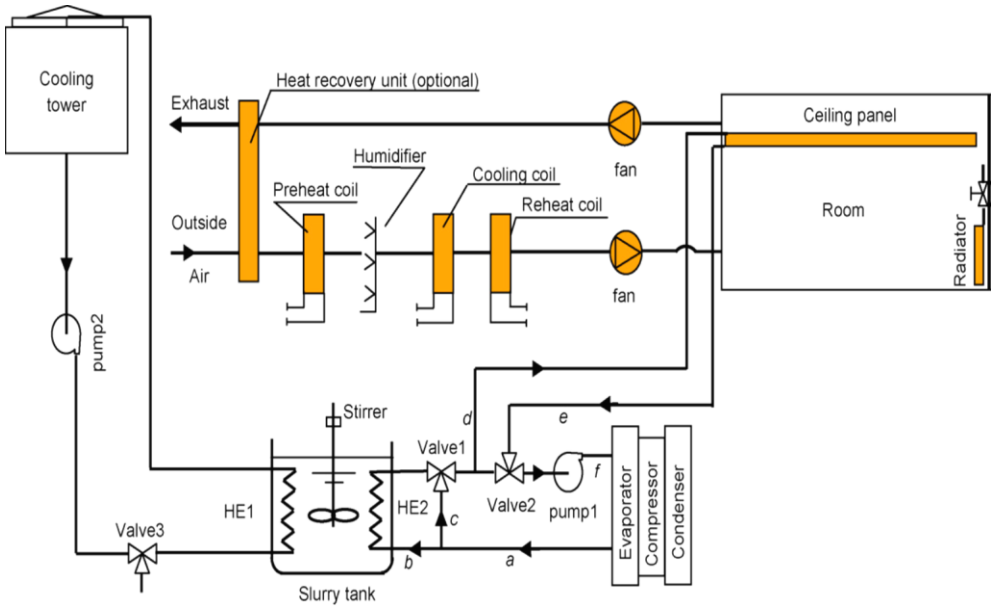

Figure 0-27: Schematic diagram of the hybrid system [70]

3.5. PCM in building envelope

The previous sections presented PCM used as separate storage unit installed with other mechanical equipment which were considered mostly as active systems. The installation of such systems needs a specific place in the building, which is considered an important disadvantage for the designers and users. As a solution for this drawback, PCM can be integrated into building envelopes i.e. walls, roofs, and floors as part of building structure or as building component and can be installed whether in passive or active system. The PCM integration into the building envelopes has attracted a great interest in the last 10 years.

3.5.1. PCM passive system applications in the building envelope

Some authors [7][66] classified passive system applications in the building envelope into two main categories:

- PCM "integrated" into building materials: when they are incorporated to a building construction material such as plaster with microencapsulated paraffin, gypsum plasterboards with microencapsulated paraffin, concrete with microencapsulated paraffin, panels with shape-stabilized paraffin [7], and blending PCM with thermal insulations. The main benefit of PCM-enhanced insulation is their capability to reduce and shift significantly the peak hour thermal loads of the building envelopes [12]. The team of Germany (2009), in a group work [67], have used microencapsulated PCM integrated into drywall panels as the interior finishing of a German house for cooling periods. These panels contain Micronal microscopic polymer spheres filled with paraffin wax developed by BASF Company. The selected PCM (Tm=26°C) starts to absorb heat when the

room temperature rises above PCM melting temperature, reducing overheating, where excess heat is stored in the walls. At night the heat is discharged, since the air temperature drops below the PCM switch temperature thanks to night ventilation. As a result, a more regular space temperature is provided, since temperature peaks are cut off, and thus the need of a mechanical conditioning system is minimized [66].

- PCM as "component": The main difference between building components equipped with PCM and PCM integrated into building materials is that a component can be manufactured before the building being constructed and have a particular design. Blinds with integrated PCM are considered as an example for PCM component. In fact, solar gains through windows are considered one of the major sources of heat input into a building. Thus, to avoid direct solar radiation, blinds equipped with PCM (Figure 0-28) can be used, it can be fixed inside the building or outside in front of the window. Integration of PCM into the internal blinds can reduce and delay the temperature rise of the blinds, and then the heat release into the room is delayed. The notion of internal blinds with integrated PCM is shown in Figure 0-29. The company ZAE Bayern and Warema (project "Innovative PCM-technology") [7], have tested a room under realistic conditions to investigate the reduction and the delay of the temperature rise of the blinds by integrating PCM. Compared to the conventional blinds, the room air temperature was around 2 K less; the temperature-rise of the blinds decreased approximately 10 K, and was delayed by about 3 hours. The numerical simulation showed that the operative temperature of the room decreased approximately 3 K and the thermal comfort in the room improved largely.

Figure 0-28: Internal blinds with integrated PCM [7]

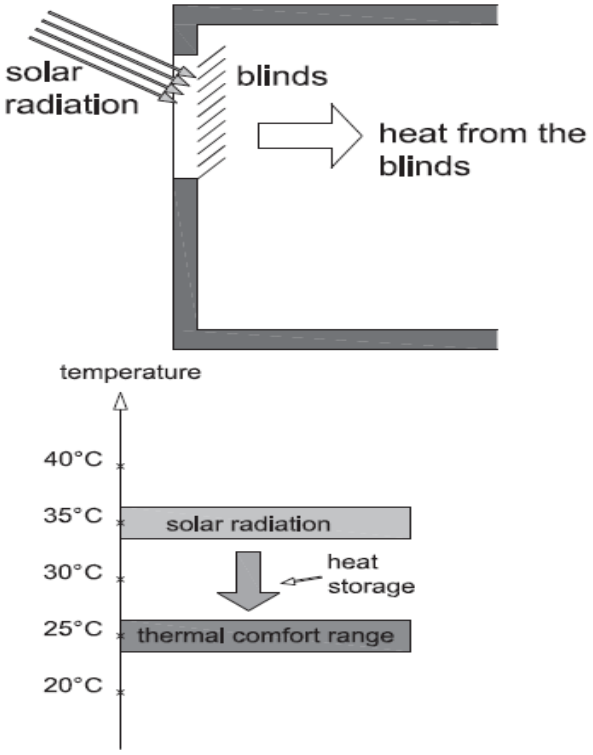

Figure 0-29: Internal blinds absorb solar radiation in order to cool the space by reducing the solar heat input [7]

Suspended ceilings with PCM are considered as an example for PCM component; salt hydrates are used and are encapsulated in plastic containers, in bags or in metal containers. The company Dörken sells a full range of PCM under the brand name DELTA®COOL system and it can be installed in ceilings or floors [7]. A system was designed by Ontario team [66] using the commercial PCM product DELTA-COOL 24 shown in Figure 0-30 which consists of salt hydrates encapsulated in 15 mm polypropylene panels with a melting temperature of 24 °C, and a solidification temperature of 22°C. A gross area of 62.1 m^2 of PCM panels was installed; each panel had a heat storage capacity of 62.6 kWh, with a melt enthalpy of 158 kJ/ kg. The team used "DRSS" concept to develop a house envelope, where exterior shades are one of the basic components that respond to the change of external conditions. The shades change their angles between perpendicular and parallel to the sun's rays as required, keeping the indoor temperature comfort. During the day, when cool is needed, the shades eliminate undesirable solar gains by preventing the solar radiation to reach the glazing, PCM remove the excess heat and then reduce the cooling peak. During the night, the PCM release the stored heat into the cool night air due to the activation of an air force night ventilation system.

Figure 0-30: Delta Cool 24, upper face of PCM panel [7]

Moreover, Kalnæs et al. [71] presented many examples of integration of phase change materials for passive systems, exploring possible areas and materials where PCM can be usefully incorporated. And they divided these examples to five different categories according to the location of integration of PCM: in walls, floors, roofs, windows/shutters, concrete, thermal insulation materials and furniture. Moreover, Pomianowski et al. [72] presented various construction materials of the building (gypsum and wallboards, concrete, bricks) which were blended or combined with PCM in passive systems. Zhue et al. [73] presented an extensive list of PCM passive systems investigated experimentally with important results. Different possibilities of the use of PCM and their application in the American Solar Decathlon, including the descriptions of the systems and the factors that affect their performance, as well as results of simulations and experimentation were presented by Ubinas et al.[66]. Soares et al [74] also explored PCM application in passive systems, and investigated the effect of these systems on the energy performance of buildings. Some examples of passive system applications are presented in the following, according to the location of PCM integration:

- *PCM in wall/wallboard*: Installation of PCM wallboards in the inner side of the building envelope is the most general and suitable solution for implementing PCM into buildings. Figure 0-31 shows PCM gypsum board. During the last years, many studies (numerical/simulation, experimental or both) investigated a large variety of this type of materials. Scalat et al. [75] believed that the human comfort can be maintained for longer periods using PCM wallboard, after the heating or cooling system was stopped. Kuznik et al. [76] investigated a renovation project in the south of Lyon-France using PCM wallboards. By testing a room in the same building that was renovated without PCM and then comparing it to the room with PCM, they concluded that the PCM increased the indoor thermal comfort, but it appeared unable to use its latent heat storage capacity for a number of durations due to the incomplete discharge overnight. Athienitis et al. [77] investigated the thermal performance of PCM gypsum board in a direct-gain outdoor test room. The results showed a reduction of the room temperature by a maximum 4°C during the daytime. Neeper [78] investigated the thermal dynamics

of room with fatty acid and paraffin waxes gypsum wallboard. The results showed that the maximum diurnal energy storage is occurred when the melting temperature of PCM was chosen close to the average room temperature.

Figure 0-31: PCM enhanced gypsum board [12]

-*PCM in floors, roofs and ceilings:* Incorporation of PCM in floors that are in direct contact with solar radiation could be an effective solution for thermal energy storage. Xu et al. [79] investigated the thermal performance of PCM floor system in passive solar buildings. This performance is affected by several factors such as the choice of covering material, thickness of PCM layer, PCM melting temperature, its thermal conductivity and heat of fusion, and the air gap between the PCM and covering material. The results showed that the thickness of PCM should not be greater than 20 mm and the heat of fusion and thermal conductivity of PCM should respectively exceed 120 kJ/ kg and 0.5 W/m K.

Incorporation of PCM into roof systems has not gotten too much attention, Pasupathy [80] investigated the performance of a double layer of PCM incorporated into roof in Chennai, India. Inorganic eutectic of hydrated salts used as PCM was incorporated into roof panels of a room and then it was compared experimentally to a room without the PCM panel. The results showed that the indoor air temperature swings can be narrowed due to the PCM roof panel, and that this system can be suitable all seasons when the upper PCM layer had a melting temperature 6–7°C greater than the ambient temperature during summer and the lower PCM layer had a melting temperature close to the indoor temperature. A naturally ventilated roof with a photovoltaic (PV) module with PCM in Oak Ridge, Tennessee was developed by Kosny et al. [81]. Reducing heating loads and cooling loads during winter and summer respectively was the main objective of this system, in winter PCM absorb heat during the day and release it at night while in summer PCM absorb excess heat. The results showed that heating loads and cooling loads were reduced by 30% and 55% during winter and

summer respectively; additionally, it was observed that peak daytime roof heat fluxes were reduced by about 90%.

-*Windows and shutters:* In cold climates great parts of energy are lost due to glazed facades, which increase the need for heating while in warm climates excessive solar heat gain increase the need for cooling, Figure 0-32 shows PCM filled window. Ismail et al. [82] investigated a glass window in a hot climate (Brazil) with incorporated PCM. After comparing PCM window with another glass window filled with absorbing gas, it was shown that the amount of heat penetrating into the room was reduced while PCM melts, even though the U-value of windows was increased due to addition of PCM. Goia et al. [83] studied the effect of PCM incorporated into glazing on the thermal comfort in three different seasons. After comparing the PCM prototype to a traditional double glazing, it was shown a significant improvement in thermal comfort conditions during all periods of the year except on cloudy days. Additionally, the authors emphasized the importance of the correct selection of PCM melting temperature. Weinläder et al. [84] investigated a solar shading system with integrated salt hydrate PCM having a melting range between 26°C and 30 °C in office rooms. After comparing rooms with PCM blinds to rooms with traditional blinds, it was shown that the air temperature is lower by about 1-2K in the PCM blinds room in summer while in winter PCM blinds do not affect the heating power. It was found that the main problem of PCM blinds is their renovation at night. The use of mechanical or natural ventilation was useful to fully regenerate the PCM at night.

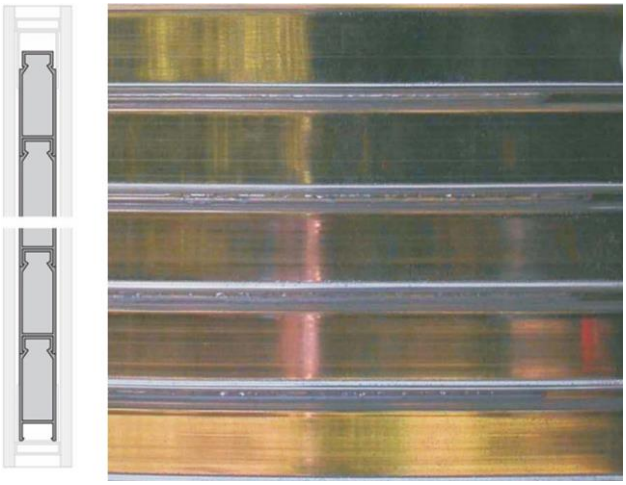

Figure 0-32:Illustration of a PCM filled window [71]

-*PCM in Concrete*: The general objective of incorporating PCM in concrete materials is to increase heat storage of heavy construction materials in buildings. A number of studies have been carried out on PCM incorporated into concrete and have shown positive results such as reducing indoor temperatures in warm climates. Entrop et al. [85] investigated experimentally the performance of PCM incorporated into concrete floors. Two rooms with PCM concrete floor as well as two rooms with regular concrete floor were constructed. The results showed that this application leads to

decrease the temperature fluctuations in the room. Cabeza et al. [86] presented a similar research, where two identical cubicles made of concrete were tested experimentally. The first one was built of traditional concrete and the other one of new concrete with microencapsulated PCM. The results showed a reduction in temperature fluctuation in the room with PCM. Arce et al. [87] continued the work presented in [86]. One of the most important obstacles found in [86] was the strong effect of solar radiation and high outdoor temperature peaks on PCM effectiveness during the summer, which leads to incomplete solidification during the night. The principal aim of this application was to rise the PCM's operation time in order to resolve the PCM cycling problem. Results showed a slight reduction in temperatures. The PCM stayed active for at least 4% more time and the problem of high temperatures was not completely solved. Royon et al. [88] tested the potential of filling hollow concrete floor with paraffin PCM having a melting temperature of 27.5°C. In summer, the results showed that the temperature was lower in the hollow concrete building which allows using such system as a passive thermal conditioner. Other passive system applications for cooling purposes [89-107] are presented in Table 0-6.

Table 0-6: PCM Passive system applications in the building envelope for cooling purposes

Ref./ Type*	Location/ climate	Used PCM properties	Installation/Strategies	Results/Conclusions
[7] S	Austin, USA / humid subtropical (hot summers and mild winters)	-PCM/graphite composite: Tm=21°C, Ts=19°C -paraffin wax: Tm=21.7°C, Ts=18.7°C -encapsulated organic material: Tm= 23°C, Ts=22°C -Encapsulated octadecane: Tm= 25.3°C, Ts=26.3°C	- Layer of PCM plasterboard located in 3 different placements with different thicknesses. - Set-point temperature schedule is created (the charging cycle of PCM is controlled).	- Use of Encapsulated octadecane→ lowest required cooling loads. - Surface area ↗↗& thickness of PCM↘↘ → more effective. - Cooling demand depends on charging cycle and peak load varies depending on set point temperature schedule. - Adding natural ventilation does not have an important effect in reducing energy consumption.
[87] E	Lleida – Spain	Microencapsulated PCM (Micronal® from BASF), Tm = 26°C & Hf = 110 kJ/kg	-PCM integrated into concrete walls Figure 0-33 (concrete contain about 5% in weight of PCM). - Awnings added to provide solar protection, reduce high wall temperatures and allow PCM solidification overnight - Two operation modes: free-cooling (windows opened only at night) and	- Using awnings → reduction of temperature peak = 6% (3–4 °C), increasing of active hours ~4–10%, & increasing in comfort time ~10–21%. - Delay of peak hours increased 36% in case of free-cooling while in case of open windows it decreased 14% - PCM phase change cycles still incomplete.

			open windows (all the time).	
[89] E, S	Tianjin-china / warm temperate semi-humid continental with cold winters and hot dry summers	-Capric acid (CA), Tm=303.35K. -Capric acid and dodecanol (CADE), Tm=299.65K. -Cp and K varies with temperature.	-2 operation mode: free cooling &opening window at night (natural ventilation) - CA panels on the outside surface of walls and roofs (PCMOW) -CADE panels on the inside surface of walls and roofs (PCMIW) Figure 0-34	- Inside surface temperatures of walls and roofs in PCMOW & PCMIW rooms < than that in room without PCM. - Performance of PCMIW is better than PCMOW especially with the condition of natural ventilation. - When PCM room temperature > comfort temperature (26°C)→ active cooling should be operated. - Heat that should be removed (ROH) is lower in case of natural ventilation than the free cooling condition. - Reduction of ROH for PCMIW up to 80%.
[90] S	Kuwait / hot climate	- n-Octadecane, Tm=27°C -n-Eicosane , Tm=37°C -P116, Tm=47°C. - Different geometries of PCM container.	- Roof-PCM system: concrete slab with cone frustum holes filled with PCM Figure 0-35. -Reducing heat flow from outdoor to indoor space by absorbing heat gain in the PCM before it reaches the indoor space.	- Significant reduction in heat gains. -heat flux reduction at the indoor space~39%. - N-Eicosane performed better than other tested PCMs. -Regarding thermal effectiveness →conical geometry is the best as a PCM container.
[91] S	-Shenyang/ severe cold - Zhengzhou/cold -Changsha/ Hot summer and cold winter -Kunming/mild -Hong Kong/ Hot summer and warm winter	octadecane paraffin with different Tm= 23,24,25°C	- PCM board (PCMB) integrated into interior surface of an external wall. - Natural cold source - reducing the utilization of AC system leading to electricity savings.	- PCM phase transition temperatures↗↗ → energy savings ↗↗ - Use of PCMB did not provide economic benefit from reduced AC utilization. - Mean electricity savings ratio =13.1%. - Optimal Tm > mean outdoor air temperature + 3°C → acceptable SPP - Colder regions → lower Tm are required - Hotter regions→higher Tm are required
[92] S	Kuwait/ hot climate	-n-Octadecane, Tm = 27°C, -n-Eicosane, Tm = 37°C, -P116, Tm = 47 ◦C, -thickness of PCM shutter varied between 0.01& 0.03 m.	-window shutter filled with PCM -Reducing solar heat gain in building through windows by absorbing it before it reaches indoor space.	-PCM with highest Tm = 47°C (close to upper temperature limit of windows) → best thermal performance. - P116 shutter → heat gain reduction= 23.29% with thickness =0.03 m to absorb large quantity of heat during the daytime.

[93] S	Beijing, China	-Different Tm, Hf, K & thickness of SSPCM -Different ACH at night and day.	-SSPCM plates as inner linings of 4 walls & ceiling. -SSPCM plates combined with night ventilation without active AC -Natural ventilation in the day and mechanical ventilation at night.	- Reduction of daily maximum temperature by 2°C -Indoor comfort improved especially in early summer days. - Optimum values for Tm, Hf, K & thickness of SSPCM are: 26°C, 160kJ/kg, 0.5w/m. °C & 20 mm respectively. - ACH at night should be at the highest possible level but ACH at daytime should be controlled. - SSPCM plates useful for free cooling application in summer.
[94] S	Hong Kong Subtropical (Hot humid summer-short mild winter)	Energain® -PCM wallboard composed of 60% microencapsulated paraffin, Tm=21.7°C	5mm PCM layer wallboard incorporated into external walls in different orientations.	- PCM integrated in eastern & western walls → better performance. - Temperature of interior surface of PCM wall stays above 28°C > Tm. - Higher Tm of 28°C-30°C should be investigated in subtropical Hong Kong climate.
[95] S	London, UK/ summer months.	- PCM with different Tm = 23, 25,27◦C, & with thicknesses of 12, 24, 36, 48 and 60 mm - wide air gaps =15, 20, 25, 30 and 35 mm	- PCM installed in the inner side of wall construction system Figure 0-36. - Integrating PCM with naturally ventilated air gaps in building envelope - Air gap is similar to ventilated façade & provides extra insulation and airflow.	-In terms of annual energy consumption (KWh/m^2) : the optimum values for Tm, PCM thickness and air gap width are 25°C, 48mm and 25 mm respectively. - Application of PCM in building reduces overheating problems & improves indoor temperature in hot periods. - Effectiveness of PCM becomes higher as temperature rise to year 2080 levels.
[96] E	Lawrence, KS, USA/ cooling seasons under full climatic conditions.	- Hydrated salt-based PCM, Tm range=18–38°C, peak Tm= 31.36 °C, starting Tm= 24.79°C - m_{total} PCM =1.5 kg/m^2	- PCM contained in thin polymer pouches, arranged in sheets laminated with aluminum foil Figure 0-37. -PCM thermal shield (PCMTS) integrated as thin layers at five locations at different depths between insulation boards & wallboard in the west & south walls	- Optimum location of PCMTS is at 1.27& 2.54cm from the wallboard in west & south wall respectively. - Peak heat flux reduction is 51.3% for south wall and 29.7% for west wall. - Peak heat flux time delayed by 6.3 h in south wall when PCMTS is next to wallboard & 2.3 h in west wall when PCMTS at 1.27cm from wallboard. - Daily heat transfer reduction= 27.1% in south wall (PCMTS at 2.54 cm from wallboard) & 3.6% in west wall (PCMTS at 5.08 cm from wallboard).
[97] E,S	Weimar, Germany	Microencapsulated paraffin with	Paraffin-modified gypsum plaster (with salt	- Peak temperature reduction~4 K. - PCM loses its storage capacity if it cannot be discharged at night after

		diameter =5 µm, Tm range= 25- 28°C.	mixture) applied on surrounding walls.	sequential hot days hence night ventilation should be used.
[98] S	Three US climate: Minneapolis, MN, Louisville, KY, and Miami, FL	-PCM wallboard containing paraffin with active temperature range of 25 °C to 27.5 °C - Volume fraction of PCM to gypsum is 25%.	PCM composite wallboard integrated in walls and roof in three different locations (exterior, center, and interior) of the multi-layered envelope surfaces	- Optimal PCM location exists depending on resistance values between external boundary conditions & PCM layer. -PCM wallboard in the middle of multilayered wall → best performance. - Use of PCM wallboard shift peak electricity load & decrease energy consumption in summer.
[99] E	Experimental room in china	Capric acid (CA) & lauric acid (LA) mixture, Tm= 20.4°C & Ts= 19.1°C.	PCM wallboards integrated in an ordinary wall (26% PCM by weight into gypsum wallboards)	PCM wallboard has high latent heat storage capacity & energy consumption in peak load shifted to off-peak load period.
[100] E	Hong Kong	Paraffin macro-encapsulated in stainless steel box k= 21.712 W/m K, Tm= 20.78°C, Hf =147.4 J/g, Ts=25.09°C, and Hs=146.9 J/g.	PCM incorporated in concrete walls in different positions: internally bonded, laminated within and externally bonded Figure 0-38.	- PCM in concrete walls regulates indoor temperature. - Effectiveness of PCM highly depends on its placement in concrete walls. - PCM laminated within concrete walls→ best temperature control: maximum temperature reduction~ 4°C. - PCM internally bonded→ best humidity control - Reduction of relative humidity providing indoor comfort. - Payback period of PCM application~11 years in public house in Hong Kong.
[101] E	Full-scale test room/ summer conditions (CETHIL-INSA de Lyon, France)	product from DuPont constituted of 60% of microencapsulated PCM with Tm=22°C.	PCM integrated in internal partition wall.	- overheating effect ↘↘ - Temperatures of wall surfaces ↘↘ improving thermal comfort conditions by radiative effects.
[102] E	Puigverd de Lleida –Spain	macro encapsulated PCM RT-27 paraffin, Tm =28°C & SP-25A8 hydrate salt, Tm= 26°C	-CSM PCM panels located between perforated bricks and polyurethane in western & southern walls and in roof Figure 0-39. -domestic heat pump as a cooling system.	- Peak temperatures reduction= 1°C, & daily temperature fluctuations were smoothed out. - In case of PCM cubicle (RT27 + PU)→ consumption of electricity reduction = 15% & CO2 emissions reduction~1–1.5 kg/year/m^2. -In case of PCM cubicle (SP25 + Alveolar)→ energy savings = 17% (2.7 kW h/m2/year).
[103] E	Solar house “Magic	ACUAL 20 PCM : multi-component mixture of	-PCM integrated in floor tiles Figure 0-40. -the tile basically consist of 4 pieces of pure clay	-PCM tiles placed in the floor are useful in summer season at night. - Tm↗↗ → the system work more efficiently as a heat sink.

	Box" located in the IES ("Instituto de Energía Solar" of Technical University of Madrid)	hydrocarbons of paraffinic composition with unsaturated additives, dyes and preservatives -Tm = 20°C &Ts=13.5°C	stoneware 20mm thick and a metal container (32mm thick) containing 4.8 l of paraffinic mixture.	- Higher effectiveness can be achieved in the sunny tiles.
[104] S	China	PCM mixture of Mn(NO3)2,6H2O and MnCl2,4H2O	-brick wall with Sierpinski carpet filled with PCM. - Thermal response of PCM brick wall is based on the enthalpy-porosity technique.	- Use of PCM in brick walls is useful for thermal comfort. - filling amount of PCM ↗↗ → temperature fluctuations ↘↘ - This model is verified experimentally.
[105] S	Periodic variations of temperatures	Salt PCM held in stasis by a perlite matrix.	-installed within the wall or ceiling insulation. - Delay peak AC request times until the evening. - 3 values of operative temperature were considered.	- With PCM, peak cooling loads reduction= 11–25%. - In case of ''insulation only'' peak reductions~19-57%
[106] E, S	Warsaw-Poland Marseille – France Cairo –Egypt / summer hot period	Bio-based PCM with properties determined by heat flow meter apparatus (HFMA).	Fiber insulations containing microencapsulated PCM integrated in the southern-oriented wood-framed wall.	Indoor set temperature = 24°C→ peak-hour heat gains ↘↘ for Marseille by 23–37% & 21–25% for Cairo; but no positive effects were observed in Warsaw.
[107] E, S	Chambery – France Catania – Italia	Paraffin (Micronal T23 BASF), Tm = 22°C & Ts = 28.5°C.	Wallboards made of aluminum honeycomb matrix contain 60% of micro-encapsulated paraffin installed in the partition walls of an office building.	- In hottest months, PCM average storage efficiency in Chambery and Catania is 50% & 39% respectively - PCM is liquid for approximately 60% of summer time. - PCM utilized only 45% of its latent heat. - Quantity & type of PCM depend on the season that one aim to improve.

*(E: experimental, S: simulation)

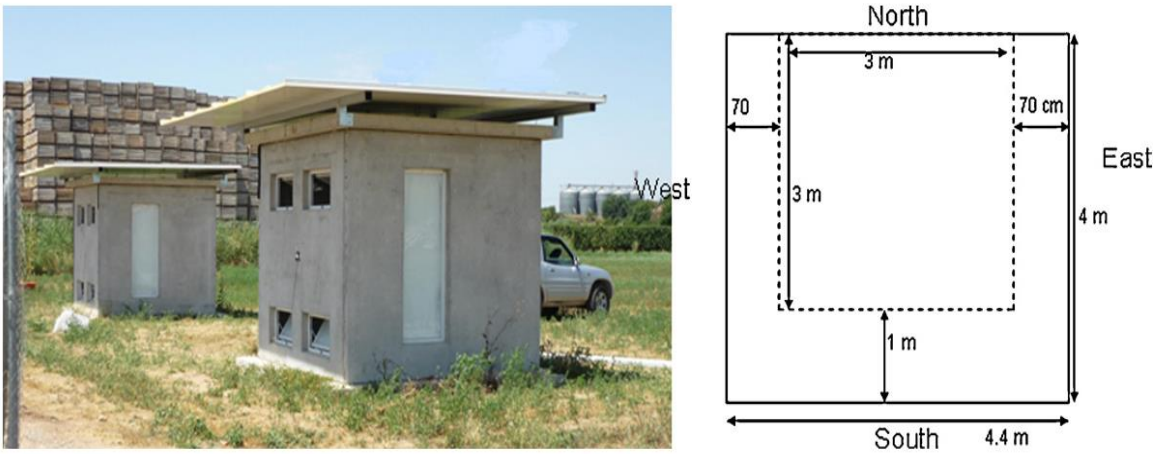

Figure 0-33: concrete cubicles with awnings (outer view and top view) [87]

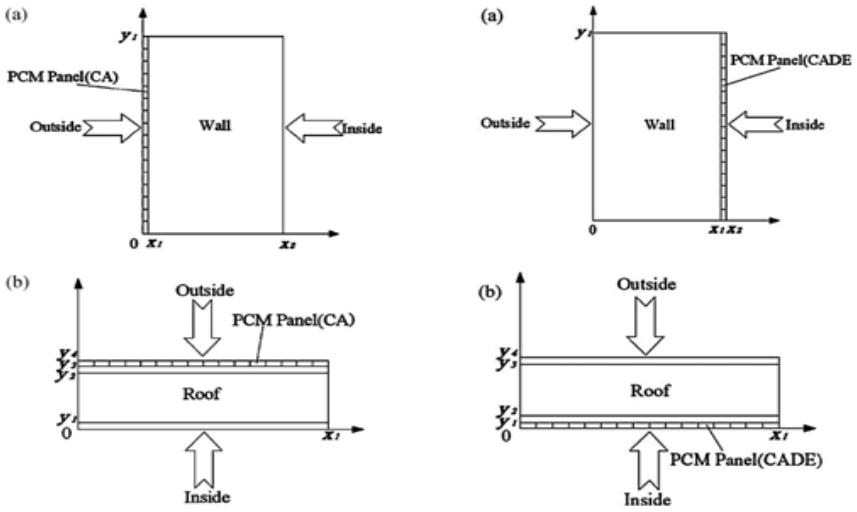

Figure 0-34: schematic of building envelope for PCM-OW(left) and PCM-IW (right) [89]

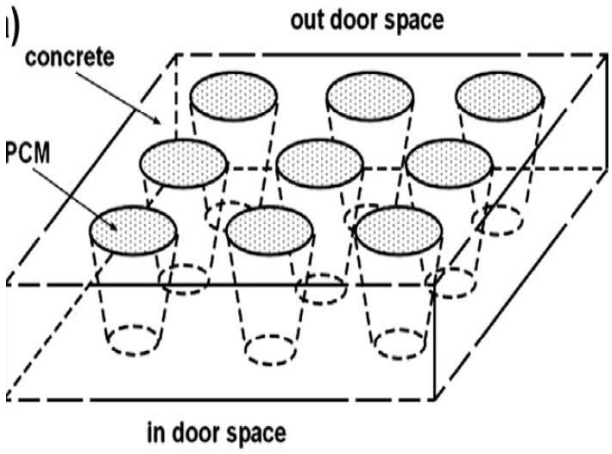

Figure 0-35: Schematic of the roof with holes filled with PCM [90]

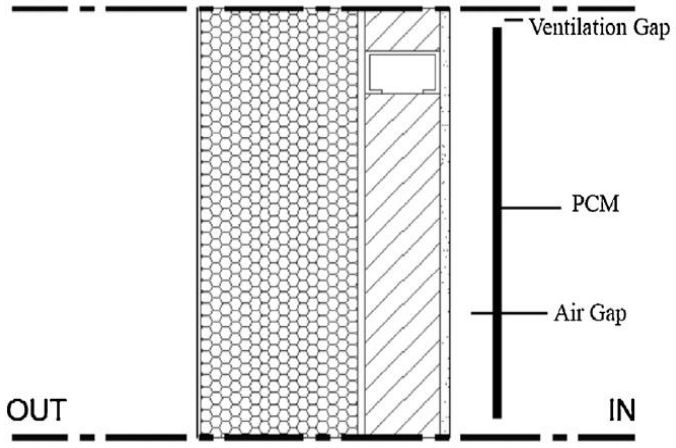

Figure 0-36: PCM installation in the wall with ventilation gap [95]

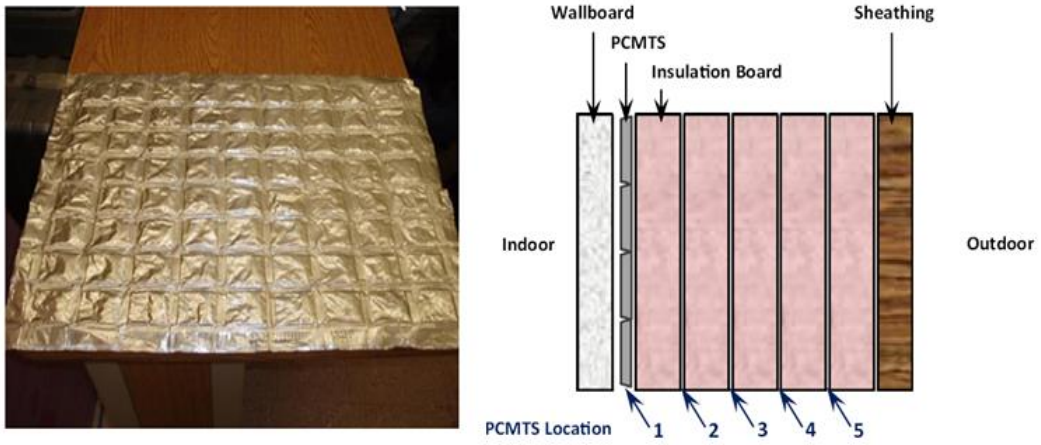

Figure 0-37: sheet of PCM thermal shield PCMTS (left) and wall section showing the PCMTS location (right) [96]

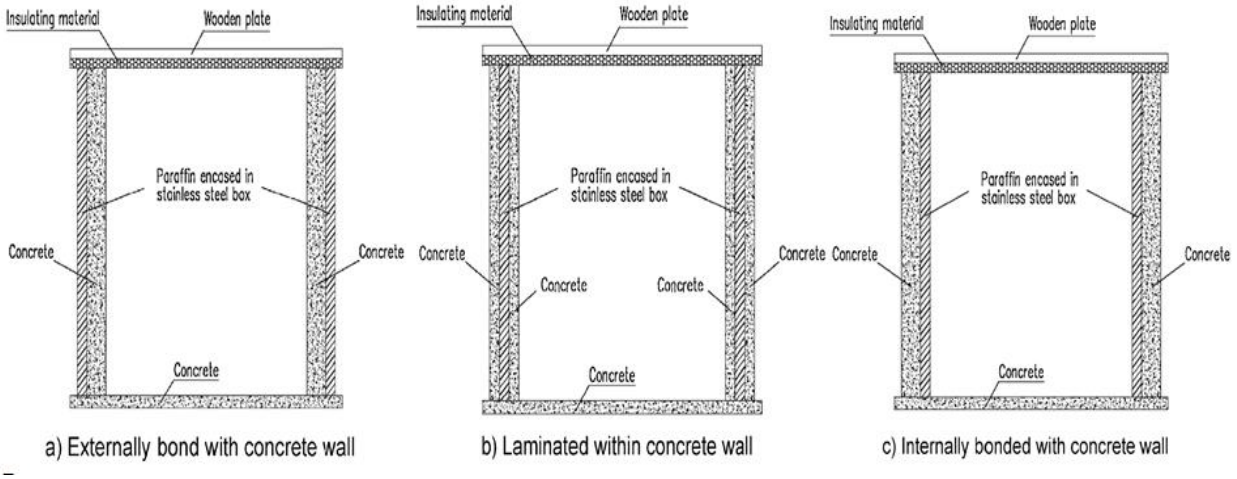

Figure 0-38: PCM layer: (a) Externally bond with concrete wall, (b) Laminated within concrete wall and (c) Internally bonded with concrete wall [100]

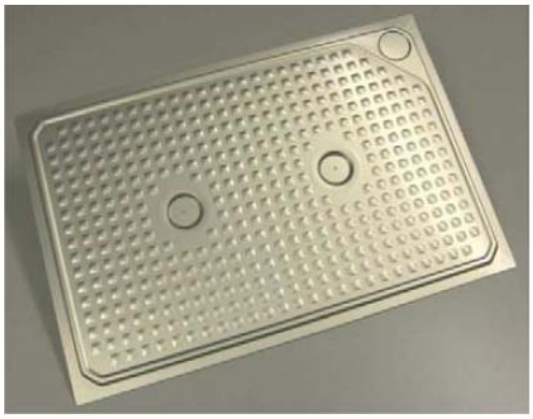

Figure 0-39: CSM panel containing PCM [102]

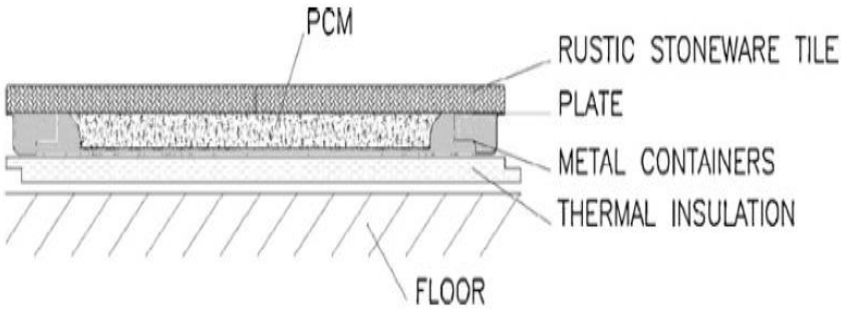

Figure 0-40: schematic of the floor with PCM integrated in tiles [103]

3.5.2. PCM active system applications in the building envelope

In contrast to passive systems for PCM integrated into building materials, PCM active systems lead to a better heat transfer coefficient by replacing the free convection by forced convection. The solidification of PCM actively can be accomplished with a minimum of energy with the help of small fans.

3.5.2.1. Active systems using air as heat transfer fluid:

- Systems integrated into the ceiling:

Providing a small fan into suspended ceilings to effectively discharge the absorbed heat, make it an active system [7]. A two-dimensional channel that directs the air flow is built in the ceiling construction. PCM located in this channel can be considered as heat storage. Cold night-air circulates in the channel, cools down the PCM and discharges the stored heat to the outside of the building. During the day, warm air from the room is compelled to move through the PCM, it is cooled and then provided to the room [108]. Figure 0-41 shows the general concept for cooling with PCM integrated into the ceiling.

The Swedish company Climator developed a system called “CoolDeck” shown in Figure 0-42. This system has been installed as part of a project in the town hall of Stevenage in England. The Cool Deck consists of the PCM C24, a salt hydrate encapsulated in bags with a melting temperature of about 24°C, a metallic channel to direct the air and a fan [109].

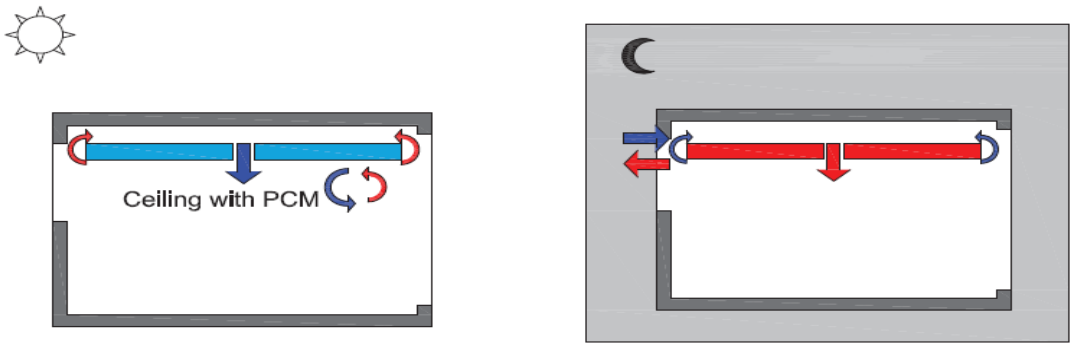

Figure 0-41: The general concept for cooling with PCM integrated into the ceiling [108]

Figure 0-42: Cool Deck C24 developed by "Climator" [7]

An active thermal storage unit in the ceiling was developed by the Team Germany (2009) [66].The application is composed of four insulated channels, with polycarbonate profiles filled with salt-hydrate PCM with a melting temperature of 26°C, the PCM system used is Delta Cool 28 by Dorken [67]. The team equips the channels with ventilation fans, grills, operable flaps, and temperature sensors. Depending on weather conditions, the COP of the system varies from 9 to 15. During the day, in cooling mode, the air in the room circulates through the ceiling and decreases its temperature. The cool air from outside, at night, blows across the ceiling and discharges the PCM.

- Systems integrated into the wall:

Since wall systems have been used for a longer time than other applications, the same concept is followed as for the ceiling in a wall construction. The system consists of bags filled with PCM, at the bottom a fan is used in order to transfer the air, openings at the top and the bottom allowing the intake and the exit of air from the room. However, it should be assured that the volume flow rate of air at

the exit does not lead to uncomfortable air velocities. An extra intake at the outside of the wall can be used optionally for direct absorption of cold night air [108].

- Systems integrated into the floor:

It is possible to integrate the same system as for the ceiling and for wall into the floor. The PCM can be directly located under the floorboards. Figure 0-43 shows the general concept for cooling with PCM integrated into the floor. During the day, the warm air from the room is taken away; it is cooled during the melting of PCM and then the cooled air is supplied back to the room providing cooling. At night, cold air circulates under the floor, cooling the PCM and discarding the stored heat [7].

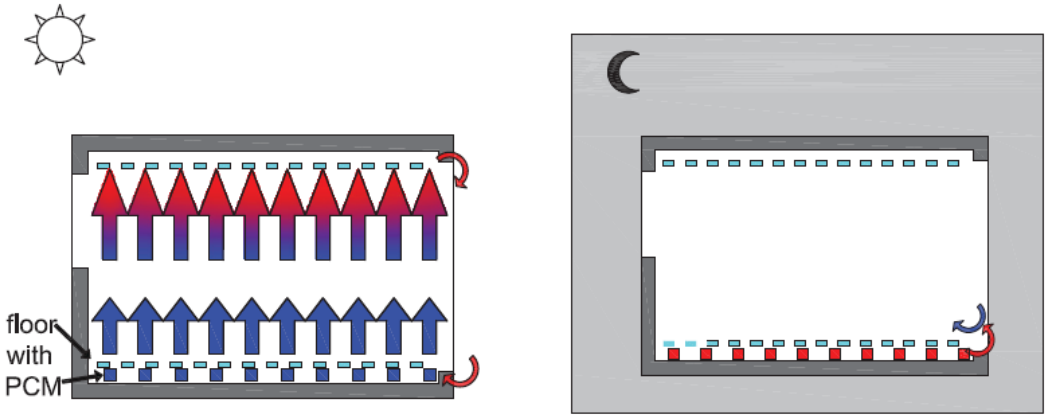

Figure 0-43: General concept for cooling with PCM integrated into the floor [7]

3.5.2.2. Active systems using a liquid as heat transfer fluid

Active systems with air thermal exchange used to reject the stored heat means that the cold night air is used as cold source. Regarding the energy consumption, it seems a very effective method, but it is not completely trusted that the night-air temperature drops to a temperature low enough to reject all the heat stored during the day [108]. It is possible to integrate systems with liquid-air thermal exchange to solve this problem, and to attach it to a cold source with a liquid heat transfer fluid.

• PCM-plaster with capillary sheets:

The capillary sheets can be fixed at the surface of the concrete wall and then cover it by a plaster layer with PCM. Integration of capillary sheets as heat exchanger into the wall is a general approach for the thermal activation of concrete walls [108].

• Cooling ceiling with PCM plasterboard:

Panels suspended from the ceiling are an example of this application; a plate for dry construction used as a wall or ceiling element, was developed by the Company ILKATHERM, which is made up of a pure-foam as an insulating layer located between two coatings made of plaster board, metal, plastics, or others [7] [108]. In this application, the coating can be PCM plasterboard. The construction and the installation of the PCM plasterboard are shown in Figure 0-44 and Figure 0-45.

Figure 0-44: Installation of ILKATHERM PCM board [108]

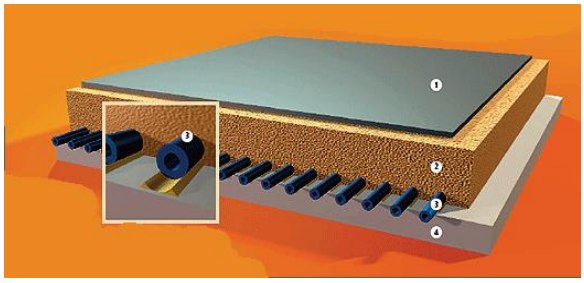

Figure 0-45: PCM board from ILKATHERM; 1) sheet metal coating, 2) PU rigid foam, 3) capillary tube mats, 4) Micronal PCM smartboard gypsum construction panel [108]

Incorporation of PCM in ceiling boards to act as air conditioning systems seems effective to shift peak loads. Kondo [110] developed a PCM ceiling board with micro capsulated PCM for an office building. At night, the cold air from the AHU flows into the ceiling and cool down the PCM ceiling board. During cooling time, the cool air from the AHU flows immediately into the room. During the peak load time, the warm air from the room circulates through the PCM ceiling board, where it is precooled before returning to the AHU. The results showed a reduction of the peak loads; however, an improvement of ceiling board is needed. Various numerical studies were also achieved on the thermal performance of this system [111][112]. Jin et al. [113] investigated an activated floor with two layers of PCM for cooling and heating. Their main objective was to find the optimal melting temperature for each PCM layer. The results showed a reduction of the floor surface temperatures fluctuations. The reduction of the fluctuations is caused not only by the latent heat capacity of PCM, but also by the implementation of additional high resistance of two layers of PCM with low thermal conductivity. Moreover, it was found that the optimal PCM melting temperature for heating and cooling were respectively 38°C and 18°C and the energy release during the peak period was increased by 41% and 38% for heating and cooling respectively. Other active system applications are presented in Table 0-7.

3.5.3. Ventilated facades principle and applications

To reduce the energy demand of a building, the careful design of its façade is considered as the most important method. Ventilated facades (VF) have been recently used in buildings and have attracted

great attention of architects and engineers, in order to fit the energy restrictions recommended by the European Directive (2010/31/EU) [114]. PCM can be introduced into the external layer of VF [115] or in its air cavity [116] [117]. During cooling season, VF with PCM can act as a free cooling system in order to avoid overheating and therefore minimize the HVAC energy consumption. VF or VDSF are considered as a special kind of envelopes, where in front of an ordinary building façade, a second skin is placed, and consequently an air cavity (channel) is created. In order to ameliorate the energy or thermal performance of the building, the air in the cavity can be naturally or mechanically ventilated [118]. Ventilated façades (VF) have the potential to ameliorate the energy efficiency of buildings, and it can be used in both new and refurbished buildings.

During the cooling period, the working principle of VF-PCM is to use the low temperatures at night to fully solidify the PCM, while during the day time, supply cold when it is needed by removing heat through melting of PCM. Figure 0-46 shows how a ventilated façade works:

(a) PCM solidification: occurs at night when the outdoor temperature is lower than the PCM phase change temperature, the air from outside enters to the channel leading to PCM solidification. To ensure the full PCM solidification, fans operating under various power rates can be used (mechanical ventilation instead of natural ventilation) increasing the convective heat exchange.

(b) PCM melting: during the day, PCM absorbs heat from the indoor air to provide cooling effect.

(c) Overheating prevention: after the PCM melting, due to the buoyancy forces, the air flows from outdoors to outdoors preventing the overheating in the air channel by natural convection.

(d) Free cooling: occurs at night when the outdoor temperature is lower than the indoor set point temperature.

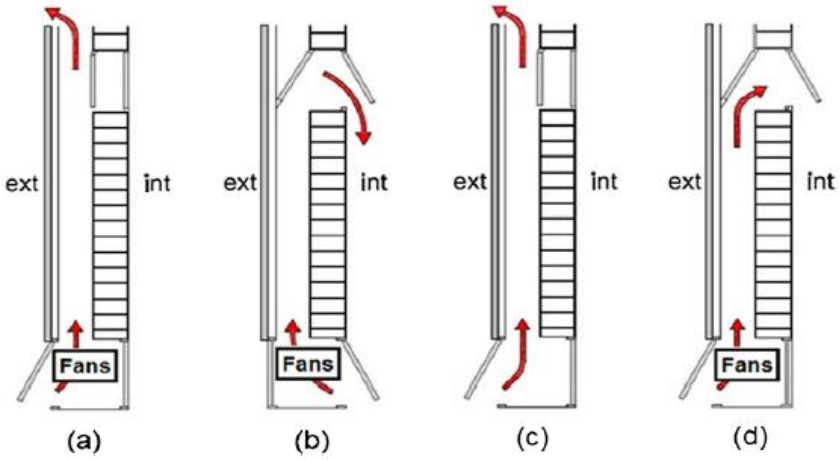

Figure 0-46: modes of operation of VF. (a) solidification process, (b) melting process, (c) overheating prevention, and (d) free cooling [116]

Ventilated facades with PCM were studied by many authors during heating period (winter season) [115][119]. However, Gracia et al. [116] investigated experimentally the efficiency of PCM-VDSF

in different cities under Mediterranean-continental climates in order to reduce cooling energy consumption; the used PCM is SP-22 with melting temperature of 21.5°C and solidification temperature of 18°C, 112 PCM panels were incorporated in the south wall and the air channel thickness was 15 cm. furthermore, natural or mechanical ventilation conditions were tested and three fans were used in the system in case of mechanical ventilation. They concluded that three possible benefits can be offered by the VDSF: free cooling, cold storage, and solar radiation protection. Free cooling can be provided for cities under "warm temperate" and "snow" main climates where the temperature swings are considered as high. The cold storage effectiveness depends highly on heat gains and the solar irradiance. The cooling supply during the day provided by the cold storage [116] strategy was about 12MJ/day; while it reaches 150 MJ/day in case of free cooling. Further, in order to optimize the charging process, a control strategy based on artificial intelligence algorithms can be used. Other VF system applications [117] [120] are presented in Table 0-7.

Table 0-7: PCM active system applications in building envelope including active VF

Ref Type*	Location/ climate	Used PCM	Installation/Strategies	Results/conclusions
[26] E, S	Lab scale experiment / Periodic variations of the temperature	Microencapsulated paraffin in gypsum (Heptadecane), Tm = 22°C & m_{total} PCM=13.3 kg/m^2	-ceiling panel with PCM incorporated in retrofitted buildings. -thermal storage controlled by an integrated water capillary tube system.	-5 cm layer of microencapsulated PCM are sufficient to keep the office temperature within the comfort range. -this system can be used in lightweight structures due to its benefits. - Fire resistance could be ensured by micro-encapsulated PCM in gypsum covered in a sheet steel tray.
[117] E	Puigverd de Lleida (Spain)/ Continental Mediterranean with severe or mild summer	- macro-encapsulated panels of salt hydrate SP-22, Tm=22°C & Ts=18°C - 112 PCM panels (1.4 kg of SP-22 each) distributed throughout the facade making 14 air flow channels.	-VF in south wall consisting of 3 fans & Six automatized gates in order to control the operational mode Figure 0-47. -the system used as a cold storage unit (an overheating protection) & as a night free cooling application.	- Night free cooling operation mode reduces cooling loads. - Cold storage sequence presents low energy storage efficiency due to significant heat gains through the outer skin. -. The system prevents effectively the overheating effect. - Effective use of VF for cooling purposes→ weather conditions & cooling demand of final users should be taken into account.
[120] E, S	Madrid Seville	- RT22 in containers, located inside an air chamber. -Tm=23°C	-Ventilated facade with fins filled with PCM. -PCM cylinders in hollow core slabs Figure 0-49. -increasing contact area between PCM & air.	- PCM located inside mechanically ventilated air layers → convective heat transfer coefficients↗↗ & control strategies used to match cooling needs of building.

			-increasing convective heat transfer coefficient & improving utilization factor.	- Use of encapsulation shapes such as fins, cylinder and sphere increase convective heat transfer coefficients & improve the use of considerable amounts of PCM.
[121] S	Catania (Southern Italy)/ hot Mediterranean climate	Wallboard panels consisting of aluminum honeycomb matrix containing 60% of microencapsulated paraffin	- PCM placed at a certain distance from the partition walls. - Narrow ventilated cavity between PCM wallboards & partition wall Figure 0-48. - Fresh air circulates according to suitable control logics.	- Ventilation occurs at night → PCM storage efficiency↗↗. - Average room operative temperature is reduced~0.4°C & indoor conditions are maintained for longer time in a comfortable range. - At night, heat stored by PCM is rejected to the air flowing into the cavity, rather than being released to room air.
[122] S	Tübingen/ Germany	PCM plates, Tm=26-28°C	- PCM in gypsum boards of top floor ceiling and wall. -Daytime mechanical ventilation with air precooling through a horizontal brine soil heat exchanger. - mechanical night ventilation	- PCM gypsum boards in ceiling and wall was not effective enough to control the room temperature level. -The problem is that during the night, the heat flux for discharging PCM was low with limited air exchange rates.
[123] E	Central Poland/daily ambient temperature oscillates in high range	Gypsum-mortar composite containing~ 27% microencapsulated PCM Figure 0-50 (Micronal DS-5008X, by BASF).), Tm= 22.8°C	-Ceiling in shape of thick board with parallel internal ventilation channels to improve night ventilation system - PCM based heat exchangers located in air ducts.	- Daily fluctuations of air temperature are eliminated & the room temperature within the comfort range. - Entire amount of PCM does not undergo complete melting & solidification. -this study needs some optimization in terms of thickness of channels and distribution of PCM in construction materials. -Numerical modeling & results of simulations of heat transfer in ceiling panel can be found in [124].
[125] S	Linköping, Sweden/ Excessive temperatures occur summertime.	-Ttransition= 19°C C_{PCM}, solid (T < 17) =2 kJ/(kg K) C_{PCM}, liquid (T > 21) = 2 kJ/(kg K) -different m_{total} PCM = 50, 100, 200, 400 kg	-External PCM night cool storage. -PCM air heat exchanger placed in an insulated box on the outside of the wall Figure 0-51.	- Indoor temperature reduction~ 0.5°C to 2°C (depending on PCM amount) in the warmest 10 days of summer season. - PCM cool storage does not provide enough cooling when the indoor temperature > 28 °C. -22–36% of the degree hours with excessive temperatures could be removed.

[126] S	Hong Kong	-PCM Hexadecane (C16H34) - Tm =18°C & Hf = 224 kJ/Kg	AC system: combination of cooled ceiling (CC) & MPCM slurry storage tank	- Tank with volume = 0.52 m^3 was sufficient to keep the indoor temperature within comfort level. - Electricity demand reduction~ 33%. - Annual energy consumption reduction= 1157Kwh.

*(E: experimental, S: simulation)

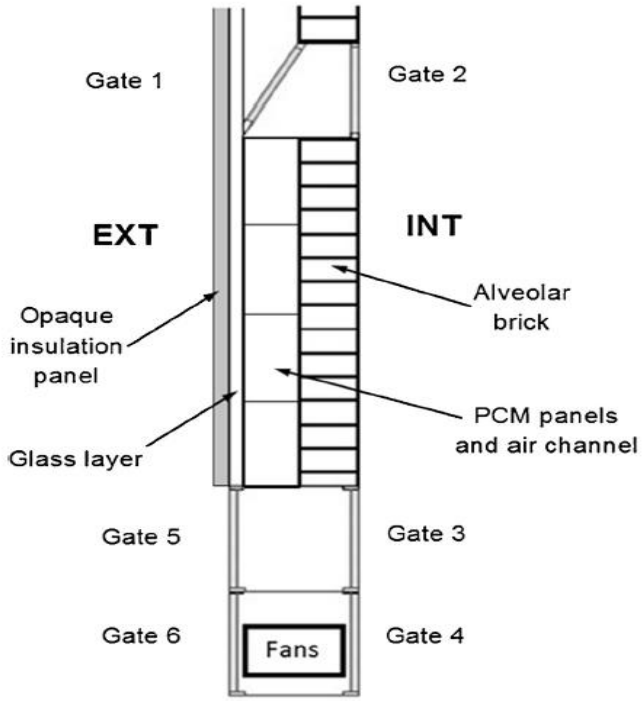

Figure 0-47: ventilated façade with the distribution of fans and automatized gates [117]

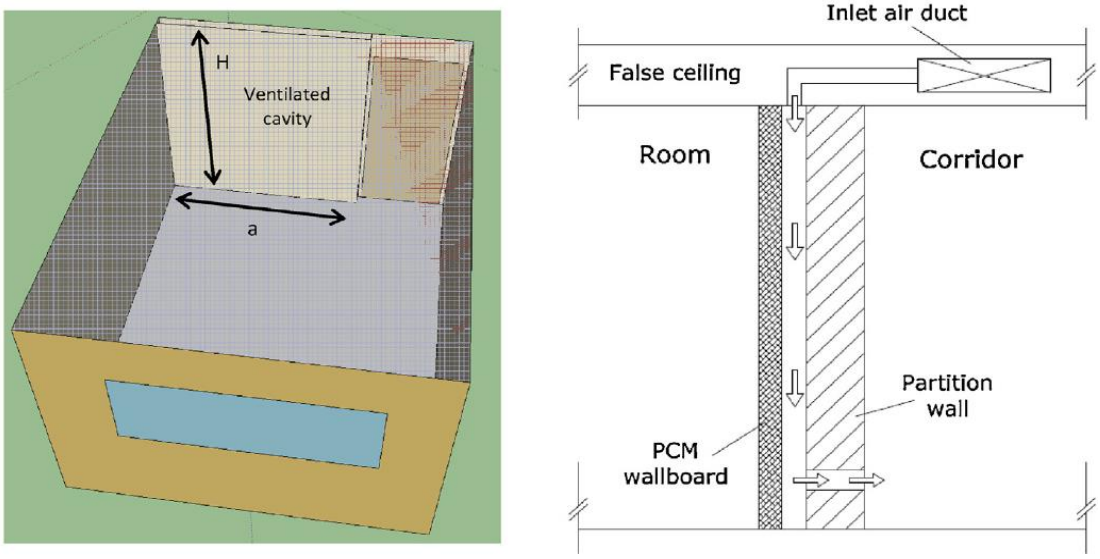

Figure 0-48: location and operation of the ventilated cavity [121]

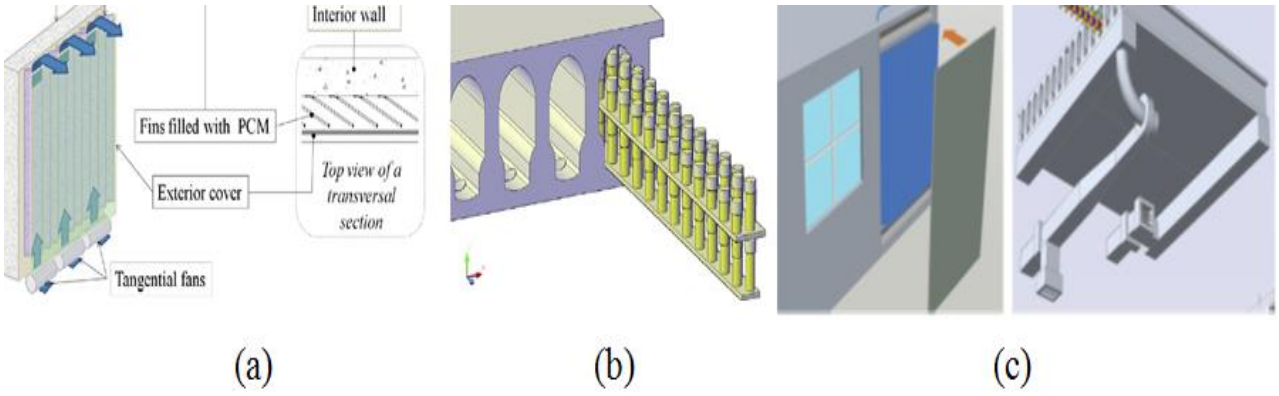

Figure 0-49: (a) Ventilated façade with fins filled with PCM, (b) PCM cylinders in hollow cores, (c) position of VF and hollow cores [120]

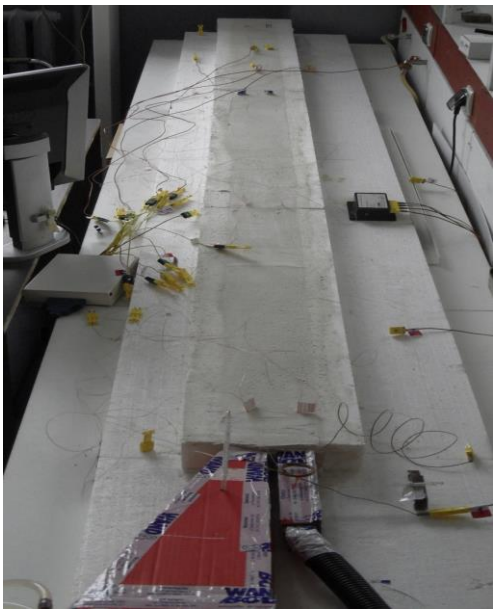

Figure 0-50: ceiling panel made of gypsum-PCM composite [123]

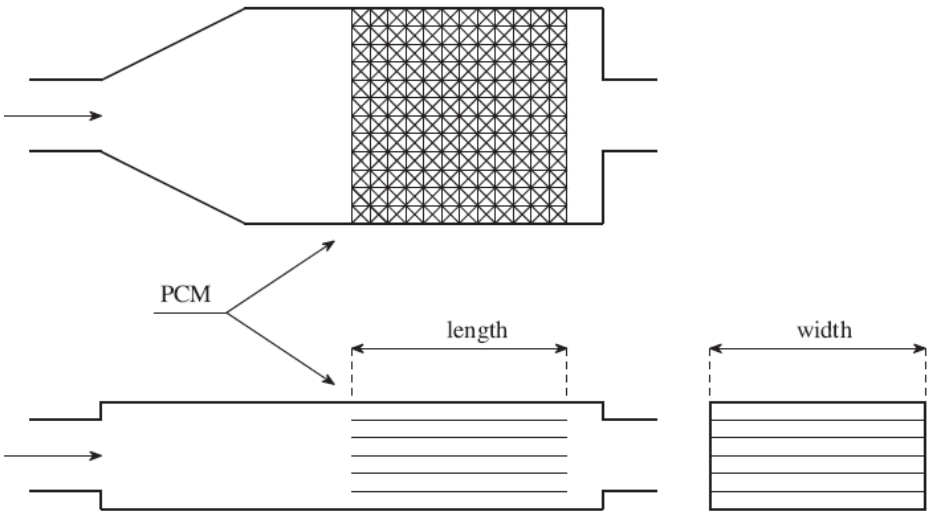

Figure 0-51: schematic of PCM heat exchanger placed in an insulated box on the outside wall [125]

4. Discussion

In building applications, PCM can be incorporated in passive or active systems. Passive systems do not require additional energy, are easy to install with integrated low consumption devices. They depend completely on the outdoor temperature and the variable weather conditions. Thereby if night temperatures do not drop considerably below the PCM phase change temperature, the PCM will not fully solidify which hinders the pursuit of its operation. In addition, among day-night cycles the heat transfer between the air and the wall limits the maximum capacity of storage which restricts the application of passive systems [46]. Furthermore, the required rate of heat exchange between the air and the PCM is not always attained. During summer season, Schossig et al. [127] proposed to increase air-change rate at night; even though natural ventilation could provide cold from outside but it may be insufficient; thus mechanical ventilation must be applied, which is considered as an active system, leading to a better heat transfer coefficient. Improving the heat transfer rates using electrical fans requires adding their energy consumption in the economic study. Active systems seem to be more efficient than the passive ones, the charge/discharge process is fully controlled, and its execution depends on several parameters besides the outdoor temperature, moreover the thermal energy storage can be obtained when it is required. On the other hand, active applications are regarded as complicated and complex systems requiring mechanical elements such as pumps and fans, in addition to a control system. In terms of the use of PCM for building applications, PCM integrated materials and PCM components are more and more easily implemented. Recently, PCM mats and boards have become available in the market which facilitates the integration of latent heat storage in lightweight construction. Originally, PCM boards were used only in passive systems, but later on it was used also for active applications [67] [66]. For space heating, the solar direct gain is the most significant strategy and the appropriate selection of the finishing material characteristics is very important in this case. Thun et al. [66] used this strategy for the PCM floor application; however this application is affected essentially by the type and the color of chosen floor finishing material since the PCM is not immediately subjected to solar radiation [66]. The heat transfer rate is reduced and delayed when the PCM is not directly in contact with solar radiation, neither with the room air. For space cooling, night ventilation and solar protection are the most important strategies. Night ventilation is advantageous in regions with large temperature swings between day and night; it can improve thermal comfort conditions and it can be achieved through window or door openings, ceiling fans and others [128]. Cooling strategies and PCM applications with active and passive systems are summarized in the synthetic diagram shown in Figure 0-52.

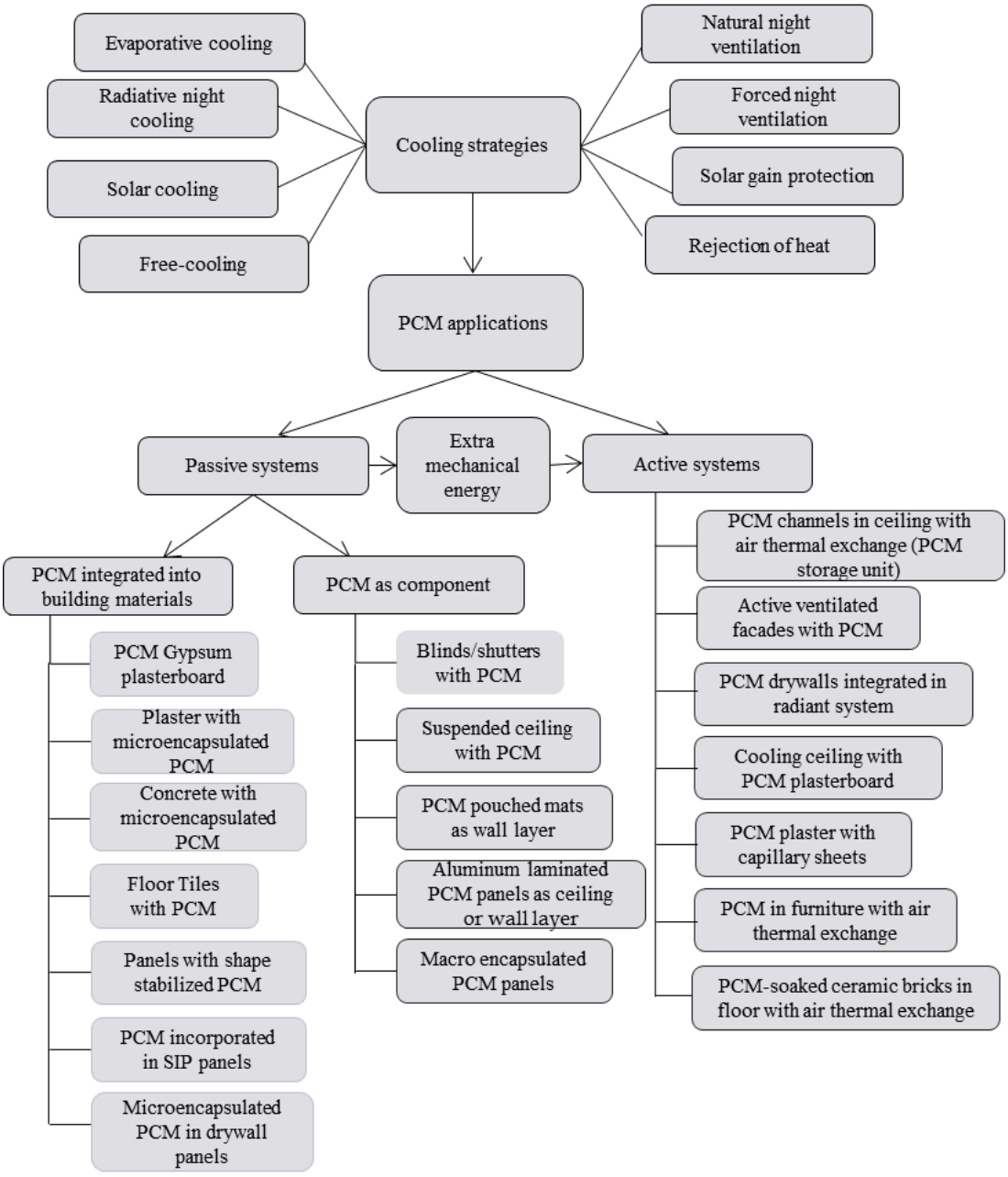

Figure 0-52: A synthetic diagram of PCM cooling applications

4.1. Factors affecting PCM selection

The integration of PCM in buildings leads to an increase in their thermal energy storage which subsequently minimizes the indoor temperature fluctuation, providing indoor thermal comfort and therefore reducing the energy consumption. Osterman et al. [24] confirmed that the use of PCM highly improves the energy performance of buildings in summer season. The efficiency of PCM strongly depends on several factors: 1) outdoor climatic conditions, 2) type of PCM, its melting temperature range and its thermo-physical properties, 3) PCM encapsulation method, 4) quantity of

PCM (effective volume and PCM layer thickness), 5) location and installation of PCM in the building , 6) purpose of PCM application; 7) way of PCM is charged/discharged (active or passive systems), 8) characteristics and orientation of the building, 9) real life conditions including heating and cooling set points, air infiltration rates, internal gains from occupancy (i.e. people (person/m^2), metabolic rate (Writing, seating, standing Cooking, cleaning… (W/person)), Lighting (W/m^2) and Electric equipment (W/m^2)) schedules), 10) solar gains, 11) orientation and reflectivity of the surfaces (solar absorbance coefficient (α)), 12) and finally investment cost and tariff structure should be taken into account.

The aim of this section is to investigate the possibility to find an optimum solution (appropriate PCM configuration) for each climate and application, in order to reduce cooling demands in hot/warm climates. It was found that the combination of building energy simulation tools and optimization tools can lead to optimize the design of buildings and HVAC systems [129][130][131][132]. Moreover, both mass of PCM and typology of PCM must be carefully designed.

4.2. Climatic conditions

As it was formerly stated, climatic conditions are one of the main factors affecting the efficiency of PCM in building applications, since the system performance is principally influenced by the outdoor weather conditions. The climate of a specified location is influenced by its latitude; terrain, ice or snow lids, and altitude, in addition to close water bodies. It can be defined as the average weather over a long period and it is categorized according to the average and the typical ranges of temperature and precipitation. Cooling and heating needs for buildings in each climatic zone can be determined according to the climatic zone conditions, and other conditions such as the kind use of building (residential, or non-residential) and internal gains from occupancy.

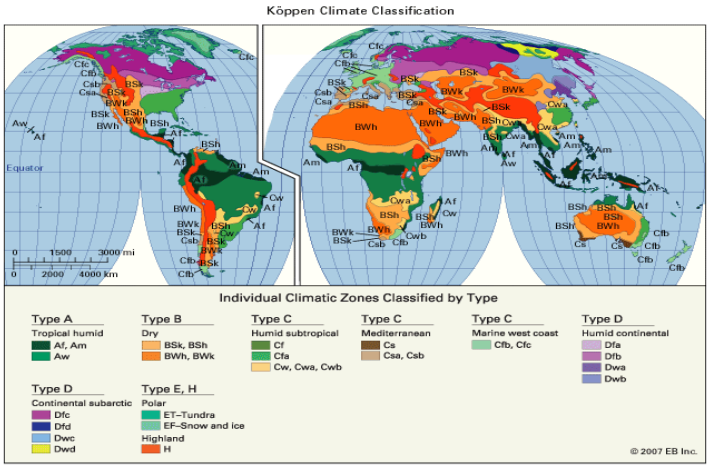

Figure 0-53: climate classification according to the Köppen–Geiger [133]

One of the most popular climate classification systems is Köppen- Geiger, Figure 0-53, it divides the main climate in five zones namely, A: equatorial, B: arid, C: warm temperate, D: snow and E: polar. Furthermore, it determines the level of precipitation W: desert, S: steppe, f: fully humid, s: summer dry, w: winter dry, m: monsoonal. Lastly, it gives details about temperature as h: hot arid, k: cold arid, a: hot summer, b: warm summer, c: cool summer, d: extremely continental, F: polar frost. For example, in Seville-Spain, the climate is considered as Csa: a Mediterranean climate with dry hot summer and mild winter while in Paris-France the climate is Cfb: Marine west coastal with warm summer, mild winter and rain all the year. In general, each climate zone has clearly different construction and design requirements. Table 0-8 shows cooling and heating requirements for each climate condition.

Table 0-8: Usual cooling & heating strategies as a function of the climate conditions [134]

climates	Cooling & heating requirements
Hot humid summer / warm winter	- Design strategies that reduce cooling energy consumption. - Orientate the building to take advantage of cooling breezes. - Shading all windows & walls. - Use low solar heat gain coefficient glazing. - Encourage natural air flow. - Use ceiling fans & other mechanical cooling equipment.
Warm and humid summer / mild winter	-. Auxiliary heating is not necessary. - Ceiling fans & high energy rated cooling appliances are required.
Hot dry summer / Warm winter	Evaporative cooling & passive solar heating are required
Hot dry summer / Cool winter	-. Evaporative cooling, ceiling fans. & night cooling - Passive & active solar heating.
Warm temperate climates	-. No auxiliary heating or cooling is required - Just may include ceiling fans.
Cool temperate climates	-. Cooling is unnecessary. - Significant level of passive / active solar heating strongly desirable if available. - Other heating systems are also needed.

Many studies were conducted in order to investigate the performance of PCM under different climates [116][135][136][137] [138]. It can be observed that the integrated PCM does not give the same advantages for all Mediterranean climates during all months of cooling season, the PCM wallboards appearing more suitable for semi-arid climate than for hot/subtropical Mediterranean climates [137]. However, Soares et al. [135] concluded that the total energy savings due to the integration of PCM-drywalls are more significant for the warmer climates, it reach 62% and 42% for Coimbra (Csb-Mediterranean climate with dry warm summer and mild winter) and Seville (Csa-Mediterranean climate with dry hot summer and mild winter) respectively. Moreover, it is observed that PCM-drywalls reduce the heating energy demand not only the cooling energy demand in warmer climates. For colder climates in Warsaw (Dfb-Moist continental with warm summer and cold winter) and Kiruna (Dfc- Subarctic with cool summer and severe winter), PCM-drywalls can reduce the heating energy demand significantly but are not attractive in terms of total energy savings due to the increase

in summer cooling loads. Finally, it was shown that the optimization of PCM-drywalls incorporation is very important and can be achieved in an annual evaluation basis instead of in a seasonal basis. Furthermore, Alam et al. [136] investigated the effect of PCM in Australian cities under different climates; they concluded that PCM can reduce the energy consumption of buildings in cities under cold, mild and warm temperate climates. However, the integration of PCM in buildings under hot and humid climate has very limited impact on the energy consumption. Usón et al. [138] considered five different climatic zones in Spain to evaluate three different commercial PCM installed on tiles. They concluded that PCM can minimize the total energy consumption and the environmental impacts. Moreover, the effective performance of PCM is heavily influenced by the climate conditions and the type of PCM introduced. Borderon et al. [139] investigated a PCM/air ventilation system storing latent heat in order to improve summer comfort conditions in four French cities (Lyon, Nice, Carpentras and Trappes) under different climates, where Carpentras is the warmest climate and Trappes is the coldest one. It was shown that the performance of the system is mainly affected by the daily amplitude of the exterior air temperature. In addition, the diurnal temperature range, which is the amplitude of the outdoor air temperature swing, is a critical factor of the applicability of PCM to reduce cooling loads [140]. Thus, when the diurnal temperature range is between 12°C and 15°C the free cooling system with incorporated PCM can be applied showing an effective performance [35].
From the above literatures, it is obvious that the effective performance of PCM is extremely related to climate conditions; therefore, it is important to choose a suitable PCM melting temperature that it is strongly conditioned by the surrounding climate.

4.3. Melting temperature of PCM

The most significant criterion for PCM selection is the required melting temperature, it is considered as the greatest influent parameter. It is very important to select the right type of PCM because, for a specific climate conditions, if the melting temperature is too low, it is difficult to maintain the indoor air temperature at a comfortable level during the night; furthermore, if the melting temperature is too high, the quantity of solar radiation heat stored by the PCM will be reduced in the daytime [141]. Additionally, the selection of a low melting temperature leads to insufficient use of PCM in the hottest months. On the other hand, a melting temperature too high could lead to a marginal feasibility during the intermediate seasons. Most of the PCM that can be applied in buildings have melting points between 18°C and 28°C, close to the human comfort temperature range. A phase change temperature outside of the operating temperature range of the storage could make the application totally useless. Partial solidification and melting of PCM can lead to insufficient thermal storage [11].

The selection of different melting temperatures depends on the main purpose of the application, which could be to save heating energy or to prevent overheating [127]. The PCM that has a good performance in the heating periods will have an insignificant impact or no effect at all in cooling periods and vice versa. Barreneche et al. [142] created a new database (software CES Selector) that helps selecting the most suitable PCM depending on the application, using data collected by Cabeza et al. [16]. They found that, for cooling applications in buildings, PCM should have melting temperatures up to 21°C. Moreover, PCM used to control the indoor comfort temperature, should have a temperature range between 20 and 30°C and this PCM are commonly used in passive systems. Furthermore, for domestic hot water application, PCM should have temperature range between 29°C and 60°C. Other authors reported that in the air conditioning applications PCM that melt below 15°C are used to store coldness, while for absorption refrigeration, the used PCM melt above 90°C and all other PCM that melt between 15°C and 90°C can be used for solar heating applications [11]. Heim and Clarke [143] showed that the optimal PCM solidification temperature is 2°C above the heating set point for the room. Peippo et al. [144] indicates that the optimal diurnal heat storage happens with a PCM melting temperature of 1–3°C above the average room temperature. Moreover, Neeper [78]tested the thermal performance of fatty acids and paraffin waxes gypsum wallboard; they found that, with a PCM melting temperature near to the average comfort room temperature, the maximum diurnal energy storage can be occurred. Additionally, for wallboard installed on external wall, the optimum value of the melting temperature depends on the outdoor temperature and the thermal resistance of the wall. Ascione et al.[137] analyzed the monthly energy improvement that can be achieved in different cities under various climates by changing the melting temperature in the range 26–29°C. They found that the most appropriate melting temperature for Ankara under semi-arid climate is 29°C leading to significant cooling energy savings in the cooling season. Otherwise, for Seville climate that has the hottest European summer, although the phase change is considerably activated, the PCM is not able to take full advantage of its storage potential. Therefore, it can be shown that it is not possible to determine an optimal melting temperature for the whole cooling period where the worst results for each melting temperature were found in August, most likely because of the incomplete solidification of PCM. Finally, it was reported that, for the Mediterranean climate the optimal range of melting temperature in the winter period is between 18°C and 22°C, while, in summer, appropriate melting temperature range is between 25 and 30°C. Usón et al [138] have analyzed three commercial PCM with melting temperatures selected within the comfort range (21–24 °C). They concluded that salt hydrates PCM with a melting temperature of 21°C can reduce the total energy consumption in the five different climate severities in Spain. Moreover, simulations have been carried out by Alam et al. [136], using BioPCM with six different melting ranges from 20PCM

(18–22°C) to 25PCM (23–27°C) in order to find the optimum PCM melting range for each climatic zone. They concluded that an optimum PCM melting range that leads to the lowest energy consumption in every month of the year can't be unique, and PCM with melting point outside the comfort or thermostat range cannot be effective and lead to decrease energy savings. Furthermore, it was found that PCM with higher melting point were more efficient during summer as well as in warm temperate climate areas, while PCM with lower melting point were most efficient during winter and perform better in cold temperate climate area. Other simulations [145] showed that a phase change temperature of 22°C, which is the mid-point of the chosen comfort range (20-24°C), was the best for the studied case. In commercial buildings, peak temperatures can be reduced by about 3-4°C, and day hours where the temperature is above 24°C can be reduced by 80%. Moreover, Fiorito [146] found that for a considered climatic zone, the PCM melting point should be selected in order to be compatible with the average maximum outdoor temperatures. Accordingly, for a free cooling system design, the PCM melting temperature is considered as a decisive factor [48], and it should be taken between 19°C and 24°C [34] [45] which intersect the range of the human comfort 23–27°C in summer conditions. Waqas and Kumar [147] have found that the performance of free cooling system in hot dry climates is better with a PCM melting temperature selected within the comfort range of the hottest month. In order to find the optimal PCM melting temperature, a new method was presented by Jiang et al. [148] for a passive solar house. They found that the optimal PCM melting point depends on the minimal limit of the indoor thermal comfort band, and its value, in china under different climates, should be taken from 1.1°C to 3.3°C greater than the minimum thermal comfort range. Soares et al. [135] investigated the impact of six different melting temperatures; they found that the optimum PCM melting temperature is higher for the warmer climates (between 22 and 26°C), and lower for colder climates (between 18 and 24°C). For better PCM performance, Farid [149] suggested to utilize in the same storage unit, more than one PCM with various melting temperatures. In order to get an effective performance all the time under different weather conditions, two layers of PCM with different melting temperature incorporated into the rooftop of the building were used [80]. Moreover, systems with different PCM having different melting temperatures are considered as an important future research, and should be developed in order to improve the building performance in both cooling and heating seasons.

From the above literatures, it can be concluded that there are different criteria to select an appropriate melting temperature whether for heating or cooling applications or both. Knowing that, the same phase change material does not provide the same advantages referring to both heating and cooling energy demands, and none of the PCM is equally effective over the year. The selection of melting temperature should be based reasonably on local thermostat set points along with the climatic

conditions. Some authors agree that high PCM melting temperatures seemed more effective for warmer climates, while low PCM melting temperature could be more efficient in colder climates, and others emphasized on the importance of selecting PCM melting temperature within the comfort range. To choose the most suitable PCM melting temperature for an application under considered climatic zone, the optimization method by testing different melting temperatures seemed the most appropriate.

4.4. Location of application: Effect of PCM surface area and thickness

In the previous section, the effectiveness of PCM was investigated in terms of selecting a suitable PCM melting temperature for a considered application. In this part, the effect of position, surface area and thickness of PCM integrated in building on energy savings will be investigated. As mentioned previously, PCM can be incorporated into wallboards, roof, underfloor, concrete, plaster, furniture, and insulation of buildings, glazing and others [66] [17][150][18][15][151]. The location of PCM, essentially in passive systems, depends on its objective and functioning [11], unlike the PCM storage units that have more options and liberty in terms of their location. Passive PCM application at the floor seems to be the best location for the heating periods; this is due to the fact that in the floor it is possible to benefit from each of the indoor air temperature and direct solar gains via the glazing. However, PCM drywalls (plasterboards, wallboards or gypsum boards) seemed more appropriate as passive systems for cooling purposes. Knowing that, night ventilation together with PCM is a very effective strategy that leads to decrease the cooling demand of buildings. Ingenious solutions [106] for reducing the cooling demand of buildings such as ventilated facade with fins filled with PCM and PCM cylinders in hollow core slabs, were created in order to increase the convective heat transfer coefficient. Therefore, they allow the use of large quantities of PCM, and improve the utilization factor of cold stored. Ceilings present considerable areas for passive heat transfer and have less risk of spillage of the macro-encapsulated PCM by drilling; however, they have lower convective heat transfer coefficients compared to walls and floor. Moreover, it was found that a PCM layer incorporated in the roof structure seemed inappropriate to improve the building energy performances [80], actually rooftop temperature increases when the PCM becomes liquid. For the purpose of reducing cooling demand and improving thermal comfort, Ascione et al. [137] installed gypsum wallboard PCM on the inner faces of the external building envelope. The results showed that the application of the PCM plaster on the whole vertical envelope leads to the highest energy savings in different climatic zones. In addition, it has been found that the cooling demand is reduced with the increment of the thickness of PCM plaster; however, authors investigated until a maximum thickness of 3 cm of PCM plaster because additional increment of PCM thickness cannot provide considerable improvements of the indoor temperature. Soares et al. [135] replaced the inner plasterboard layers of the exterior walls, partition wall and roof by a PCM-drywall layer. In all studied cases, they found

that the optimum thickness of the PCM-drywalls was equal to 4cm. Moreover, in terms of surfaces solar absorbance, lower values (α = 0.3) are better for warmer climates while higher values (α= 0.9) are better for colder climates. Alam et al.[136] investigated energy savings for different locations of PCM (east wall, North wall, West wall, South wall, North wall and roof, West wall and roof, South wall and roof, east wall and roof, all walls, all walls and roof) where the thickness of PCM layer was calculated by dividing the PCM volume by the surface area of the applied location. For a specified amount of PCM, it was shown that energy savings and therefore effectiveness of PCM increase with the decrease of the thickness of PCM layer and the increase of surface area until an optimum level.

During a phase change daily cycle, the PCM volume must be chosen so that PCM mass could be melted and solidified entirely. During the cooling season, if the PCM volume is very high, the solidification process time may be longer than the time of low temperatures at night. Similarly, in winter, if the PCM volume is very high, the PCM cannot be completely melted because the sunshine time could be shorter than the time required for the heat penetration in the PCM. Furthermore, increasing the surface area of the applied location of PCM, leads to an increase of the heat transfer rate between this area and the PCM. At a constant PCM volume, the thickness of PCM layer is thinner when the surface area increases. Therefore, melting and solidification processes become more effective.

The total energy exchanged due to the enthalpy content in the PCM (i.e. the overall latent heat storage capability) can be calculated using Eq. 0-1 [138]:

$$E_{latent} = n.m.H_f \quad \textbf{Eq. 0-1}$$

Where, m is the mass of the PCM, n is the number of phase changes that occur during a specified period of time and H_f is the PCM latent heat.

For a better evaluation of the impact of PCM position and thickness, Konstantinidis [7] calculated the total amount of PCM necessary to absorb the surplus heat for cooling periods. The average daily cooling load E_{daily} was determined. Therefore, the diurnal energy stored in the PCM is given by Eq. 0-2:

$$E_{daily} = m_{cp}.H_f \quad \textbf{Eq. 0-2}$$

Where, m_{cp} is the specific mass of PCM and H_f is the latent enthalpy of the material.

Therefore, the required mass of PCM is calculated and subsequently the required PCM volume is given by Eq. 0-3:

$$PCM\ Volume = m(PCM)/\rho(PCM) \quad \textbf{Eq. 0-3}$$

4.5. HVAC controls

According to the indoor microclimate, two types of study can be carried out:

- Without including the HVAC system (naturally ventilated building): to find out the effect of PCM on the temperature fluctuations in the considered indoor space, where the temperature is free-running, and the potential of PCM in reducing peaks. In this case the hourly temperature data must be given.
- Including the HVAC system (air-conditioned building): to calculate the energy consumptions, and thus the energy savings. In this case, the indoor temperature is controlled and a schedule of set points must be made.

5. Conclusion

A review of PCM applications for cooling purposes, and factors affecting the effectiveness of PCM were discussed in this article. Many experimental and modeling-simulation studies have been presented, showing the effect of PCM on the buildings thermal performance. The use of PCM in buildings seems to be very beneficial; PCM can decrease energy consumption, shift the peak loads of cooling energy demand, decrease temperature fluctuations providing a thermally comfortable environment, and reduce the electricity consumption. Free cooling applications are effective when the diurnal temperature variations are large (up to15°C). When HVAC system is used, PCM act as a cold storage unit, shifting the peak loads to low electricity rate periods. Integrating PCM in the building envelope prevents the raise of the indoor temperature improving the thermal comfort. However, many drawbacks have been found in PCM applications, mainly the non-use of considerable portions of employed PCM due to the low convective heat transfer coefficients, incomplete solidification of PCM at night and the limited contact area between the air and PCM.

Several solutions have been proposed, such as the use of proper control strategy, forced ventilation to increase the convective heat transfer, and adequate design of the heat exchangers. Moreover, using fins, cylinders, and spheres to encapsulate the PCM could improve the use of considerable amounts of PCM and increase the convective heat transfer coefficients. Paraffin was mostly used in cooling applications; however, salt hydrates and fatty acids were used in some cases. Selecting the most suitable PCM for a specific climate and a specific application was discussed. The melting temperature is the most influential parameter, some authors approve that high PCM melting temperatures seemed more effective for warmer climates, while low PCM melting temperature could be more efficient in colder climates, and others emphasized on the importance of selecting PCM melting temperature within the comfort range then an optimization method by testing different melting temperatures is required. Moreover, systems with different PCM having different melting temperatures are considered as an important future research and should be developed in order to improve the building performance in both cooling and heating seasons. Moreover, for a specified amount of PCM, it was shown that energy savings and therefore effectiveness of PCM increase with the decrease of the

thickness of PCM layer and the increase of surface area until a certain optimum level. The selection of an appropriate amount of PCM needed for thermal storage still requires also further research. A general topology diagram summarizing the PCM application in buildings is presented in Figure 0-54.

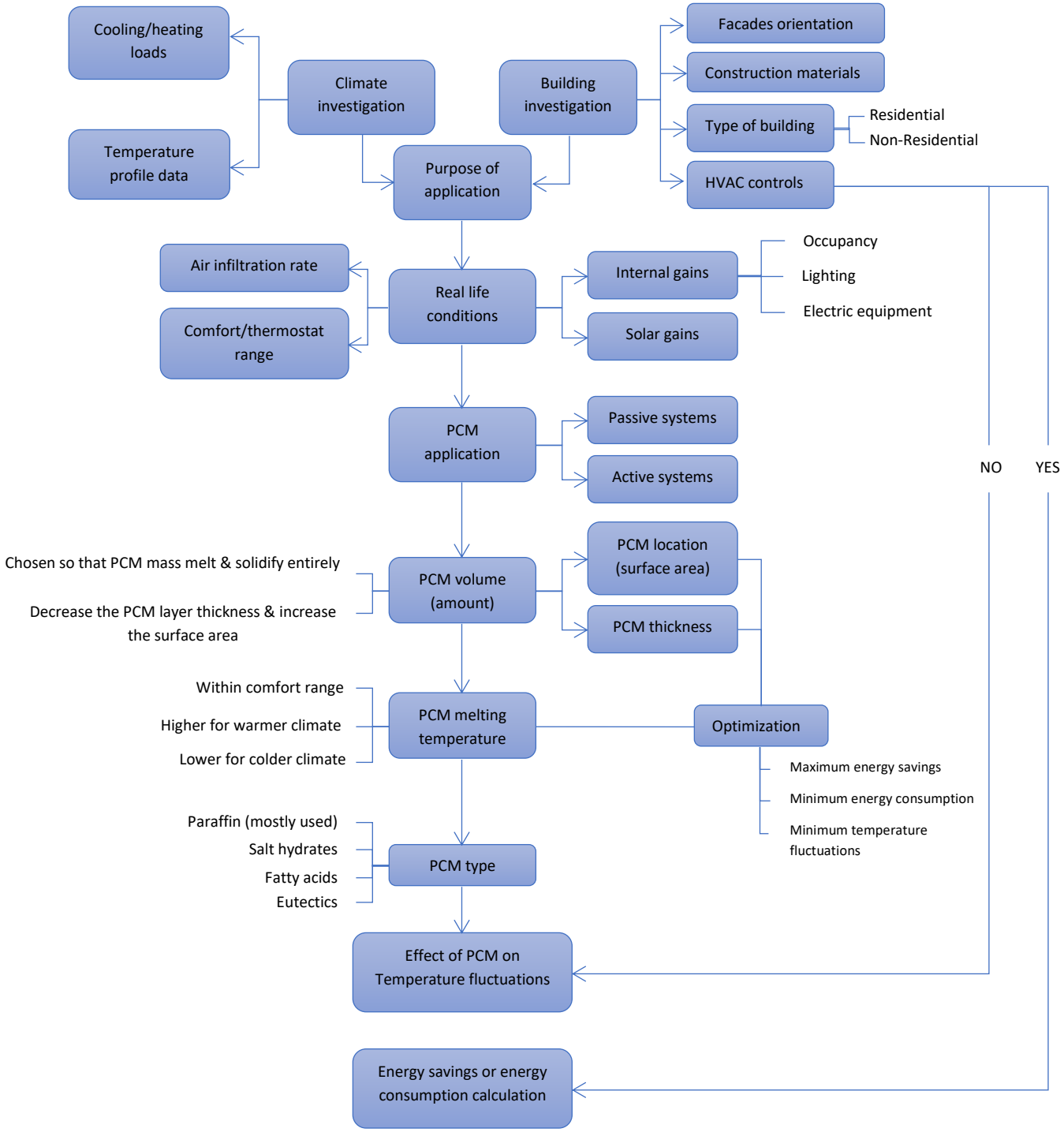

Figure 0-54: A typology diagram of PCM in building applications

6. *Résumé en français*

Matériaux à changement de phase (MCP) pour les applications de refroidissement dans les bâtiments : une revue

Une revue des applications de matériaux à changement de phase (MCP) pour le refroidissement des bâtiments, et les facteurs affectant l'efficacité de MCP ont été discutés dans ce chapitre. De nombreuses études expérimentales et numériques ont été présentées, montrant l'effet de MCP sur la performance thermique des bâtiments. L'utilisation de MCP dans les bâtiments dans des systèmes passifs ou actifs semble être très bénéfique ; les matériaux à changement de phase peuvent réduire la consommation d'énergie, déplacer les pointes de charge de la demande énergétique de refroidissement, diminuer les fluctuations de la température, fournir un environnement thermiquement confortable et réduire la consommation d'électricité. Les applications de refroidissement naturel (free-cooling) sont efficaces lorsque les variations de température diurnes sont importantes (jusqu'à 15°C). Lorsque le système de chauffage, de ventilation et de climatisation (HVAC) est utilisé, les MCP agissent comme une unité de stockage de froid, déplaçant les pointes de charge à des périodes où l'électricité est bon marché. L'intégration de MCP dans l'enveloppe du bâtiment empêche l'augmentation de la température intérieure en été et améliore à son tour le confort thermique.

Cependant, de nombreux inconvénients ont été trouvés dans les applications de MCP, principalement la non-utilisation de portions considérables du MCP en raison des faibles coefficients de transfert de chaleur par convection, la solidification incomplète du MCP la nuit et la zone de contact limitée entre l'air et le MCP. Plusieurs solutions ont été proposées, telles que l'utilisation d'une stratégie de contrôle appropriée, la ventilation forcée pour augmenter le transfert de chaleur par convection et la conception adéquate des échangeurs de chaleur. De plus, l'utilisation d'ailettes, de cylindres et de sphères pour encapsuler les MCP pourrait augmenter la quantité de MCP utilisée ainsi que les coefficients de transfert de chaleur par convection. La paraffine est principalement utilisée dans les applications de refroidissement ; cependant, les hydrates de sel et les acides gras ont été utilisés dans certains cas.

La sélection des MCP les plus appropriés pour un climat spécifique et pour une application spécifique a été aussi discutée. La température de fusion est le paramètre le plus influent, certains auteurs admettent que des températures de fusion élevées semblent plus efficaces pour les climats plus chauds, tandis que les températures de fusion basses peuvent être plus efficace dans les climats froids. D'autres ont insisté sur l'importance de choisir la température de fusion de MCP dans la plage de confort, puis d'effectuer une optimisation en testant différentes températures de fusion au sein de la plage de confort. En plus, les systèmes avec plusieurs MCP ayant des températures de fusion

différentes sont considérés comme une recherche future importante, et devraient être développés afin d'améliorer la performance du bâtiment dans les deux saisons de refroidissement et de chauffage. Par ailleurs, pour une quantité précisée du MCP, il a été montré que les économies d'énergie et donc l'efficacité du MCP augmentent avec la diminution de l'épaisseur de la couche du MCP et l'augmentation de la surface d'échange jusqu'à un certain niveau optimal. La sélection d'une quantité appropriée de MCP pour le stockage thermique nécessite également d'autres recherches complémentaires. Finalement, un diagramme topologique résumant les méthodes de choix des MCP dans les bâtiments est présenté.

References

[1] "IEA_Solar_HC_Roadmap_FoldOut_Print.pdf." .
[2] C. Initiative, "Buildings and Climate Change http://admin.indiaenvironmentportal.org.in/files/SBCI-BCCSummary.pdf," 2009.
[3] "http://www.iea.org/Textbase/npsum/building2013SUM.pdf." .
[4] "European Union, Directive 2012/27/EU of the European parliament and of the council efficiency." Official Journal of the European Union, 25-Oct-2012.
[5]."https://ec.europa.eu/energy/sites/ener/files/documents/2014_final_report_eu_building_heat_demand.pdf. "
[6] European Commission, Joint Research Centre, and European Technology Platform on Renewable Heating and Cooling (RHC-Platform), *2020-2030-2050, common vision for the renewable heating and cooling sector in Europe: European technology platform on renewable heating and cooling*. Luxembourg: EUR-OP, 2011.
[7] C. V. Konstantinidou and A. Novoselac, "Integration of thermal energy storage in buildings," *Univ. Tex. Austin*, 2010.
[8] X. Wang, D. Chen, and Z. Ren, "Global warming and its implication to emission reduction strategies for residential buildings," *Build. Environ.*, vol. 46, no. 4, pp. 871–883, Apr. 2011.
[9] L. Pérez-Lombard, J. Ortiz, and C. Pout, "A review on buildings energy consumption information," *Energy Build.*, vol. 40, no. 3, pp. 394–398, Jan. 2008.
[10] Agence internationale de l'énergie and Organisation de coopération et de développement économiques, *Energy technology perspectives: scenarios & strategies to 2050 : in support of the G8 Plan of action.* Paris: OECD, IEA, 2006.
[11] M. M. Farid, A. M. Khudhair, S. A. K. Razack, and S. Al-Hallaj, "A review on phase change energy storage: materials and applications," *Energy Convers. Manag.*, vol. 45, no. 9–10, pp. 1597–1615, Jun. 2004.
[12] J. Kośny, *PCM-Enhanced Building Components*. Cham: Springer International Publishing, 2015.
[13] H. Mehling and L. F. Cabeza, *Heat and Cold Storage with PCM: An up to Date Introduction in to Basics and Applications*. Springer, 2008.
[14] S. N. AL-Saadi and Z. (John) Zhai, "Modeling phase change materials embedded in building enclosure: A review," *Renew. Sustain. Energy Rev.*, vol. 21, pp. 659–673, May 2013.
[15] R. Baetens, B. P. Jelle, and A. Gustavsen, "Phase change materials for building applications: A state-of-the-art review," *Energy Build.*, vol. 42, no. 9, pp. 1361–1368, Sep. 2010.
[16] L. F. Cabeza, A. Castell, C. Barreneche, A. de Gracia, and A. I. Fernández, "Materials used as PCM in thermal energy storage in buildings: A review," *Renew. Sustain. Energy Rev.*, vol. 15, no. 3, pp. 1675–1695, Apr. 2011.
[17] A. M. Khudhair and M. M. Farid, "A review on energy conservation in building applications with thermal storage by latent heat using phase change materials," *Energy Convers. Manag.*, vol. 45, no. 2, pp. 263–275, Jan. 2004.
[18] F. Kuznik, D. David, K. Johannes, and J.-J. Roux, "A review on phase change materials integrated in building walls," *Renew. Sustain. Energy Rev.*, vol. 15, no. 1, pp. 379–391, Jan. 2011.
[19] S. A. Memon, "Phase change materials integrated in building walls: A state of the art review," *Renew. Sustain. Energy Rev.*, vol. 31, pp. 870–906, Mar. 2014.
[20] S. M. Hasnain, "Review on sustainable thermal energy storage technologies, part I: heat storage materials and techniques," *Energy Convers. Manag.*, vol. 39, no. 11, pp. 1127–1138, 1998.
[21] N. Artmann, R. L. Jensen, H. Manz, and P. Heiselberg, "Experimental investigation of heat transfer during night-time ventilation," *Energy Build.*, vol. 42, no. 3, pp. 366–374, Mar. 2010.
[22] M. Santamouris, K. Pavlou, A. Synnefa, K. Niachou, and D. Kolokotsa, "Recent progress on passive cooling techniques," *Energy Build.*, vol. 39, no. 7, pp. 859–866, Jul. 2007.
[23] U. Desideri, S. Proietti, and P. Sdringola, "Solar-powered cooling systems: Technical and economic analysis on industrial refrigeration and air-conditioning applications," *Appl. Energy*, vol. 86, no. 9, pp. 1376–1386, Sep. 2009.
[24] E. Osterman, V. V. Tyagi, V. Butala, N. A. Rahim, and U. Stritih, "Review of PCM based cooling technologies for buildings," *Energy Build.*, vol. 49, pp. 37–49, Jun. 2012.

[25] A. Waqas and Z. Ud Din, “Phase change material (PCM) storage for free cooling of buildings—A review,” *Renew. Sustain. Energy Rev.*, vol. 18, pp. 607–625, Feb. 2013.
[26] M. Koschenz and B. Lehmann, “Development of a thermally activated ceiling panel with PCM for application in lightweight and retrofitted buildings,” *Energy Build.*, vol. 36, no. 6, pp. 567–578, Jun. 2004.
[27] D. W. Hawes, D. Feldman, and D. Banu, “Latent heat storage in building materials,” *Energy and Buildings*, pp. 77–86, 1993.
[28] A. . Futane, S. R. Karale, and U. S. Wamkhede, “A review on free cooling through heat pipe by using phase change materials,” *nternational Journal of Engineering Science and Technology*, pp. 4556–4563., 2011.
[29] C. Liang and X. Lingling, “Microencapsulation of butyl stearate as a phase change material by interfacial polycondensation in a polyurea system,” *Energy Conversion and Management*, p. 50 (3) 723–729., 2009.
[30] P. Kauranen, and K. Peippo, “An organic PCM storage system with adjustable melting temperature,” *Solar Energy 46 (5) (1991) 275–278.*
[31] V. V. Tyagi and D. Buddhi, “Thermal cycle testing of calcium chloride hexahydrate as a possible PCM for latent heat storage,” *Solar Energy Materials and Solar Cells*, 92 (8) ( ) 891–899 2008.
[32] M. Thambidurai, K. Panchabikesan, K. M. N, and V. Ramalingam, “Review on phase change material based free cooling of buildings—The way toward sustainability,” *J. Energy Storage*, vol. 4, pp. 74–88, Dec. 2015.
[33] S. Kamali, “Review of free cooling system using phase change material for building,” *Energy Build.*, vol. 80, pp. 131–136, Sep. 2014.
[34] V. Butala and U. Stritih, “Experimental investigation of PCM cold storage,” *Energy Build.*, vol. 41, no. 3, pp. 354–359, Mar. 2009.
[35] V. A. A. Raj and R. Velraj, “Review on free cooling of buildings using phase change materials,” *Renew. Sustain. Energy Rev.*, vol. 14, no. 9, pp. 2819–2829, Dec. 2010.
[36] B. Zalba, J. M. Marín, L. F. Cabeza, and H. Mehling, “Free-cooling of buildings with phase change materials,” *Int. J. Refrig.*, vol. 27, no. 8, pp. 839–849, Dec. 2004.
[37] A. H. Mosaffa, C. A. Infante Ferreira, F. Talati, and M. A. Rosen, “Thermal performance of a multiple PCM thermal storage unit for free cooling,” *Energy Convers. Manag.*, vol. 67, pp. 1–7, Mar. 2013.
[38] A. H. Mosaffa, C. A. Infante Ferreira, M. A. Rosen, and F. Talati, “Thermal performance optimization of free cooling systems using enhanced latent heat thermal storage unit,” *Appl. Therm. Eng.*, vol. 59, no. 1–2, pp. 473–479, Sep. 2013.
[39] M. R. Anisur, M. A. Kibria, M. H. Mahfuz, R. Saidur, and I. H. S. C. Metselaar, “Cooling of air using heptadecane phase change material in shell and tube arrangement: Analytical and experimental study,” *Energy Build.*, vol. 85, pp. 98–106, Dec. 2014.
[40] F. Rouault, D. Bruneau, P. Sebastian, and J. Lopez, “Numerical modelling of tube bundle thermal energy storage for free-cooling of buildings,” *Appl. Energy*, vol. 111, pp. 1099–1106, Nov. 2013.
[41] E. Osterman, V. Butala, and U. Stritih, “PCM thermal storage system for ‘free’ heating and cooling of buildings,” *Energy Build.*, Jul. 2015.
[42] A. A. R. Darzi, S. M. Moosania, F. L. Tan, and M. Farhadi, “Numerical investigation of free-cooling system using plate type PCM storage,” *Int. Commun. Heat Mass Transf.*, vol. 48, pp. 155–163, Nov. 2013.
[43] A. Lazaro, P. Dolado, J. M. Marín, and B. Zalba, “PCM–air heat exchangers for free-cooling applications in buildings: Experimental results of two real-scale prototypes,” *Energy Convers. Manag.*, vol. 50, no. 3, pp. 439–443, Mar. 2009.
[44] G. Tan and D. Zhao, “Study of a thermoelectric space cooling system integrated with phase change material,” *Appl. Therm. Eng.*, vol. 86, pp. 187–198, Jul. 2015.
[45] K. Yanbing, J. Yi, and Z. Yinping, “Modeling and experimental study on an innovative passive cooling system—NVP system,” *Energy Build.*, vol. 35, no. 4, pp. 417–425, 2003.
[46] S. Takeda, K. Nagano, T. Mochida, and K. Shimakura, “Development of a ventilation system utilizing thermal energy storage for granules containing phase change material,” *Sol. Energy*, vol. 77, no. 3, pp. 329–338, Sep. 2004.
[47] A. Waqas and S. Kumar, “Thermal performance of latent heat storage for free cooling of buildings in a dry and hot climate: An experimental study,” *Energy Build.*, vol. 43, no. 10, pp. 2621–2630, Oct. 2011.

[48] C. Arkar, B. Vidrih, and S. Medved, “Efficiency of free cooling using latent heat storage integrated into the ventilation system of a low energy building,” *Int. J. Refrig.*, vol. 30, no. 1, pp. 134–143, Jan. 2007.
[49] U. Stritih and V. Butala, “Experimental investigation of energy saving in buildings with PCM cold storage,” *Int. J. Refrig.*, vol. 33, no. 8, pp. 1676–1683, Dec. 2010.
[50] J. R. Turnpenny, D. W. Etheridge, and D. A. Reay, “Novel ventilation system for reducing air conditioning in buildings. Part II: testing of prototype,” *Appl. Therm. Eng.*, vol. 21, no. 12, pp. 1203–1217, 2001.
[51] K. Nagano, S. Takeda, T. Mochida, K. Shimakura, and T. Nakamura, “Study of a floor supply air conditioning system using granular phase change material to augment building mass thermal storage—Heat response in small scale experiments,” *Energy Build.*, vol. 38, no. 5, pp. 436–446, May 2006.
[52] J. N. W. Chiu, P. Gravoille, and V. Martin, “Active free cooling optimization with thermal energy storage in Stockholm,” *Appl. Energy*, vol. 109, pp. 523–529, Sep. 2013.
[53] H.-M. Henning, “Solar assisted air conditioning of buildings – an overview,” *Appl. Therm. Eng.*, vol. 27, no. 10, pp. 1734–1749, Jul. 2007.
[54] M. Helm, C. Keil, S. Hiebler, H. Mehling, and C. Schweigler, “Solar heating and cooling system with absorption chiller and low temperature latent heat storage: Energetic performance and operational experience,” *Int. J. Refrig.*, vol. 32, no. 4, pp. 596–606, Jun. 2009.
[55] M. Helm, K. Hagel, W. Pfeffer, S. Hiebler, and C. Schweigler, “Solar Heating and Cooling System with Absorption Chiller and Latent Heat Storage – A Research Project Summary,” *Energy Procedia*, vol. 48, pp. 837–849, 2014.
[56] A. Gil, C. Barreneche, P. Moreno, C. Solé, A. Inés Fernández, and L. F. Cabeza, “Thermal behaviour of d-mannitol when used as PCM: Comparison of results obtained by DSC and in a thermal energy storage unit at pilot plant scale,” *Appl. Energy*, vol. 111, pp. 1107–1113, Nov. 2013.
[57] A. Gil, E. Oró, A. Castell, and L. F. Cabeza, “Experimental analysis of the effectiveness of a high temperature thermal storage tank for solar cooling applications,” *Appl. Therm. Eng.*, vol. 54, no. 2, pp. 521–527, May 2013.
[58] A. Gil, E. Oró, L. Miró, G. Peiró, Á. Ruiz, J. M. Salmerón, and L. F. Cabeza, “Experimental analysis of hydroquinone used as phase change material (PCM) to be applied in solar cooling refrigeration,” *Int. J. Refrig.*, vol. 39, pp. 95–103, Mar. 2014.
[59] J. F. Belmonte, M. A. Izquierdo-Barrientos, P. Eguía, A. E. Molina, and J. A. Almendros-Ibáñez, “PCM in the heat rejection loops of absorption chillers. A feasibility study for the residential sector in Spain,” *Energy Build.*, vol. 80, pp. 331–351, Sep. 2014.
[60] F. Agyenim, M. Rhodes, and I. Knight, “The use of phase change material (PCM) to improve the coefficient of perform-ance of a chiller for meeting domestic cooling in Wales,” in *2nd PALENC Conference and 28th AIVC Conference on Building Low Energy Cooling and Advanced Ventilation Technologies in the 21sr Century, Crete island, Greece*, 2007.
[61] G. Fang, S. Wu, and X. Liu, “Experimental study on cool storage air-conditioning system with spherical capsules packed bed,” *Energy Build.*, vol. 42, no. 7, pp. 1056–1062, Jul. 2010.
[62] N. Chaiyat, “Energy and economic analysis of a building air-conditioner with a phase change material (PCM),” *Energy Convers. Manag.*, vol. 94, pp. 150–158, Apr. 2015.
[63] F. Bruno, N. H. S. Tay, and M. Belusko, “Minimising energy usage for domestic cooling with off-peak PCM storage,” *Energy Build.*, vol. 76, pp. 347–353, Jun. 2014.
[64] D. Zhao and G. Tan, “Numerical analysis of a shell-and-tube latent heat storage unit with fins for air-conditioning application,” *Appl. Energy*, vol. 138, pp. 381–392, Jan. 2015.
[65] M. Yamaha and S. Misaki, “The Evaluation of Peak Shaving by a Thermal Storage System Using Phase-Change Materials in Air Distribution Systems,” *HVACR Res.*, vol. 12, 2006.
[66] E. Rodriguez-Ubinas, L. Ruiz-Valero, S. Vega, and J. Neila, “Applications of Phase Change Material in highly energy-efficient houses,” *Energy Build.*, vol. 50, pp. 49–62, Jul. 2012.
[67] “solardecathlon.” .
[68] S. Zhang and J. Niu, “Cooling performance of nocturnal radiative cooling combined with microencapsulated phase change material (MPCM) slurry storage,” *Energy Build.*, vol. 54, pp. 122–130, Nov. 2012.
[69] R. Ansuini, R. Larghetti, A. Giretti, and M. Lemma, “Radiant floors integrated with PCM for indoor temperature control,” *Energy Build.*, vol. 43, no. 11, pp. 3019–3026, Nov. 2011.
[70] X. Wang, J. Niu, and A. H. C. van Paassen, “Raising evaporative cooling potentials using combined cooled ceiling and MPCM slurry storage,” *Energy Build.*, vol. 40, no. 9, pp. 1691–1698, Jan. 2008.

[71] S. E. Kalnæs and B. P. Jelle, "Phase change materials and products for building applications: A state-of-the-art review and future research opportunities," *Energy Build.*, vol. 94, pp. 150–176, May 2015.
[72] M. Pomianowski, P. Heiselberg, and Y. Zhang, "Review of thermal energy storage technologies based on PCM application in buildings," *Energy Build.*, vol. 67, pp. 56–69, Dec. 2013.
[73] N. Zhu, Z. Ma, and S. Wang, "Dynamic characteristics and energy performance of buildings using phase change materials: A review," *Energy Convers. Manag.*, vol. 50, no. 12, pp. 3169–3181, Dec. 2009.
[74] N. Soares, J. J. Costa, A. R. Gaspar, and P. Santos, "Review of passive PCM latent heat thermal energy storage systems towards buildings' energy efficiency," *Energy Build.*, vol. 59, pp. 82–103, Apr. 2013.
[75] S. Scalat, D. Banu, D. Hawes, J. Parish, F. Haghighata, and D. Feldman, "Full scale thermal testing of latent heat storage in wallboard," *Sol. Energy Mater. Sol. Cells*, vol. 44, no. 1, pp. 49–61, 1996.
[76] F. Kuznik, J. Virgone, and K. Johannes, "In-situ study of thermal comfort enhancement in a renovated building equipped with phase change material wallboard," *Renew. Energy*, vol. 36, no. 5, pp. 1458–1462, May 2011.
[77] A. Athienitis, C. Liu, D. Hawes, D. Banu, and D. Feldman, "Investigation of the thermal performance of a passive solar test-room with wall latent heat storage," *Build Env.*, 1997.
[78] D. A. Neeper, "Thermal dynamics of wallboard with latent heat storage," *Sol. Energy*, vol. 68, no. 5, pp. 393–403, 2000.
[79] X. Xu, Y. Zhang, K. Lin, H. Di, and R. Yang, "Modeling and simulation on the thermal performance of shape-stabilized phase change material floor used in passive solar buildings," *Energy Build.*, vol. 37, no. 10, pp. 1084–1091, Oct. 2005.
[80] A. Pasupathy and R. Velraj, "Effect of double layer phase change material in building roof for year round thermal management," *Energy Build.*, vol. 40, no. 3, pp. 193–203, Jan. 2008.
[81] J. Kośny, K. Biswas, W. Miller, and S. Kriner, "Field thermal performance of naturally ventilated solar roof with PCM heat sink," *Sol. Energy*, vol. 86, no. 9, pp. 2504–2514, Sep. 2012.
[82] K. A. R. Ismail, C. T. Salinas, and J. R. Henriquez, "Comparison between PCM filled glass windows and absorbing gas filled windows," *Energy Build.*, vol. 40, no. 5, pp. 710–719, Jan. 2008.
[83] F. Goia, M. Perino, and V. Serra, "Improving thermal comfort conditions by means of PCM glazing systems," *Energy Build.*, vol. 60, pp. 442–452, May 2013.
[84] H. Weinlaeder, W. Koerner, and M. Heidenfelder, "Monitoring results of an interior sun protection system with integrated latent heat storage," *Energy Build.*, vol. 43, no. 9, pp. 2468–2475, Sep. 2011.
[85] A. G. Entrop, H. J. H. Brouwers, and A. H. M. E. Reinders, "Experimental research on the use of micro-encapsulated Phase Change Materials to store solar energy in concrete floors and to save energy in Dutch houses," *Sol. Energy*, vol. 85, no. 5, pp. 1007–1020, May 2011.
[86] L. F. Cabeza, C. Castellón, M. Nogués, M. Medrano, R. Leppers, and O. Zubillaga, "Use of microencapsulated PCM in concrete walls for energy savings," *Energy Build.*, vol. 39, no. 2, pp. 113–119, Feb. 2007.
[87] P. Arce, C. Castellón, A. Castell, and L. F. Cabeza, "Use of microencapsulated PCM in buildings and the effect of adding awnings," *Energy Build.*, vol. 44, pp. 88–93, Jan. 2012.
[88] L. Royon, L. Karim, and A. Bontemps, "Thermal energy storage and release of a new component with PCM for integration in floors for thermal management of buildings," *Energy Build.*, vol. 63, pp. 29–35, Aug. 2013.
[89] X. Kong, S. Lu, Y. Li, J. Huang, and S. Liu, "Numerical study on the thermal performance of building wall and roof incorporating phase change material panel for passive cooling application," *Energy Build.*, vol. 81, pp. 404–415, Oct. 2014.
[90] E. M. Alawadhi and H. J. Alqallaf, "Building roof with conical holes containing PCM to reduce the cooling load: Numerical study," *Energy Convers. Manag.*, vol. 52, no. 8–9, pp. 2958–2964, Aug. 2011.
[91] X. Sun, Q. Zhang, M. A. Medina, and K. O. Lee, "Energy and economic analysis of a building enclosure outfitted with a phase change material board (PCMB)," *Energy Convers. Manag.*, vol. 83, pp. 73–78, Jul. 2014.
[92] E. M. Alawadhi, "Using phase change materials in window shutter to reduce the solar heat gain," *Energy Build.*, vol. 47, pp. 421–429, Apr. 2012.
[93] G. Zhou, Y. Yang, X. Wang, and S. Zhou, "Numerical analysis of effect of shape-stabilized phase change material plates in a building combined with night ventilation," *Appl. Energy*, vol. 86, no. 1, pp. 52–59, Jan. 2009.
[94] A. L. S. Chan, "Energy and environmental performance of building façades integrated with phase change material in subtropical Hong Kong," *Energy Build.*, vol. 43, no. 10, pp. 2947–2955, Oct. 2011.

[95] S. M. Sajjadian, J. Lewis, and S. Sharples, "The potential of phase change materials to reduce domestic cooling energy loads for current and future UK climates," *Energy Build.*, vol. 93, pp. 83–89, Apr. 2015.
[96] K. O. Lee, M. A. Medina, E. Raith, and X. Sun, "Assessing the integration of a thin phase change material (PCM) layer in a residential building wall for heat transfer reduction and management," *Appl. Energy*, vol. 137, pp. 699–706, Jan. 2015.
[97] C. Voelker, O. Kornadt, and M. Ostry, "Temperature reduction due to the application of phase change materials," *Energy Build.*, vol. 40, no. 5, pp. 937–944, Jan. 2008.
[98] S. D. Zwanzig, Y. Lian, and E. G. Brehob, "Numerical simulation of phase change material composite wallboard in a multi-layered building envelope," *Energy Convers. Manag.*, vol. 69, pp. 27–40, May 2013.
[99] L. Shilei, F. Guohui, Z. Neng, and D. Li, "Experimental study and evaluation of latent heat storage in phase change materials wallboards," *Energy Build.*, vol. 39, no. 10, pp. 1088–1091, Oct. 2007.
[100] X. Shi, S. A. Memon, W. Tang, H. Cui, and F. Xing, "Experimental assessment of position of macro encapsulated phase change material in concrete walls on indoor temperatures and humidity levels," *Energy Build.*, vol. 71, pp. 80–87, Mar. 2014.
[101] F. Kuznik, J. Virgone, and J.-J. Roux, "Energetic efficiency of room wall containing PCM wallboard: A full-scale experimental investigation," *Energy Build.*, vol. 40, no. 2, pp. 148–156, Jan. 2008.
[102] A. Castell, I. Martorell, M. Medrano, G. Pérez, and L. F. Cabeza, "Experimental study of using PCM in brick constructive solutions for passive cooling," *Energy Build.*, vol. 42, no. 4, pp. 534–540, Apr. 2010.
[103] I. Cerón, J. Neila, and M. Khayet, "Experimental tile with phase change materials (PCM) for building use," *Energy Build.*, vol. 43, no. 8, pp. 1869–1874, Aug. 2011.
[104] C. Zhang, Y. Chen, L. Wu, and M. Shi, "Thermal response of brick wall filled with phase change materials (PCM) under fluctuating outdoor temperatures," *Energy Build.*, vol. 43, no. 12, pp. 3514–3520, Dec. 2011.
[105] C. K. Halford and R. F. Boehm, "Modeling of phase change material peak load shifting," *Energy Build.*, vol. 39, no. 3, pp. 298–305, Mar. 2007.
[106] J. Kosny, E. Kossecka, A. Brzezinski, A. Tleoubaev, and D. Yarbrough, "Dynamic thermal performance analysis of fiber insulations containing bio-based phase change materials (PCMs)," *Energy Build.*, vol. 52, pp. 122–131, Sep. 2012.
[107] G. Evola, L. Marletta, and F. Sicurella, "A methodology for investigating the effectiveness of PCM wallboards for summer thermal comfort in buildings," *Build. Environ.*, vol. 59, pp. 517–527, Jan. 2013.
[108] H. Mehling and L. F. Cabeza, "Heat and cold storage with PCM," *Hand Book Publ. Springer Ger.*, 2008.
[109] F. Kaltenbach, "PCM Latent Thermal Storage Media Heating and Cooling without Energy Consumption," pp. 544–549, 2005.
[110] T. Kondo and T. Ibamoto, "Research on Thermal Storage Using Rock Wool Phase-Change Material Ceiling Board," *ASHRAE Trans.*, vol. 112, no. 1, Jan. 2006.
[111] S. M. Vakilaltojjar and W. Saman, "Analysis and modelling of a phase change storage system for air conditioning applications," *Appl. Therm. Eng.*, vol. 21, no. 3, pp. 249–263, 2001.
[112] W. Saman, F. Bruno, and E. Halawa, "Thermal performance of PCM thermal storage unit for a roof integrated solar heating system," *Sol. Energy*, vol. 78, no. 2, pp. 341–349, Feb. 2005.
[113] X. Jin and X. Zhang, "Thermal analysis of a double layer phase change material floor," *Appl. Therm. Eng.*, vol. 31, no. 10, pp. 1576–1581, Jul. 2011.
[114] "Directive 2010/31/EU of the European Parliament and of the Council on the Energy Performance of Buildings." 19-May-2010.
[115] G. Diarce, A. Urresti, A. García-Romero, A. Delgado, A. Erkoreka, C. Escudero, and Á. Campos-Celador, "Ventilated active façades with PCM," *Appl. Energy*, vol. 109, pp. 530–537, Sep. 2013.
[116] A. de Gracia, L. Navarro, A. Castell, and L. F. Cabeza, "Energy performance of a ventilated double skin facade with PCM under different climates," *Energy Build.*, vol. 91, pp. 37–42, Mar. 2015.
[117] A. de Gracia, L. Navarro, A. Castell, Á. Ruiz-Pardo, S. Álvarez, and L. F. Cabeza, "Thermal analysis of a ventilated facade with PCM for cooling applications," *Energy Build.*, vol. 65, pp. 508–515, Oct. 2013.

[118] N. Safer, M. Woloszyn, and J. J. Roux, “Three-dimensional simulation with a CFD tool of the airflow phenomena in single floor double-skin facade equipped with a venetian blind,” *Sol. Energy*, vol. 79, no. 2, pp. 193–203, Aug. 2005.
[119] A. de Gracia, L. Navarro, A. Castell, Á. Ruiz-Pardo, S. Alvárez, and L. F. Cabeza, “Experimental study of a ventilated facade with PCM during winter period,” *Energy Build.*, vol. 58, pp. 324–332, Mar. 2013.
[120] S. Álvarez, L. F. Cabeza, A. Ruiz-Pardo, A. Castell, and J. A. Tenorio, “Building integration of PCM for natural cooling of buildings,” *Appl. Energy*, vol. 109, pp. 514–522, Sep. 2013.
[121] G. Evola, L. Marletta, and F. Sicurella, “Simulation of a ventilated cavity to enhance the effectiveness of PCM wallboards for summer thermal comfort in buildings,” *Energy Build.*, vol. 70, pp. 480–489, Feb. 2014.
[122] U. Eicker, “Cooling strategies, summer comfort and energy performance of a rehabilitated passive standard office building,” *Appl. Energy*, vol. 87, no. 6, pp. 2031–2039, Jun. 2010.
[123] M. Jaworski, “Thermal performance of building element containing phase change material (PCM) integrated with ventilation system – An experimental study,” *Appl. Therm. Eng.*, vol. 70, no. 1, pp. 665–674, Sep. 2014.
[124] M. Jaworski, P. Łapka, and P. Furmański, “Numerical modelling and experimental studies of thermal behaviour of building integrated thermal energy storage unit in a form of a ceiling panel,” *Appl. Energy*, vol. 113, pp. 548–557, Jan. 2014.
[125] J. Persson and M. Westermark, “Phase change material cool storage for a Swedish Passive House,” *Energy Build.*, vol. 54, pp. 490–495, Nov. 2012.
[126] X. Wang and J. Niu, “Performance of cooled-ceiling operating with MPCM slurry,” *Energy Convers. Manag.*, vol. 50, no. 3, pp. 583–591, Mar. 2009.
[127] P. Schossig, H. Henning, S. Gschwander, and T. Haussmann, “Micro-encapsulated phase-change materials integrated into construction materials,” *Sol. Energy Mater. Sol. Cells*, vol. 89, no. 2–3, pp. 297–306, Nov. 2005.
[128] Y. Zhang, G. Zhou, K. Lin, Q. Zhang, and H. Di, “Application of latent heat thermal energy storage in buildings: State-of-the-art and outlook,” *Build. Environ.*, vol. 42, no. 6, pp. 2197–2209, Jun. 2007.
[129] M. Wetter and J. Wright, “A comparison of deterministic and probabilistic optimization algorithms for nonsmooth simulation-based optimization,” *Build. Environ.*, vol. 39, no. 8, pp. 989–999, Aug. 2004.
[130] E. Asadi, M. G. da Silva, C. H. Antunes, and L. Dias, “A multi-objective optimization model for building retrofit strategies using TRNSYS simulations, GenOpt and MATLAB,” *Build. Environ.*, vol. 56, pp. 370–378, Oct. 2012.
[131] A. Hasan, M. Vuolle, and K. Sirén, “Minimisation of life cycle cost of a detached house using combined simulation and optimisation,” *Build. Environ.*, vol. 43, no. 12, pp. 2022–2034, Dec. 2008.
[132] M. Fesanghary, S. Asadi, and Z. W. Geem, “Design of low-emission and energy-efficient residential buildings using a multi-objective optimization algorithm,” *Build. Environ.*, vol. 49, pp. 245–250, Mar. 2012.
[133] M. Kottek, J. Grieser, C. Beck, B. Rudolf, and F. Rubel, “World Map of the Köppen-Geiger climate classification updated,” *Meteorol. Z.*, vol. 15, no. 3, pp. 259–263, Jun. 2006.
[134] C. Reardon, “Design for climate, passive design.” 2013.
[135] N. Soares, A. R. Gaspar, P. Santos, and J. J. Costa, “Multi-dimensional optimization of the incorporation of PCM-drywalls in lightweight steel-framed residential buildings in different climates,” *Energy Build.*, vol. 70, pp. 411–421, Feb. 2014.
[136] M. Alam, H. Jamil, J. Sanjayan, and J. Wilson, “Energy saving potential of phase change materials in major Australian cities,” *Energy Build.*, vol. 78, pp. 192–201, Aug. 2014.
[137] F. Ascione, N. Bianco, R. F. De Masi, F. de’ Rossi, and G. P. Vanoli, “Energy refurbishment of existing buildings through the use of phase change materials: Energy savings and indoor comfort in the cooling season,” *Appl. Energy*, vol. 113, pp. 990–1007, Jan. 2014.
[138] A. Aranda-Usón, G. Ferreira, A. M. López-Sabirón, M. D. Mainar-Toledo, and I. Zabalza Bribián, “Phase change material applications in buildings: An environmental assessment for some Spanish climate severities,” *Sci. Total Environ.*, vol. 444, pp. 16–25, Feb. 2013.
[139] J. Borderon, J. Virgone, and R. Cantin, “Modeling and simulation of a phase change material system for improving summer comfort in domestic residence,” *Appl. Energy*, vol. 140, pp. 288–296, Feb. 2015.
[140] S. Medved and C. Arkar, “Correlation between the local climate and the free-cooling potential of latent heat storage,” *Energy Build.*, vol. 40, no. 4, pp. 429–437, Jan. 2008.

[141] W. Xiao, X. Wang, and Y. Zhang, “Analytical optimization of interior PCM for energy storage in a lightweight passive solar room,” *Appl. Energy*, vol. 86, no. 10, pp. 2013–2018, Oct. 2009.
[142] C. Barreneche, H. Navarro, S. Serrano, L. F. Cabeza, and A. I. Fernández, “New Database on Phase Change Materials for Thermal Energy Storage in Buildings to Help PCM Selection,” *Energy Procedia*, vol. 57, pp. 2408–2415, 2014.
[143] D. Heim and J. A. Clarke, “Numerical modelling and thermal simulation of PCM–gypsum composites with ESP-r,” *Energy Build.*, vol. 36, no. 8, pp. 795–805, Aug. 2004.
[144] K. Peippo, P. Kauranen, and P. Lund, “Multicomponent PCM wall optimized for passive solar heating,” *Energy Build.*, 1991.
[145] C. Kendrick and N. Walliman, “Removing unwanted heat in lightweight buildings using phase change materials in building components: simulation modelling for PCM plasterboard,” *Archit. Sci. Rev.*, vol. 50, no. 3, pp. 265–273, 2007.
[146] F. Fiorito, “Phase-change Materials for Indoor Comfort Improvement in Lightweight Buildings. A Parametric Analysis for Australian Climates,” *Energy Procedia*, vol. 57, pp. 2014–2022, 2014.
[147] A. Waqas and S. Kumar, “Utilization of Latent Heat Storage Unit for Comfort Ventilation of Buildings in Hot and Dry Climates,” *Int. J. Green Energy*, 2011.
[148] F. Jiang, X. Wang, and Y. Zhang, “A new method to estimate optimal phase change material characteristics in a passive solar room,” *Energy Convers. Manag.*, vol. 52, no. 6, pp. 2437–2441, Jun. 2011.
[149] M. M. Farid, “Solar energy storage with phase change,” *J. Sol. Energy Res.*, 1986.
[150] V. V. Tyagi and D. Buddhi, “PCM thermal storage in buildings: A state of art,” *Renew. Sustain. Energy Rev.*, vol. 11, no. 6, pp. 1146–1166, Aug. 2007.
[151] D. Zhou, C. Y. Zhao, and Y. Tian, “Review on thermal energy storage with phase change materials (PCMs) in building applications,” *Appl. Energy*, vol. 92, pp. 593–605, Apr. 2012.

Annex B: Graphical user interface GUI

GUIs, also known as graphical user interfaces or UIs, provide point-and-click control of software applications, eliminating the need to learn a language or type commands to run the application. The image processing toolbox needs to be installed.

A GUI is created to model the phase change problem in rectangular cavity in presence of natural convection and radiation. The inputs need to be inserted: thermo-physical and optical PCM properties, geometry of the PCM container, mesh size, boundary and initial conditions, in addition to time step and number of time steps. Two commands are used to define these inputs: ‘edit text’ and ‘static text’ and the values are tagged in the main program (.m file).

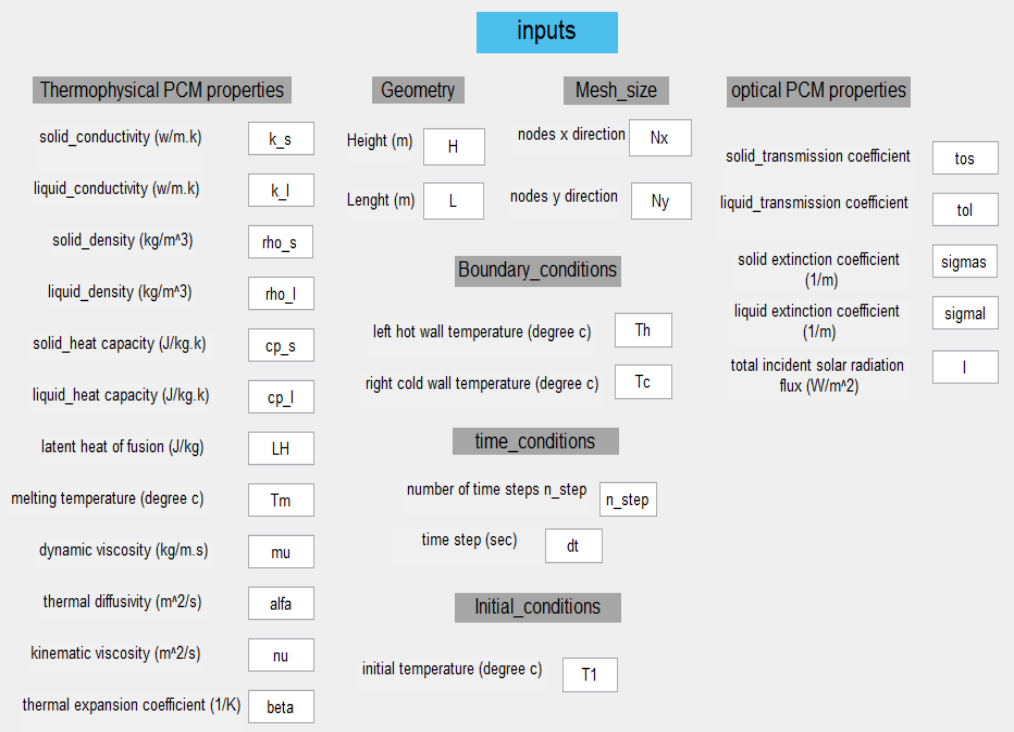

As outputs the GUI provides the average liquid fraction, the average position of the melting front and the position of melting front at different instants for both cases (phase change with natural convection and phase change e with natural convection radiation). Three commands are used to show the results: ‘push bottom’, ‘axes’ and ‘pop up menu’.

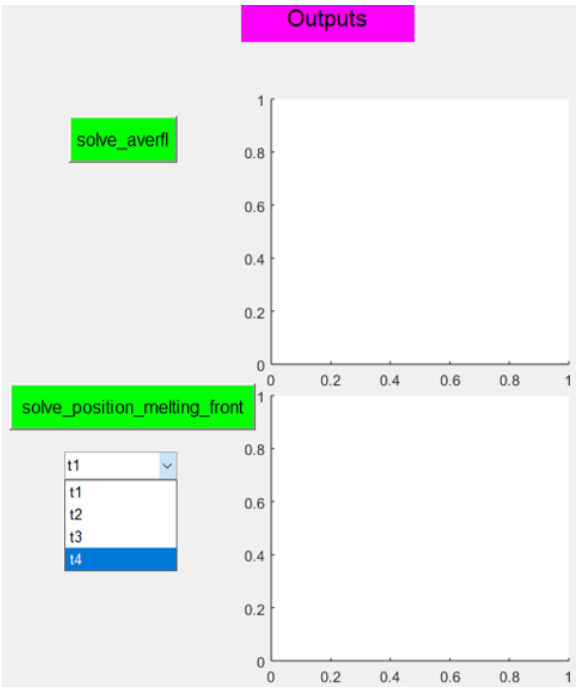
Outputs
solve_averfl
solve_position_melting_front
t1
t1
t2
t3
t4
0
0.2
0.4
0.6
0.8
1

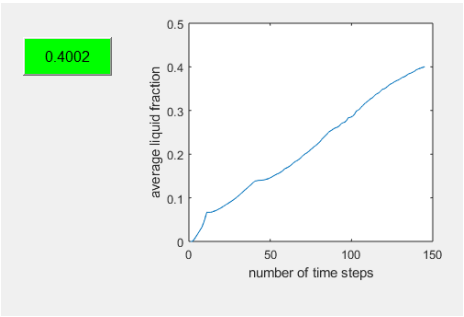
0.4002
average liquid fraction
number of time steps
0
0.1
0.2
0.3
0.4
0.5
50
100
150

Annex C: List of Publications

The results of the current work are published in peer-reviewed journals. Four journal papers are published, and one is submitted:

- **Farah Souayfane**, Farouk Fardoun, Pascal Henry Biwole. "Phase Change Materials (PCM) for cooling applications in buildings: A review". ***Energy and Buildings, Elsevier, 2016, 129, pp.396-431*.**
- **Farah Souayfane**, Pascal Henry Biwole, Farouk Fardoun. "Melting of a phase change material in presence of natural convection and radiation: A simplified model". ***Applied Thermal Engineering, Elsevier, 2018, 130, pp.660 – 671***
- **Farah Souayfane**, Pascal Henry Biwole, Farouk Fardoun. "Thermal behavior of a translucent superinsulated latent heat energy storage wall in summertime". ***Applied Energy, 2018, 217, pp. 390-408.***
- **Farah Souayfane**, Farouk Fardoun, Pascal Henry Biwole. "Energy Performance and Economic Analysis of a TIM-PCM Wall Under Different Climates". ***Submitted to Energy, revision requested, 2018*.**
- Pascal Henry Biwole, Dominic Groulx, **Farah Souayfane**, Tim Chiu. "Influence of fin size and distribution on solid-liquid phase change in a rectangular enclosure". ***International Journal of Thermal Sciences, Elsevier, 2018, 124, pp.433 - 446.***

International Conference Papers:

- **Farah Souayfane**, Pascal Henry Biwole, Farouk Fardoun. "Melting of a phase change material in presence of natural convection and radiation: A simplified model for engineering applications". ***Thermal and fluid engineering conference (TFEC),*** Fort Lauderdale, USA, March 2018.
- **Farah Souayfane**, Pascal Henry Biwole, Farouk Fardoun. "Modèle simplifié pour la prise en compte de la convection naturelle dans la modélisation du changement de phase solide-liquide". ***XIIIème Colloque Interuniversitaire Franco-Québécois sur la Thermique des Systèmes***, Saint Lo, France, May 2017.
- **Farah Souayfane**, Farouk Fardoun, Pascal Henry Biwole. "Different mathematical models of convection during phase change". ***Renewable Energies for Developing Countries (REDEC), Third international conference***, Beirut, Lebanon, July 2016

Press release in the Science Trends website:

Farah Souayfane, Pascal Henry Biwole, Farouk Fardoun & Patrick Achard "**Novel translucent superinsulated latent heat storage wall''** *https://sciencetrends.com/novel-translucent-superinsulated-latent-heat-storage-wall/*